The application of microfaunal and sedimentological data for Holocene landscape and sea-level reconstructions on the German North Sea coast

Inaugural-Dissertation

zur

Erlangung des Doktorgrades

der Mathematisch-Naturwissenschaftlichen Fakultät

der Universität zu Köln

Köln, 2021

vorgelegt von

Juliane Scheder

aus Bad Homburg

Berichterstatter/Gutachter:	Prof. Dr. Helmut Brückner
	Prof. Dr. Martin Melles
	Apl. Prof. Dr. Peter Frenzel
Tag der mündlichen Prüfung:	26.06.2020

Abstract

Detailed reconstructions of palaeo-landscape and sea-level changes on the German North Sea coast are crucial for the understanding of coastal evolution, dynamic forming processes and local controlling mechanisms of coastal and sea-level changes. This research contributes to reconstructing Holocene coastal changes in the German Bight and provides a high-resolution relative sea-level (RSL) curve for the tidal basin of Norderney by applying a novel approach of a transfer function (TF) based on microfaunal data. Based on this new knowledge, future projections of RSL rise can be supported and, thus, future coastal-protection measures can be better adjusted.

This study focuses on sediment archives from two different study areas: (1) the Jade-Weser region and (2) the East Frisian islands, which were both investigated for their sedimentological, geochemical and microfaunal characteristics. This leads to the reconstruction of phases of coastal pro- and retrogradation, which can be related to existing RSL curves. However, uncertainties due to peat compaction, indicative meaning of peats and missing reliable quantitative data remain. Therefore, in a new approach, modern associations of foraminifers and ostracods were investigated at the southern coast of Spiekeroog. These exhibit a vertical zonation, which is mainly influenced by the elevation relative to the mean sea level and therefore suitable for the development of a TF for RSL change. Such a TF relates the modern elevation to the relative species frequency of foraminifer and ostracod associations and enables the determination of elevations of fossil samples relative to the palaeo sea level from fossil microfaunal assemblages. For the first time, a combined dataset of foraminifers and ostracods is used for TF development, showing a clear improvement in terms of vertical error (RMSEP) and correlation (R^2_{boot}) compared to using exclusively foraminifers. The final TF provides a vertical error of ±29.7 cm, which is a significant improvement compared to the error ranges of solely peat-based RSL reconstructions. This improved TF was applied to Holocene samples from the tidal basin of Norderney.

Due to the intense sediment reworking of the tidal-flat deposits, as revealed by the chronological data (^{14}C dating), the resulting RSL curve reconstructs the RSL evolution until ~2500 cal BP. In this time range, the deceleration of the RSL rise is clearly evident, and the smaller error range compared to that of existing peat-based RSL curves from the southern North Sea region especially highlights the potential of fossil salt-marsh deposits for TF applications. Comparison to the available sea-level related peat data from the same cores suggests a compaction of at least ~0.7–0.9 m, whereas some deposits seem to have undergone double compaction effects due to the existence of an intercalated peat. The latter led to

uncertainties concerning the third and last phase (~3700–2500 cal BP) of the TF-based RSL curve. Moreover, comparison to a local peat-based RSL curve for the tidal basin of Langeoog reveals potential changes in palaeo-tidal range that occurred after ~6100 cal BP. Here, the TF data may indicate a stronger rise of mean high water compared to mean low water, since the data plot below the base of basal peat data points from Langeoog, which suggests a course too low for the curve. This could also be explained by a combination of the indicated compaction effects and palaeo-tidal changes. Finally, by comparing it with existing peat-based curves from Belgium and the Netherlands, the RSL curve for Norderney confirms regional differences in glacial isostatic adjustment (GIA).

In sum, this study provides valuable insights into the Holocene coastal and RSL evolution in the German Bight, where reconstructions have so far been hampered by less precise RSL index points. TF development based on microfaunal data offers new perspectives for understanding the RSL evolution at a much higher resolution. Consequently, it can be considered a useful tool also for other coastal areas in that it allows a more precise differentiation and quantification of all underlying processes, both at a local and regional scale.

Kurzzusammenfassung

Detaillierte Rekonstruktionen von Paläolandschafts- und Meeresspiegelveränderungen der Deutschen Nordseeküste sind von essenzieller Bedeutung für das Verständnis der Küstenentwicklung, der dynamischen Formungsprozesse und der lokalen Kontrollmechanismen von Meeresspiegelveränderungen.

Diese Arbeit liefert einen Beitrag zur Rekonstruktion der holozänen Küstenentwicklung in der Deutschen Bucht und stellt eine hochauflösende Meeresspiegelrekonstruktion für das Gezeitenbecken der Insel Norderney vor, welche durch einen neuen Forschungsansatz verwirklicht wird. Dieser beruht auf der Anwendung einer Mikrofauna-Transferfunktion. Basierend auf den gewonnenen Erkenntnissen können Zukunftsprognosen im Hinblick auf den relativen Meeresspiegelanstieg Unterstützung erfahren und somit Küstenschutzmaßnahmen zielgerichteter angepasst werden.

In dieser Arbeit werden Sedimentarchive in zwei verschiedenen Untersuchungsgebieten (Jade-Weser-Region und Ostfriesische Inseln) vor dem Hintergrund ihrer sedimentologischen, geochemischen und mikrofaunistischen Charakteristika untersucht. Letztlich besteht das Ziel darin, eine Rekonstruktion von Phasen der Küstenprogradation und -retrogradation zu erreichen. Diese Phasen lassen sich bestehenden relativen Meeresspiegelkurven (RMS-Kurven) zuordnen. Jedoch können Unsicherheiten aufgrund von Torfkompaktion und der indikativen Bedeutung von Torf sowie aufgrund des Fehlens verlässlicher quantitativer Daten nicht vollständig ausgeräumt werden. Als Konsequenz hieraus wurden in einem neuen Forschungsansatz rezente Foraminiferen- und Ostrakodenvergesellschaftungen an der südlichen Küste der Insel Spiekeroog untersucht. Diese weisen eine Vertikalzonierung auf, die hauptsächlich durch die Höhe relativ zum Meeresspiegel bestimmt wird. Somit erweist sich der Rezentdatensatz als geeignet für die Erstellung einer Transferfunktion (TF) für RMS-Veränderungen. Eine solche TF stellt einen statistischen Zusammenhang zwischen der heutigen Höhe und der relativen Artenverteilung der Foraminiferen und Ostrakoden her. Im Umkehrschluss ermöglicht dies die Bestimmung der Höhe einer fossilen Probe relativ zum Paläomeeresspiegel anhand der fossilen Artenverteilung. Zum ersten Mal wird eine Kombination aus Foraminiferen und Ostrakoden für eine derartige TF verwendet. Diese Tatsache bietet eine deutliche Verbesserung des vertikalen Fehlers (RMSEP) und der Korrelation (R^2_{boot}) im Vergleich zum bisher üblichen Ansatz (exklusiv Foraminiferen). Die finale TF ermöglicht die Bestimmung des RMS mit einem vertikalen Fehler von ±29,7 cm. Im Vergleich zu Fehlerbereichen torfbasierter RMS-Rekonstruktionen stellt dies einen deutlichen Fortschritt dar.

Die neue TF wurde auf holozäne Sedimentproben aus dem Gezeitenbecken der Insel Norderney angewendet. Aufgrund der durch die Datierungsergebnisse (Radiokohlenstoffdatierung) aufgedeckten starken Umlagerungseffekte im gesamten Wattbereich reicht die resultierende RMS-Kurve nur bis ca. 2500 Jahre vor heute. In dem aufgeführten Zeitraum zeigt sie deutlich die bekannte Verlangsamung des RMS nach dem starken postglazialen Anstieg. Sie weist hierbei einen meist kleineren Fehlerbereich auf als existierende torfbasierte Kurven des südlichen Nordseeraums. Im besonders kleinen Fehlerbereich der Salzwiesensedimente zeigt sich zudem das hohe Potential dieses Ablagerungsraums für TF-basierte RMS-Rekonstruktionen. Des Weiteren liefert ein Vergleich mit Torfen aus denselben Bohrkernen wertvolle Einblicke in potenzielle Kompaktionsraten, die auf mindestens ~0,7–0,9 m eingeschätzt werden. Allerdings scheinen manche Ablagerungen aufgrund eines eingeschalteten Torfs zusätzlich zum Basistorf einen doppelten Kompaktionseffekt erfahren zu haben. Dieser Umstand führt dazu, dass die dritte und letzte Phase (~3700–2500 Jahre vor heute) der RMS-Kurve mit stärkeren Unsicherheiten behaftet ist. Ein Vergleich der Kurve mit einer neuen torfbasierten RMS-Kurve des Gezeitenbeckens der Insel Langeoog lässt Veränderungen des Tidenhubs nach ~6100 Jahren vor heute vermuten. Die TF-basierte Kurve liegt hier unterhalb der Basis des Basistorfs. Hiervon ausgehend deutet sich ein seither stärkerer Anstieg des mittleren Tidehochwassers im Vergleich zum mittleren Tiedeniedrigwasser an, aufgrund dessen die TF den RMS unterschätzen würde. Letztlich bestätigt der niedrigere Verlauf der Kurve im Vergleich zu Kurven aus anderen Regionen der südlichen Nordsee (Belgien, Niederlande) bekannte regionale Unterschiede in glazialisostatischen Senkungsraten.

Abschließend lässt sich festhalten, dass die vorliegende Arbeit wertvolle Einblicke in die holozäne Küsten- und Meeresspiegelentwicklung in der Deutschen Bucht liefert, in der bisherige Rekonstruktionen durch unpräzise RMS-Indikatoren beeinträchtigt sind. Die Entwicklung einer mikrofaunabasierten TF liefert neue und detailreiche Erkenntnisse für ein vertieftes Verständnis der RMS-Entwicklung. Hieraus ergibt sich, dass sie auch in anderen Küstenbereichen als wertvolles Werkzeug zur Bestimmung lokaler und regionaler Unterschiede eingesetzt werden sollte.

Acknowledgements

This PhD thesis provides the opportunity to express my gratitude to a number of people who have helped and supported me over the last few years.

First of all, I would like to thank my supervisor Prof. Dr. Helmut Brückner for enabling the cooperation between the Institute of Geography (University of Cologne) and the Lower Saxony Institute for Historical Coastal Research (NIhK), which made my participation in the WASA Project possible. Furthermore, I would like to thank him for stirring my interest and encouraging my passion for the natural sciences, both through his inspiring teaching during my studies, and through numerous discussions about the North Sea which motivated and guided the writing of my thesis.

Besides my supervisor at the University of Cologne I would like to thank Prof. Dr. Felix Bittmann, head of the WASA Project and of the NIhK, for providing me with the opportunity to be a part of this project and focus the topic of my thesis around it.

I owe the biggest gratitude to the other members of my doctoral committee, especially Dr. Friederike Bungenstock and Dr. Max Engel, who were my mentors during and since my Master thesis. I am extremely grateful for their support and counsel in times of doubt, as well as for their patience, helpfulness and support. They never grew tired of providing explanations and joining discussions, even when obstacles occurred. Dr. Anna Pint earns my deep gratitude with her constant concern and support, content-related and mental, which helped me through the most difficult moments. All three were always there for questions, discussions and for the ups and downs during the time of my research.

Many thanks also go to Apl. Prof. Dr. Peter Frenzel, who not only co-supervised this thesis, but also supported me in terms of all the microfaunal and statistical issues arising throughout my PhD research, offering advice and practical assistance wherever he could. Furthermore, I would like to thank both him and Anna Pint for the research idea, which led to the execution and existence of this research.

My sincere thanks also go to Prof. Dr. Martin Melles who agreed to be co-supervisor of this thesis, despite the content lying outside of his usual research fields. He, Prof. Dr. Frank Schäbitz and Dr. Hannes Laermanns were members of the commission during my PhD defense, which I gratefully acknowledge.

I thank the whole WASA group and the team of the NIhK who were always supportive and helpful when needed. Special thanks go to Susanne Sisenop and Claudia Schulenberg for logistics and during grain-size measurements, Dr. Frank Schlütz for data exchange and

support in interpreting peat data, Tina Kunde for helping solve different issues, Dr. Dirk Enters for providing me with information and statistical support, Dr. Kristin Thomsen, née Haynert, for inspiration and discussions about foraminifers, Spiekeroog, salt-marsh vegetation and macrofauna, and Dr. Achim Wehrmann for providing the means for the additional dating within the project that helped unravel new aspects of the reconstructions. Kristin Thomsen and Achim Wehrmann also opened the possibility for me to use their samples for improving the transfer function. Anika Symanczyk, Anna-Sophie Kühl, Annastasia Elschner and Luise Schenk-Schlautmann were a great support in the laboratory and we had exciting discussions about all our North Sea topics and beyond.

In the context of statistical help I also owe great thanks to Dr. Yvonne Milker for her patience in helping me identify the potential obstacles during the development of the transfer function.

I am grateful for the support of Friederike Bungenstock, Anna Pint and David Scheder during field work campaigns with occasionally uncomfortable conditions (North Sea weather).

I greatly appreciate the whole working group of Prof. Dr. Helmut Brückner for productive discussions, welcome distractions and for making me feel a valuable member of the group as a scientist as well as a person. I am especially thankful to my dear colleagues and friends Dr. Melanie Bartz and Dr. Hannes Laermanns, who always created a friendly and productive but still personal atmosphere in the office. They accompanied me through the ups and downs, offering motivation, moral support, discussions and social life.

Dr. Max Engel, Dr. Melanie Bartz, Dr. Anna Pint, Dr. Alicia Medialdea Utande, Ms. Tasnim Patel, Ms. Maike Norpoth and Mr. Alan Palmer are thanked for proofreading this thesis.

The VolkswagenStiftung and the Ministry for Science and Culture of Lower Saxony funded this research as part of the WASA Project (project no. VW ZN3197). The Graduate School of Geosciences (GSGS) of the University of Cologne provided me with a Start-up Honours Grant 2016A for starting my research, with travel grants for participating in national and international conferences, and with a one-month Fellowship Grant in 2019. I gratefully acknowledge all of this financial support.

Finally, I would like to express my deepest gratitude to my family: my mother Michaela Scheder, who supported me for longer than I could have imagined, and, most of all, my husband David Scheder, who has always been my safe haven, my greatest support and who showed great understanding and patience, especially during the last months.

Table of Contents

Abstract I

Kurzzusammenfassung III

Acknowledgements V

Table of Contents VII

List of Figures X

List of Tables XIII

1 Introduction 1

1.1 The WASA Project 1

1.2 Landscape reconstructions and relative sea-level (RSL) research on the German North Sea coast – state of the art 2

1.3 Objectives of the present study 4

1.4 Research design and applied methodology 7

1.4.1 Field work 7

1.4.2 Sedimentology and geochemistry 9

1.4.3 Microfauna 10

1.4.4 Radiocarbon (^{14}C) dating 11

1.4.5 Data processing 11

1.4.6 Outline of the study 12

1.5 The study area 13

1.5.1 Geological background of the North Sea 13

1.5.2 Palaeo- and recent climate 14

1.5.3 Holocene sea-level changes 15

1.5.4 Recent dynamics on the German North Sea coast 17

1.5.5 Anthropogenic influences and human-environment interactions 19

1.5.6 The East Frisian islands of Spiekeroog and Norderney 19

2 Fossil bog soils (‘dwog horizons’) and their relation to Holocene coastal changes in the Jade Weser region, southern North Sea, Germany 21

3 Multi-proxy reconstruction of Holocene paleoenvironments from a sediment core retrieved from the Wadden Sea near Norderney, East Frisia, Germany 55

4 Microfauna- and sedimentology-based facies analysis for palaeolandscape reconstruction in the back-barrier area of Norderney (NW Germany) 71

5 Vertical and lateral distribution of Foraminifera and Ostracoda in the East Frisian Wadden Sea – developing a transfer function for relative sea-level change 102

6 Unravelling Holocene relative sea-level change in the southern North Sea using an improved microfauna-based transfer function 115

6.1 Introduction 116

6.2 Methods 118

6.2.1 Field work 118

6.2.2 Laboratory analyses 119

6.2.3 Data processing 120

6.3 Results of the modern samples 121

6.4 Results and interpretation of the statistical analyses 122

6.4.1 The combined modern training set 122

6.4.2 Final transfer function (TF) 123

6.5 Results and interpretation of the Holocene sediment cores 125

6.6 Discussion 129

6.6.1 Evaluation of sample material for TF application 129

6.6.2 The resulting RSL curve 129

6.6.3 Evaluation of the reconstructed RSL development 132

6.7 Conclusion and outlook 136

6.8 Acknowledgements 137

6.9 References 138

6.S1. Applied Methods (outside main focus of the paper) 146

6.S1.1 Laboratory analyses – Core drillings 146

6.S1.2 Data processing – Core drillings 147

6.S2. Results – modern samples and core drillings 147

6.S2.1 Microfauna – taxa and ecological information 147

6.S2.2 Results of modern samples 151
6.S2.3 Sedimentological, geochemical and microfaunal results of core drillings ..154
7 Discussion 163
7.1 Holocene coastal changes in NW Germany....163
7.2 A transfer function for relative sea-level change 174
7.3 RSL reconstructions for Norderney using microfaunal data 180
8 Conclusion and Outlook 189
References 192
Paper contribution....XV
Erklärung XVI
Curriculum Vitae XVIII

List of Figures

Fig. 1.1 The research design of this study 8
Fig. 1.2 Photographic documentation of field work 9
Fig. 1.3 Shaded relief map of the southern North Sea 14
Fig. 1.4 Time/depth diagram of sea-level rise 16
Fig. 1.5 Ternary diagram showing the classification of exemplary tidal-flat samples 18

Fig. 2.1 The study area (Weser marshland) 24
Fig. 2.2 The study area with locations of all 221 archive drillings 26
Fig. 2.3 Map of the study area with locations of stratigraphic cross sections and drilling sites. 27
Fig. 2.4 Sedimentological and foraminiferal data of the complete drilling LAN 3 29
Fig. 2.5 Detailed photographs of the different facies 30
Fig. 2.6 SEM images of selected specimens of the most frequent foraminiferal species 31
Fig. 2.7 Cross section 1, situated in the north of the study area 32
Fig. 2.8 Cross section 4, situated in the west of the study area 33
Fig. 2.9 PCA biplot of the sedimentological and foraminiferal data of LAN 3 34
Fig. 2.10 Schematical illustration of the facies interpretations for the whole study area 35
Fig. 2.11 Idealised facies model in relation to the sea-level curve for the Jade Weser region ... 38
Fig. 2.12 Core photo, schematic drawing and core description of LAN 1 41
Fig. 2.13 Core photo, schematic drawing and core description of LAN 2 42
Fig. 2.14 Core photo, schematic drawing and core description of LAN 3, Part 1 43
Fig. 2.15 Core photo, schematic drawing and core description of LAN 3, Part 2 44
Fig. 2.16 Core photo, schematic drawing and core description of LAN 3, Part 3 45
Fig. 2.17 Sedimentological and foraminiferal data of the complete drilling LAN 1 47
Fig. 2.18 Sedimentological and foraminiferal data of the complete drilling LAN 2 48
Fig. 2.19 Cross section 2, situated in the centre of the study area 49
Fig. 2.20 Cross section 3, situated in the south of the study area 50
Fig. 2.21 Cross section 5, situated in the east of the study area 51
Fig. 2.22 PCA biplot of the sedimentological and foraminiferal data of LAN 1 51
Fig. 2.23 PCA biplot of the sedimentological and foraminiferal data of LAN 2 52

Fig. 3.1 Regional overview of the Wassen Sea 58
Fig. 3.2 Stratigraphy of core VVC 17 60
Fig. 3.3 Stratigraphy of core VVC 17 with radiocarbon and laboratory results 62
Fig. 3.4 Stratigraphy of core VVC 17 with XRF scanning results 63
Fig. 3.5 Scatter plot documenting the correlation between TOC and inc/coh 64
Fig. 3.6 PCA biplot of coh-normalized elemental data 64
Fig. 3.7 Sea-level record for the southern North Sea 66
Fig. 3.S1 Pollen and non-pollyn palynomorph diagram of selected taxa for core VVC 17 69

Fig. 3.S2 Diatom, foraminifer and ostracod diagram for core VVC 17 70

Fig. 4.1 Study area 74
Fig. 4.2 Scanning electron microscope images of frequently documented foraminifera 76
Fig. 4.3 Sedimentological, geochemical and microfaunal results of N77 77
Fig. 4.4 Sedimentological, geochemical and microfaunal results of N49 78
Fig. 4.5 PCA biplot of N 77 79
Fit. 4.6 PCA biplot of N49 (lower part) 79
Fig. 4.7 PCA biplot of all cores 80
Fig. 4.8 Stratigraphic cross section of the subsurface in the back-barrier of Norderney 81
Fig. 4.S1 Sedimentological, geochemical and microfaunal results of N44 89
Fig. 4.S2 Sedimentological, geochemical and microfaunal results of N45 90
Fig. 4.S3 Sedimentological, geochemical and microfaunal results of VC13 91
Fig. 4.S4 PCA biplot of N49 (upper part of the core, Unit F) 92
Fig. 4.S5 PCA biplot of VC13 92
Fig. 4.S6 PCA biplot of N44 (lower part of the core) 93
Fig. 4.S7 PCA biplot of N45 93

Fig. 5.1 Overview of the study area 104
Fig. 5.2 Photographic documentation of the study area during low tide 105
Fig. 5.3 Elevation profile of the investigated surface transect 107
Fig. 5.4 Microfaunal, sedimentological and geochemical results 107
Fig. 5.5 PCA biplot of the investigated surface transect 108
Fig. 5.6 CCA biplot of the investigated surface transect 108
Fig. 5.7 DCA plot showing the length of the environmental gradient 109
Fig. 5.8 Results of testing the transfer function by bootstrapping cross-validation 109
Fig. 5.P1 SEM images of frequently documented foraminifer and ostracod species 110

Fig. 6.1 Study area 117
Fig. 6.2 RDA plot of supra- to intertidal foraminifers in relation to oxygen and TOC 122
Fig. 6.3 PCA biplot of the combined modern dataset 123
Fig. 6.4 Results of testing of the transfer function by bootstrapping cross-validation 124
Fig. 6.5 Stratigraphic cross section of the subsurface in the back-barrier of Norderney 125
Fig. 6.6 RSL envelope curve for the tidal basin of Norderney 130
Fig. 6.7 RSL curve for Norderney combined with available peat data 131
Fig. 6.8 Compilation of previous RSL curves and the Norderney curve 132
Fig. 6.9 Compilation of the RSL curve for Norderney and new data from Langeoog 135
Fig. 6.10 Schematic depiction of changes in tidal range and relative position of TF sample 136
Fig. 6.S2.1 SEM images of frequently documented foraminifer and ostracod species 164
Fig. 6.S2.2 Sedimentological, geochemical and microfaunal results of VVC16 169
Fig. 6.S2.3 Sedimentological, geochemical and microfaunal results of N49 170

Fig. 6.S2.4 Sedimentological, geochemical and microfaunal results of N43 171
Fig. 6.S2.5 Sedimentological, geochemical and microfaunal results of VC03 172
Fig. 6.S2.6 Sedimentological, geochemical and microfaunal results of VC13..... 173
Fig. 6.S2.7 Sedimentological, geochemical and microfaunal results of N44 174
Fig. 6.S2.8 Sedimentological, geochemical and microfaunal results of N45 175

Fig. 7.1 Test application of a TF based on modern data of Lehmann (2000)..... 173
Fig. 7.2 Compilation of the TF data and new data from Langeoog..... 187

List of Tables

Tab. 2.1 The chronology and different settlement layers of the dwelling mound 'Barward'..... 25
Tab. 2.2 Information about ^{14}C dating and calibration 31
Tab. 2.3 Extract of the most important storm surges of the North Sea 37
Tab. 2.4 Abundant foraminiferal species and their ecological characteristics 46
Tab. 2.5 Compilation of the data used for PCA of LAN 1 52
Tab. 2.6 Compilation of the data used for PCA of LAN 2 53
Tab. 2.7 Compilation of the data used for PCA of LAN 3 53

Tab. 3.1 AMS-radiocarbon dates 61

Tab. 4.1 Radiocarbon ages and calibration information.....81
Tab. 4.S1 Abundant foraminifer and ostracod species and their ecological characteristics..... 87
Tab. 4.S2 Grain-size data of all investigated cores..... 94
Tab. 4.S3 Geochemical data of all investigated cores..... 95
Tab. 4.S4 Foraminifer and ostracod counts of all investigated cores..... 98

Tab. 6.1 AMS ^{14}C data chart..... 126
Tab. 6.S2.1 List of foraminifers, mean density and standard deviation..... 151
Tab. 6.S2.2 Total organic carbon (TOC) values..... 152
Tab. 6.S2.3 Replicated oxygen values, mean oxygen ± standard deviation..... 152
Tab. 6.S2.4 Foraminifer- and ostracod counts of the combined dataset..... 153

Chapter 1

1 Introduction

1.1 The WASA Project

The WASA Project (*'The Wadden Sea as an archive of landscape evolution, climate change and settlement history: exploration – analysis – predictive modelling'*) is funded by the 'Niedersächsisches Vorab' of the VolkswagenStiftung within the funding initiative 'Küsten und Meeresforschung in Niedersachsen' of the Ministry for Science and Culture of Lower Saxony, Germany (project VW ZN3197) (https://nihk.de/index.php?id=483&L=1). It is a collaboration of the Lower Saxony Institute for Historical Coastal Research (Wilhelmshaven, Germany), 'Senckenberg am Meer' (Wilhelmshaven, Germany), the 'Niedersächsischer Landesbetrieb für Wasserwirtschaft, Küsten- und Naturschutz, Forschungsstelle Küste' (Norderney, Germany) and the University of Bremen (Germany). This interdisciplinary project combines methods of sedimentology, geophysics, geochemistry, palaeobiology, archaeology and offshore engineering for the analysis of marine sediment archives. The aim of the project is the reconstruction of Holocene palaeo-landscapes, which shall provide the basis for the identification of potential archaeological settlement areas (archaeoprognosis).

Due to the rising temperatures after the last glacial maximum (LGM), approximately 20 ka (kiloyears = 1000 years) ago, and the associated sea-level rise (Lambeck et al., 2014), the North Sea coast experienced several stages of coastal evolution (Bungenstock and Schäfer, 2009). These are recorded by an alternation of peats, overlying the Pleistocene sediments indicating coastal swamp landscapes, deposits of sheltered coastal areas like in salt marshes and deposits of higher dynamic conditions, such as those seen in tidal flats or channels. These alternations document repeated coastline pro- and retrogradation, which led to the burial of human and animal habitats and the possible conservation of these drowned areas over thousands of years (Bittmann, 2019). Numerous, mostly scattered archaeological findings within the present-day Wadden Sea area indicate that settlements did exist in these areas, confirming the Wadden Sea to be a unique archive of environmental and cultural history (Jöns, 2015). This archive is investigated by the application of a multi-proxy approach (comprising: hydro-acoustics, granoulometry, geochemistry, micro- and macrofaunal investigations, pollen and botanical analysis, diatom analysis, radiocarbon dating and archaeological investigations) within the WASA project, in order to reconstruct the

post-glacial landscape development, sedimentary processes as well as the relative sea-level (RSL) development and climatic changes (Bittmann, 2019).

A grid of over 120 drillings is investigated within the WASA Project, mainly concentrating on the back-barrier and offshore area of the East Frisian island of Norderney with additional drillings around Spiekeroog (Fig. 1.3). In order to generate information over larger areas and correlate depositional units, additional hydro-acoustic investigations are carried out. The retrieved data are combined using geo-information systems and interpreted to develop maps of palaeo-landscapes and potential former settlement areas (Bittmann, 2019). In order to develop these maps, knowledge about the RSL history is essential, which is why RSL reconstructions are a crucial component of the project. Thus, this PhD thesis will give new insights into the Holocene landscape and RSL evolution in the back-barrier area of Norderney, an area where RSL research is rather underexplored and associated with large uncertainties. Due to restrictions arising when reconstructing the RSL development from peat layers or when drawing conclusions on the RSL from landscape reconstructions (Behre, 2007; Bungenstock and Schäfer, 2009; Bungenstock and Weerts, 2010, 2012; Baeteman et al., 2011), a novel approach is used in this thesis, which has so far not been applied to the southern North Sea coast.

1.2 Landscape reconstructions and relative sea-level (RSL) research on the German North Sea coast – state of the art

Landscape and RSL reconstructions on the German North Sea coast have been connected for a long time due to the fact that mainly peat layers were frequently used as sea-level index points (Denys and Baeteman, 1995; De Groot et al., 1996; Baeteman, 1999; Freund and Streif, 2000; Kiden et al., 2002; van de Plassche et al., 2005; Behre, 2007; Bungenstock and Schäfer, 2009; Karle et al., 2017; Meijles et al., 2018). However, post-depositional and auto-compaction represents a source of significant uncertainties, wherefore there have been several approaches to quantify the effect of compaction and its impact on RSL reconstructions (Paul and Barras, 1998; Bird et al., 2004; Long et al., 2006). Along the east coast of England, average compaction rates of 0.4±0.3 mm/a for peats in Holocene sequences have been inferred (Horton and Shennan, 2009). The auto-compaction of peat by oxidation and decomposition can lead to subsidence of the surface of several metres over centuries (e.g. Long et al., 2006; Weerts, 2013). As a result, mid- to late Holocene peat-based curves may suffer from large error ranges of up to 3–5 m (Long et al., 2006; Vink et al., 2007; Bungenstock and Schäfer, 2009; Bungenstock and Weerts, 2010, 2012; Baeteman et al., 2011). Furthermore, the indicative meaning of peat, only having an indirect relation to the sea level, is still not entirely resolved (Baeteman, 1999; van de Plassche et al., 2005;

Bungenstock and Schäfer, 2009; Wolters et al., 2010). The general assumption is that basal peats approximately correlate with coastal mean high water (MHW), whereas local differences in tidal range, caused by different effects, can lead to the peat reflecting any level between mean sea level (MSL) and MHW, but never below MSL (Vink et al., 2007). Furthermore, not all basal peats are valid RSL indicators, since their formation is not always linked to the sea level, demonstrated for example by an early Holocene basal peat from the Borkum Riffground, southern North Sea, that started to grow when sea level was ~17 m lower (Wolters et al., 2010). Earlier investigations already described sea level-independent paludification related to specific topographic conditions (Jelgersma, 1961; Lange and Menke, 1967; Baeteman, 1999). Therefore, when using widespread basal or intercalated peat layers as RSL index points, close investigation concerning formation processes is needed (Bungenstock and Schäfer, 2009; Bungenstock and Weerts, 2010).

A RSL drop or stagnation can cause oxidative decomposition of peats associated with pedogenesis. If the so-formed bog soils are subsequently buried during marine inundations, they are called *dwog* horizons, usually occurring within the first 3 m of the subsurface as intercalated humic or highly iron-affected horizons (Streif, 1990). During the Bronze Age, several of these *dwog* horizons formed in the southern North Sea region (Schoute et al., 1981). Since their formation in the coastal marshlands requires a dropping groundwater level, which is directly related to the RSL, they can also be used as RSL index points (Streif, 1990, 2004).

Another possibility to draw conclusions on RSL developments is using archaeological information, for example by investigating different elevation stages of dwelling mounds. Dwelling mounds ('Wurten") are typical for the German North Sea coast since the 1st century BC, which were raised continuously following the rising RSL. Thus, their specific, archaeologically dated levels can also be used as RSL index points (Behre, 2007; Aufderhaar et al., 2013).

In order to avoid compaction-prone peats and the indirect relation of peats and *dwog* horizons, RSL change can be reconstructed using salt-marsh foraminifers. They are shell-bearing protists and occur in very specific assemblages based on habitat conditions. The distribution of taxa in modern intertidal environments can be used to develop a transfer function (TF), modelling the relation between elevations and relative abundances of foraminifer species. This enables the determination of palaeo-water depths with a precision of up to 10–15% of the tidal range, hence a decimetre-scale precision in mesotidal environments (Leorri et al., 2010; Kemp et al., 2012; Barlow et al., 2013; Edwards and Wright, 2015). This approach has been established over the last two decades mainly in North America, Denmark and on the British Isles (Scott et al., 2001; Gehrels et al., 2002; Gehrels and Newman, 2004;

Pedersen et al., 2009; Engelhart and Horton, 2012; Kemp et al., 2012, 2013). This thesis presents the first microfossil-based TF for the southern part of the German Bight (Scheder et al., 2019), where in a pioneering attempt ostracod, (small crustaceans with a bivalve calcified carapace) assemblages, are combined with foraminifers, leading to a reduced error range of the TF. Furthermore, the first application of this TF for RSL reconstruction is presented in this thesis.

Regardless of the used RSL index points and their suitability, RSL reconstructions on the German North Sea coast have to be realised on a local basis and cannot be extrapolated for the complete German Bight, as for local differences in compaction rates, glacial isostatic adjustment (GIA), tidal range, halokinetics of buried Permian salt layers, etc. This is why separate RSL curves are required for each tidal basin of the coast (Bungenstock and Schäfer, 2009; Bungenstock and Weerts, 2010, 2012; Baeteman et al., 2011).

1.3 Objectives of the present study

In NW Germany, sediment archives have been used for reconstructing Holocene environmental and RSL changes using sedimentological as well as archaeological information (e.g. Behre, 2007; Bungenstock and Schäfer, 2009; Karle et al., 2017). However, high-resolution RSL reconstructions with acceptable error ranges are so far lacking for the German North Sea coast, which is why the Holocene RSL history in the area is still associated with significant uncertainties. Holocene landscape reconstructions have so far been the first step towards drawing conclusions on the RSL history, followed by peat-based reconstructions. However the need for more precise reconstructions, also using quantitative data, has been widely expressed (Vink et al., 2007; Bungenstock and Schäfer, 2009; Bungenstock and Weerts, 2010, 2012; Baeteman et al., 2011; Meijles et al., 2018). This study aims at using multiple approaches in order to get an understanding of the Holocene landscape and sea-level change in the area of the southern North Sea coast. Therefore, sedimentological information is combined with microfaunal investigations to improve interpretations, reduce uncertainties and generate additional information on environmental conditions and water depths.

Hypothesis 1 – The reconstruction of Holocene coastal changes in the southern North Sea region can be connected to the RSL evolution

<u>Objective A: Reconstructing Holocene landscape changes in the ‘Land Wursten’ region</u>

The ‘Land Wursten’ region was subject to substantial landscape changes. It represents a former marsh island, which was formed during the post-glacial sea-level rise and is perched

between a Pleistocene *Geest* ridge and the Weser estuary. Sedimentological and microfaunal investigations on sediment cores shall provide information on depositional environments and their connection with layer information of archive core data, in order to reconstruct the development of a larger area. Furthermore, *dwog* horizons known from this area shall be identified and assigned to settlement stages of the adjacent dwelling mound 'Barward' (Asmus, 1949; Siegmüller, 2017).

Objective B: Reconstructing Holocene landscape changes in the back-barrier of Norderney

The East Frisian island of Norderney belongs to the chain of barrier islands, which formed since the deceleration of the post-glacial RSL rise (6–7 ka BP) (Freund and Streif, 2000; Flemming, 2002; Bungenstock and Schäfer, 2009). The present-day back-barrier area was subject to massive landscape changes since the last glaciation, which mainly are connected to the Holocene transgression. Sedimentological, geochemical and microfaunal investigations shall provide information about depositional environments and their correlation over a drilling transect shall enable palaeo-landscape reconstruction.

Objective C: Relating coastal changes to the local RSL history

Every reconstructed facies layer in the study area has a specific relation to RSL, lying either above, at or below it (e.g. Streif, 2004). Thus, the study shall draw detailed conclusions on the position of the identified facies layers relative to the MSL, enabling statements about the RSL development at the corresponding time.

Hypothesis 2 – Reconstructions of the Holocene RSL on the southern North Sea coast can be improved by using a transfer function based on microfaunal data

Objective D: Investigating the vertical and lateral zonation of foraminifer and ostracod associations on the southern coast of Spiekeroog

Precise data on vertical and lateral foraminifer and ostracod associations are mandatory to establish a RSL TF. A surface transect (Transect 1) on the southern coast of the East Frisian island of Spiekeroog provides an ideal area with minimal anthropogenic influences due to its location adjacent to the national park 'Niedersächsisches Wattenmeer'. The vertical and lateral zonation of foraminifers and ostracods shall be investigated in relation to environmental parameters (grain-size distribution, organic, nitrogen and carbonate content and salinity) and the elevation relative to MSL in order to identify the main driving parameters for the distribution of foraminifers and ostracods.

Objective E: Using a combination of foraminifers and ostracods for TF development

So far, studies about RSL-related TFs use exclusively foraminifer associations (e.g. Kemp et al., 2012; Milker et al., 2016, 2017; Müller-Navarra et al., 2016, 2017). The additional use of ostracods, occurring within the same sediment fraction as foraminifers, shall provide additional ecological information for more detailed reconstructions of the lower intertidal and the uppermost subtidal areas. Therefore, a combined dataset of foraminifers and ostracods shall provide a TF with a better performance than one using only foraminifer associations.

Objective F: Comparing the TF with presently used RSL index points

Basal and intercalated peats have widely been used as RSL index points, but they are associated with partially large uncertainties due to their unclarified indicative meaning and vulnerability to compaction, leading to large error ranges (Bungenstock and Schäfer, 2009; Wolters et al., 2010; Baeteman et al., 2011). The microfauna-based TF shall provide a vertical error smaller than the one usually provided by peat-based RSL reconstructions, since compaction-prone layers can be omitted. Furthermore, the TF shall provide a clear indicative meaning with a direct relation to the sea level and enable the avoidance of uncertainties resulting from relocated peat layers.

Hypothesis 3 – The application of a microfauna-based TF leads to more precise RSL reconstructions for the East Frisian islands

Objective G: Improving the performance of the TF

Most studies base their TF on a minimum of 40 samples and result in smaller error ranges (Kemp et al., 2012; Müller-Navarra et al., 2016, 2017; Milker et al., 2017). Therefore, we expect to be able to improve the performance of the TF by increasing the number of samples. Besides the 16 samples taken from the surface transect on the southern coast of Spiekeroog, an additional transect (Transect 2) investigated by colleagues from the WASA Project in the adjacent area will be included and new modelling shall provide a final TF with a smaller error range than before.

Objective H: Reconstructing the Holocene RSL history for Norderney

Understanding the local landscape evolution shall enable the identification of sediment layers, which are suitable for the application of the TF. Hence, the inter- and supratidal layers can be used for RSL reconstruction, in order to get more precise results than the relative conclusions drawn from landscape reconstructions. Therefore, the final and improved TF shall be applied to the relevant sediment layers of the WASA cores in order to create a RSL curve for the East Frisian island of Norderney. This curve shall provide smaller error ranges

than previous peat-based RSL curves and is therefore discussed in terms of comparability and improvement.

1.4 Research design and applied methodology

The palaeogeographical research performed in this PhD thesis (Fig. 1.1) investigates the modern environmental conditions in connection to microfaunal associations as well as successions of Holocene depositional environments on the East Frisian coast, NW Germany, in order to reconstruct the landscape formation during the Holocene as well as the RSL development of the last ~6 ka. Further details on the methodology can be found in the individual thematic chapters.

1.4.1 Field work

Prior to the start of the WASA Project, the field work for the modern samples (Transect 1) started in 2015 and was complemented in 2017. Surface samples were taken along a transect (c. 1180 m) from supratidal to shallow subtidal areas on the southern coast of the East Frisian island of Spiekeroog (Fig. 1.2) in steps of 15 cm elevation difference using steel sampling rings (Eijkelkamp, 5 cm diameter, Fig. 1.2d). For differentiation between living and dead individuals, samples were preserved with Ethanol mixed with rose Bengal (Walton, 1952; Edwards and Wright, 2015). Additional sediment samples were taken for sedimentological and geochemical analyses and salinity was measured in the water samples (contingent on coverage), either in the field or in the laboratory using a conductivity meter CO310 (VWR). Precise elevation measurements were conducted at each sampling station using a differential global navigation satellite system (GDNSS, Topcon Hiper Pro). Alongside the sampling, the typical vegetation in the salt marsh (supratidal areas) was documented.

Three core drillings were conducted in the ‘Land Wursten’ area in 2013, during the course of the Master’s thesis (preceding this PhD thesis), using an Atlas Copco percussion coring device (cobra mk 1) and open steel probes (5 and 6 cm diameter) to study the *dwog* horizons of the Wesermarsch. The cores were documented after schemes of Ad-hoc-Arbeitsgruppe Boden (2005). Sampling was conducted selectively according to facies changes.

Eight core drillings were conducted in the back-barrier area of Norderney (2016–2019, Fig. 1.2e–f) using a vibrocorer (Wacker Neuson IE high-frequency vibrator head and generator) and aluminium tubes (8 cm diameter) in the tidal flat, and a vibrocorer VKG-6 (VC600, med consultants GmbH) and plastic liners (10 cm diameter) for drillings from the research vessel “*MS Burchana*” in the tidal channels. Core opening and macroscopic description after

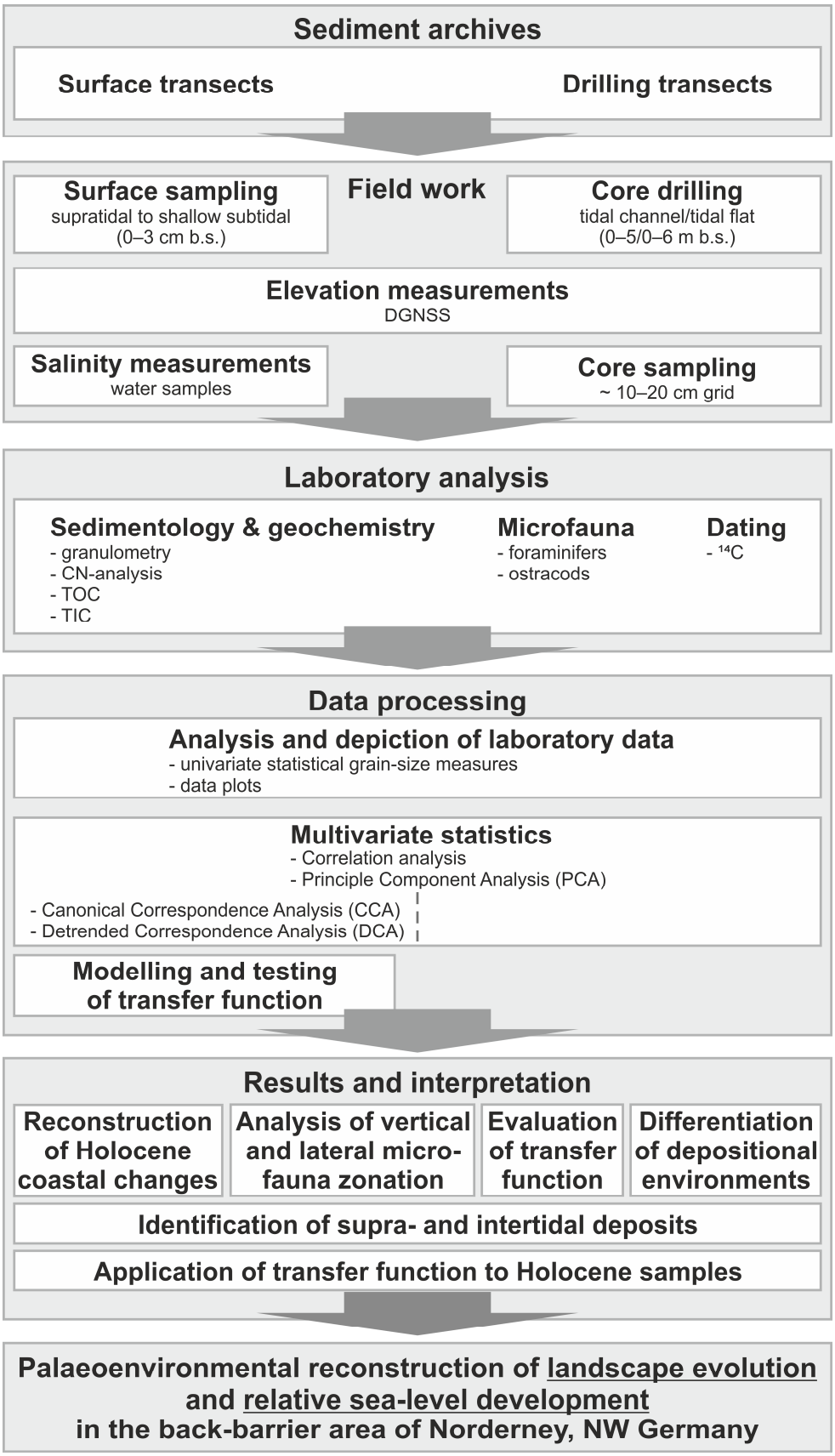

Fig. 1.1 The research design of this study (own design, inspired by M. Bartz 2018).

Preuß et al. (1991) was performed at the Institute of Geography of the University of Bremen (Germany) and the Lower Saxony Institute for Historical Coastal Research (Wilhelmshaven,

Germany). Core sampling followed a 10- or 20-cm grid, where appropriate with additional samples in smaller-scale layers.

Fig. 1.2 Photographic documentation of field work. a: view from the salt marsh of Spiekeroog towards the tidal flat, b: looking for the next sampling point in the tidal flat via elevation measurements (DGNSS), c: DGNSS base station with trigonometric point on top of a summer dyke, d: surface sampling in the salt marsh, e: drilling process in the tidal flat using a self-built vibrocoring drill hammer, f: extraction process of the core by manual chain hoist. a–d: own photos (2015 & 2017), e–f: (Francesca Bulian 2017).

1.4.2 Sedimentology and geochemistry

In order to determine the sediment origin and assess depositional environments, the sediment characteristics were analysed in the Laboratory for Physical Geography of the University of Cologne. The grain-size distribution was measured using a laser particle size analyser LS 13320 (Beckman Coulter, laser beam 780 nm) applying the Fraunhofer optical mode (Eshel et al., 2004), in order to support the interpretation of hydro-energetic levels and sediment origin and to unravel connections to the occurring microfaunal associations (Blott et al., 2004; Frenzel et al., 2010). This analysis was performed for all fossil (drill cores) and modern samples (Transect 1).

For the ‘Land Wursten’ cores, the content of organic matter was quantified by the loss on ignition (LOI) using a muffle furnace after DIN 19684-3 in order to support identification of

dwog horizons and interpretation of sediment origin (Barsch et al., 2000; Blume et al., 2011). The carbonate ($CaCO_3$) content was measured volumetrically after Scheibler (DIN ISO 10693), in order to verify field-defined sediment strata (Barsch et al., 2000; Blume et al., 2011). Furthermore, pedogenetic iron oxides (oxalate extract after Tamm, 1932; Schwertmann, 1964 and dithionite extract after Mehra and Jackson, 1958) were quantified, for *dwog* identification by means of atomic absorption spectrometry (AAS).

In order to establish information about the organic, nitrogen and carbonate content of the surface samples and Norderney cores, which will provide indications on dynamic levels, sediment origin and nutrient availability, the concentration of total organic carbon (TOC, constituting c. 50% of the organic matter) was measured using an elemental analyser Vario EL Cube (elementar). This enabled simultaneous measurement of nitrogen (N) and subsequent determination of total inorganic carbon (TIC, constituting c. 12% of the calcium carbonate [$CaCo_3$]). The inferred C/N ratio provides information about the origin of the organic matter (aquatic/terrestrial) again supporting the interpretation of depositional environments (Last and Smol, 2001).

1.4.3 Microfauna

Foraminifers and ostracods build very specific associations based on habitat conditions, which is what makes them excellent proxies for past ecological conditions (e.g. Frenzel et al., 2010; Frenzel and Boomer, 2005; Leorri et al., 2010; Milker et al., 2015). To test the vertical distribution of living individuals, several of the 5-cm thick samples were split into 1-cm thick slices for further investigation. After testing the possible effects of drying on the fragile tests of agglutinated foraminifers (De Rijk, 1995; Edwards and Wright, 2015), foraminifers and ostracods were counted dry using a light stereo microscope. Foraminifer taxa were identified based on descriptions and illustrations in Gehrels and Newman (2004), Horton and Edwards (2006) and Murray (2006) and ostracod taxa identification followed descriptions in Athersuch et al. (1989) and Frenzel et al. (2010). Due to problems in differentiating between juvenile individuals of *Leptocythere*, species were grouped under *Leptocythere* spp. for both the modern and fossil samples. The genus *Jadammina*, which is used in the first study (Chapter 2), is replaced by *Entzia* for the other studies based on the taxonomic reasoning of Filipescu and Kaminski (2011), regarding *Entzia* as a senior synonym of *Jadammina*. Differentiation between living and dead individuals for the modern samples was based on the well-preserved soft parts of ostracods and on the staining of foraminifers. Since initial testing of the vertical distribution of living individuals showed significant numbers within the upper 3 cm, these were combined for the analysis, whereas the lower 2 cm were discarded. The amounts of analysed and residual material were weighed in order to

enable extrapolation and calculation of total microfaunal concentrations for both modern and fossil samples.

1.4.4 Radiocarbon (^{14}C) dating

In order to provide a chronological framework for the Holocene landscape changes, ^{14}C-AMS (Accelerator Mass Spectrometry) dating was carried out using the radioactive decay of the third oxygen isotope (calculated half-time period 5730 ±40 years) after being cut off of carbon uptake (death of an organism) (Hajdas, 2008). Bulk samples of *dwog* horizons and peat, macro-remains, and calcareous shells of molluscs (bivalves) and foraminifers were used for ^{14}C datings and processed at the ^{14}CHRONO Centre of the Queens University of Belfast (United Kingdom), the Poznan Radiocarbon Laboratory (Poland) and Beta Analytic Inc. (USA). Calib (v. 7.1) and R software (rbacon, v. 2.3.9.1) and IntCal13 and Marine13 calibration curves (Reimer et al., 2013; Blaauw and Christen, 2019) were used for calibration and age-depth modelling and marine datings were corrected for reservoir effect, using the offset and uncertainty recently determined by Enters et al. (2021).

1.4.5 Data processing

For modern and fossil samples, univariate statistical grain-size measures were calculated after (Folk and Ward, 1957) using the GRADISTAT Excel tool (Blott and Pye, 2001). Depiction of the data was accomplished by the creation of data plots using the software Grapher (v. 8.0.278–9.4.819) and the drawing application CorelDRAW X8 (v. 18.1.690).

Foraminifer and ostracod associations and environmental parameters of modern and fossil samples were analysed by means of multivariate statistics (Principle Component Analysis, PCA) after the calculation of Pearson correlation coefficients between the environmental parameters and microfaunal data. The latter helps to detect possible auto-correlations between the parameters, whereas the PCA supports the evaluation of driving environmental factors and the facies interpretation. Further multivariate statistics (CCA, DCA) were performed exclusively for the modern samples, in order to identify the main environmental driving factors of taxa composition and test whether taxa show unimodal or linear response along the environmental gradient. Correlation analysis and multivariate statistics were carried out using the software PAST (v. 3.2.1) (Hammer et al., 2001).

The TF was developed from the modern training set and tested using bootstrapping cross-validation (1000 cycles) using the software C2 (v. 1.7.7.) (Juggins, 2007).

1.4.6 Outline of the study

Following this introductive first chapter, including a description of the project, methodology and study area, this PhD thesis can be subdivided into two main sections: Part I deals with landscape reconstructions and possible conclusions on RSL changes (Chapters 2, 3 and 4), whereas Part II focuses on a more precise approach for RSL reconstructions (Chapters 5 and 6). A major aim was to confirm that this more precise approach is able to provide less uncertain results than inferences drawn from landscape reconstructions and is also better than the commonly used peat-based RSL index points.

Chapter 2 investigates the palaeo-landscape development in the Jade Weser region by using a combination of archive data and new drillings and by focusing on *dwog* horizons, their implications for RSL reconstructions as well as their connection to early settlement activities. It was possible to correlate the identified *dwog* horizons with stagnation phases of the regional RSL. These results are part of the preceding Master thesis and are published in *Journal of Coastal Conservation* (Scheder et al., 2018).

Chapter 3 focuses on palaeoenvironmental reconstructions in the vicinity of the East Frisian island of Norderney by means of high-resolution stratigraphic, geochemical and palaeobiological analyses on one selected WASA core. This sedimentary record provides information about the coastal evolution since ~7000 cal BP, including variations induced by RSL changes. Finally, the data are related to further published RSL data and included into an existing RSL curve. These results are published in *Estuarine, Coastal and Shelf Science* (Bulian et al., 2019).

Chapter 4 describes the palaeo-landscape evolution in the back-barrier area of the island of Norderney based on a sedimentary record of five WASA core drillings as well as additional archive data, which are interpreted in terms of facies changes and RSL changes. The record reaches from Pleistocene aeolian and glacio-fluvial deposits over basal peat to the present-day tidal-flat deposits, showing an overall continuous RSL rise during the Holocene transgression, except for one core, which indicates a short-term phase of stagnation or slow RSL rise. These results are published in *Netherlands Journal of Geosciences* (Elschner et al., 2021).

Chapter 5 covers an approach for more precise RSL reconstructions. A TF for RSL change is established from a modern training set on the southern coast of the East Frisian island of Spiekeroog (Transect 1). For the first time, a combination of foraminifers and ostracods is used for TF development, leading to an improved performance. Since applications for the southern part of the German North Sea coast are lacking so far, this new approach shall provide the possibility for more precise, high-resolution RSL reconstructions independent

of compaction-prone peats. These results are published in *Geologica Belgica* (Scheder et al., 2019).

Chapter 6 focuses on the improvement of the existing TF (Chapter 5) as well as the application of the improved TF in order to establish a RSL curve for the island of Norderney. Additional samples from Spiekeroog indeed help to improve the performance of the TF, whereas additional WASA cores and radiocarbon dates from Norderney complement and refine the palaeo-landscape reconstructions made in Chapter 4, unravelling relocation effects highly affecting the complete tidal-flat deposits. Finally, the TF is applied to suitable samples of the WASA cores and the resulting curve is discussed in terms of comparability to existing curves and local effects. These results were submitted to *Journal of Quaternary Science* (Scheder et al., *submitted*).

Chapter 7 discusses all results with respect to the working hypotheses (Chapter 1.3).

Chapter 8 presents a conclusion and outlook of this cumulative PhD thesis.

1.5 The study area

1.5.1 Geological background of the North Sea

The North Sea is a shallow shelf sea that represents a young and dynamic sedimentary environment of mainly late Pleistocene and Holocene age. Therefore, older lithological units are mostly buried, except for those uplifted due to salt tectonics, like the island of Heligoland, where Triassic (red sand stone and shell limestone) and Cretaceous layers were tipped and uplifted by ~4000 metres, above the present sea level, by underlying Zechstein salt deposits (Streif, 1990). However, the main forming processes happened during the Quaternary and especially the Pleistocene, when the North Sea was repeatedly overprinted by the Fennoscandian and UK ice sheets (Streif, 2004). Within the three youngest Pleistocene glaciations – Elsterian (~400–245 ka BP [kiloyears before present]), Saalian (~230–128 ka BP) and Weichselian (~117–11.6 ka BP) – the ice sheets, connected to sea-level lowstands, extended far inland (Fig. 1.3) with thicknesses of over 1000 m, leaving systems of subglacial valleys originating from meltwater runoff as well as high end moraines (Streif, 2004). In between these glaciations, the interglacials – Holsteinian and Eemian – were connected to marine transgressions and associated with the deposition of marine sediments. The glaciation with the largest southward ice extent was the Saalian glaciation, overprinting the landscape previously formed during the Elsterian glaciation in Northern Germany, which led to a levelling of the surface on the German North Sea coast. During the Weichselian, the ice sheet did not reach the German North Sea coast. Most of Northern Germany was subject to periglacial conditions associated with the accumulation of aeolian and glacio-

fluvial sands that form the oldest Pleistocene surface, hence, the Holocene base, which in Germany is called *geest* (Ehlers and Gibbard, 2004; Streif, 2004; Ehlers et al., 2011). After the last glacial maximum (LGM,~20 ka BP), the sea level began to rise from its lowstand about 130 m below the present level leading to a coastline shift of about 600 km to the south (Streif, 2004). This post-glacial transgression that continued throughout the following and present-day Holocene interglacial controlled the processes shaping the present-day coastal landscape of the German North Sea.

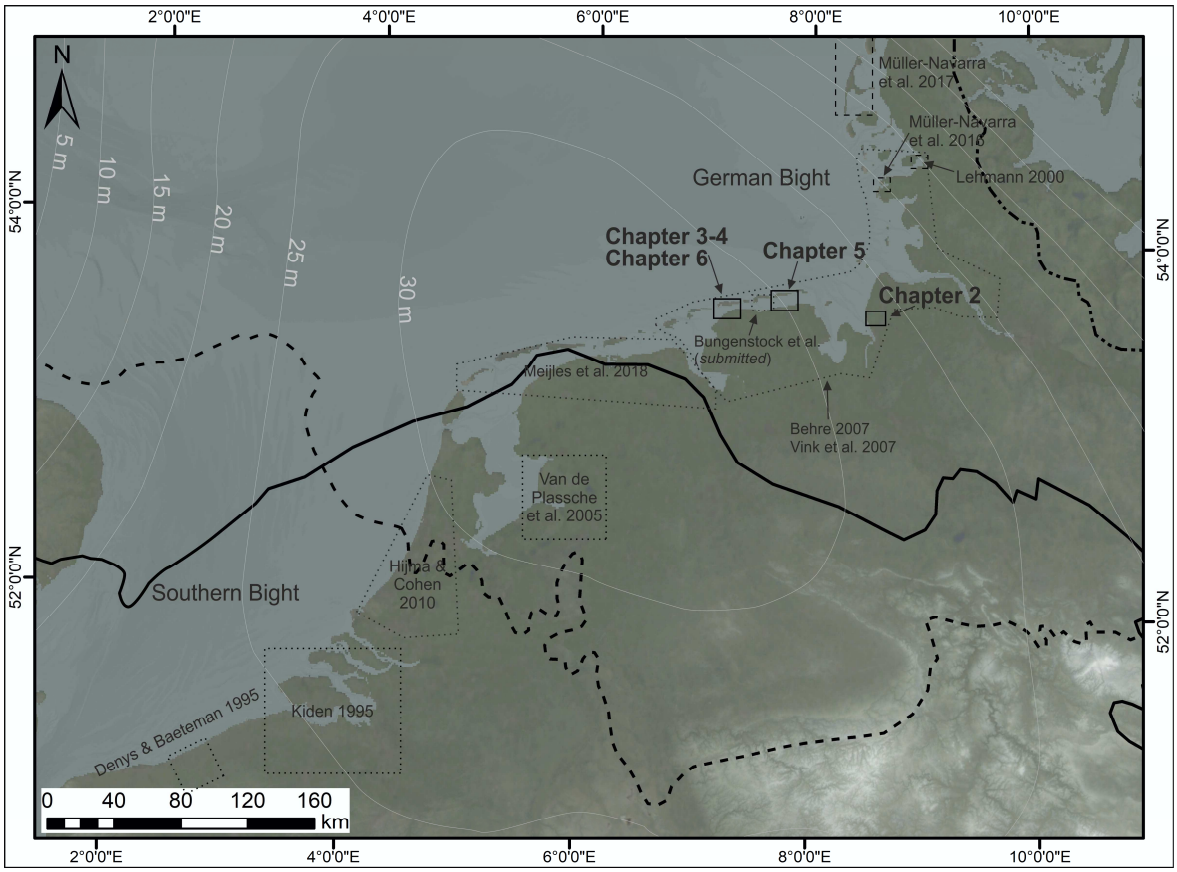

Fig. 1.3 Shaded relief map of the southern North Sea with maximum Quaternary ice extents, GIA (white isolines: subsidence in m since the last glacial; after Weerts, 2013), study areas and studies mentioned in this PhD thesis. Ice extents (Ehlers et al., 2011): solid: Elsterian glaciation, dashed: Saalian glaciation, dash-dotted: Weichselian glaciation. Study areas: solid: own research presented in this thesis, dashed: TF studies in the northern part of the German Bight, dotted: selected previous RSL reconstructions for the southern North Sea, which are used for comparison.

1.5.2 Palaeo- and recent climate

The Quaternary palaeo-climate was dictated by the mentioned alternation of glacial and interglacial periods, causing high eustatic sea-level fluctuations. The Elsterian glaciation (from ~400 ka BP) was characterised by subarctic conditions with an ice extent reaching the margins of the Central German Uplands within at least two advances (Streif, 2004; Ehlers et al., 2011). The beginning of the Holsteinian interglacial is marked by the progres-

sive melting of the ice sheets (from ~245 ka BP) resulting from a transition to boreal conditions and leading to a eustatic transgression. Around 230 ka BP, climatic conditions deteriorated again, and the Saalian glaciation was characterised by three different ice advances (Fuhne, Drenthe and Warthe) with at least one warmer period (Dömnitz). The maximum ice extent reached up tothe border of the German low mountain ranges (Streif, 1990, 2004; Ehlers et al., 2011). The climatic improvements (from ~128 ka BP) during the Eemian interglacial led to a climatic optimum and a marine transgression almost till the present-day coastline (Streif, 1990, 2004). Starting ~117 ka BP, climatic deteriorations resulted in the Weichsel glaciation with several short interstadial periods and a sea-level lowstand of ~-130 m during the LGM. The maximum ice extent did not reach further than the river Elbe. The start of the Holocene is marked by the improvement of climatic conditions (~11.6 ka BP), which caused the melting of the Weichselian ice sheets and a transgression lasting until today (Streif, 2004).

Recent conditions are characterised by a humid tempered climate (Cfb after Köppen-Geiger classification) (Kottek et al., 2006; Beck et al., 2018).

1.5.3 Holocene sea-level changes

Streif (2004) reports three main transgression phases for the southern North Sea in Holocene times whereas other authors focus on more local reconstructions (De Groot et al., 1996; Kiden et al., 2002; van de Plassche et al., 2005; Bungenstock and Schäfer, 2009; Baeteman et al., 2011; Meijles et al., 2018). Fig. 1.4 shows the Holocene transgression since the LGM from a compilation of a global eustatic sea-level curve (Lambeck et al., 2014) and several local curves from the southern North Sea (Denys and Baeteman, 1995; Shennan et al., 2000; Meijles et al., 2018). The general phases of the transgression for the North Sea described by Streif (2004) slightly differ from the phases reported for the global eustatic transgression (Lambeck et al., 2014), showing a clear delay. However, since Streif's (2004) curve before 10.25 ka BP is only a rough estimate, a general trend similar to the global curve can be expected.

The first transgression phase started after the LGM, initiated by warmer climatic conditions around 18 ka BP. During the first phase (18–10.25 ka BP), Streif (2004) estimated a rate of ~0.6 m per century to about 72 m below the present-day sea-level. This phase was characterised by phases of deceleration during the still colder phases of the terminal Weichselian which is visible from a phase of almost constant sea level before 15 ka BP in the global eustatic sea-level curve. Within this phase, the main global phase of deglaciation is documented around 16.5–8.2 ka BP and a period of faster rise, due to a meltwater pulse, occurred around ~14.5–14 ka BP (Lambeck et al., 2014), which probably also influenced the

North Sea. The Younger Dryas, a phase with a slower rise between ~12.5 and ~11.5 ka BP, is estimated in the curve by Streif (2004) and visible as a step prior to the following phase.

The second phase (10.25–7.1 ka BP) was characterised by rates of ~1.5 m per century increasing to ~2.1 m per century towards the end of this phase. Tidal-flat sedimentation was widespread in the southern North Sea and fully marine conditions were established around 7 ka BP. The associated rise in groundwater levels led to the formation of swamps close to the transgressive coastline, enabling the growth of the so called basal peat, which is widely spread along the German North Sea coast overlying the Holocene base (Streif, 2004). The rise for the southern North Sea is described steeper than it is on a global scale (Lambeck et al., 2014).

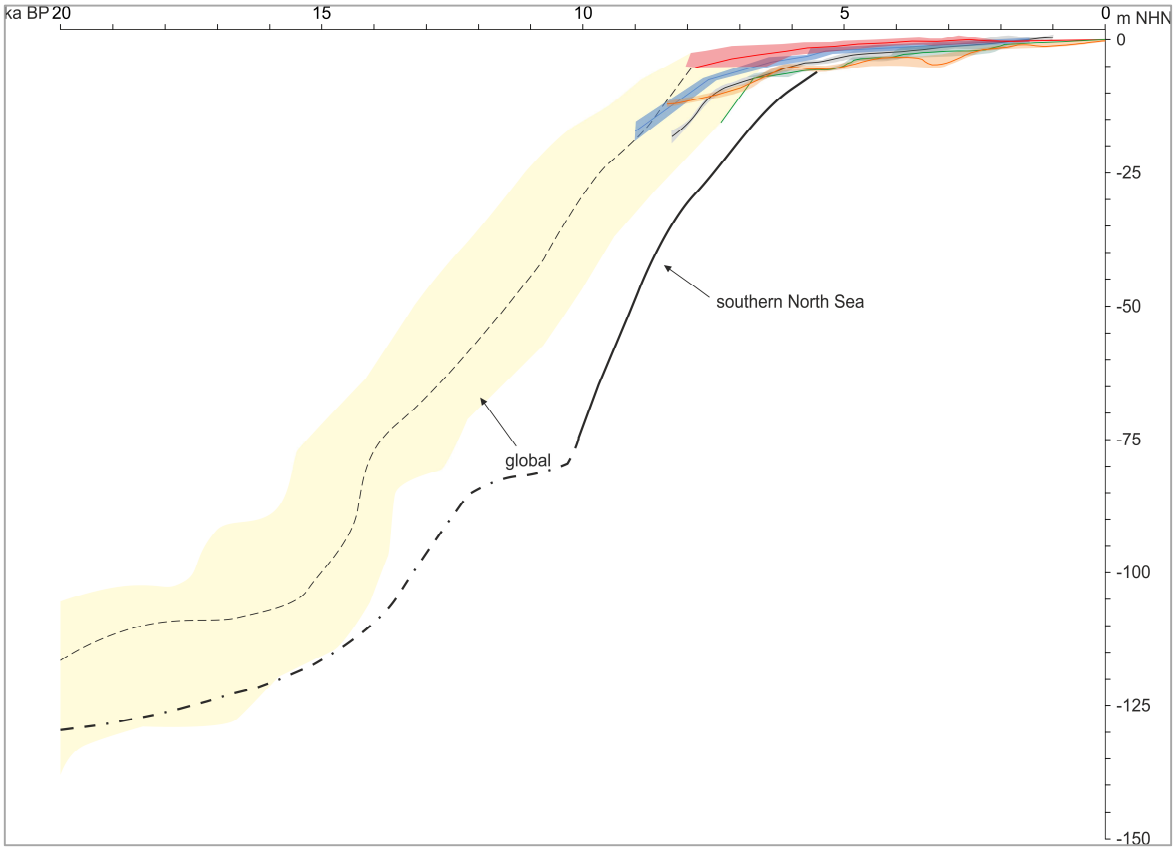

Fig. 1.4 Time/depth diagram of sea-level rise from the lowstand during the LGM to the present. Compilation of different (relative) sea-level curves. Yellow: global eustatic sea-level curve (Lambeck et al., 2014), black: RSL curve for the southern North Sea (Streif, 2004), blue: RSL curve Belgium (Denys and Baeteman, 1995), red: RSL curve British Isles (Shennan et al., 2000), grey: RSL curve Dutch Wadden Sea (Meijles et al., 2018), green: RSL curve Langeoog, Germany (Bungenstock and Schäfer, 2009), orange: RSL curve Denmark (Pedersen et al., 2009).

The third phase (~7.5 ka BP until today) shows a RSL rise of ~0.3 m per century. During this third phase, the present-day landscape of the German North Sea coast was shaped. Phases of stagnation or decelerated RSL rise led to the formation of peats, which are intercalated in the tidal-flat sediments within the stratigraphy of the North Sea coast. These have

been subject to many discussions about Holocene sea-level variations and how to interpret them with regard to coastal pro- and retrogradation (Streif, 2004; Behre, 2007; Bungenstock and Weerts, 2010, 2012; Baeteman et al., 2011). These ongoing discussions led to a re-consideration of the use of peats as sea-level index points and highlighted the need for more precise data (Chapter 1.2). Different local RSL curves of the third phase provide different trends, verifying the importance of local reconstructions for each tidal basin.

1.5.4 Recent dynamics on the German North Sea coast

The present-day coastal landscape in NW Germany was and is influenced by a variety of dynamic processes that started when the post-glacial transgression decelerated around 7 ka BP (Freund and Streif, 2000; Flemming, 2002; Streif, 2004; Bungenstock and Schäfer, 2009). On the natural side, these influences include the slowly ongoing sea-level rise, tidal dynamics, prevailing currents, storms and GIA, whereas another important factor is the anthropogenic influence (see section 1.5.5).

The German North Sea coast is characterised by semi-diurnal tides with locally different tidal ranges due to local topography, the geographical situation and the position relative to the amphidromic points. While two amphidromic points exist in the North Sea area, significant impact on the German Bight comes from the one east of the British Isles. The highest tides in the German Bight occur in the Jade Weser region (macro-tidal with tidal range of up to 4 m), whereas the rest of the coastal area experiences meso-tidal conditions (Streif, 2004; Bungenstock and Weerts, 2012). In the East Frisian area, the tides and the prevalent eastward longshore current induced the formation of two characteristic landscape units during the Holocene; barrier islands and tidal flats.

The barrier islands of East Frisia belong to the chain of barrier islands reaching from the Netherlands to the Jade Bay. Their formation started around 6–7 ka BP from an interaction of waves, the longshore current and sediment supply, when spits or sand bars formed at the seaward edges of Pleistocene *geest* ridges enabling the deposition of aeolian sediments. These dune islands were stabilised by primary vegetation and grew into their present-day size through further aeolian accumulation (Flemming, 2002). Between the islands, tidal currents have eroded and preserved deep channels, so-called *gats* ('Seegatten'), that enable the water masses to enter and exit the back-barrier areas of the islands and also prevent barrier islands from merging. Due to the ongoing sea-level rise and prevalent current directions, since their formation, the islands as well as the channels have shifted several kilometres in a south-easterly direction and reached their present-day position around 2 ka BP (Streif, 1990; Freund and Streif, 2000; Flemming, 2002). In the Jade Weser region, the macro-tidal conditions prevent the formation of barrier islands.

The tidal flats formed simultaneously with the barrier islands due to the tides transporting suspended sediments to the area closest to the coastline. During the short time of stagnation of the tidal current during high tide, sediment is deposited forming the tidal flats, which grow constantly higher, keeping up with the rising sea level (Streif, 1990, 2004). The German Wadden Sea (UNESCO world heritage since 2009, Strempel, 2016) belongs to one of the greatest connected Wadden areas worldwide, with a length of ~450 km from the Netherlands to Denmark. It shows three main types of deposits – sandflats, mixed flats and mudflats – which are classified based on their grain-size distribution (Fig. 1.5) and dependent on hydro-dynamics and water depth (Streif, 1990). Since different species of foraminifers and ostracods prefer different substrates, their distribution within these tidal-flat types should also differ, providing a possible driving factor for vertical zonations of microfaunal associations. The fourth type (fat/sticky mudflats) has almost completely disappeared.

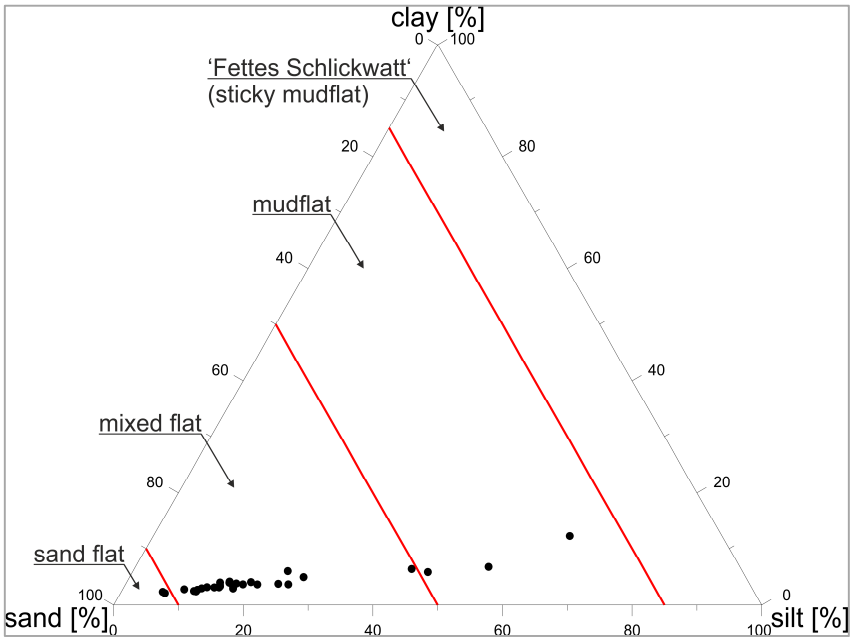

Fig. 1.5 Ternary diagram showing the classification of exemplary tidal-flat samples (unpublished) from a surface transect near Harlesiel, NW Germany, after Sindowski (1973). The transect was investigated for complementation of the TF but turned out to be subject to too high anthropogenic influences. Nevertheless, each sample can be clearly assigned to one of the tidal-flat types from its grain-size distribution (own design, 2019, terms after Reineck & Siefert, 1980).

At some point, the constantly vertically growing tidal flats reach above the mean high tide level, where halophytes, salt-tolerant plants, start to settle, catching more and more sediment whilst reducing the hydro-energetic levels. This way, the salt marshes are formed from former tidal-flat areas on the mainland coast as well as on the back-barrier coast of the East Frisian islands. In general, the hydro-energetic levels lead to a fining trend in grain sizes from tidal flats over salt marshes to the mainland (Nyandwi and Flemming, 1995). Lying in the supratidal area, salt marshes are only inundated during spring tides and high-energy

events, like storm surges, and represent the natural part of the marshlands as the transitional landscape unit between marine and terrestrial environments (Streif, 1990; Bungenstock and Weerts, 2012).

The only short-term and high-energy events with an essential influence on the coastal landscape of NW Germany are storm surges, which are generally caused by atmospherical parameters, but can be intensified by astronomical events such as spring-tide situations (Streif, 1990). Large parts of the course of the present-day coastline were created by the severe storm surges of Medieval times. These widened the estuaries and inundated huge areas which had to then be reclaimed by men, for example the Jade Bay (Flemming, 2002; Streif, 2004). The most crucial influence on storm surge levels is given by anthropogenic factors.

1.5.5 Anthropogenic influences and human-environment interactions

Since the beginning of human settlement along the German North Sea coast, there have been severe interferences in the dynamic processes and associated land-sea interactions. For a long time, humans had to adapt to local conditions of rising sea levels shifting their settlement areas (Gerdes et al., 2003). Around the turn of era, they started protecting their settlements from rising sea and storm-surge levels by the construction of dwelling mounds which went on, in two phases, until AD 1100. Around that time, the dyke construction began and the first continuous dyke system existed by ~AD 1300, representing the most significant anthropogenic interference with natural coastal dynamics (Gerdes et al., 2003; Bungenstock and Schäfer, 2009). The dyked areas, the so called *Polders*, had to be drained for agricultural use, which resulted in subsidence of the surface and in even more disastrous consequences in the event of dyke breaches during storm surges (Gerdes et al., 2003). Furthermore, the dyke systems led to the narrowing of flooding areas and an enhanced damming effect, which lead to a significant rise in storm-surge levels. Due to a slowly increasing understanding of these effects and changes in the need of agricultural areas, the land-reclamation measures are currently slowly being turned into measures of enlargement of the flooding areas, for example by renaturation of dyked areas or opening of dykes in order to create dedicated flooding basins (Reise, 2015).

1.5.6 The East Frisian islands of Spiekeroog and Norderney

The present-day mean tidal range varies along the East Frisian coast within meso-tidal conditions from 2.4 m at Borkum in the west up to 2.9 m at Wangerooge in the east (Streif, 1990; BSH, 2018). According to the shore-normal energy gradient (Nyandwi and Flemming, 1995), an offshore-coarsening trend in grain sizes can be observed. Although this general

trend can be locally interrupted by tidal channels, old channel fillings or depressions, the barrier islands do not disturb it, wherefore there is no fining trend in grain size in the southern salt marshes of the islands. Both Spiekeroog and Norderney are underlain by salt domes from red sandstone and shell limestone times at their western ends (Streif, 1990).

Spiekeroog is situated between the two tidal inlets 'Otzumer Balje' and 'Harle' at about 7 km distance from the mainland. It extends across an area of ~21 km² (Streif, 1990) and is characterised by a mean tidal range of 2.7 m (BSH, 2018). The back-barrier tidal flat shows salinities around 30 psu (practical salinity units) close to the main tidal channel and a little lower towards the mainland (Kaiser and Niermeyer, 1999). The tidal flat transitions towards the island into a salt marsh, which is characterised by a more or less typical vegetation pattern. The high to mid salt marsh exhibits sea lavender (*Limonium vulgare*), the adjacent 'Andel' Zone of the lower salt marsh is characterised by andel grass (*Puccinellia maritima*) and salt bush (*Atriplex halimus*) and the Glasswort Zone (pioneer zone) contains typical cord grass (*Spartina anglica*) and glasswort (*Salicornia europea*) (Streif, 1990; Gerlach, 1999).

Norderney is situated between the two tidal inlets 'Norderneyer Seegat' and 'Wichter Ee' at about 4 km distance from the mainland. Extending across an area of ~25 km² it has a mean tidal range of 2.5 m (BSH, 2018). The salinity in the tidal basin lies around 33 psu (COSYNA data web portal (CODM), https://codm.hzg.de/codm/). Its back-barrier tidal flat also transitions into a salt marsh on the southern coast of the island. The detailed vegetation zones have not been investigated in this study but are expected to be similar to the typical zonation described above.

Chapter 2

2 Fossil bog soils ('dwog horizons') and their relation to Holocene coastal changes in the Jade Weser region, southern North Sea, Germany

Juliane Scheder[1,2], Max Engel[2], Friederike Bungenstock[1], Anna Pint[2], Annette Siegmüller[1], Stephan Schwank[1], Helmut Brückner[2]

[1] Lower Saxony Institute for Historical Coastal Research, Viktoriastraße 26/28, 26382 Wilhelmshaven, Germany

[2] Institute of Geography, University of Cologne, Albertus-Magnus-Platz, 50923 Köln (Cologne), Germany

Abstract

After the deceleration of the postglacial marine transgression, the German North Sea coast was subject to deposition of a complex pattern of subtidal to terrestrial facies. This study aims at reconstructing these facies changes in the 'Land Wursten' region (Lower Saxony) by focussing on socalled dwog horizons (incipient soil horizons of the preengineered salt marshes). We explore their implications for relative sea-level reconstructions and their indication for early settlement activities. Archive drilling data (1960, provided by the 'Landesamt für Bergbau, Energie und Geologie') were analysed to create five high-resolution stratigraphic cross sections. Three new drilling records were subjected to sedimentological and microfaunal investigations and interpreted to verify and calibrate the archive data. Two dwog horizons were found and 14C-AMS dated. We found basal salt marsh deposits inundated by a high-energy event and covered by tidal flat sediments. The thick tidal flat unit is again overlain by salt marsh deposits indicating the transition from a shallow marine to a terrestrial environment where dwogs were developed and covered by episodic marine incursions. The ages of the dwogs (1128–969 cal BC; cal AD 1426–1467) do not correlate with known layers of adjacent settlement sites and are critically discussed. However, we show that they correlate with phases of stagnant regional relative sea level (RSL) and can be used as RSL indicators. The combined archive and modern data provide valuable information for the RSL reconstruction and palaeoenvironmental changes. However, further research is recommended to accomplish more detailed information about coastal response during the Holocene sea-level changes and implications for settlement dynamics.

Keywords

North Sea, Holocene, Landscape changes, Palaeoenvironment, Relative sea-level changes, Settlement history

Published in *Journal of Coastal Conservation* 22 (2018), 51-69.

https://doi.org/10.1007/s11852-017-0502-z

J Coast Conserv (2018) 22:51–69
DOI 10.1007/s11852-017-0502-z

Fossil bog soils ('*dwog* horizons') and their relation to Holocene coastal changes in the Jade Weser region, southern North Sea, Germany

Juliane Scheder[1,2] · **Max Engel**[2] · **Friederike Bungenstock**[1] · **Anna Pint**[2] · **Annette Siegmüller**[1] · **Stephan Schwank**[1] · **Helmut Brückner**[2]

Received: 30 August 2016 / Revised: 9 December 2016 / Accepted: 2 March 2017 / Published online: 7 April 2017
© Springer Science+Business Media Dordrecht 2017

Abstract After the deceleration of the postglacial marine transgression, the German North Sea coast was subject to deposition of a complex pattern of subtidal to terrestrial facies. This study aims at reconstructing these facies changes in the 'Land Wursten' region (Lower Saxony) by focussing on so-called *dwog* horizons (incipient soil horizons of the pre-engineered salt marshes). We explore their implications for relative sea-level reconstructions and their indication for early settlement activities. Archive drilling data (1960, provided by the 'Landesamt für Bergbau, Energie und Geologie') were analysed to create five high-resolution stratigraphic cross sections. Three new drilling records were subjected to sedimentological and microfaunal investigations and interpreted to verify and calibrate the archive data. Two *dwog* horizons were found and ^{14}C-AMS dated. We found basal salt marsh deposits inundated by a high-energy event and covered by tidal flat sediments. The thick tidal flat unit is again overlain by salt marsh deposits indicating the transition from a shallow marine to a terrestrial environment where *dwogs* were developed and covered by episodic marine incursions. The ages of the *dwogs* (1128–969 cal BC; cal AD 1426–1467) do not correlate with known layers of adjacent settlement sites and are critically discussed. However, we show that they correlate with phases of stagnant regional relative sea level (RSL) and can be used as RSL indicators. The combined archive and modern data provide valuable information for the RSL reconstruction and palaeoenvironmental changes. However, further research is recommended to accomplish more detailed information about coastal response during the Holocene sea-level changes and implications for settlement dynamics.

Keywords North Sea · Holocene · Landscape changes · Palaeoenvironment · Relative sea-level changes · Settlement history

Electronic supplementary material The online version of this article (doi:10.1007/s11852-017-0502-z) contains supplementary material, which is available to authorized users.

✉ Juliane Scheder
scheder@nihk.de

[1] Lower Saxony Institute for Historical Coastal Research, Viktoriastraße 26/28, 26382 Wilhelmshaven, Germany

[2] Institute of Geography, University of Cologne, Albertus-Magnus-Platz, 50923 Köln (Cologne), Germany

Introduction

During the Holocene, the glacio-eustatic transgression caused a southward shift of the North Sea coast of about 600 km in total (Streif 2004). In Early Holocene times, brackish conditions established in the southern North Sea. The rising groundwater level caused the formation of swamps on top of the Pleistocene sands ('Geest') close to the former coastline. They appear as basal peats in the stratigraphy covered by intertidal and subtidal sediments (Streif 2004; Bungenstock and Schäfer 2009). Fully marine conditions were established since 7000 BP (years before present) when the eustatic sea-level rise decelerated (Freund and Streif 2000; Bungenstock and Schäfer 2009). Subsequently, the accumulation of marine and terrestrial sediments was controlled by sediment supply, tidal dynamics, local relative sea-level (RSL) evolution and short-term events in addition to the slowly continuing eustatic sea-level rise (Falk 2003). Humans started to interfere with these processes by first settling on levee dykes since the 1st mill. BC (millennium before Christ), and later right inside the marshes (Behre 2004). Settlements were protected by the construction of dwelling mounds since AD 50 (anno domini), ring

dykes since AD 1100, and first continuous dyke systems parallel to the coast since AD 1300, which fundamentally changed flooding regimes and sediment fluxes (Gerdes et al. 2003; Bungenstock and Schäfer 2009).

Both in the pre-dyke era and the High Middle Ages to the Early Modern Period, when dykes were often prone to failure, land surfaces were episodically flooded during severe storm surges. Covered by fine sandy to muddy deposits, bog soils became preserved. They are referred to as *dwog* horizons (Streif 1990). These *dwog* horizons provide evidence for former RSL and sometimes show a lateral transition to intercalated peat beds indicating coastal progradation (Behre 2007; Bungenstock and Weerts 2012). Therefore, *dwog* horizons are important features to reconstruct Holocene coastal changes as they are a clear sign of relatively stable, terrestrial environmental conditions in the perimarine marshes.

The widespread intercalated peat beds are often used as RSL index points (e.g. Streif 2004; Behre 2007; Bungenstock and Schäfer 2009), even though significant uncertainties have to be considered. Regional palaeogeographic conditions play an important role when interpreting intercalated peats as sea-level markers: Baeteman (1999), for example, showed that intercalated peat beds are not necessarily associated with sea-level changes, but related to sedimentological control of tidal channel and creek networks in the supratidal zone creating upsilting environments which favour salt marshes to encroach and later peat vegetation. Kiden et al. (2008) describe the so-called floodbasin effect that is seen behind closing coasts. There, peat growth starts to develop due to the decreasing influence of the sea in a cut-off basin. Furthermore, the intercalated peat beds are prone to post-depositional compaction with locally different compaction rates depending on the underlying fine-grained Holocene sediments (e.g. Paul and Barras 1998; Allen 1999; Long et al. 2006; Bungenstock and Schäfer 2009; Brain et al. 2012).

This study aims at reconstructing Holocene coastal changes in connection with the RSL history in the 'Land Wursten' region (Lower Saxony) and their implications for regional settlement practices mainly based on sedimentological and microfaunal analyses. The main objectives are:

(i) Determining facies types in the study area using new sediment cores and identifying *dwog* horizons;
(ii) Combining and correlating facies of the new sediment cores and archived core logs in order to establish detailed stratigraphic cross sections and reconstructing the spatial distribution and lateral development of the *dwog* horizons;
(iii) Reconstructing coastal changes in the 'Land Wursten' region based on vertical and lateral facies changes and relating them to RSL;
(iv) Deriving repercussions for the local settlement history by focussing on landscape reconstruction in the area of the adjacent dwelling mound 'Barward' (Asmus 1949).

Study area

Physical setting

The study area is located in the 'Land Wursten' region northeast of the Weser estuary (Fig. 1). It represents a marsh environment (*'Wurster Marsch'*) or former marsh island, formed during the postglacial sea-level rise. 'Land Wursten' is perched between the Pleistocene 'Geest' ridge *'Hohe Lieth'* (c. 1 km to the east) and the wide-open Weser estuary (c. 2.2 km to the west) (Haarnagel 1979). It combines two geological subunits: A palaeo-estuary of the river Weser, providing sandy (lower subsurface) and clayey (upper subsurface) sediments, characterises the eastern part, whereas the western part mainly consists of silty to fine sandy deposits. Both are separated by a 500–1000 m-wide transition zone, where the silty to fine sandy sediments transported from the west were deposited partially on top of the clayey sediments of the palaeo-estuary. Most of the study area is located in the palaeo-estuary area, while the prehistoric dwelling mound 'Barward' is located in the transitional zone. The western border of the study area is marked by a levee dyke, followed by younger westward marshes. The Pleistocene sands and the overlying basal peat lie below 10 m b.s. (below surface) (Schneeberg 1962).

The area experiences a humid temperate climate (Cfb) with mean precipitation of 720–840 mm/a, mean annual temperatures of 8.5–9.0 °C and predominant westerly winds (Schneeberg 1962). Severe storm surges occur in winter when cyclones spinning off from the Iceland Depression reach the German Bight and, due to the narrow shape of the Weser estuary and a tidal range of >3.5 m, may reach disastrous levels (Streif 1990).

Sea-level history

After the Last Glacial Maximum (LGM), in particular since 16.5 ka ago, eustatic sea level rose rapidly from c. 120–135 m below its present position with an average rate of 12 m/ka until the Early Holocene (Lambeck et al. 2014). Rising levels inundated the Dogger Bank and between 10,000 and 8400 BP brackish conditions established in the southern North Sea. After the fast transgression before 7000–6000 BP (e.g. Freund and Streif 2000; Bungenstock and Schäfer 2009; Bungenstock and Weerts 2010) the decelerated sea-level rise of the Late Holocene was characterised by more local influences (e.g. tidal range, coastal geography, regional glacio-isostatic adjustment) (Vink et al. 2007; Lambeck et al. 2014).

The Mid- to Late Holocene transgression was interrupted by phases of deceleration, stagnation and even lowering of the RSL indicated by transgressive and regressive sediment

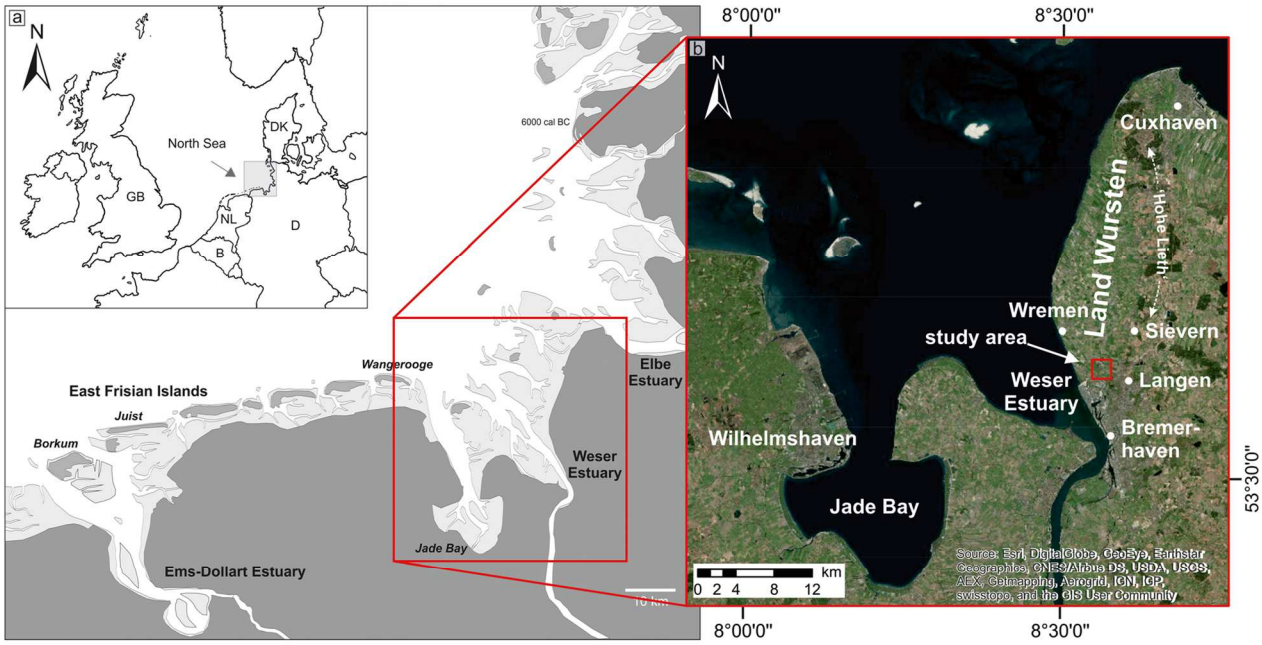

Fig. 1 The study area (Weser marshland). a: General overview of the southern North Sea; b: Jade Weser region with the 'Land Wursten' region in the east. The red box marks the location of the study area (see Figs. 2 and 3) (sources: Esri, Digital Globe, GeoEye, Earthstar Geographics, CNES/Airbus DS, USDA, USGS, AEX, Getmapping, Aerogrid, IGN, IGP, swisstopo, and the GIS User Community)

overlaps within the stratigraphy of the North Sea coast (Streif 2004). However, these could also be interpreted as lateral shifts (progradation and retrogradation) of the coastline controlled by sediment supply (Bungenstock and Schäfer 2009).

In general, the facies changes visible in the wedge-shaped Holocene coastal sediment body do not simply depend on eustatic sea-level change. They are also influenced by the ratio of accommodation space and sediment supply. With a sufficiently large sediment supply a coastline is able to prograde, even during RSL rise (e.g. Baeteman 1999; Beets and van der Spek 2000). Moreover, the German North Sea coast is characterised by (i) glacio-isostatic subsidence due to the collapsing glacial forebulge of the Fennoscandic ice sheet, and (ii) tectonic subsidence, both of which influence regional RSL (Kiden et al. 2002; Busschers et al. 2007; Vink et al. 2007). In addition, local halokinetic effects due to salt diapirism (salts from the Zechstein) (Streif 1990) should be considered.

Also, periods of higher storm activity resulting in deposition of marine clastic sediments above peats or *dwog* horizons may imply an increasing rate of RSL rise.

Dwog horizons

While a stagnating or slowly rising RSL supports the expansion of fens above former brackish and tidal areas, a RSL drop causes oxidative decomposition of peats and pedogenesis (soils), or a development of fen-vegetation into upland moors (bog peats) (Freund and Streif 2000; Streif 2004). Fossilized bog soils buried after marine inundation – *dwog* horizons – formed in several stages in the southern North Sea region during the Bronze Age (Brand et al. 1965; Schoute et al. 1981). They occur within 2–3 m b.s. as intercalated brownish black humic horizons (humic *dwog*) or as horizons highly affected by iron (iron *dwog*). From a pedological point of view, the humic *dwog* represents a fossil humic topsoil whereas the iron *dwog* is a fossil groundwater horizon (Streif 1971, 1990; Ad-Hoc-Arbeitsgruppe Boden 2005).

In the wet depressions of the marsh, soil formation is only possible under subaerial conditions and with a dropping groundwater level enabling the expansion of vegetation (Streif 1971). Since groundwater and RSL are directly related, *dwog* horizons are useful indicators of RSL and mean high-tide level, respectively, indicating a decreasing marine influence (Streif 1990). Even though assumptions about the degree of groundwater level fall are difficult, the formation of a *dwog* horizon seems possible after a drop of a few dm. Furthermore, the characteristic feature of a *dwog* horizon is its sudden burial by sediment. Therefore, the presence of a *dwog* horizon overlain by a sandy to muddy layer may provide evidence for former storm surges, depositing clastic material on top above a sharp lower boundary, often followed by a new pedogenetic phase (Streif 1971).

Hence, *dwog* horizons can provide significant data for the reconstruction of Holocene coastal changes and RSL histories, since they indicate not only a decrease in marine

influence but also the fact that terrestrial conditions lasted long enough for soil formation to start. It is surprising how rarely their potential has been used for these purposes in the past.

Archaeology

At the time of the first settlement of the 'Land Wursten' region in the second half of the first century BC, it was characterised by the already mentioned levee dyke and the resulting marsh island both interspersed by tidal channels (Schmid 1978). A chain of prehistoric flat settlements was established on the levee (Aufderhaar et al. 2013; Aufderhaar 2016), which, after the first century AD, were gradually raised using stacking manure and 'Klei' sods (clayey to silty sediments) from the surrounding area (Haarnagel 1979; Hayen et al. 1981). The levee was adjacent to a tidal flat in the west. The best investigated of these dwelling mounds is Feddersen Wierde (Haarnagel 1979), about 5 km north of 'Barward'.

The prehistoric dwelling mound 'Barward' has a diameter of 300 m in total, but is separated into a northern and a southern part through a former drainage channel. The much lower southern part was excavated from 1939 to 1940 in the course of the construction of military installations (Genrich 1941). A settlement from the Pre-Roman Iron Age until at least the fourth century AD along with a stepwise elevation was proved (Aufderhaar et al. 2013; Aufderhaar 2016), characterised by the settlement layers already described by Asmus (1949) (Table 1).

The combined dwelling mound settlements that first appeared during the second century AD played an important role at the North Sea coast. Even after the beginning of dyke construction they remained important, since initially dykes were not completely storm surge safe and the risk of inundations remained (Asmus 1949).

Methods

Analysis of archive data

221 handwritten drilling records from 1960 from 1 to 10 m depth, which were the basis for the Geological-Pedological Map (1:5000) 231727 Imsum-Ost (cf. Fig. 2), were digitalised using both Excel and the software GeODin and searched for documentation of potential *dwog* horizons. The records were provided by the 'Landesamt für Bergbau, Energie und Geologie' (LBEG) in Hannover and are spread across the study area. GeODin was used to create five stratigraphic cross sections in the study area, each over a distance of about 2 km. The geological coastal map of LBEG (2016) was accessed through the 'NIBIS® Kartenserver' (http://nibis.lbeg.de/cardomap3) and used to complete the stratigraphic cross sections with the Holocene base. The archive drilling profiles were also used to find suitable locations for new sediment cores.

Field work

Three new sediment cores (LAN 1–3) were taken in November 2013 in order to validate the transcription and interpretation of the archive data (see Fig. 3). An Atlas Copco percussion coring device (Cobra mk 1) and open steel probes of 5 and 6 cm diameter were used. The cores were photographed and documented in the field using schemes of Ad-Hoc-Arbeitsgruppe Boden (2005). The cores were sampled selectively according to the facies changes determined in the field.

Laboratory analyses

Sedimentological and microfaunal analyses were conducted in the Laboratory for Physical Geography at the University of Cologne in order to characterise different facies types.

Table 1 The chronology and different settlement layers of the dwelling mound 'Barward' (Asmus 1949)

Time of settlement	Elevation (m) relative to NN (German Ordinance Datum close to mean sea level)	Type of settlement	Comments
First century BC	~0.6	Flat settlement	Destruction during storm surge
First century BC	~0.6	Flat settlement	Built directly on the residual of the previous layer
First century AD	0.9–1.0	Individual dwelling mounds ('Einzelhofwurten')	First elevation (~30 cm); individual dwelling mounds for each building; banks of Klei around individual dwelling mounds indicate increased flooding risk
Second century AD	~1.2	Combined dwelling mound ('Dorfwurt')	Second elevation (~30 cm); different animal bones (horses, cattle, sheep, pigs, dogs)
Second to third century AD	~1.5–1.6	Combined dwelling mound	Third elevation (~30 cm); much lower density of settlement traces than before
Abandonment of the dwelling mound and end of the prehistoric settlement (probably used as farmland)			
c. 1000–1100 AD	~2.35	Combined dwelling mound	Reoccupation during Middle Ages; fourth and strongest elevation (homogeneous sandy Klei instead of manure and Klei sods); occasional pottery fragments but no other settlement traces

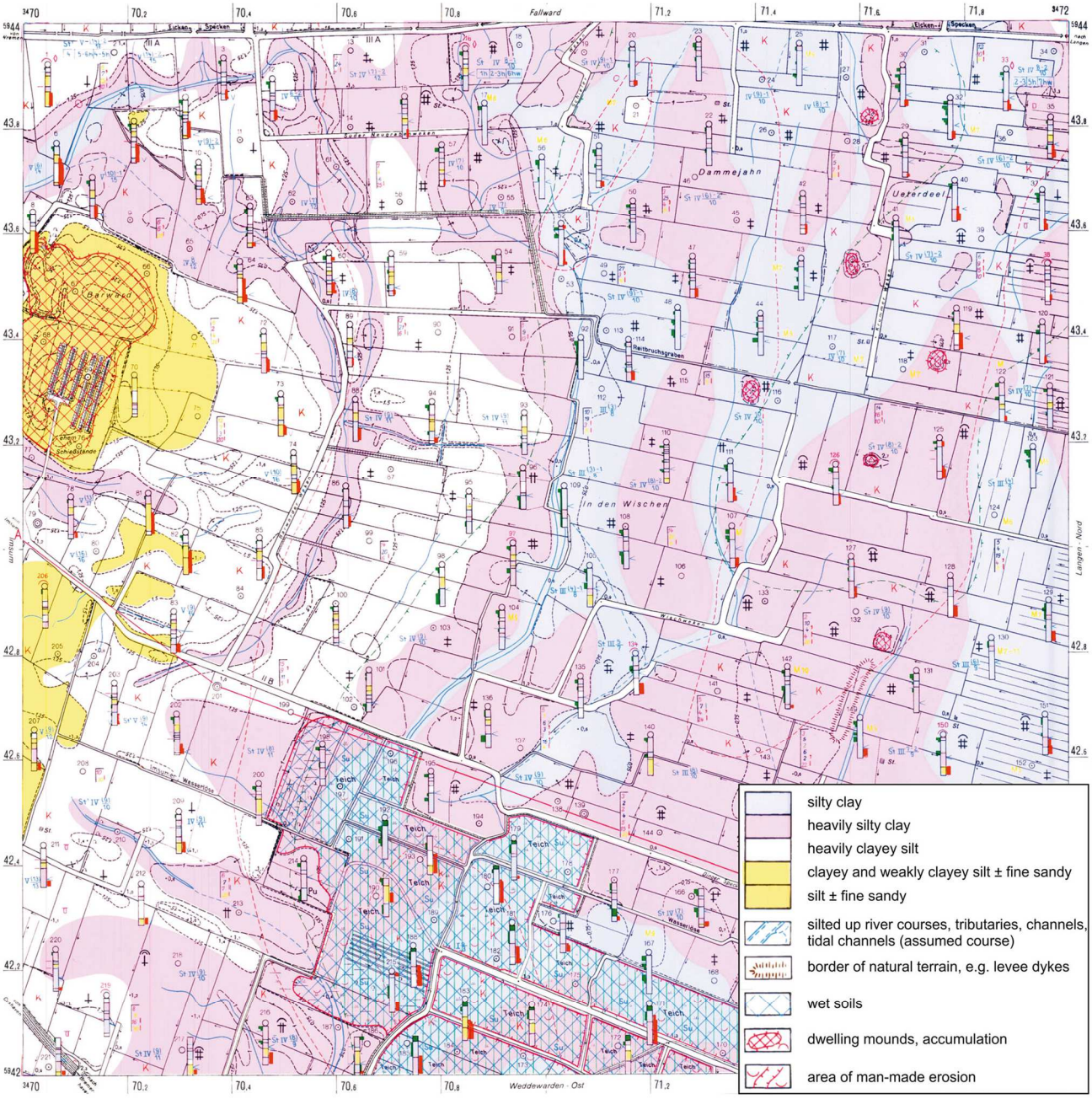

Fig. 2 The study area (see red box in Fig. 1b) with locations of all 221 archive drillings. The dwelling mound 'Barward' can be seen in the western part of the map marked by yellow colour. The complete colour and symbol key can be seen in the original map sheet (Geological-Pedological Map [1:5000] 231727 Imsum-Ost [1960])

Samples for sedimentological analyses were dried at 30 °C, carefully grinded in a mortar by hand and sieved in order to separate the matrix material (<2 mm), which was then measured using a laser particle size analyser (Beckman Coulter LS 13320) with a laser beam (wavelength 780 nm) applying the Frauenhofer optical mode (Eshel et al. 2004). The calculation of univariate statistical measures after Folk and Ward (1957) was accomplished using GRADISTAT software (Blott and Pye 2001). End-member modelling using R software was applied to disentangle distinct groups of different grain-size distributions and identify a restricted number of endmembers. We use the algorithm of Dietze et al. (2012), which is based on a principal component analysis (PCA), factor rotation, variable data scaling, and a non-negative least-square estimate; all steps of the analysis are presented in Dietze et al. (2012).

The amount of organic matter was quantified by the loss on ignition (LOI) using sample amounts of 5–8 g (DIN 19684–3; Barsch et al. 2000; Blume et al. 2011). Carbonate content

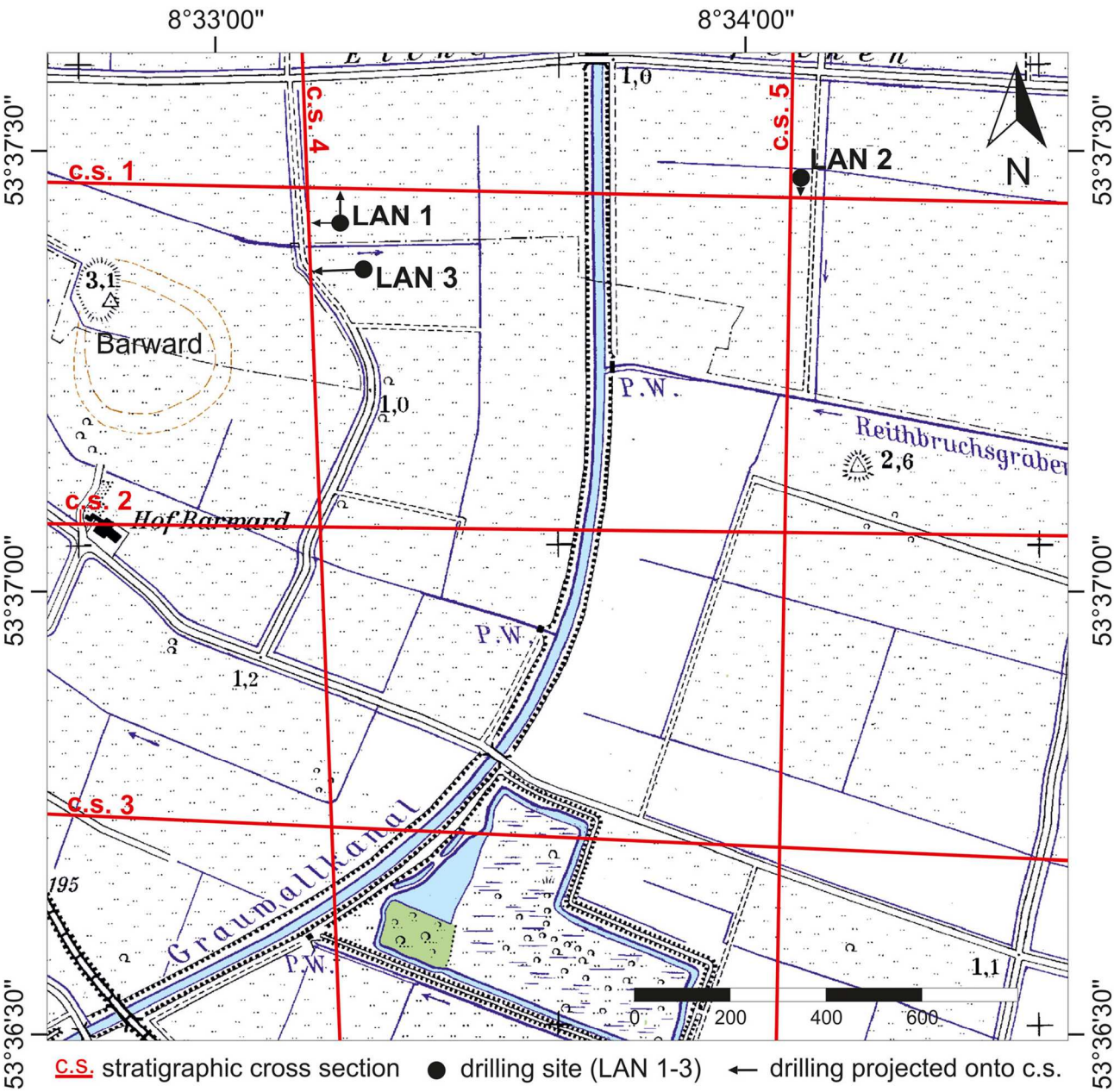

Fig. 3 Map of the study area (see red box in Fig. 1b) with locations of stratigraphic cross sections (red lines) and drilling sites LAN 1–3. The channel in the centre of the map ('Grauwallkanal') did not exist in 1960 (section of the topographic map 1:25,000 2317 Langen)

($CaCO_3$) was volumetrically measured after Scheibler (DIN ISO 10693). Pedogenetic iron oxides were quantified in order to identify *dwog* horizons. Therefore, the more active amorphous part was determined from an oxalate extract after Tamm (1932) and Schwertmann (1964), whereas the more crystalline fraction was measured from a dithionite extract after Mehra and Jackson (1958). The extracted iron oxides were measured by means of atom absorption spectrometry (AAS). The relation of both fractions provides information on pedogenetic intensity, the degree of weathering or aging of soil horizons.

Since species of Ostracoda and Foraminifera are often confined to particular habitats, they also serve as proxies for reconstructing sedimentary environments (De Deckker and Forester 1988; Handl et al. 1999; Frenzel and Boomer 2005; Murray 2006; Pint et al. 2015). The samples were pre-treated with $Na_4P_2O_7$ and slowly shaken overnight in an agitation device (cf. Handl et al. 1999). Afterwards they were washed over sieves with 63 μm and 100 μm meshes. The remaining sediment for both fractions was air-dried for about 24 h (Forester 1988) and the 100 μm fraction was analysed for its microfossil

content. Counting and determination was carried out using a light stereo microscope. If possible, at least 100 individuals were counted for each sample in order to receive appropriate statistical values. A total of 57 samples were analysed. Foraminifera were classified to at least genus level based on the online database 'World Register of Marine Species' (WoRMS) (WoRMS Editorial Board 2016), the foraminifera.eu database (Hesemann 2015) and Murray (2006).

Principal component analysis (PCA) was carried out using the software PAST v.3.06 (Hammer et al. 2001) and the parameters foraminiferal taxa, mean grain size, sand amount, organic matter and carbonate content. PCA allows a statistical grouping of all samples with similar environmental or sedimentological variables in order to support the facies interpretation. Due to their very similar dimensions, the parameters were not normalised or standardised prior to the PCA.

Two bulk samples of two different *dwog* horizons were dated by ^{14}C-AMS (Accelerator Mass Spectrometry) at the ^{14}CHRONO Centre of the Queens University of Belfast to infer ages of the *dwog* horizons. Calib Rev. 7.1 software (Reimer et al. 2013) was applied for calibration and the data was corrected for δ^{13}C values. Data are reported at the 2σ confidence level (i.e. 95% probability).

Data were charted using the software Grapher (v. 8.0.278) and the drawing application CorelDRAW X5 (v. 15.0.0.486).

Results

Sedimentology of the new drillings

LAN 3, the longest new core (11 m b.s.), provides the basis for the identification and characterisation of facies A–G. It is situated approximately 230 m northeast of the prehistoric dwelling mound 'Barward' (Fig. 3). The drilling site is a fallow agricultural field densely covered with grass. Puddles form due to a lacking drainage system. The surface level is 1.28 m a.s.l. (m above present mean sea level), hence, the end depth of the core is −9.72 m a.s.l. A detailed description of all cores is presented in Figs. 12–16 (online supplement [onl. Suppl.]), while sedimentological and foraminiferal data of LAN 3 are depicted in Fig. 4 (other cores in Figs. 17–18 [onl. Suppl.]); Fig. 5 shows detailed photographs of the identified facies. Table 4 (onl. Suppl.) lists the ecological characteristics of the foraminiferal species and in Fig. 6 examples of the most frequent species are presented.

Facies A is found in two sections of the sequence (−9.72 to −6.44 m a.s.l. [A1] and −0.72 to 0.23 m a.s.l. [A2]). It is characterised by muddy sand, grey in A1 and greyish yellow brown in A2, where it gradually changes to sandy mud. Both sections show varying amounts of silt and fine sand. A1 exhibits occasional mollusc fragments, very thin black organic layers and a muddy lamination, whereas A2 is characterised by fine sand laminae, traces of oxidation ('rust') and a layer of plant remains. Variance in grain-size distributions is mostly explained by endmember 2 in A1 and endmember 1 in A2. LOI and $CaCO_3$ values show an approximately parallel decreasing trend in A1 and decrease both in the lower part of A2 as well. Above −0.72 m a.s.l., they show different courses as LOI values decrease after a first increase, whereas $CaCO_3$ values decrease rapidly. The foraminiferal association (Fig. 6) is dominated by *Haynesina germanica, Ammonia tepida* and *Cribroelphidium williamsoni* (in ranking order). In A1, *C. williamsoni* is less frequent than the other two species, whereas in A2, it is for most parts more frequent than *A. tepida* but still less than *H. germanica*. One single specimen of *Triloculina oblonga* was documented in A1. A2 exhibits two specimens of *Trochammina inflata* and one of *Jadammina macrescens*. A2 is also present in the other two sediment cores (bottom to 0.10 m a.s.l. in LAN 1; −0.87 to −0.38 m a.s.l. in LAN 2, Figs. 17–18 [onl. Suppl]).

Facies B is found in two sections of LAN 3 (−6.44 to −6.38 m a.s.l. [B1] and −6.31 to −6.27 m a.s.l. [B2]) and in one additional section of LAN 2 (−0.38 to −0.27 m a.s.l. [B3]). It is characterised by black organic-rich mud without any macroscopic plant remains. All three sections show relatively high LOI values (B1 < B2 < B3). Endmember 4 characterises B1, while grain-size distribution in B2, which is even finer, is best explained by endmembers 1 and 2. Mollusc fragments and remains occur at the upper boundaries of B1 and B2, which shows the highest $CaCO_3$ value of the complete core. The foraminiferal association of B1 and B2 is dominated by *H. germanica,* accompanied by *A. tepida* and *C. williamsoni*. However, in B1 *A. tepida* is more frequent than *C. williamsoni*, which is reversed in B2. Furthermore, B1 includes one specimen of *T. oblonga* (<1%). In contrast to that, B3 exhibits exclusively three specimens of *Trochammina inflata*.

Facies C occurs from −6.38 to −6.31 m a.s.l. [C1], 0.65 to 0.75 m a.s.l. [C2] and 0.81 to 0.98 m a.s.l. [C3]). C1 is characterised by grey muddy sand with remains of B1 in the lower part, whereas C2 and C3 are characterised by brownish grey sandy mud with traces of oxidation. A specific stratigraphic position between two peat layers (C1) and two thin humic layers (C2, C3), respectively, is characteristic of Facies C. Foraminifers were only found in C1, where a slight dominance of *A. tepida* along with *C. williamsoni* and *H. germanica* was identified. However, C3 is also present in LAN 1 (0.86 to 0.96 m a.s.l.), where foraminifers occur equally dominated by *A. tepida* and *H. germanica* accompanied by *C. williamsoni*.

Facies D is present from −6.27 to −1.82 m a.s.l. in LAN 3 and is characterised by alternating grey muddy sand and sand, i.e. varying silt and fine sand amounts. In the lower part, scores of endmember 3 are highest, whereas in the upper part, variances in grain-size distribution are explained by both, endmember 2 and 3. LOI values are at a low level, whereas $CaCO_3$ varies between 2 and 3%. The foraminiferal

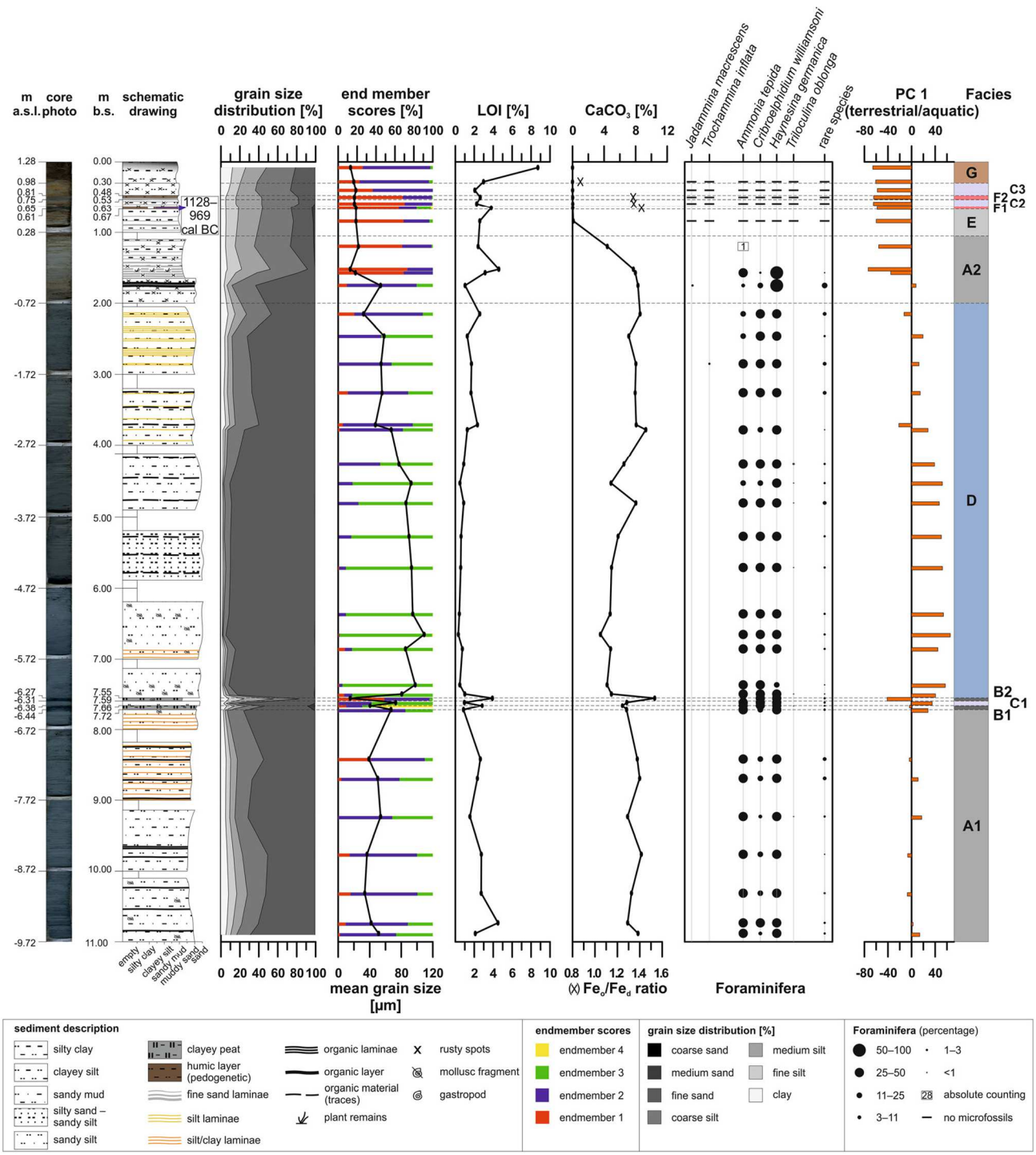

Fig. 4 Sedimentological and foraminiferal data of the complete drilling LAN 3. Depths are given in m b.s. as well as m a.s.l. Identified facies units are presented in the column on the right (see Fig. 8 for the colour key, 'Sedimentology of the new drillings' for description and Fig. 10 for interpretation)

association is again characterised by *H. germanica*, *A. tepida* and *C. williamsoni*. *A. tepida* dominates the lower and *H. germanica* the upper half of the section. Few individuals of *T. oblonga* also occur. Facies D is also present in LAN 2 from the bottom to −0.81 m a.s.l.

Facies E (0.23 to 0.61 m a.s.l. in LAN 3) is quite similar to the upper part of A2 in terms of grain-size distribution and LOI, except for the total absence of $CaCO_3$, traces of oxidation and microfossils. It also occurs in LAN 1 (0.10 to 0.80 m a.s.l.) and LAN 2 (−0.27 to 0.58 m a.s.l.).

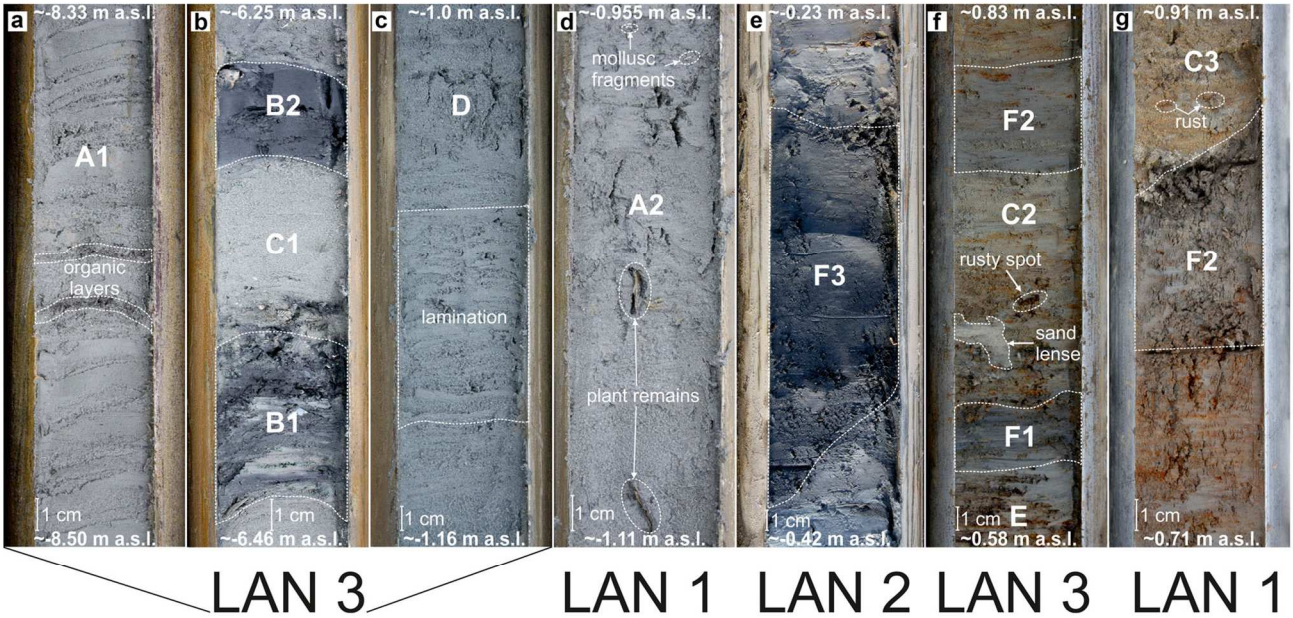

Fig. 5 Detailed photographs of the different facies (bottom [left] to the top [right]). For interpretations of facies units A–G see Fig. 10. a: Facies A1 with organic layers (LAN 3); b: Facies B1 and B2 with intercalated C1 (LAN 3); c: Facies D with lamination (LAN 3); d: Facies A2 with mollusc fragments and plant remains (LAN 1); e: Facies F3 (LAN 2); f: Facies E, F1 and F2 with intercalated C2, traces of oxidation and sand lense (LAN 3); g: Facies F2 overlain by C3 (LAN 1)

Facies F is found in two sections of LAN 3 (0.61 to 0.65 m a.s.l. [F1] and 0.75 to 0.81 m a.s.l. [F2]). It is characterised by brownish black to brownish grey sandy mud. Both sections show a quite high level of activity of pedogenetic iron oxides visible in Fe_o/Fe_d values, traces of oxidation and are void of $CaCO_3$ and microfossils. ^{14}C-dating results of F1 from LAN 3 lead to the Late Bronze Age (1128–969 cal BC). Since F2 also occurs in LAN 1 (0.80 to 0.86 m a.s.l.), it was also dated leading to the Late Middle Ages (cal AD 1426–1467) (Table 2).

Facies G (0.98 to 1.28 m a.s.l.) is characterised by dull yellowish brown to dark brown sandy mud with an upwards increasing clay amount. LOI values show a strong increase towards the surface and only weak traces of oxidation are present. Facies G is also present in LAN 1 (0.96 to 1.19 m a.s.l.) and LAN 2 (0.58 to 0.88 m a.s.l.).

Stratigraphic cross sections

The identified facies units A–G were correlated with 61 existing archive drillings in order to create five stratigraphic cross sections showing the subsurface of the study area (Figs. 7, 8 and 19–21 [onl. Suppl.])

As the cross sections show, the subsurface is mainly characterised by Facies A and D. A channel structure in the western part of the study area, running around the dwelling mound, is incised into the sediments of Facies D (c.s. [cross section] 1, 2 and 4; Figs. 3, 7, 8 and 19 [onl. Suppl.]). Further smaller channel structures are visible in the southwest and also in the southeast.

At least two different layers of Facies F could be identified in the study area, which in some areas show lateral facies transitions and change into two of three identified layers of Facies B (possible correlation with B3). However, there are a few profiles, which do not exhibit any layers of Facies F nor B in the northwest, visible in c.s. 1 (Figs. 3 and 7), and one in the central south within a former clay pit, visible in c.s. 3 (Fig. 20 [onl. Suppl.]). As described above, F1 (LAN 3, c.s. 4, Figs. 3 and 8) was ^{14}C-dated to the Late Bronze Age and dominates the area around the dwelling mound. F2 (LAN 1, c.s. 1, Fig. 7), predominant in the north-eastern area, was associated with Medieval times (Late Middle Ages).

The present-day surface mostly follows the existing channel structures as it shows depressions in these areas. None of the investigated drillings reaches the Holocene base, which exhibits a general southward lowering trend. In the western area, this trend is stronger than in the eastern area and the Holocene base clearly ascends eastwards.

Discussion and synthesis

PCA (principle component analysis)

The PCA, combining LOI, $CaCO_3$ and foraminiferal data, was carried out in order to corroborate and fine-tune the facies classification. The most relevant axes for LAN 3 are PC 1 and PC 2, describing variances of 79.62% and 14.74%. Since the variance

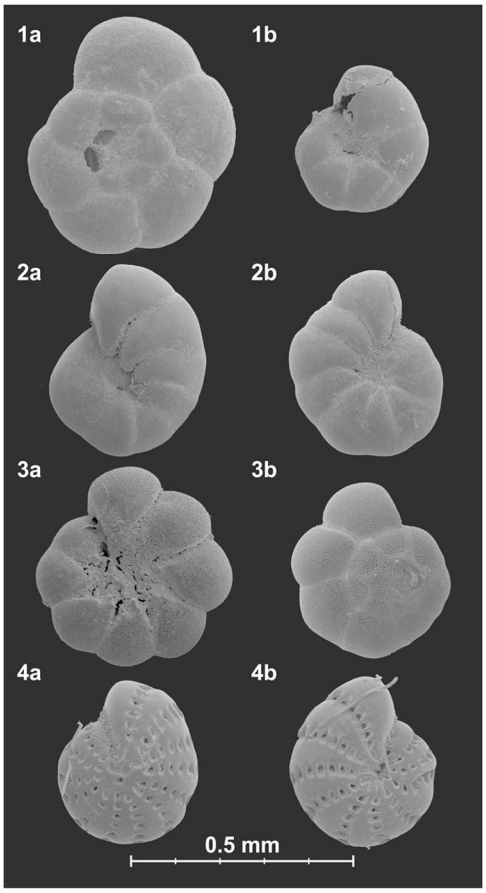

Fig. 6 Scanning electron microscope images of selected specimens of the most frequent foraminiferal species. For ecological information see Table 4 (onl. Suppl.). 1: *Trochammina inflata* (Montagu 1808); 2: *Haynesina germanica* (Ehrenberg 1840); 3: *Ammonia tepida* (Cushman 1926); 4: *Cribroelphidium williamsoni* (Haynes 1973)

value of PC 3 is only 2.81%, only the biplot of PC 1 and PC 2 is considered and presented in Fig. 9. The PCA biplots for LAN 1 and 2 are shown in Figs. 22 and 23 (onl. Suppl.). Three groups were identified. Group 1 is bound to PC 1, characterised by the absence of Foraminifera and includes samples of Facies A, C, E, F and G. The two samples (belonging to Facies A and B) of group 2, which is bound to PC 2 and PC 1, are characterised by a low mean grain size and sand amount combined with moderate LOI values and a higher $CaCO_3$ content. Group 3 can be divided into two subgroups (a and b). Both subgroups mainly differ in grain size and foraminiferal characteristics. 3 a (mainly relating to Facies A) shows mean grain sizes of mainly <63 μm (silt), and a sand amount of <73%, whereas 3 b (mainly relating to Facies D) has higher mean grain sizes of >72 μm (fine sand) containing a higher sand amount of >81%. Furthermore, subgroup 3 a is dominated by *Haynesina germanica*, whereas 3 b is slightly dominated by *Ammonia tepida* (not visible in Fig. 9, but from the foraminiferal data of these samples [Table 7; onl. Suppl.]).

Thus, PC 1 is characterised by the absence of Foraminifera on the negative and their occurrence on the positive side. Hence, PC 1 describes the habitat opposing terrestrial and aquatic conditions (cf. Fig. 4). On the other hand, PC 2 is characterised by *H. germanica* on the positive and the sand amount and mean grain size on the negative side. Since *H. germanica* is common in finer-grained sediments (Murray 2006), this suggests the interpretation of PC 2 as grain-size component. However, the space between *H. germanica* and *A. tepida* could also relate to salinity, which would suggest PC 2 as salinity component. The low variance of PC 2 prohibits a final interpretation.

Facies interpretation

All interpreted facies are depicted in a schematical drawing in Fig. 10.

Facies A – salt marsh environment (transitional facies above mean sea level)

This facies is characterised by an environment of medium energetic levels implied especially by the grain-size distribution and the high mud content. It represents salt marshes, characterised by laminae that form due to occasional inundations delivering new sediments eroded during high tide rise from the tidal flats and

Table 2 Information about ^{14}C dating and calibration provided by the 14CHRONO Centre of the Queens University of Belfast. The ages marked with an asterisk were used for this article

Lab. ID	Sample ID	Material	Conventional ^{14}C age	Cal BC/AD		Rel. area under probability distr.	
				1 sigma	2 sigma	1 sigma	2 sigma
UBA-26110	LAN 1/3	fossil top soil horizon (bulk sample)	443 ± 22	AD 1436–1451	AD 1426–1467*	1.000	1.000
UBA-26111	LAN 3/6	fossil top soil horizon (bulk sample)	2873 ± 31	1109–1097 BC	1188–1180 BC	0.103	0.009
					1156–1147 BC	0.897	0.011
					1128–969 BC*		0.925
					962–932 BC		0.055

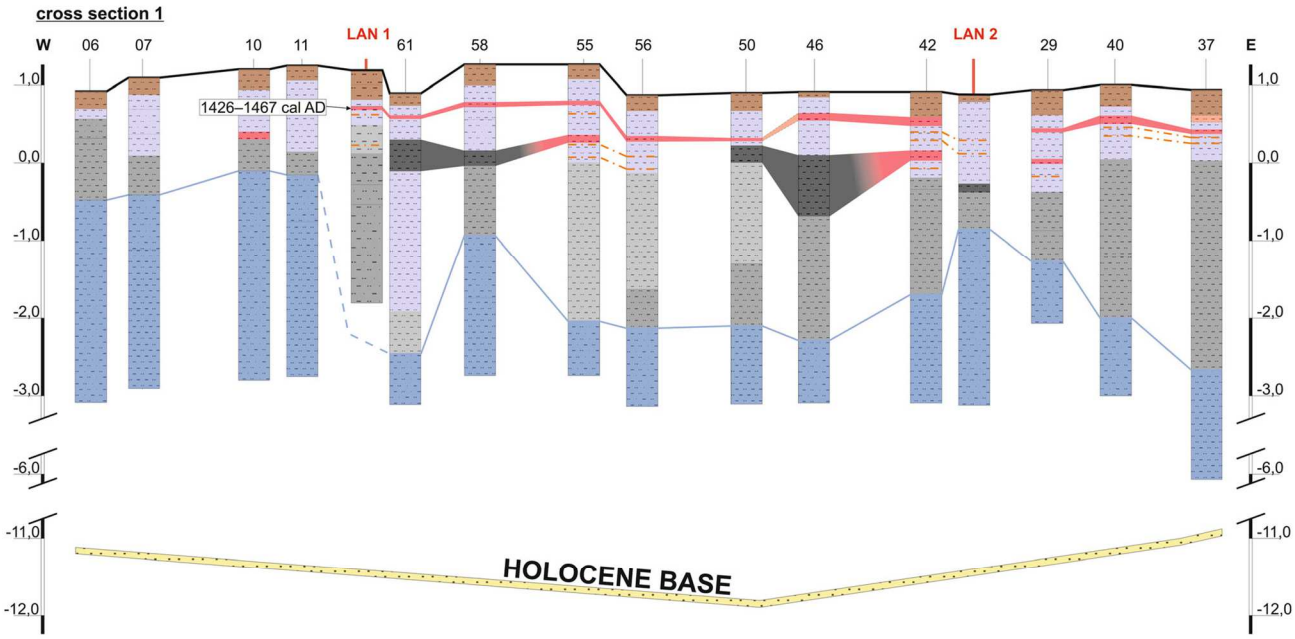

Fig. 7 Cross section 1, situated in the north of the study area (cf. Figs. 2 and 3). The section includes two of the new drillings (LAN 1 and 2). If possible, stratigraphic layers were correlated. The numbers on top are the drilling numbers of 1960 and 2013. The Holocene base was modelled from the geological coastal map of LBEG (2016). For descriptions and interpretations of facies units A–G see previous subchapter and Fig. 10 and for the uniform colour key see Fig. 8

slopes seawards of the tidal flats (Bungenstock and Weerts 2012). The most abundant foraminiferal species, *Haynesina germanica*, *Ammonia tepida* and *Cribroelphidium williamsoni*, are calcareous, euryhaline intertidal species tolerant of brackish waters, which occur in very shallow coastal waters, tidal flats and also in (salt) marshes (Lehmann 2000; Frenzel et al. 2005; Murray 2006; Horton and Edwards 2006). They only occur at the western drilling sites LAN 1 and 3, whereas LAN 2 shows a completely different picture (at least for A2). The present *Trochammina inflata* and *Jadammina macrescens* are agglutinated, euryhaline (high- to mid-) marsh species, which tolerate brackish, shallow waters (Frenzel et al. 2005; Murray 2006) and corroborate the interpretation of a salt marsh. The PCA (Fig. 9) groups all samples of A1 into the same group (3 a) and separates A2 into a lower (group 3 a – salt marsh) and an upper (group 1 – terrestrial) part, implying a transition from aquatic to more terrestrial conditions.

Facies B – peat layer (swamp formation above mean sea level)

This facies is characterised by 'clayey peats' (Schneeberg 1962), which do not exhibit any macroscopic plant remains. The foraminiferal association of the lower two peat layers B1 and B2, which are only visible in the western drilling LAN 3, shows similar characteristics as in the underlying salt marsh (A1). Furthermore, the PCA grouped B1 and A1 within group 3 a. These results imply a similar environment of deposition for B1 and A1. Nevertheless, the grain-size distribution (endmember scores) and organic content clearly differentiate this facies from the salt marsh. The upper peat layer B3 from LAN 2 differs from the underlying salt marsh (A2), since the before frequently occurring marsh species *T. inflata* is barely present within the peat. The peat layers formed out of the decaying salt marsh vegetation, which most likely destroyed most of the agglutinated shells. The fact that B3 in the east is only visible in LAN 2 could be due to insecure interpretations of the handwritten archive drilling protocols of the surrounding area.

Facies C – marine inundation (high-energy event above mean sea level)

The grain-size distribution, mean grain size and very limited thickness of this facies indicate an episodic, high-energy depositional process. Considering this higher energy level, the fact that the PCA groups the layer with most of Facies D (group 3 b) and the stratigraphic position of all three layers C1–3 between either two peat layers or on top of a humic layer with indications of pedogenesis, this facies can be associated with severe marine inundation of the salt marsh during storm surges. The reworked and frayed parts of the underlying peat (B1) visible in C1 support this interpretation. The foraminiferal association of this section also implies a shallow marine (brackish) input, which, however, cannot be specified through the present intertidal species. As for LAN 3, C2 and C3 are void

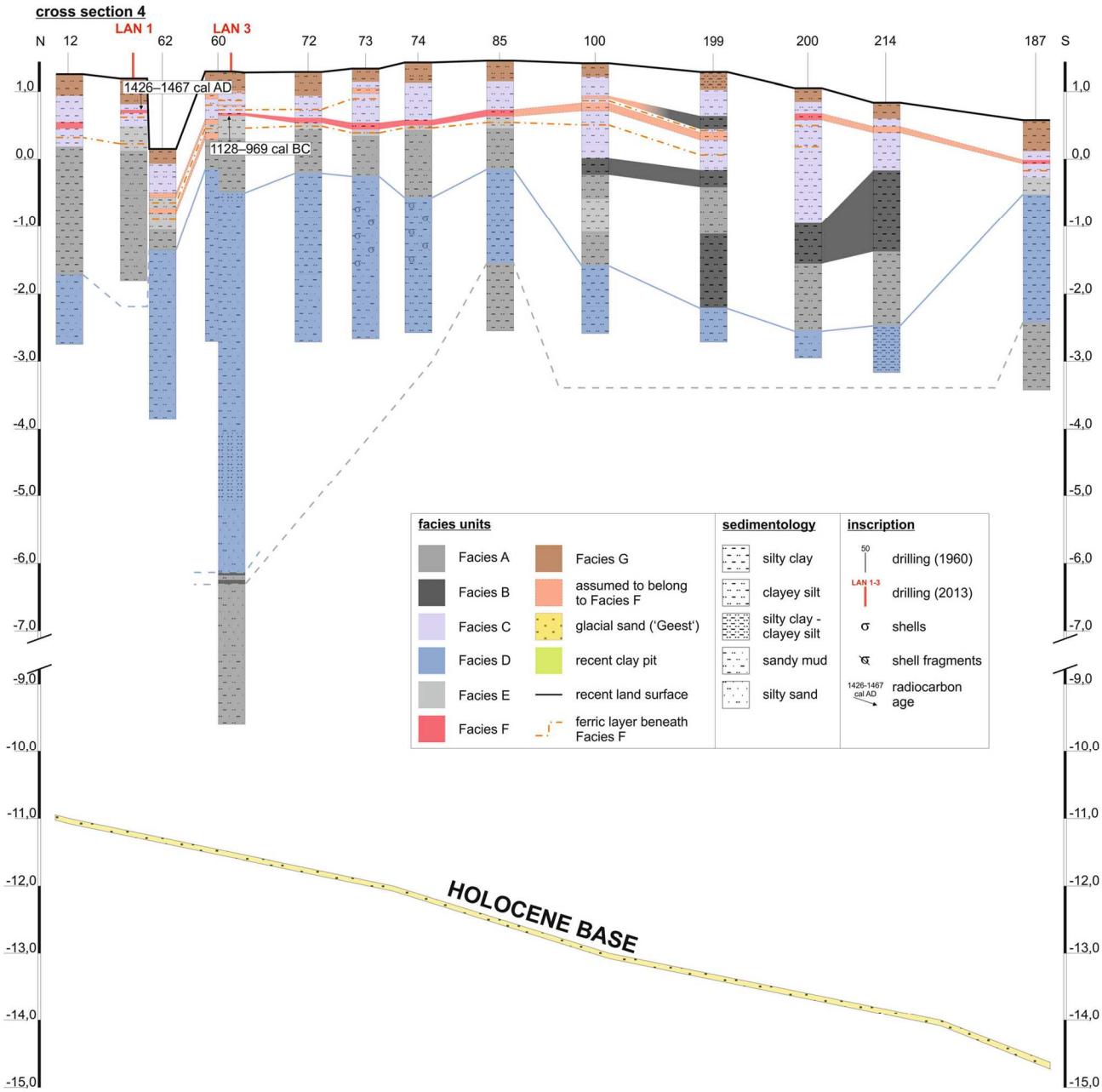

Fig. 8 Cross section 4, situated in the west of the study area (cf. Figs. 2 and 3). The section includes two of the new drillings (LAN 1 and 3). If possible, stratigraphic layers were correlated. The numbers on top are the drilling numbers of 1960 and 2013. The Holocene base was modelled from the geological coastal map of LBEG (2016). For descriptions and interpretations of facies units A–G see previous subchapter and Fig. 10

of microfossils, possibly due to post-depositional carbonate solution, whereas the inundation layer in LAN 1 (C3) again contains the three shallow marine, intertidal species *H. germanica*, *A. tepida*, *C. williamsoni*.

Facies D – tidal flat (marine facies at mean sea level)

The grain-size distribution (coarsest endmember dominates), indicating a much higher-energetic environment than before, the high carbonate content, organic laminae, implying periodical inundations, and the presence of mollusc fragments suggest a deposition in a tidal flat environment. The dominance of the three already mentioned shallow marine, intertidal foraminifer species does also fit this interpretation. However, a difference is noticeable between the lower and upper part of the facies, as the lower is dominated by *A. tepida* and the upper by *H. germanica*. The upper part of the tidal sediments (starting at −2.72 m a.s.l. in the west and

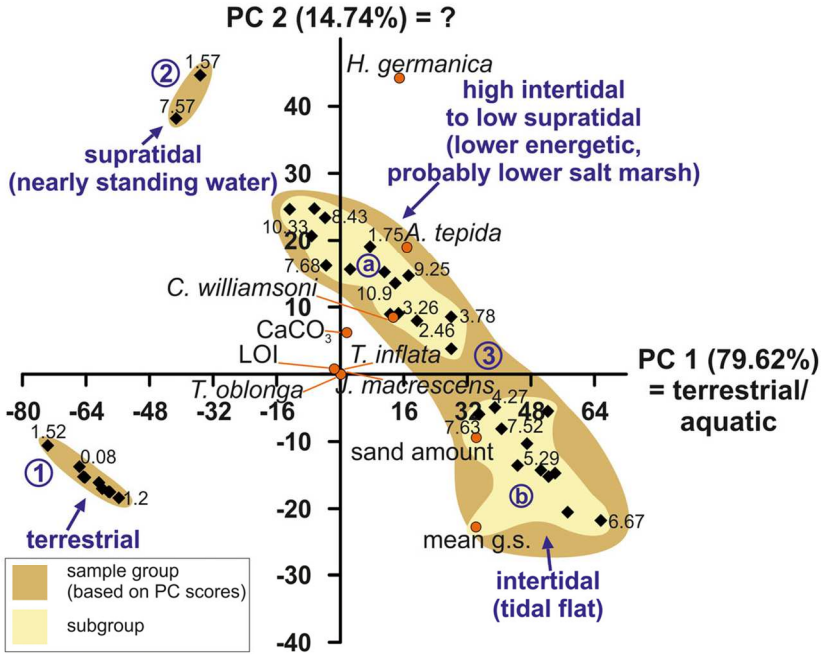

Fig. 9 PCA biplot of the sedimentological and foraminiferal data of LAN 3. Samples are represented by black rhombs (including sample depth in m b.s.) and variables by orange circles. Blue numbers represent groups identified by the PCA of LAN 3. Due to reasons of readability and clarity only representative depths are depicted for each group. For the depth profile of PC 1 see Fig. 4 and for the used data see Table 7 (onl. Suppl)

−2.22 m a.s.l. in the east) most likely represents the transition to a following salt marsh, i.e. the aggradation above sea level. The decreasing energy level in the upper part reflected by the shift from the higher-energy endmember 3 to the lower-energy endmember 2 confirms this assumption as well as the fact that the PCA combines the lower part in group 3 b and the upper part with the salt marsh samples (group 3 a). The data imply a less high energetic level and poorer sorting in the east (LAN 2) closer to the 'Geest', which is reasonable, since sorting, grain size and energy level decrease in an inland direction from tidal flats over salt marshes to terrestrial environments (Falk 2003).

Facies E – decalcified marsh (terrestrial facies above mean sea level)

This facies is characterised by a very low-energetic environment. It is comparable to the underlying salt marsh A2, but with the major difference of a lack of carbonates (and thus microfossils), which indicates the ageing of the marsh that grew above the supratidal area. These post-depositional changes may be the reason why A2 and E show different patterns of endmember scores than A1. The PCA grouping this layer with other terrestrial samples (group 1) also supports this interpretation.

Facies F – dwog horizon (stable terrestrial conditions; pedogenesis above mean sea level)

At the surface of the decalcified marsh a humic topsoil formed, void of microfossils. In the western part this is given through the existence of two different *dwog* horizons combined in the terrestrial group 1 of the PCA. The visual identification due to its dark colour and crumbly structure (Streif 1990) is supported by the absence of carbonate and the high activity levels of pedogenetic iron oxides (Figs. 4 and 17 [onl. Suppl.]). In the East (LAN 2), none of the humic *dwog* horizons occur. However, the highly iron-affected upper half of Facies E could represent one or two iron *dwog*s, which are often underlying the humic *dwog*. This could only be confirmed by further analyses of pedogenetic iron oxides.

Facies G – recent humic topsoil (terrestrial facies above mean sea level)

This facies is characterised by terrestrial conditions, indicated by the grain-size distribution, the upwards increasing organic content as well as the affiliation to group 1 of the PCA. Hence, this unit represents soil formation at the recent land surface after the reclamation of land through the construction of dykes.

Correlation with other facies models

The Facies A, B and possibly the transitory part of D can be associated with *quiet reach* sediments as classified by Wartenberg et al. (2013), which can be characterised by both, direct connection to the North Sea or isolated lagoonal conditions. The lower part of Facies D, however, probably relates to the *dymanic deposits* of Wartenberg et al. (2013), which are characterised by coarser-grained

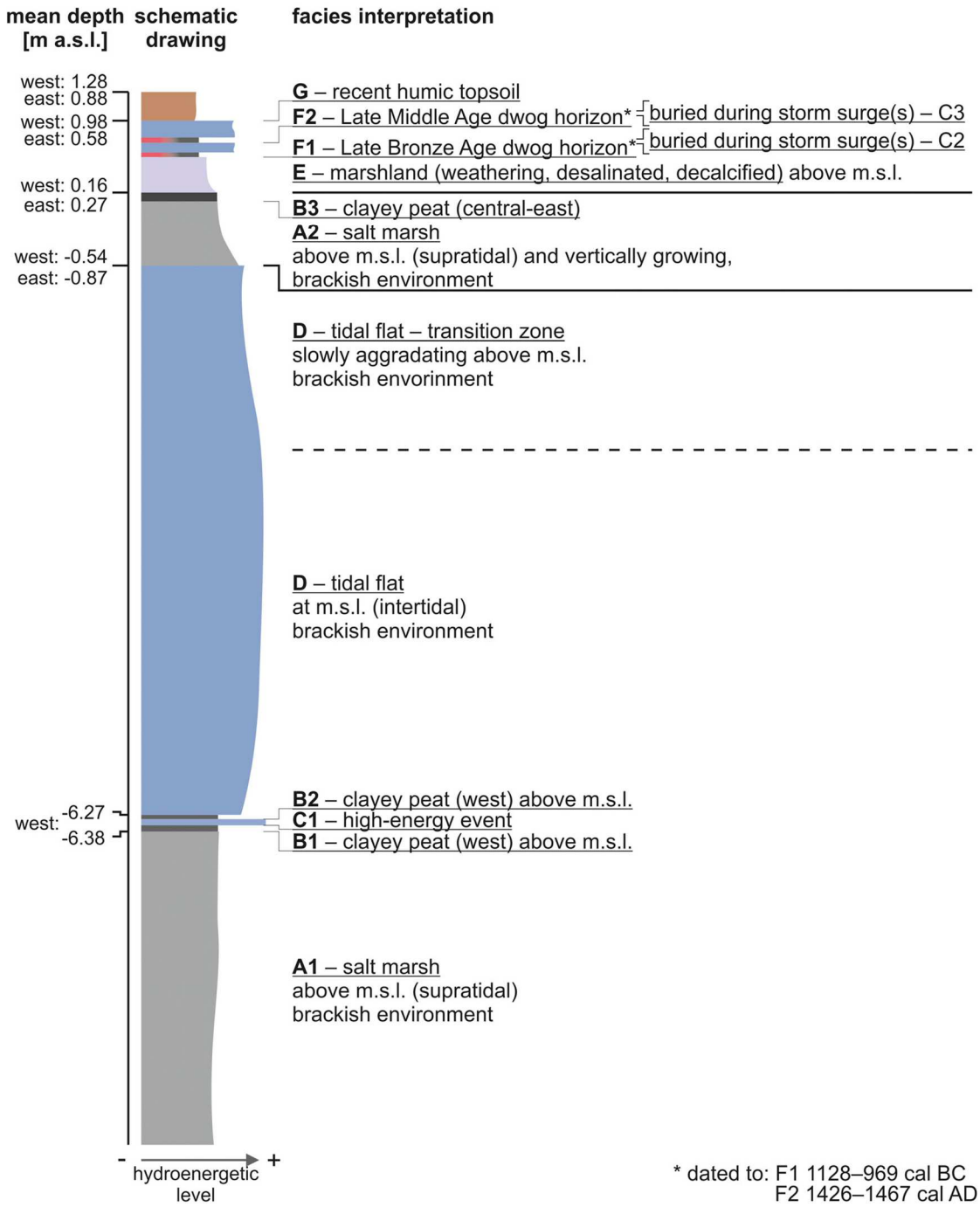

Fig. 10 Schematical illustration of the facies interpretations for the whole study area derived from the archive data as well as the new drillings. Eastern depths are based on LAN 2, western depths on LAN 1 and 3. The colour key of the stratigraphic cross sections (Fig. 8) was used for this standard profile and 'm.s.l.' stands for 'mean sea level' at the time of deposition (in contrast to present mean sea level [s.l.] within the text)

sediments implying relatively higher-energetic conditions. Finally, the marine inundations of Facies C associate with the classified *partings*, which are characterised by thin intercalated clastic layers within a peat (see also Bruns et al. 2015) – in our record with additional occurrence between fossil topsoils.

Reconstructing coastal landscape formation

The investigated record starts with a salt marsh environment. One archive drilling from the south-eastern part of the study area (146; visible in c.s. 3 and c.s. 5; Figs. 20 and 21 [onl. Suppl.]) shows the existence of another layer of tidal

sediments beneath this first salt marsh horizon A1. Formations like this have been discussed in terms of a progradation and retrogradation of the coastline connected to sediment supply and accommodation space (e.g. Bungenstock and Weerts 2010, 2012). Considering a period of increased sediment supply at the beginning of the investigated sedimentary sequence, the development of a salt marsh could probably be justified. Since the deposition of and on tidal flats depends on the sediment supply of both the North Sea (c. 90%) and the rivers (c. 10%) (Hoselmann and Streif 2004), these environments are highly sensitive to changes in either one of them. The deceleration of the transgression could probably have caused a smaller accommodation space/sediment supply ratio leading to a prograding coastline. Furthermore, periods of repeated marine inundations (spring tides or storm surges), if not too intense, cause the deposition of massive sediment loads in the vegetated zones associated with a vertical and lateral growth of the salt marsh areas (Bungenstock and Weerts 2012). However, an increased fluvial sediment supply controlled by the river Weser must also be considered. A combined effect of anthropogenic influences, given through new agricultural techniques, and more humid climate conditions during the Holocene climatic optimum, causing increased soil erosion and floodplain deposits, is possible (Kalis et al. 2003). Further investigations are needed in order to confirm a possible fluvial sediment origin in the eastern part of the study area.

Out of decaying salt marsh vegetation, the peat B1 developed, which was probably partially eroded and buried during the high-energy marine inundation C1. Assuming one single event, either a storm surge, an extremely high tide (spring tide) or a combination of both is possible. This event layer could possibly correlate with the incisive event marker Wartenberg et al. (2013) documented for the time period of c. 3600–2400 cal BC. However, this should be verified by further investigations. It was followed by a re-establishment of previous conditions with the formation of the peat B2.

Subsequently a tidal flat D most certainly developed due to the continuing transgression, perhaps with an increased rate, because the growth of the peat could not keep up with the rising sea (cf. Bungenstock and Weerts 2012). The tidal flat was characterised by several tidal channels, visible in the cross sections (Figs. 7, 8 and 19–21 [onl. Suppl.]), one running in the east of the later settlement area.

As the tidal flat slowly aggradated above the mean high-tide level, the record shows a transition to the second salt marsh environment A2. This facies change reflects the typical dynamics of the North Sea coast. Hence, it probably developed due to the vertical growth of the tidal flat and represents a transitional facies between marine and terrestrial environments (Bungenstock and Weerts 2012). In this case, an increased sediment supply from the sea is most likely the reason for this transition. A period of repeated flooding of the higher parts of the tidal flat (spring tides, storm surges) possibly deposited remarkable amounts of sediment, which were trapped by vegetation resulting in an increased aggradation and a possible progradation of the coastline. Some of the tidal currents were infilled during this phase (cf. c.s. 1–5; Figs. 7, 8 and 19–21 [onl. Suppl.]). In the east, this salt marsh is taken over by swamp formation B3, whereas in the west and northwest it shows signs of an initial transition to terrestrial conditions, implied by upwards decreasing energy levels. The foraminiferal association also supports this development.

Under predominant subaerial conditions the area was exposed to processes of subsidence, desalination and oxidation (iron oxides) leading to the complete decalcification in the course of soil formation (Müller-Ahlten 1994) represented in Facies E.

The *dwog* horizon F1 on top represents the land surface of the Late Bronze Age. Considering correct relative ages (see following subchapter), only LAN 3, which, instead of LAN 1, is not located in the tidal channel east of 'Barward', exhibits the older *dwog* F1. This could imply that the tidal channel was still active at that time. F1 was buried during a marine inundation C2, which could have been a single storm surge or a period of increased storm activity combined with an increased RSL rise. Wartenberg et al. (2013) also report an incisive event for the time from c. 1000–400 cal BC, which, provided that the age is correct, approximately matches this inundation C2. The tidal channel probably was infilled during or after it, since the following dwog F2 was identified above it. The high number of storm surges during the Middle Ages until the eighteenth century is related to C3 burying this Late Medieval land surface. A very thin intercalated fine-grained layer within C3 supports this assumption, since a series of storm surges is most certainly characterised by occasional calmer phases with standing water enabling the deposition of finer sediments.

After the effects of this stormy period had weakened, the recent land surface G could develop.

Chronology of the *dwog* horizons

The age of the older *dwog* F1 (1128–969 cal BC) approximately matches a *dwog* Bungenstock (2008) assumed for the Late Bronze Age to Early Iron Age. Furthermore, the sea-level curve (Bungenstock and Weerts 2010; Fig. 11) shows a stagnation or a very slow rise of the RSL in this phase and Wartenberg et al. (2013) report a high-energy event in the time after c. 1000 cal BC. However, there are also contradictory statements, as Schneeberg (1962) describes the sedimentation environment at this time as a brackish estuary and Haarnagel (1979) reports that the levee in the west, which protected the hinterland enabling soil formation, did not exist until the last centuries BC. This might indicate that the date underlies one or several methodological errors. The contamination with allochthonous carbon from the east could be possible, but this does not seem reasonable, since the transport medium remains uncertain. The incorporation of older ^{14}C from groundwater seems more likely, as pedogenesis in the marsh is strongly related to groundwater levels.

However, since the more recent studies provide ages in support of our data, a local or regional pedogenesis in the study area seems possible for the Late Bronze Age – even though 'Barward' was not inhabited at this time, which is also visible in the curve, since its first settlement layer dates to c. 50–1 BC (see Fig. 10).

The younger *dwog* (F2, sampled from LAN 1), which dates to cal AD 1426–1467, seems too young, since the marshlands of the 'Land Wursten' region were completely dyked by the fifteenth century (first consistent dyke line c. AD 1300 [Bungenstock and Schäfer 2009]) questioning the origin of the clastic layer (C3) above the *dwog*. Hence, this age either underlies methodological errors or this sedimentary sequence represents an event of greater significance. The methodological error would be given through contamination with younger carbon in terms of bioturbation (pre-sampling), field sampling, fungal growth (sample storage) or pre-treatment in the laboratory. Considering a correct age, the overlying sediment layer could only result from a short-term event like a storm surge or a period of increased storm activity. Table 3 shows five important storm surges from the beginning of the 16th to the early seventeenth century AD all affecting the coast at or near the study area. Dyke breaches are only documented for one of these storm surges. The clastic layer could have been deposited during one of these or by several storm surges at short intervals (e.g. 1509 and 1511). Another possible explanation for the clastic layer above the *dwog* at this position could be the reactivation of the drainage system of 'Barward' in the course of the short reoccupation during the Middle Ages (Table 1). However, this does not explain its extensive occurrence even in non-tidal-channel areas and the foraminiferal association does not support this assumption. Hence, as explained in the previous subchapter, a series of storm surges seems most likely in this case.

Both age estimates leave uncertainties; thus, they should be verified by dating further *dwog* horizons or under- and overlying strata.

Correlation of the facies with existing RSL data

We tried to relate the facies model to an existing relative sea-level curve for the Jade Weser region published by Bungenstock and Weerts (2010) with data of the curve of Behre (2007) (Fig. 11). The curve was modified by means of excluding compaction-prone index points, which creates a curve with less variations.

The salt marsh in Facies A1 is situated in the supratidal area of frequent inundation and reflects a stagnation or slowly rising phase of the RSL history. We assume a relation of this facies to the slower RSL rise between c. 5200 and 3200 cal BC. The overlying peats B1 and B2 as well as the possible storm surge in between (C1) probably also relate to this stagnation phase. The following tidal flat in Facies D clearly reflects a transgressive phase and thus can be related to the time period from c. 3200–2600 cal BC. However, the described transition to the overlying salt marsh in the upper part of the tidal sediments could already relate to the following deceleration of the sea-level rise. This decelerated rise from c. 2600–1100 cal BC probably is represented by the salt marsh in Facies A2 as well as the decalcified marsh in Facies E. The subsequent and even slower RSL rise between c. 1100 cal BC and the turn of the eras depicted in the curve matches the age of the older *dwog* horizon F1 (1128–969 cal BC). The latter was probably covered during several storm surges or spring tides (C2) combined with a generally increased RSL rise in the time between the turn of the eras and cal AD 300. Then, our record shows a hiatus, since the younger *dwog* F2 (cal AD 1426–1467) does not directly follow in time. However, its age still matches the regressive or stagnation phase from c. cal AD 300 until 1644 shown in the curve. *Dwog* F2 was probably covered by a series of storm surges, which are not documented in the modified sea-level curve.

Conclusions and future perspectives

The applied sedimentological, microfaunal and statistical methods in combination with the analysis of the extensive archive drilling data provide a valuable dataset for the reconstruction of Holocene coastal and environmental changes in the 'Land Wursten' region (research goals i–iii).

The combined sedimentary record shows a number of facies changes probably related to RSL changes or

Table 3 Extract of the most important storm surges of the North Sea reported from historical sources (Streif 1990)

Storm surge name	Date	Affected area	Dyke breach
Cosmas and Damian Flood	26/09/1509	Between Netherlands and Weser	Not documented.
Antonius Flood	16/01/1511	Jade Bay	Yes
3rd All Saints' Day Flood ('Allerheiligenflut')	31/10/1532	Between English Channel and Jutland	Not documented
4th All Saints' Day Flood ('Allerheiligenflut')	01/11/1570	Between Flanders and Eiderstedt	Not documented
Shrovetide Flood ('Fastnachtsflut')	26/02/1625	Between Maas and Jutland	Not documented

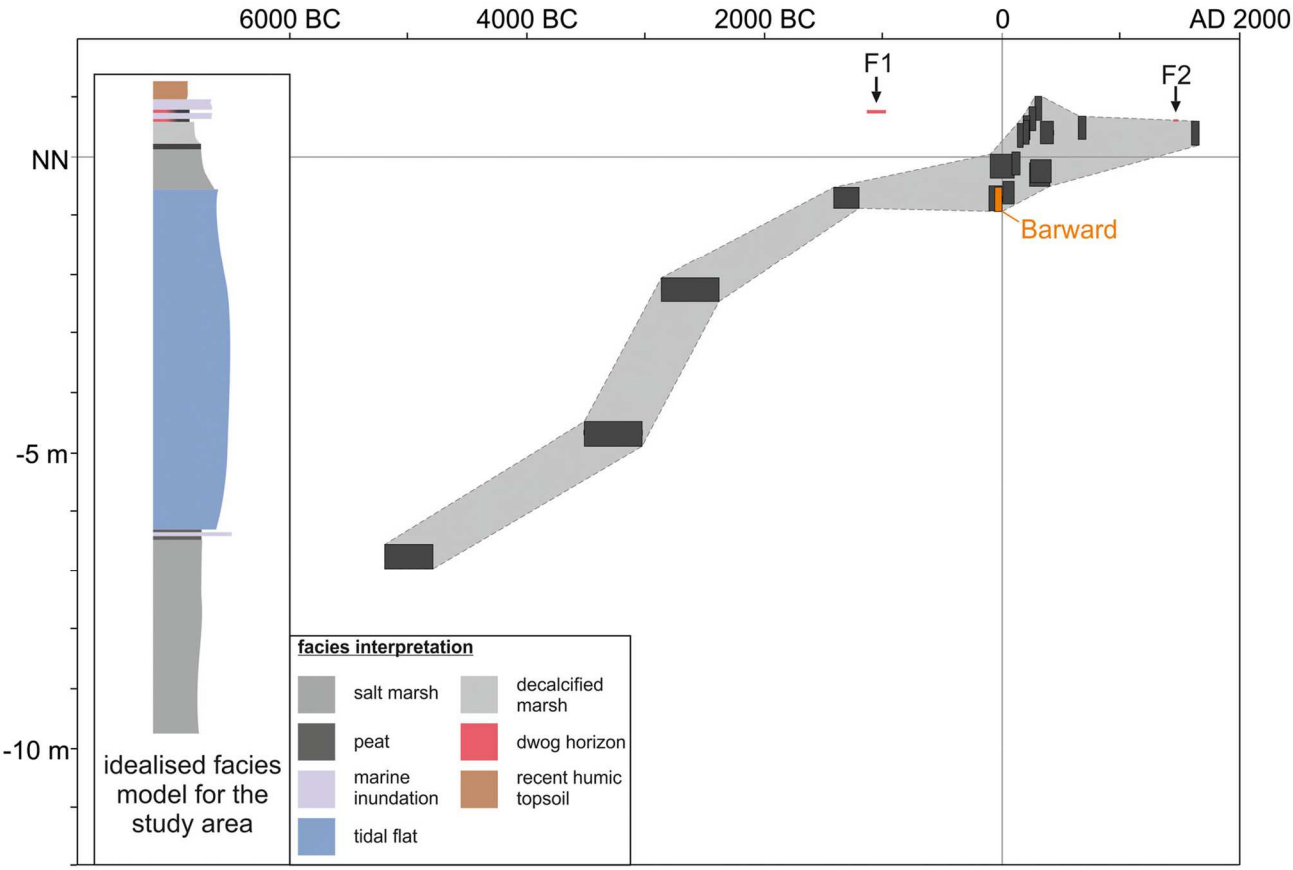

Fig. 11 Idealised facies model from Fig. 10 in relation to the sea-level curve for the Jade Weser region (*modified after* Bungenstock and Weerts 2010; original curve for whole German Bight by Behre 2007; separated into different tidal basins). Compaction-prone data points have been excluded. The ages of the two *dwog* horizons were integrated but not combined with the curve, since compaction rates are not known. The age of the settlement layer of 'Barward' is marked in order to show that there is no possible correlation with our data

changes in the rate of RSL rise. However, these facies changes may also imply aggradation, progradation and retrogradation of the coastline, which can be caused by changes in sediment supply, accomodation space and/or climatic conditions. Other important influences are anthropogenic impacts and interactions with natural processes, increasing constantly since c. 7500 BP, e.g. farming activities, which have enhanced soil erosion in a massive way, changing sediment loads of rivers since c. 6300 BP (cf. Kalis et al. 2003). Dyke construction represents another huge anthropogenic impact since the Middle Ages (Gerdes et al. 2003; Bungenstock and Schäfer 2009), since it caused considerable reductions of inundation areas of the North Sea and thus an increased damming effect. Hence, the most disastrous storm surges happened after the completion of the first continuous dyke system (c. AD 1300). These effects could even be exacerbated by the future rising global eustatic sea level.

We were able to relate the investigated record, including the *dwog* horizons, to existing RSL data for the Jade Weser region. However, due to the lack of datings, most of the correlations are based on assumptions and comparable results from former investigations in different areas. The (decalcified) salt marsh facies can be related to phases of a slowly rising RSL (5200–3200 cal BC and 2600–1100 cal BC), whereas the tidal sediments probably correlate with the faster RSL rise (3200–2600 cal BC) and the *dwog* horizons with local or regional phases of stagnation or a barely rising RSL (1100 cal BC until the turn of the eras and cal AD 300–1644).

We were able to identify and trace the *dwog* horizons throughout the study area. As their radiocarbon ages do not match the age of the known settlement layers of the dwelling mound, no conclusions on implications of the identified coastal changes for the dwelling mound 'Barward' could be drawn (research goal iv).

Hence, further investigations are necessary in order to get more information on local compaction and verify the ages of the *dwog* horizons to possibly achieve a correlation with settlement layers of 'Barward'.

Acknowledgements The 'Landesamt für Bergbau, Energie und Geologie' in Hannover is acknowledged for providing access to the archive of drilling records. We thank David Scheder for considerable help during field campaigns, Peter Frenzel for thecreation of the scanning

electron microscope images and Ines Bruns for support in the application of GeODin. Radiocarbon dating was funded through a Max Delbrück Prize for Junior Researchers awarded to Max Engel, a measure of the future concept of the University of Cologne in the framework of the Excellence Initiative (DFG ZUK 81/1).

References

Ad-hoc-Arbeitsgruppe Boden (2005) Bodenkundliche Kartieranleitung, 5th edn. Bundesanstalt für Geowissenschaften und Rohstoffe, Hannover

Allen JRL (1999) Geological impacts on coastal wetland landscapes: some general effects of sediment autocompaction in the Holocene of Northwest Europe. The Holocene 9:1–12. doi:10.1191/095968399674929672

Asmus WD (1949) Neuere Ausgrabungen in der Eisenzeitlichen Dorfsiedlung auf der Barward bei Dingen. Kr Wesermünde Hammaburg 2:116–130

Aufderhaar I (2016) Sievern, Ldkr. Cuxhaven – Analyse einer Zentralregion von der ausgehenden Vorrömischen Eisenzeit bis in das 6. Jh. n. Chr. Studies in Landscape and Settlement History in the Southern North Sea Region 8, Wilhelmshaven

Aufderhaar I, Brandt I, Schwank S, Siegmüller A (2013) Aktuelle Untersuchungen im Umfeld der Wurt Fallward, Ldkr Cuxhaven. Nachrichten des Marschenrates zur Förderung der Forschung im Küstengebiet der Nordsee 50:41–44

Baeteman C (1999) The Holocene depositional history of the Ijzer palaeovalley (western Belgian coastal plain) with reference to the factors controlling the formation of intercalated peat beds. Geol Belg 2:39–72

Barsch H, Billwitz K, Bork H (eds) (2000) Arbeitsmethoden in Physiogeographie und Geoökologie. Justus Perthes Verlag Gotha GmbH, Gotha

Beets DJ, van der Spek AJF (2000) The Holocene evolution of the barrier and back-barrier basins of Belgium and the Netherlands as a function of late Weichselian morphology, relative sea-level rise and sediment supply. Geol Mijnb 79:3–16. doi:10.1017/S0016774600021533

Behre K-E (2004) Coastal development, sea-level change and settlement during the later Holocene in the Clay District of lower Saxony (Niedersachsen), northern Germany. Quatern Int 112:37–53. doi:10.1016/S1040-6182(03)00064-8

Behre K-E (2007) A new Holocene Sea-level curve for the southern North Sea. Boreas 36:82–102. doi:10.1111/j.1502-3885.2007.tb01183.x

Blott SJ, Pye K (2001) Gradistat: a grain size distribution and statistics package for the analysis of unconsolidated sediments. Earth Surf Proc Land 26:1237–1248. doi:10.1002/esp.261

Blume HP, Stahr K, Leinweber P (2011) Bodenkundliches Praktikum. Eine Einführung in pedologische Arbeiten für Ökologen, Land- und Forstwirte, Geo- und Umweltwissenschaftler. Spektrum, Heidelberg

Brain MJ, Long AJ, Woodroffe SA, Petley DN, Milledge DG, Parnell AC (2012) Modelling the effects of sediment compaction on salt marsh reconstructions of recent sea-level rise. Earth Planet Sc Lett 345–348:180–193. doi:10.1016/j.epsl.2012.06.045

Brand G, Hagemann BP, Jelgersma S, Sindowski K-H (1965) Die lithostratigraphische Unterteilung des marinen Holozäns an der Nordseeküste. Geol Jahrb 82:365–384

Bruns I, Bungenstock F, Wolters S, Freund H (2015) Klastische Lagen in eingeschalteten Torfen im niedersächsischen Küstenholozän–Anzeiger für synsedentäre oder postsedentäre Einzelereignisse. Siedlungs- und Küstenforschung im südlichen Nordseegebiet 38: 257–269

Bungenstock F (2008) Zur Paläogeographie des jungbronze- bis früheisenzeitlichen Siedlungsplatzes Rodenkirchen-Hahnenkooper Mühle, Ldkr Wesermarsch. Probleme der Küstenforschung im südlichen Nordseegebiet 32:181–195

Bungenstock F, Schäfer A (2009) The Holocene relative sea-level curve for the tidal basin of the barrier island Langeoog, German bight, southern North Sea. Glob Planet Chang 33:34–51. doi:10.1016/j.gloplacha.2008.07.007

Bungenstock F, Weerts HJT (2010) The high-resolution Holocene sea-level curve for Northwest Germany: global signals, local effects or data-artefacts? Int J Earth Sci 99:1687–1706. doi:10.1007/s00531-009-0493-6

Bungenstock F, Weerts HJT (2012) Holocene relative sea-level curves for the German North Sea coast. Int J Earth Sci 101:1083–1090. doi:10.1007/s00531-011-0698-3

Busschers FS, Kasse C, van Balen RT, Vandenberghe J, Cohen KM, Weerts HJT, Wallinga J, Johns C, Cleveringa P, Bunnik FPM (2007) Late Pleistocene evolution of the Rhine-Meuse system in the southern North Sea basin: imprints of climate change, sea-level oscillation and glacio-isostacy. Quaternary Sci Rev 26:3216–3248. doi:10.1016/j.quascirev.2007.07.013

De Deckker P, Forester RM (1988) The use of ostracods to reconstruct continental palaeoenvironmental records. In: De Deckker P, Colin JP, Peypouquet JP (eds) Ostracoda in the earth sciences. Elsevier, Amsterdam, Oxford, pp 175–199

Dietze E, Hartmann K, Diekmann B, Ijmker J, Lehmkuhl F, Opitz S, Stauch G, Wünnemann B, Borchers A (2012) An end-member algorithm for deciphering modern detrital processes from lake sediments of Lake Donggi, NE Tibetan plateau, China. Sediment Geol 243–244:169–180. doi:10.1016/j.sedgeo.2011.09.014

Eshel G, Levy GJ, Mingelgrin U, Singer MJ (2004) Critical evaluation of the use of laser diffraction for particle-size distribution analysis. Soil Sci Soc Am J 68:736–743. doi:10.2136/sssaj2004.7360

Falk GC (2003) Die Paläogeomorphologie ausgewählter Standorte der Schleswig-Holsteinischen Nordseeküste in Früh- und Mittelholozän. PhD thesis. Technische Universität Berlin

Folk RL, Ward WC (1957) Brazos River bar: a study in the significance of grain size parameters. J Sediment Petrol 27:3–26. doi:10.1306/74D70646-2B21-11D7-8648000102C1865D

Forester RM (1988) Nonmarine calcareous microfossil sample preparation and data acquisition procedures. US Geological Survey Technical Procedure HP-78(R1):1–9

Frenzel P, Boomer I (2005) The use of ostracods from marginal marine, brackish waters as bioindicators of modern and Quaternary environmental change. Palaeogeogr Palaeocl 225:68–92. doi:10.1016/j.palaeo.2004.02.051

Frenzel P, Tech T, Bartholdy J (2005) Checklist and annotated bibliography of recent Foraminiferida from the German Baltic Sea coast. Stud Geol Polon 124:67–85

Freund H, Streif H (2000) Natürliche Pegelmarken für Meeresspiegelschwankungen der letzten 2000 Jahre im Bereich der Insel Juist. Petermann Geogr Mitt 143:34–45

Genrich (1941) Bericht über die Untersuchungen auf der Barward. Probleme der Küstenforschung im südlichen Nordseegebiet 2: 157–170

Gerdes G, Petzelberger BEM, Scholz-Böttcher BM, Streif H (2003) The record of climatic change in the geological archives of shallow marine, coastal and adjacent lowland areas of northern Germany. Quaternary Sci Rev 22:101–124. doi:10.1016/S0277-3791(02)00183-X

Haarnagel W (1979) Die Grabung Feddersen Wierde. Methode, Hausbau, Siedlungs- und Wirtschaftsformen sowie Sozialstruktur. Textband. Steiner, Wiesbaden

Hammer Ø, Harper DAT, Ryan PD (2001) PAST: Palaeontological statistics software package for education and data analysis. Palaeontol Electron 4(1):article4

Handl M, Mostafawi N, Brückner H (1999) Ostracodenforschung als Werkzeug der Paläogeographie. In: Brückner H (ed) Dynamik, Datierung, Ökologie und Management von Küsten. Marburger Geographische Schriften 134:116–153

Hayen H, Tidow K, Ullemeyer R (1981) Einzeluntersuchungen zur Feddersen Wierde. Steiner, Wiesbaden

Hesemann M (2015) The foraminifera.eu database: concept and status. Palaeontol Electron 18.3.48A: 1–14

Horton BP, Edwards RJ (2006) Quantifying Holocene Sea level chance using intertidal foraminifera: lessons from the British isles, vol 40. Special Publication, Cushman Foundation for Foraminiferal Research

Hoselmann C, Streif H (2004) Holocene sea-level rise and its effect on the mass balance of coastal deposits. Quatern Int 112:89–103. doi:10.1016/S1040-6182(03)00067-3

Kalis AJ, Merkt J, Wunderlich J (2003) Environmental changes during the Holocene climatic optimum in Central Europe – human impact and natural causes. Quaternary Sci Rev 22:33–79. doi:10.1016/S0277-3791(02)00181-6

Kiden P, Denys L, Johnston P (2002) Late Quaternary sea-level change and isostatic and tectonic land movements along the Belgian–Dutch North Sea coast: geological data and model results. J Quaternary Sci 17:535–546. doi:10.1002/jqs.709

Kiden P, Makaske B, van de Plassche O (2008) Waarom verschillen de zeespiegel—reconstructies voor Nederland? Gronboor Hamer 3(4): 54–61

Lambeck K, Rouby H, Purcell A, Sun Y, Sambridge M (2014) Sea level and global ice volumes from the last glacial maximum to the Holocene. P Natl Acad Sci USA 111:15296–15303. doi:10.1073/pnas.1411762111

LBEG (2016) Geologische Küstenkarte von Niedersachsen 1: 25 000 – Relief der Holozänbasis http://nibis.lbeg.de/net3/public/ikxcms/default.aspx?pgid=151. Accessed 28 June 2016

Lehmann G (2000) Vorkommen, Populationsentwicklung, Ursache fleckenhafter Besiedlung und Fortpflanzungsbiologie von Foraminiferen in Salzwiesen und Flachwasser der Nord- und Ostseeküste Schleswig-Holsteins. PhD thesis. University of Kiel

Long AJ, Waller MP, Supples P (2006) Driving mechanisms of coastal change: peat compaction and the destruction of late Holocene coastal wetlands. Mar Geol 225:63–84. doi:10.1016/j.margeo.2005.09.004

Mehra OP, Jackson ML (1958) Iron oxide removal from soils and clays by a dithionite-citrate system buffered with sodium bicarbonate. Clay Clay Miner 7(1):317–327. doi:10.1346/CCMN.1958.0070122

Müller-Ahlten W (1994) Zur Genese der Marschböden. II. Kalksedimentation, Entkalkung. J Plant Nutr Soil Sc 157:333–343. doi:10.1002/jpln.19941570504

Murray JW (2006) Ecology and applications of benthic foraminifera. Cambridge University Press, Cambridge

Paul MA, Barras BF (1998) A geotechnical correction for post-depositional sediment compression: examples from the forth valley, Scotland. J Quaternary Sci 13:171–176. doi:10.1002/(SICI)1099-1417(199803/04)13:2<171::AID-JQS369>3.0.CO;2-Z

Pint A, Frenzel P, Horne DJ, Franke J, Daniel T, Burghardt A, Funai B, Lippold K, Daut G, Wennrich V (2015) Ostracoda from inland waterbodies with saline influence in Central Germany: implications for palaeoenvironmental reconstruction. Palaeogeogr Palaeocl 419: 37–46. doi:10.1016/j.palaeo.2014.07.042

Reimer PJ, Bard E, Bayliss A, Beck JW, Blackwell PG, Ramsey CB, Buck CE, Cheng H, Edwards RL, Friedrich M, Grootes PM, Guilderson TP, Haflidason H, Hajdas I, Hatté C, Heaton TJ, Hoffmann DL, Hogg AG, Hughen KA, Kaiser KF, Kromer B, Manning SW, Niu M, Reimer RW, Richards DA, Scott EM, Southon JR, Staff RA, Turney CSM, van der Plicht J (2013) IntCal13 and Marine13 radiocarbon age calibration curves 0–50,000 years cal BP. Radiocarbon 55:1869–1887. doi:10.2458/azu_js_rc.55.16947

Schmid P (1978) Siedlung und Wirtschaft in den Jahrhunderten vor und nach der Zeitwende im Küstengebiet der südlichen Nordsee. Berichte zur deutschen Landeskunde 52:137–157

Schneeberg HA (1962) Beiheft zur geologisch-bodenkundlichen Karte 1: 5000, Blatt Imsum-Ost. Niedersächsisches Landesamt für Bodenforschung, Hannover

Schoute JFT, Griede JW, Mook WG, Roeleveld W (1981) Radiocarbon dating of vegetation horizons. Geol Mijnb 60:453–459

Schwertmann U (1964) Differenzierung der Eisenoxide des Bodens durch Extraktion mit Ammoniumoxalat-Lösung. J Plant Nutr Soil Sc 105:194–202. doi:10.1002/jpln.3591050303

Streif H (1971) Stratigraphie und Faziesentwicklung im Küstengebiet von Woltzeten in Ostfriesland. Beihefte zum Geologischen Jahrbuch 119, Hannover

Streif H (1990) Das Ostfriesische Küstengebiet. Nordsee, Inseln, Watten und Marschen. Sammlung Geologischer Führer 57. Gebr. Borntraeger, Berlin, Stuttgart

Streif H (2004) Sedimentary record of Pleistocene and Holocene marine inundations along the North Sea coast of lower Saxony, Germany. Quatern Int 112:3–28. doi:10.1016/S1040-6182(03)00062-4

Tamm O (1932) Über die Oxalat-Methode in der chemischen Bodenanalyse. Medd Stat Skogsforsoks Stockholm 27:1–20

Vink A, Steffen H, Reinhardt L, Kaufmann G (2007) Holocene relative sea-level change, isostatic subsidence and the radial viscosity of the mantle of Northwest Europe (Belgium, the Netherlands, Germany, southern North Sea). Quaternary Sci Rev 26:3249–3275. doi:10.1016/j.quascirev.2007.07.014

Wartenberg W, Vött A, Freund H, Hadler H, Freche M, Willershäuser T, Schnaidt S, Fischer P, Obrocki L (2013) Evidence of isochronic transgressive surface within the Jade Bay tidal flat area, southern German North Sea coast – Holocene event horizons of regional interest. Z Geomorphol (Suppl) 57(4):229–256. doi:10.1127/0372-8854/2013/S-00150

WoRMS Editorial Board (2016) World Register of Marine Species. URL: http://www.marinespecies.org. Accessed 12 Jul 2016. doi:10.14284/170

– Online Supplement –

Fossil bog soils (‘*dwog* horizons’) and their relation to Holocene coastal changes in the Jade Weser region, southern North Sea, Germany

Journal of Coastal Conservation

Juliane Scheder[1,2] • Max Engel[2] • Friederike Bungenstock[1] • Anna Pint[2] •
Annette Siegmüller[1] • Stephan Schwank[1] • Helmut Brückner[2]

[1] Lower Saxony Institute for Historical Coastal Research, Viktoriastraße 26/28, 26382 Wilhelmshaven, Germany

[2] Institute of Geography, University of Cologne, Albertus-Magnus-Platz, 50923 Köln (Cologne), Germany

Juliane Scheder: scheder@nihk.de

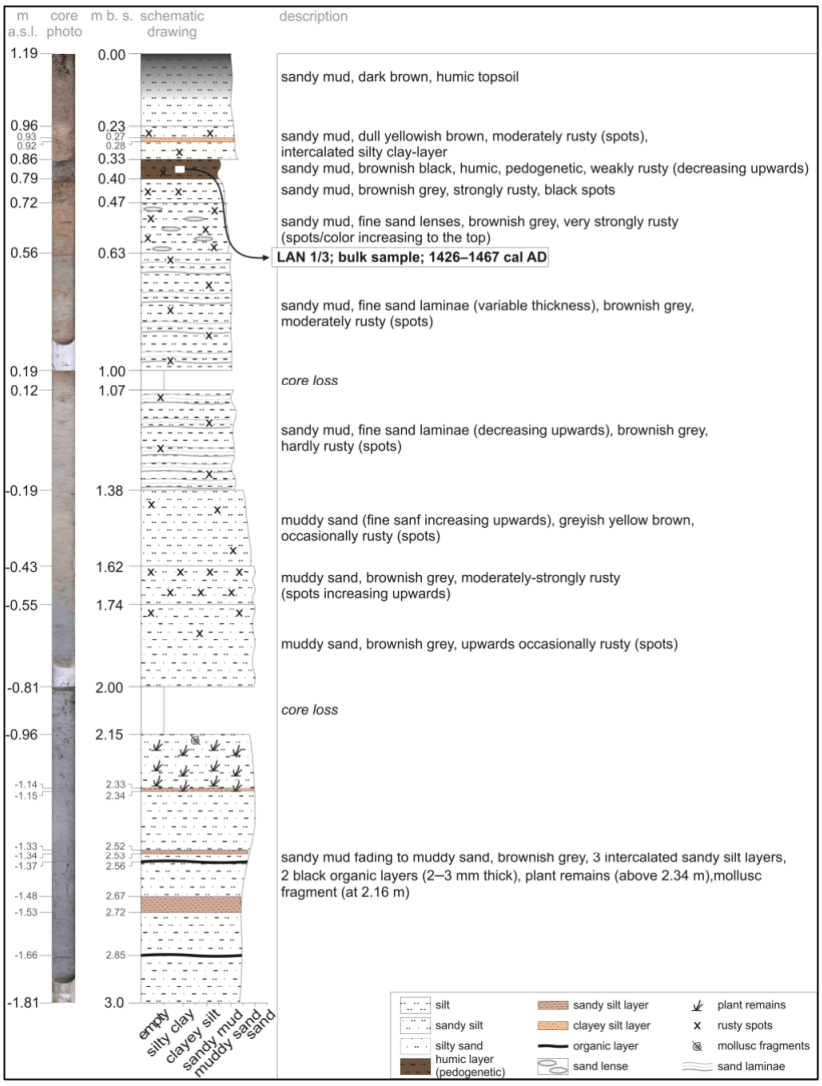

Fig. 12 Core photo, schematic drawing and core description of LAN 1. Depths are given in m b.s. (metres below surface) as well as m a.s.l. (metres below present mean sea level)

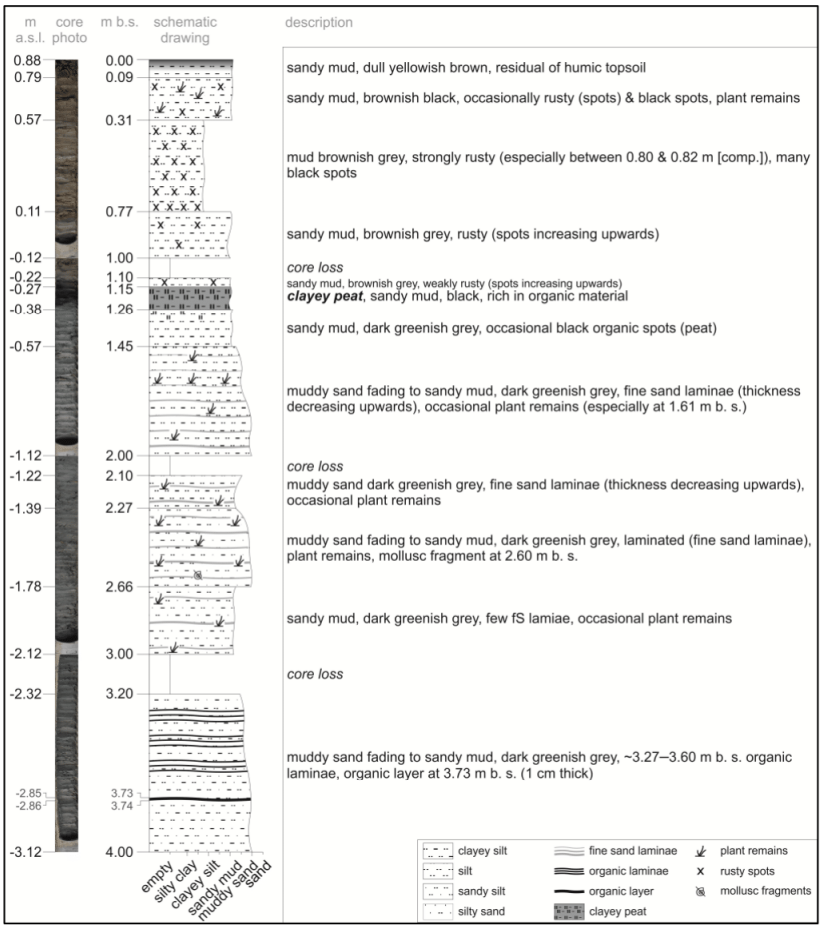

Fig. 13 Core photo, schematic drawing and core description of LAN 2. Depths are given in m b.s. as well as m a.s.l.

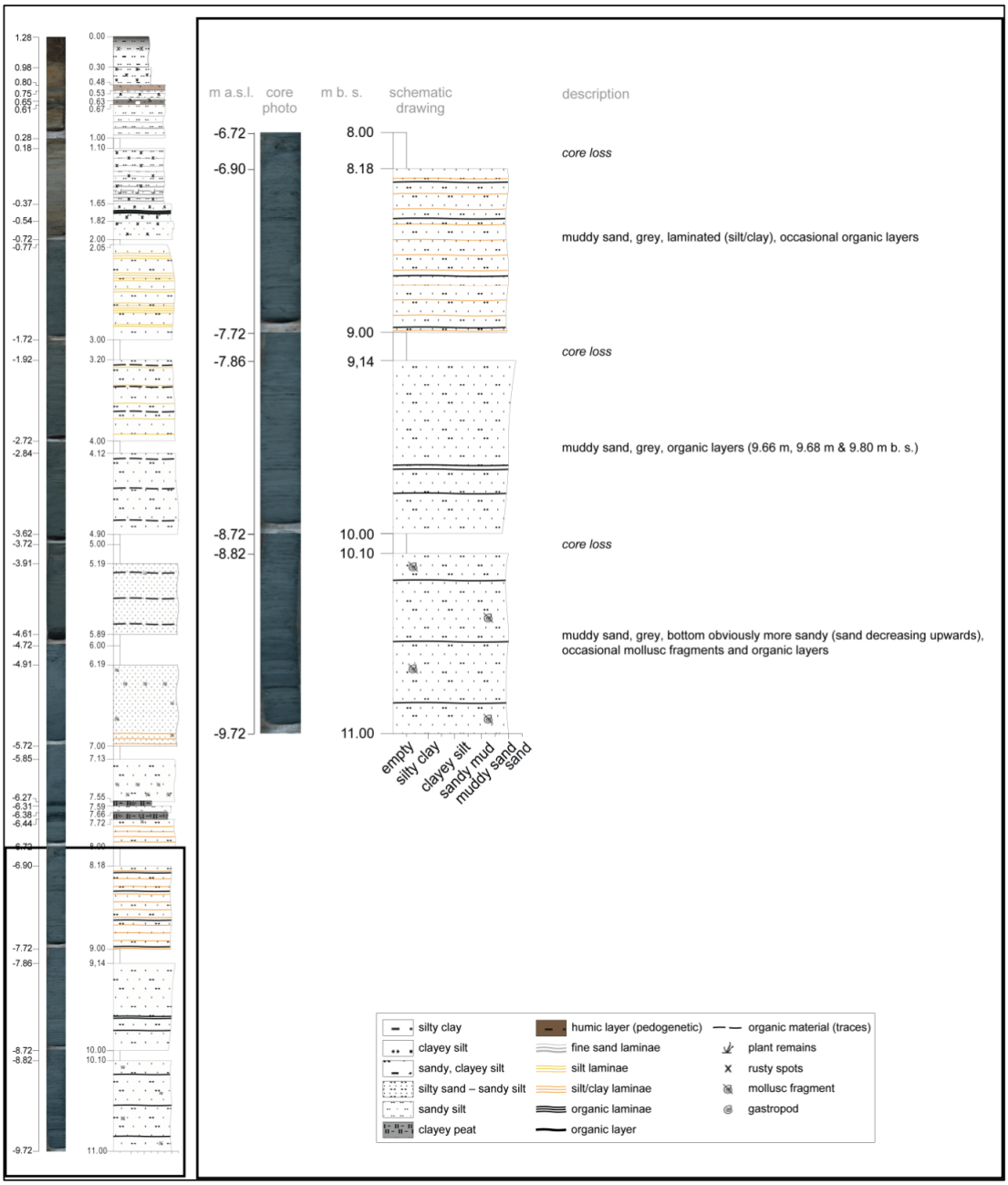

Fig. 14 Core photo, schematic drawing and core description of LAN 3. Depths are given in m b.s. as well as m a.s.l. Part 1 of the core description, metres 11–8 (Parts 2 and 3 in Figs. 14 and 15)

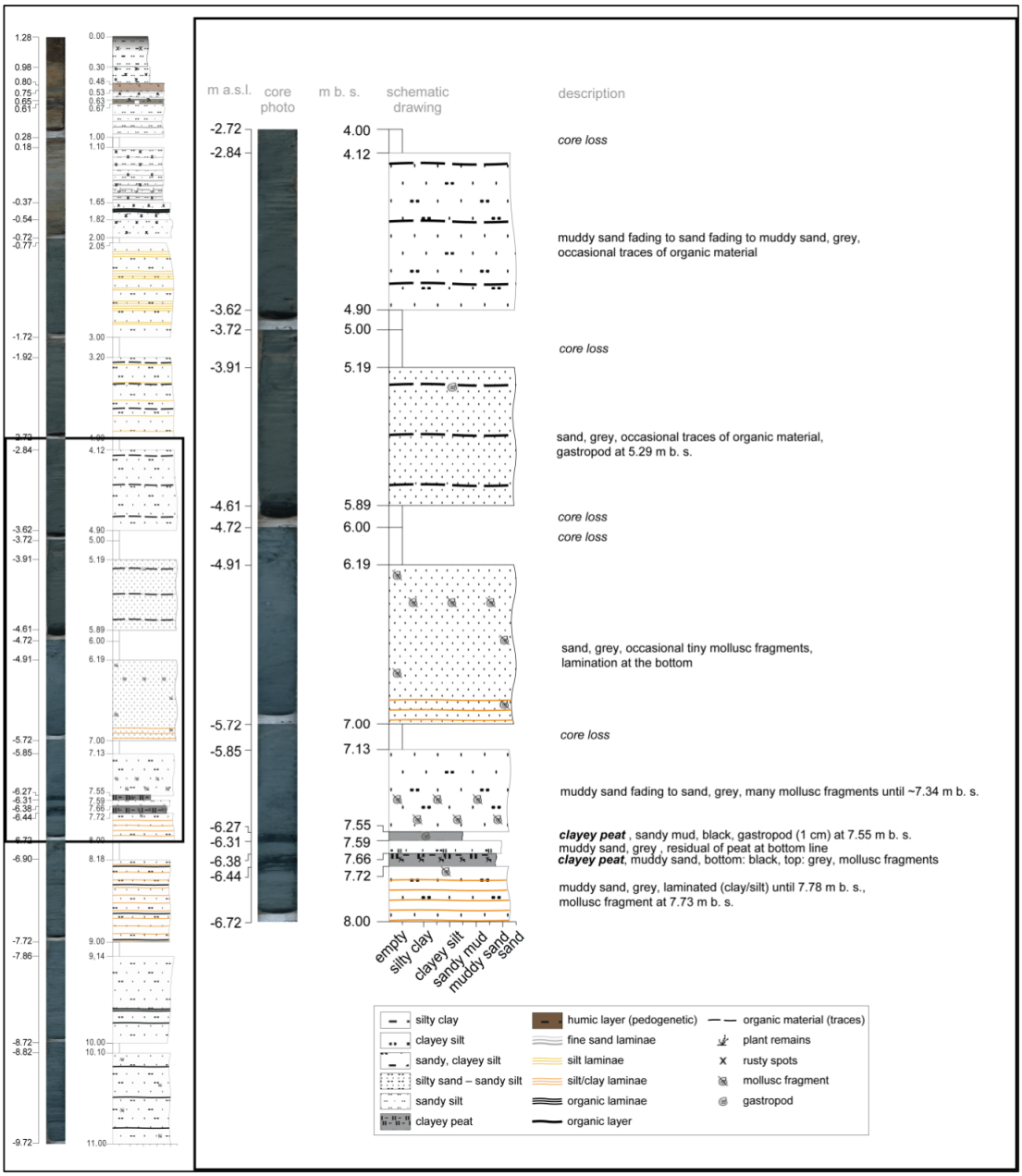

Fig. 15 Core photo, schematic drawing and core description of LAN 3. Depths are given in m b.s. as well as m a.s.l. Part 2 of the core description, metres 8–4 (Parts 1 and 3 in Figs. 13 and 15)

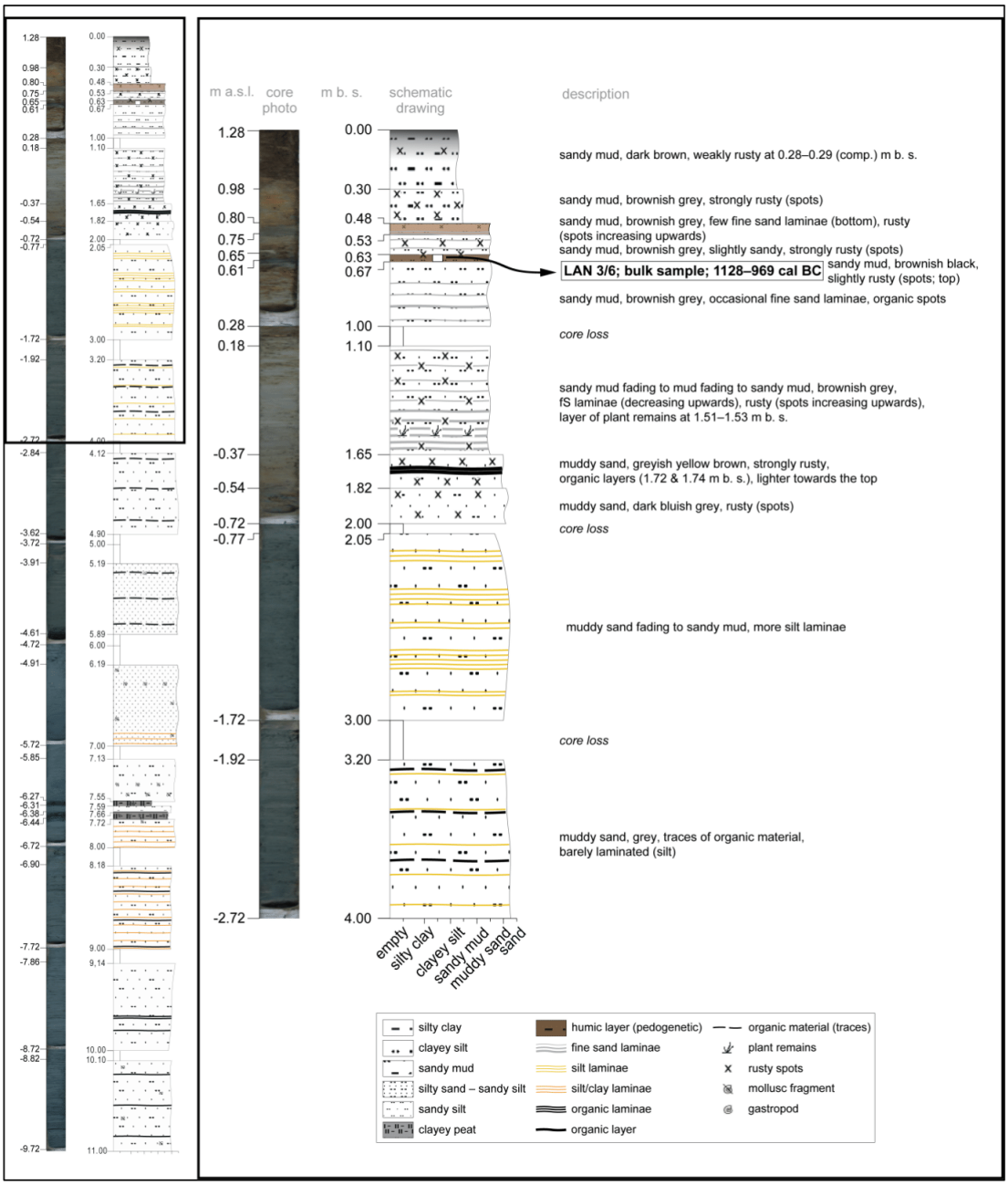

Fig. 16 Core photo, schematic drawing and core description of LAN 3. Depths are given in m b.s. as well as m a.s.l. Part 3 of the core description, metres 4–0 (Parts 1 and 2 in Figs. 13 and 14)

Table 4 Abundant foraminiferal species and their ecological characteristics (for visual information see Fig. 6 [main article])

Ammonia tepida (Cushman, 1926)					
Order	**Suborder**	**Superfamily**	**Family**	**Subfamily**	**Genus**
Foraminifera	Rotaliina	Rotaliacea	Rotaliidae	Ammoniinae	*Ammonia*
Ecology: Sheltered, shallow marine, often slightly brackish, intertidal environments, may extend onto low and mid marshes (Murray 2006).					

Cribroelphidium williamsoni (Haynes, 1973)					
Order	**Suborder**	**Superfamily**	**Family**	**Subfamily**	**Genus**
Foraminifera	Rotaliina	Rotaliacea	Elphidiidae	Elphidiinae	*Cribroelphidium*
Ecology: Shallow parts of intertidal mud flats, estuaries, lagoons and sea-bound parts of salt marshes (Murray 2006); mainly less than 20 cm water depth, found in 0.1 to 0.5 m water depth and between 8 and 19 psu on mud to medium sand, also within the phytal zone, brackish water species, mainly temperate climate (Lehmann, 2000)					

Haynesina germanica (Ehrenberg, 1840)					
Order	**Suborder**	**Superfamily**	**Family**	**Subfamily**	**Genus**
Foraminifera	Rotaliina	Nonionacea	Nonionidae	Nonioninae	*Haynesina*
Ecology: Middle and low marshes, tidal flats (Horton and Edwards 2006); shallow marine, intertidal environments, may extend onto low and mid marshes (Murray 2006)					

Jadammina macrescens (Brady, 1870)				
Order	**Suborder**	**Family**	**Subfamily**	**Genus**
Foraminifera	Trochamminina	Trochamminina	Jadamminina	*Jadammina*
Ecology: Euryhaline species, land-bound parts of salt marshes, also on sand flats, in 0.1 to 0.3 m water depth and 8.5 to 19 psu on mud to medium sand and within the phytal zone of the southern Baltic; extremely euryhaline (Lehmann 2000); controlled more by substrate than salinity (Murray 2006)				

Triloculina oblonga (Montagu, 1803)					
Order	**Suborder**	**Superfamily**	**Family**	**Subfamily**	**Genus**
Foraminifera	Miliolina	Miliolacea	Hauerinidae	Miliolinellinae	*Triloculina*
Ecology: Salt marshes (Lehmann 2000)					

Trochammina inflata (Montagu, 1808)				
Order	**Suborder**	**Family**	**Subfamily**	**Genus**
Foraminifera	Trochamminina	Trochamminina	Trochamminina	Trochammina
Ecology: Euryhaline brackish water species, shallow water, typical for salt marshes (Lehmann 2000); high and middle marsh environments (Horton and Edwards 2006)				

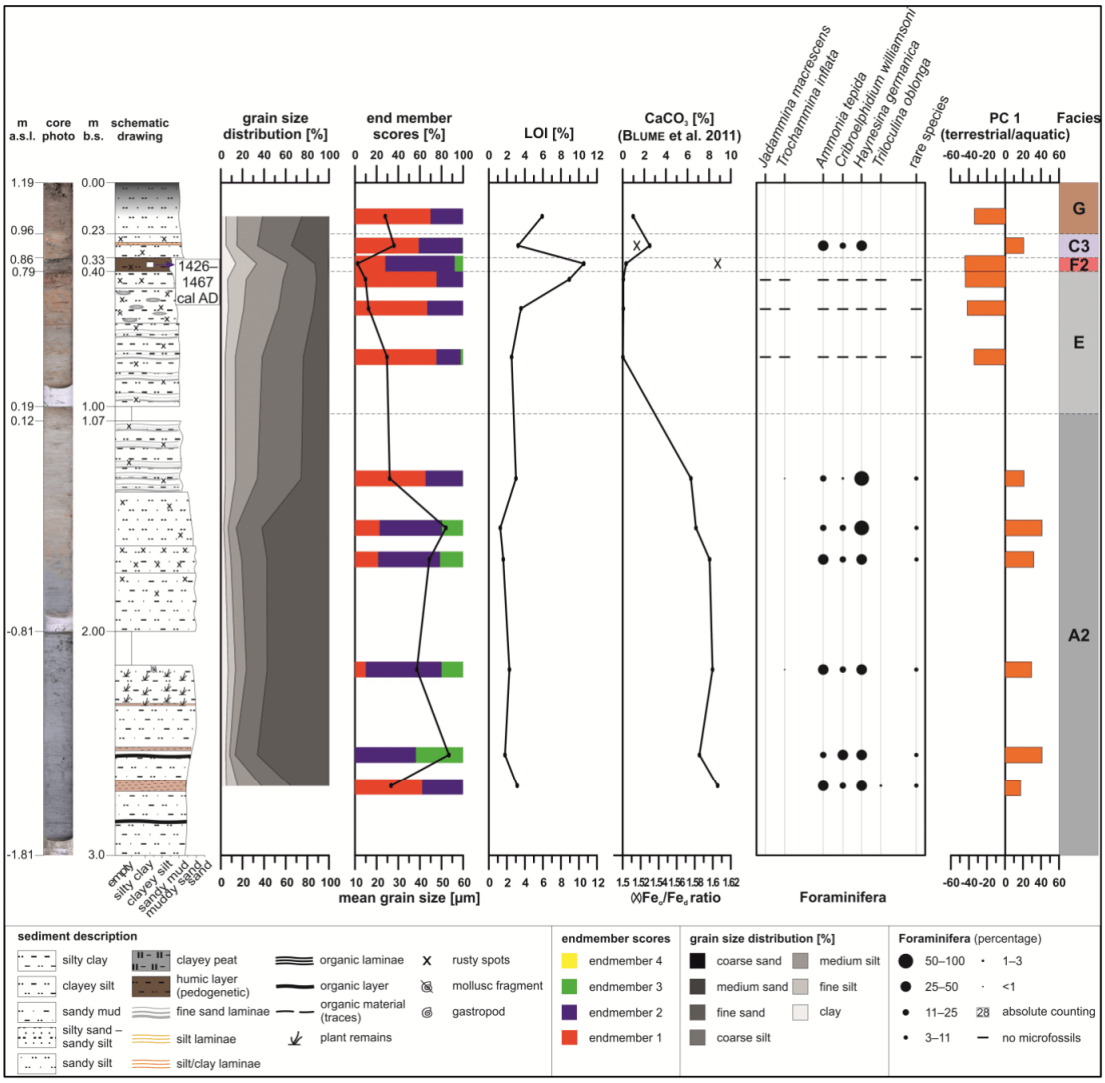

Fig. 17 Sedimentological and foraminiferal data of the complete drilling LAN 1. Depths are given in m b.s. as well as m a.s.l. Identified facies units are presented in the column on the right (see Figs. 19–21 for the used colour key and Fig. 11 [main article] for interpretation)

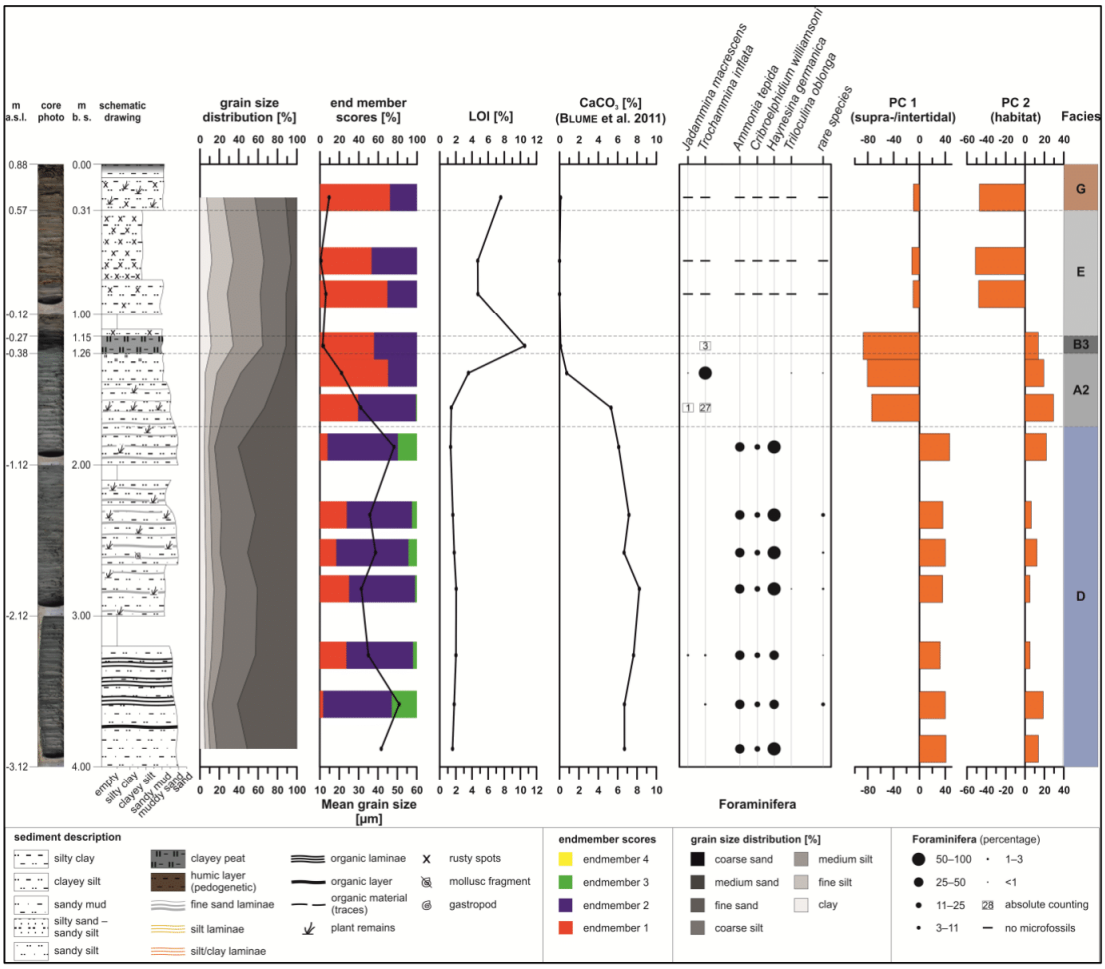

Fig. 18 Sedimentological and foraminiferal data of the complete drilling LAN 2. Depths are given in m b.s. as well as m a.s.l. Identified facies units are presented in the column on the right (see Figs. 19–21 for the used colour key and Fig. 11 [main article] for interpretation)

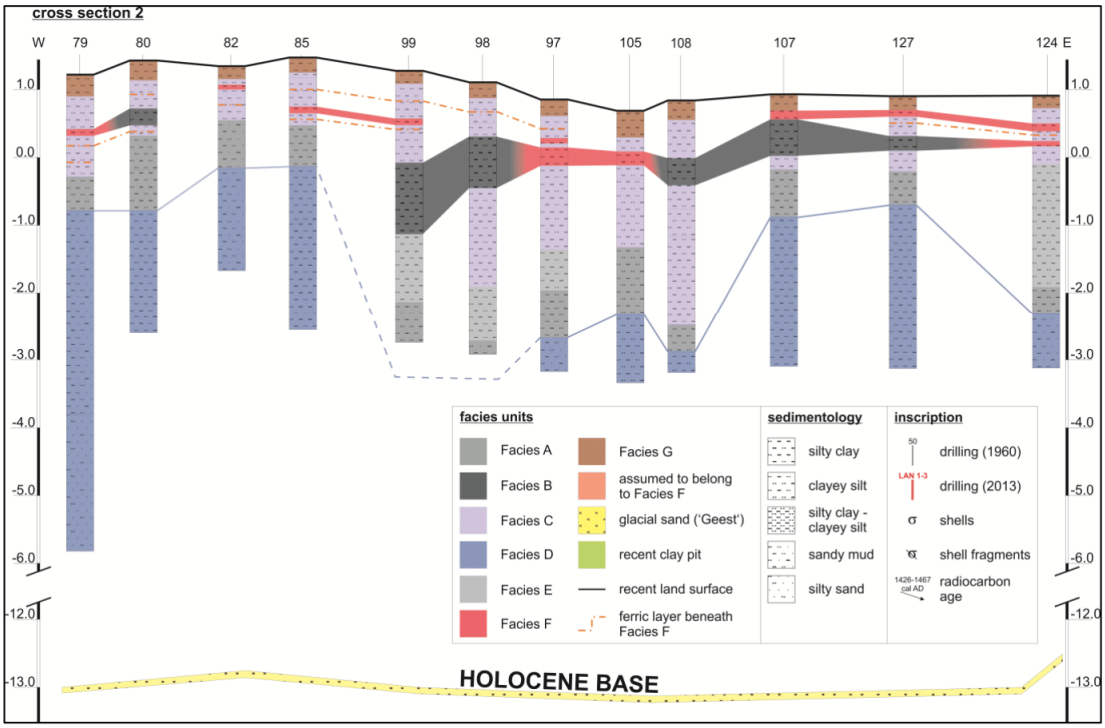

Fig. 19 Cross section 2, situated in the centre of the study area (cf. Figs. 2 and 3). If possible, stratigraphic layers were correlated. The numbers on top are the drilling numbers of 1960. The Holocene base was modelled from the geological coastal map of LBEG (2016). For interpretations of facies units A–G see Fig. 10 (main article)

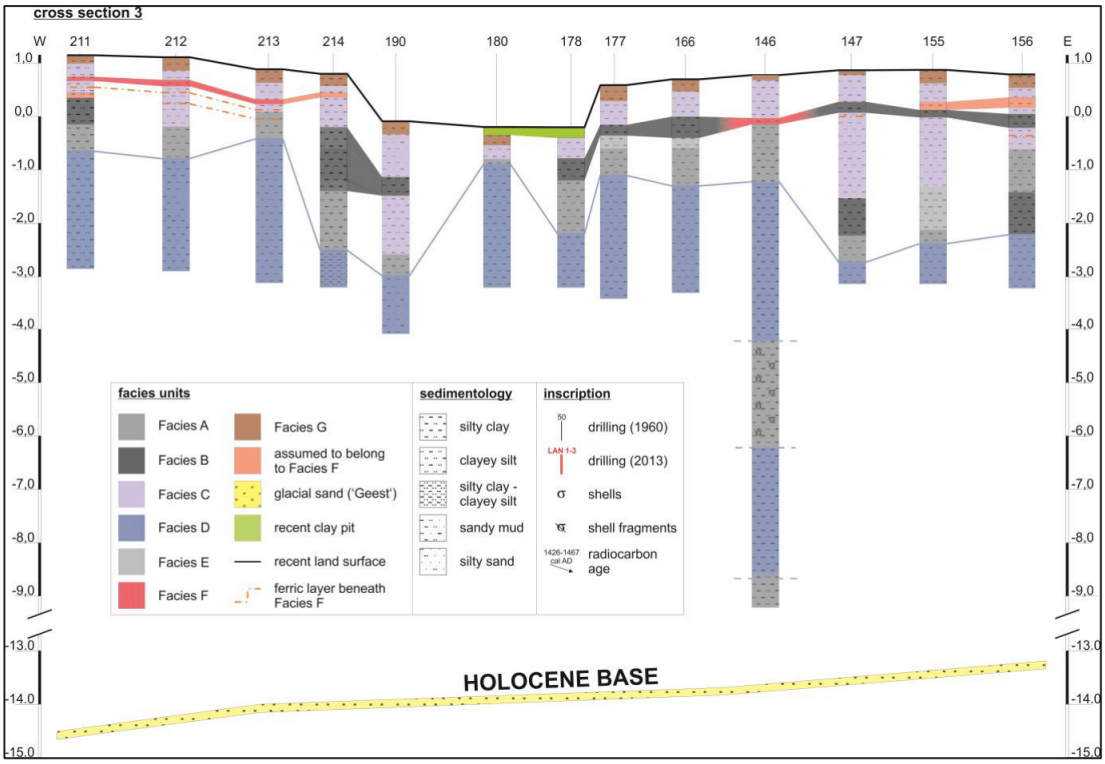

Fig. 20 Cross section 3, situated in the south of the study area (cf. Figs. 2 and 3). If possible, stratigraphic layers were correlated. The numbers on top are the drilling numbers of 1960. The Holocene base was modelled from the geological coastal map of LBEG (2016). For interpretations of facies units A–G see Fig. 10 (main article)

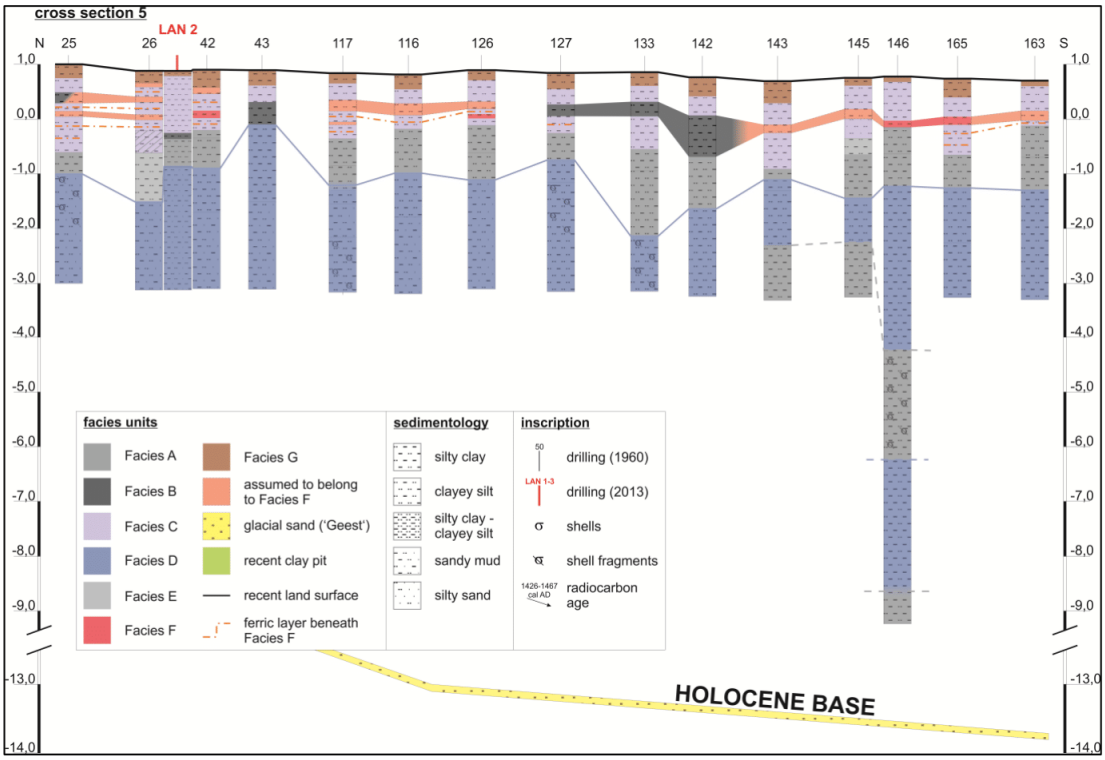

Fig. 21 Cross section 5, situated in the east of the study area (cf. Figs. 2 and 3). The section includes one of the new drillings (LAN 2). If possible, stratigraphic layers were correlated. The numbers on top are the drilling numbers of 1960 and 2013. The Holocene base was modelled from the geological coastal map of LBEG (2016). For interpretations of facies units A–G see Fig. 10 (main article)

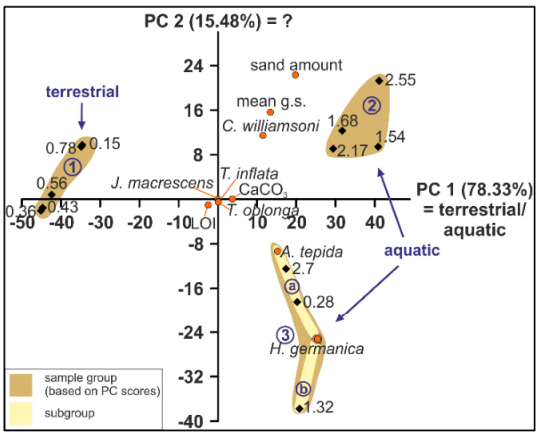

Fig. 22 PCA biplot of the sedimentological and foraminiferal data of LAN 1. Samples are represented by black rhombs (including sample depth in m b.s.) and variables by orange circles. Blue numbers represent groups identified by the PCA of LAN 1. For the depth profile of PC 1 see Fig. 17 and for the used data see Table 5

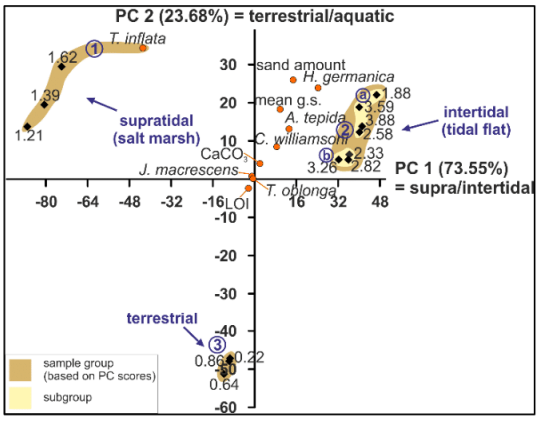

Fig. 23 PCA biplot of the sedimentological and foraminiferal data of LAN 2. Samples are represented by black rhombs (including sample depth in m b.s.) and variables by orange circles. Blue numbers represent groups identified by the PCA of LAN 2. For the depth profiles of PC 1 and 2 see Fig. 18 and for the used data see Table 6

Table 5 Compilation of the data used for PCA of LAN 1 (for the diagram see Fig. 22).

Sample ID	Mean depth [m b.s.]	*Jadammina macrescens* [%]	*Trochammina inflata* [%]	*Ammonia tepida* [%]	*Cribroelphidium williamsoni* [%]	*Haynesina germanica* [%]	*Triloculina oblonga* [%]	mean grain size [µm]	sand amount [%]	LOI [%]	CaCO3 [%]
LAN 1/1	0.15	0.00	0.00	0.00	0.00	0.00	0.00	23.99	24.97	5.92	0.97
LAN 1/2	0.28	0.00	0.00	44.44	11.11	44.44	0.00	28.05	34.65	3.25	2.51
LAN 1/3	0.36	0.00	0.00	0.00	0.00	0.00	0.00	11.21	12.98	10.54	0.32
LAN 1/4	0.43	0.00	0.00	0.00	0.00	0.00	0.00	14.85	11.29	8.93	0.06
LAN 1/5	0.56	0.00	0.00	0.00	0.00	0.00	0.00	16.27	14.27	3.57	0.06
LAN 1/6	0.78	0.00	0.00	0.00	0.00	0.00	0.00	24.78	23.67	2.53	0.03
LAN 1/7	1.32	0.00	0.92	21.10	2.75	70.64	0.00	26.06	25.54	3.01	6.31
LAN 1/8	1.54	0.00	0.00	23.73	19.49	50.85	0.00	52.01	61.98	1.27	6.78
LAN 1/9	1.68	0.00	0.00	33.33	24.32	36.04	0.00	44.38	57.27	1.60	8.04
LAN 1/10	2.17	0.00	0.90	32.43	22.52	36.94	0.00	38.60	57.14	2.28	8.31
LAN 1/11	2.55	0.00	0.00	17.69	32.65	44.90	0.00	53.41	66.21	1.79	7.10
LAN 1/12	2.69	0.00	0.00	29.25	19.81	44.34	2.68	26.66	35.39	3.15	8.79

Table 6 Compilation of the data used for PCA of LAN 2 (for the diagram see Fig. 23)

Sample ID	Mean depth [m b.s.]	*Jadammina macrescens* [%]	*Trochammina inflata* [%]	*Ammonia tepida* [%]	*Cribroelphidium williamsoni* [%]	*Haynesina germanica* [%]	*Triloculina oblonga* [%]	mean grain size [µm]	sand amount [%]	LOI [%]	CaCO3 [%]
LAN 2/1	0.22	0.00	0.00	0.00	0.00	0.00	0.00	14.79	11.72	7.56	0.10
LAN 2/2	0.64	0.00	0.00	0.00	0.00	0.00	0.00	10.32	5.94	4.71	0.00
LAN 2/3	0.86	0.00	0.00	0.00	0.00	0.00	0.00	13.11	11.12	4.73	0.00
LAN 2/4	1.21	0.00	100.00	0.00	0.00	0.00	0.00	11.43	11.27	10.54	0.10
LAN 2/5	1.39	0.94	97.17	0.00	0.00	0.00	0.94	21.20	19.44	3.56	0.74
LAN 2/6	1.62	3.57	96.43	0.00	0.00	0.00	0.00	31.14	33.54	1.43	5.32
LAN 2/7	1.88	0.00	0.00	22.22	17.09	60.68	0.00	48.29	60.57	1.35	6.11
LAN 2/8	2.33	0.00	0.00	25.66	18.58	51.33	0.00	35.80	42.58	1.63	7.16
LAN 2/9	2.58	0.00	0.00	29.06	15.38	52.99	0.00	38.76	50.80	1.80	6.66
LAN 2/10	2.82	0.00	0.00	27.03	17.12	53.15	0.90	31.42	40.72	2.04	8.24
LAN 2/11	3.26	1.94	1.94	29.13	24.27	41.75	0.00	35.05	42.82	2.01	7.64
LAN 2/12	3.59	0.00	1.90	34.29	20.00	40.00	0.00	50.96	61.28	1.79	6.70
LAN 2/13	3.88	0.00	0.00	29.70	17.82	52.48	0.00	41.69	51.22	1.59	6.71

Table 7 Compilation of the data used for PCA of LAN 3 (for the diagram see Fig. 9 [paper])

Sample ID	Mean depth [m b.s.]	*Jadammina macrescens* [%]	*Trochammina inflata* [%]	*Ammonia tepida* [%]	*Cribroelphidium williamsoni* [%]	*Haynesina germanica* [%]	*Triloculina oblonga* [%]	mean grain size [µm]	sand amount [%]	LOI [%]	CaCO3 [%]
LAN 3/1	0.08	0.00	0.00	0.00	0.00	0.00	0.00	15.71	20.75	8.72	0.00
LAN 3/2	0.28	0.00	0.00	0.00	0.00	0.00	0.00	19.77	24.34	2.98	0.00
LAN 3/3	0.40	0.00	0.00	0.00	0.00	0.00	0.00	22.38	26.14	2.06	0.01
LAN 3/4	0.50	0.00	0.00	0.00	0.00	0.00	0.00	20.60	17.82	2.63	0.02
LAN 3/5	0.59	0.00	0.00	0.00	0.00	0.00	0.00	20.59	17.22	2.26	0.03
LAN 3/6	0.65	0.00	0.00	0.00	0.00	0.00	0.00	22.66	25.39	3.80	0.03
LAN 3/7	0.84	0.00	0.00	0.00	0.00	0.00	0.00	22.57	22.85	2.58	0.10
LAN 3/8	1.20	0.00	0.00	0.00	0.00	0.00	0.00	25.67	26.26	2.41	4.41
LAN 3/9	1.52	0.00	0.00	0.00	0.00	0.00	0.00	15.29	7.88	4.59	7.71

– Continued on next page –

Sample ID	Mean depth [m b.s.]	*Jadammina macrescens* [%]	*Trochammina inflata* [%]	*Ammonia tepida* [%]	*Cribroelphidium williamsoni* [%]	*Haynesina germanica* [%]	*Triloculina oblonga* [%]	mean grain size [µm]	sand amount [%]	LOI [%]	CaCO3 [%]
LAN 3/10	1.57	0.00	0.00	40.34	2.52	56.30	0.00	21.93	17.52	3.15	7.97
LAN 3/11	1.75	1.22	0.00	8.54	13.41	62.20	0.00	53.73	63.14	1.03	8.30
LAN 3/13	2.15	0.00	0.00	24.00	28.00	45.00	0.00	32.17	46.39	2.58	8.57
LAN 3/14	2.46	0.00	0.00	23.36	30.84	42.99	0.00	58.17	72.05	1.26	7.13
LAN 3/15	2.85	0.00	1.79	26.79	19.64	41.96	0.00	54.40	68.09	1.70	8.03
LAN 3/16	3.26	0.00	0.00	29.52	26.67	40.00	0.00	55.59	67.02	1.66	7.94
LAN 3/17	3.71	0.00	0.00	0.00	0.00	0.00	0.00	47.18	59.63	2.34	8.07
LAN 3/18	3.78	0.00	0.00	33.66	18.81	46.53	0.00	67.22	74.83	1.26	9.29
LAN 3/19	4.27	0.00	0.00	34.00	29.00	35.00	1.00	77.08	83.66	0.89	6.51
LAN 3/20	4.54	0.00	0.00	23.29	24.53	49.38	0.31	92.46	90.54	0.48	4.87
LAN 3/21	4.82	0.00	0.00	31.54	30.00	34.62	0.77	85.93	88.73	0.88	8.03
LAN 3/22	5.29	0.00	0.00	37.62	29.70	29.70	0.00	89.81	89.86	0.61	5.77
LAN 3/23	5.73	0.00	0.00	40.38	25.96	29.81	0.96	93.01	89.88	0.57	4.94
LAN 3/24	6.38	0.00	0.00	28.83	33.33	35.14	0.00	94.53	91.47	0.42	4.77
LAN 3/25	6.67	0.00	0.00	34.58	30.84	32.71	0.00	109.06	94.73	0.32	3.54
LAN 3/26	6.87	0.00	0.00	43.27	28.85	25.00	0.00	85.36	84.50	0.74	4.83
LAN 3/27	7.38	0.00	0.00	46.85	29.73	22.52	0.00	97.70	91.46	0.47	4.38
LAN 3/28	7.52	0.00	0.00	42.06	26.17	29.91	0.93	80.67	82.21	1.00	4.93
LAN 3/29	7.57	0.00	0.00	23.01	28.32	46.90	0.00	15.17	16.95	3.92	10.42
LAN 3/30	7.63	0.00	0.00	37.72	31.58	28.95	0.00	72.92	81.21	0.96	6.87
LAN 3/31	7.68	0.00	0.00	33.02	26.42	36.79	0.94	40.38	52.82	2.84	6.32
LAN 3/32	7.74	0.00	0.00	38.68	19.81	38.68	0.00	66.94	75.82	0.86	6.85
LAN 3/33	8.43	0.00	0.00	27.88	17.31	49.04	0.00	38.89	54.56	2.64	8.21
LAN 3/34	8.71	0.00	0.00	35.64	13.86	44.55	0.00	50.14	66.82	2.33	8.51
LAN 3/35	9.25	0.00	0.00	40.57	11.32	45.28	0.94	53.77	71.20	1.54	6.97
LAN 3/36	9.78	0.00	0.00	34.26	19.44	45.37	0.00	36.52	50.20	2.75	8.72
LAN 3/37	10.33	0.00	0.00	37.38	23.36	37.38	0.00	33.70	52.37	2.73	7.47
LAN 3/38	10.75	0.00	0.00	33.33	26.67	38.10	0.00	41.76	60.41	4.50	6.98
LAN 3/39	10.90	0.00	0.00	33.06	22.31	42.98	0.00	51.26	68.71	2.11	8.30

Chapter 3

3 Multi-proxy reconstruction of Holocene paleoenvironments from a sediment core retrieved from the Wadden Sea near Norderney, East Frisia, Germany

Francesca Bulian[a], Dirk Enters[b,a], Frank Schlütz[b], Juliane Scheder[b], Katharina Blume[b], Bernd Zolitschka[a], Felix Bittmann[b]

[a] University of Bremen, Institute of Geography, GEOPOLAR, Celsiusstr. 2, D-28359, Bremen, Germany

[b] Lower Saxony Institute for Historical Coastal Research, Viktoriastraße 26/28, D-26382, Wilhelmshaven, Germany

Abstract

The coastal area of the southern North Sea passed through several stages of development during the Holocene starting with swamps and bogs on Pleistocene sands. These were covered due to the rising sea-level by brackish and intertidal sediments with intercalated peat layers indicating repeated shoreline replacements. Such sedimentary archives are excellent sources for environmental reconstructions and potentially suited to deliver a regional sea-level curve. We analysed a 4.6 m-long sediment core recovered south of the island of Norderney (East Frisia, Germany) using a multiproxy approach. The record comprises a vertical stack of changing sedimentary facies, including a basal peat and a second peat layer intercalated between marine sediments, which provides a sedimentological record of local coastal evolution since 7000 cal. BP. High-resolution stratigraphic, geochemical and paleobiological analyses enables reconstructing environmental variability in response to sea-level changes including a short-lived transgressive-regressive cycle. This took place around 6000 cal. BP and lasted only a few hundred years. Our multiproxy approach demonstrates that the combined analyses of geochemical and biological parameters in concert with statistical evaluation are indispensable for the reconstruction of coastal evolution and short-term sea-level fluctuations.

Keywords

Wadden Sea, Holocene, High-resolution stratigraphy, XRF scanning, Multi-proxy approach, Holocene sea-level rise

Published in *Estuarine, Coastal and Shelf Science* 225 (2019), 106251.
https://doi.org/10.1016/j.ecss.2019.106251

Estuarine, Coastal and Shelf Science 225 (2019) 106251

Contents lists available at ScienceDirect

Estuarine, Coastal and Shelf Science

journal homepage: www.elsevier.com/locate/ecss

Multi-proxy reconstruction of Holocene paleoenvironments from a sediment core retrieved from the Wadden Sea near Norderney, East Frisia, Germany

Francesca Bulian[a,*], Dirk Enters[b,a], Frank Schlütz[b], Juliane Scheder[b], Katharina Blume[b], Bernd Zolitschka[a], Felix Bittmann[b]

[a] University of Bremen, Institute of Geography, GEOPOLAR, Celsiusstr. 2, D-28359, Bremen, Germany
[b] Lower Saxony Institute for Historical Coastal Research, Viktoriastraße 26/28, D-26382, Wilhelmshaven, Germany

ARTICLE INFO

Keywords:
Wadden sea
Holocene
High-resolution stratigraphy
XRF scanning
Multi-proxy approach
Holocene sea-level rise

ABSTRACT

The coastal area of the southern North Sea passed through several stages of development during the Holocene starting with swamps and bogs on Pleistocene sands. These were covered due to the rising sea-level by brackish and intertidal sediments with intercalated peat layers indicating repeated shoreline replacements. Such sedimentary archives are excellent sources for environmental reconstructions and potentially suited to deliver a regional sea-level curve. We analysed a 4.6 m-long sediment core recovered south of the island of Norderney (East Frisia, Germany) using a multiproxy approach. The record comprises a vertical stack of changing sedimentary facies, including a basal peat and a second peat layer intercalated between marine sediments, which provides a sedimentological record of local coastal evolution since 7000 cal. BP. High-resolution stratigraphic, geochemical and paleobiological analyses enables reconstructing environmental variability in response to sea-level changes including a short-lived transgressive-regressive cycle. This took place around 6000 cal. BP and lasted only a few hundred years. Our multiproxy approach demonstrates that the combined analyses of geochemical and biological parameters in concert with statistical evaluation are indispensable for the reconstruction of coastal evolution and short-term sea-level fluctuations.

1. Introduction

Global climate warming after the Last Glacial Maximum started around 18,000 cal. (calibrated) BP and was accompanied by a more or less continuous rise in sea level. Streif (2004) proposed a general scheme of the sea-level history for the southern North Sea, highlighting three major periods. The first period lasted ca. 6500 years (18,000–11,500 cal. BP), during which the sea level rose to 70 m below present-day sea level (bsl) from its low stand at about 130 m bsl. Marine transgression started with erosional processes, followed by re-deposition of clastic glacial and marine sediments directly above terrestrial, glacio-fluvial and glacial deposits in the North Sea basin (Streif, 2004). The second period of sea–level rise started with Melt Water Pulse-1B (MWP-1B; Lambeck et al., 2014) at around 11,500–11,300 cal. BP and ended at ca. 8000 cal. BP encompassing the Early Holocene. During this period, the sea level rose to 25 m bsl accompanied by a rapid, unidirectional landward shift of the shoreline. Mostly, a thin peat layer has formed before being covered by marine sediments. The average rate of sea-level rise was about 2.1 m per century compared to 1.5 m per century before (Streif, 1990). The progressive inundation translocated eroded glacial deposits and Holocene marine sediments landwards leading to a wedge-shaped sedimentary body of Holocene coastal sediments (Streif, 2004).

The evolution of today's Wadden Sea back-barrier tidal flats and the configuration of the present-day coastline started around 8000 cal. BP after the North Sea basin was successively inundated by the continuing sea-level rise (Vos and van Kesteren, 2000; van der Spek, 2018). This shallow intertidal zone, bordered by barrier islands to the open sea and by the mainland coast landward, represents a highly dynamic depositional setting mainly affected by tidal energy fluxes (Flemming, 2012). The marine ingression into the present-day Wadden Sea area obstructed the drainage of the hinterland, which triggered a rise of the groundwater level and a large scale paludification (Behre, 2004) forming a belt of peatlands ("basal peat") that continuously migrated landwards. Since approximately 6800 cal. BP the sea-level rise slowed down to 0.2–0.3 m per century (Vos and van Kesteren, 2000; Bazelmans et al., 2012; van der Spek, 2018). At the same time, crustal adjustment in response to a decrease of glacial ice pressure on Scandinavia and peat consolidation

* Corresponding author. University of Salamanca, Department of Geology, Plaza de los Caidos s/n, 37008, Salamanca, Spain.
E-mail addresses: fra.bulian@usal.es (F. Bulian), enters@uni-bremen.de (D. Enters), schluetz@nihk.de (F. Schlütz), schederj@uni-koeln.de (J. Scheder), blume@nihk.de (K. Blume), zoli@uni-bremen.de (B. Zolitschka), bittmann@nihk.de (F. Bittmann).

https://doi.org/10.1016/j.ecss.2019.106251
Received 15 February 2019; Received in revised form 7 June 2019; Accepted 13 June 2019
Available online 20 June 2019
0272-7714/ © 2019 Elsevier Ltd. All rights reserved.

caused the land to sink gradually by about 0.1 m per century (Vink et al., 2007). During this process, the lower courses of the rivers turned into micro tidal estuaries (created as a consequence of sea-level ingression into the river mouths and not due to tides; Davis and Flemming, 1995; Streif, 2002) and the peatlands were covered by tidal flat deposits (Freund et al., 2004). However, the Holocene transgression did not advance continuously, since it was interrupted by repeated periods of regression (Behre, 2007). This is documented by peat layers intercalated into silty and clayey tidal sediments (Freund et al., 2004) as well as by formation of thin humic soil horizons (cf. Streif, 2004; Scheder et al., 2018). A particularly favourable period for such intercalated peat layer formation occurred between 5000 and 4800 cal. BP ("Middle Peat") and between 3500 and 3000 cal. BP. A further regressional period dated to ca. 2000 cal. BP (Streif, 1990; Behre, 2004) caused widespread soil-formation and the most recent peat generation at the transition to uplands.

However, only few studies have investigated the long-term evolution of the North Sea and its coastal area (e.g. Behre, 2004; Bungenstock and Schäfer, 2009; Meijles et al., 2018) by relying not only on stratigraphic interpretations of sediment cores but also on combining radiocarbon ages, pollen and plant macrofossils, diatoms, foraminifera and geochemical data. The study presented here has two main objectives: (1) reconstructing the changing terrestrial and marine Holocene paleoenvironments at high-temporal resolution using a multi-proxy approach and (2) providing new insights into the relationship between the Wadden Sea stratigraphy and general Holocene sea-level fluctuations. Our results, even if based on a single core study, contribute to recent efforts to gain better knowledge about potential human settlement sites in the Wadden Sea during prehistoric time periods (e.g. Karle and Goldhammer, 2018) and will also improve our understanding of how coastal wetlands have responded to past sea-level changes, which is mandatory to predict reliable future scenarios.

2. Study site, materials and methods

The study site is located in the back-barrier area of the East Frisian Islands in a 4-6 m-deep tidal channel branching from the Juist-Norderney tidal inlet, northeast of the river Ems estuary (Fig. 1B). The coring site is characterized by semidiurnal tides with a mean tidal range of 2.4 m (± 0.7 m due to neap and spring tides; Jacobs and De Batist, 1996).

2.1. Coring

Sediment core VVC 17 was obtained on 21/09/2016 using a 5 m-long Vibracorer (VKG-6) from the research vessel Burchana (operated by *Niedersächsischer Landesbetrieb für Wasserwirtschaft, Küsten und Naturschutz* - NLWKN, Norderney research station) south of the barrier island of Norderney (53°40′27.01″ N, 7° 8′3.06″ E, Fig. 1). The sediment surface of VVC 17 is 3.75 m bsl NHN (Normalhöhennull), referenced to the Amsterdam gauge. After drilling, the 455.5 cm long core was cut into four sections of 101.5, 120, 120 and 114 cm length.

2.2. Laboratory analyses

2.2.1. Core description, smear slides and subsampling

After splitting the cores lengthwise, the archive half was photographed and stored at 4 °C in a cold room at the University of Bremen. The working half was described macroscopically, including sediment-type and structures, colour, accessory materials (e.g. fossils and plant remains), organic horizons, type of contacts between layers and carbonate content (test with 10% HCl). Visual description was complemented by microscopic inspection of smear slides from selected depths. In total, 44 smear slides were taken (every ~10 cm), which allowed a rapid identification of sediment components such as microfossils or organic matter and to evaluate form and size of mineral grains.

2.2.2. Granulometry

In order to quantify the grain size distribution, 85 samples were taken along the working half following lithological criteria. No samples were taken from peat layers. First, 0.5–1 g of clayey and 2–5 g of sandy sediments were treated with hydrogen peroxide (H_2O_2; 30%) to destroy organic matter, then decalcified with hydrochloric acid (HCl; 10%) and treated with sodium hydroxide (NaOH; 20%) in order to remove biogenic silica. The samples were then dispersed with 20 ml of Calgon (37.5 g/L $NaPO_3$ + 7.94 g/L Na_2CO_3) and placed overnight on a shaking platform. All samples were analysed by laser diffraction using a Coulter LS 200 instrument capable of measuring the particle range 0.02–2000 µm. The grain size scale used is a modified Udden–Wentworth scale implemented in the software package GRADISTAT (Blott and Pye, 2001).

2.2.3. XRF core-scanning

All sections were scanned using the ITRAX XRF core-scanner (Cox Analytical Systems) for the detection of major and trace elements using a Mo tube with a step size of 1 mm and an acquisition time of 10 s. Tube settings were kept constant for all sections at 60 kV and 40 mA (except for core section 2 with 45 mA). Elements with count rates lower than 15 cps were discarded.

In order to account for matrix differences (Weltje and Tjallingii, 2008), XRF scanning data were normalized by Mo-coh (coherent scatter at the same energy as tube anode radiation) and element-log ratios were calculated. The elemental data sets were smoothed using a seven-point moving average to improve data visualization.

A principal component analysis (PCA) was performed on selected elements from the normalized dataset using R (R Development Core Team, 2008). Logarithmic transformations of data were necessary to achieve a normal distribution. The final dataset consisted of 14 variables: 13 elements and the value of the ratio between incoherent (Compton) and coherent (Raleigh) X-ray scatter intensities from the X-ray tube (inc/coh), which was used as an indicator for organic matter content (Ohlendorf et al., 2015). Other parameters were not used for PCA because of the considerably lower number of datapoints. Nevertheless, TOC data were correlated with inc/coh in order to verify the dependence between both parameters and to document the applicability of the ratio as indicator of organic matter.

In addition, a Bartington point sensor (MS2F) mounted on an automatic core logging system was used to obtain a high-resolution record of bulk magnetic susceptibility of the split core sections.

2.2.4. Carbon, nitrogen and sulphur analyses

For geochemical analyses (CNS) 176 (1 cm-thick) discrete samples were taken with trimmed plastic syringes at 4 cm resolution in minerogenic sediments and at 2 cm resolution in peat units. The samples were freeze-dried for at least 48 h using a Steris Lyovac GT2 freeze-drier. Finally, the samples were homogenised by grounding with a pestle in an agate mortar.

Determination of total carbon (TC), total nitrogen (TN) and total sulphur (TS) was carried out with an Euro EA – CHNSO Elemental Analyser. Sample amounts of 10–20 mg were analysed using tin capsules and vanadium pentoxide (V_2O_5) as catalyst. For analyses of total organic carbon (TOC), silver capsules were used without vanadium pentoxide. Inorganic carbon (carbonates) were then destroyed with increasingly stronger HCl (3% up to 20%) in order to measure TOC. The amount of total inorganic carbon (TIC) was calculated as difference between TC and TOC following the equation: TIC = TC-TOC. However, a reliable determination of TIC was impossible in peat units containing more than 30% TC, since the inaccuracies of TC and TOC determinations were larger than the expected TIC concentration, resulting in negative or unrealistic high TIC values. Preliminary XRD analyses and the lack of reaction with HCl confirm that no carbonates are present in

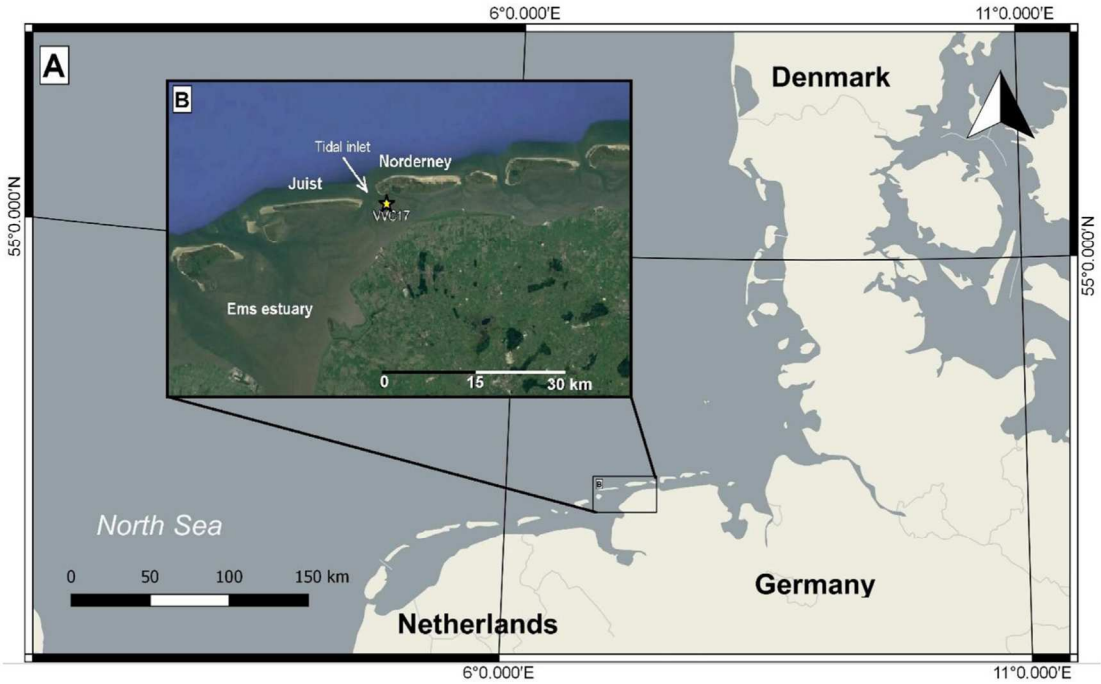

Fig. 1. a) Regional overview of the Wadden Sea (Quantum Gis 2. 18. 9), b) VVC 17 core location with respect to main geomorphological features (Google Earth Pro, 2017) and coring site marked by a yellow star. (For interpretation of the references to colour in this figure legend, the reader is referred to the Web version of this article.)

the peat samples.

The C/N ratio has been calculated as weight ratio according to the equation C/N = TOC/TN (C/N = TC/TN for peat units), which is commonly used in back-barrier environments as an indicator of the source of sediment organic matter (Fujine, 2008; Armynot du Châtelet et al., 2009).

2.2.5. Palynology

Pollen and non-pollen palynomorphs (NPP: fungal and other spores, algae, zoological remains etc.) were studied to reconstruct the regional palaeoecological conditions and local changes. Samples of 1 ml were treated with potassium hydroxide (KOH), hydrochloric acid (HCl), hydrofluoric acid (HF; ~40%) and acetolysis including the addition of *Lycopodium* spores as exotic marker to calculate pollen concentrations. Ultrasonic sieving removed particles < 5 μm before mounting in Glycerol and studying with a light microscope (400x, 1000x oil emersion and phase contrast). Until now 23 samples are preliminarily analysed with a total of about 80 pollen taxa and 50 NPP types. The identification is based on published references (Beug, 2004; van Geel and Aptroot, 2006) as well as on personal and institutional collections. For comparison with the existing literature, all percentage values of pollen and NPP refer to the tree pollen sum calculated without shrubs (*Corylus*, *Myrica*, Ericaceae). The pollen diagram includes selected taxa arranged in ecological groups and is divided into five local pollen zones (A-E) based on changes in taxa abundance and sedimentology.

2.2.6. Diatoms

For the analysis of subfossil diatoms, 60 samples were taken in 4–32 cm intervals according to the lithology. Samples were treated with hydrogen peroxide (H_2O_2) and HCl (Kalbe and Werner, 1974), mounted on slides using Naphrax and subsequently counted up to 500 valves using a Zeiss Axioplan microscope (oil immersion Plan-Apochromat lens, magnification 1000×, numerical aperture 1.4). The determination of diatom species follows Krammer & Lange-Bertalot (1986–1991), Lange-Bertalot et al. (2000) and the database of the Leibniz Institute for Baltic Sea Research, Warnemünde. For the reconstruction of paleosalinities, a salinity index was calculated according to Ziemann (1971) and Ziemann and Schulz (1999). A simplified approach was used classifying the species into three salinity classes (Lange-Bertalot et al., 2000): oligohalob (−30 < H < 30), mesohalob (30 < H < 70) and polyhalob (H > 70).

$$H = \frac{\sum h_H - \sum h_x}{\sum h} * 100$$

H = salinity index (Halobienindex)
h_H = total abundance of polyhalob, mesohalob and oligohalob species
h_x = total abundance of halophob species
h = total abundance of all identified taxa

2.2.7. Foraminifera and ostracoda

Species assemblages of foraminifera and ostracoda were analysed for a total of 15 samples, taken in different intervals according to lithological criteria. Due to their varying preferences of particular habitats, these species provide valuable information for reconstructing sedimentary environments (Frenzel and Boomer, 2005; Murray, 2006). Samples were mixed with water and shaken overnight in an agitation device. Afterwards they were washed over sieves with mesh sizes of 63 and 100 μm. The remaining sediment of the 63 μm fraction was air-dried for about 24 h and stored for archive purposes (Scheder et al., 2018) while the 100 μm fraction remained wet for analyses as recommended for highly organic coastal sediments (e.g. Müller-Navarra et al., 2016). Counting and species identification was performed using a stereo microscope. Where possible, at least 100 individuals were counted for each sample in order to obtain appropriate statistical values. Foraminifera were classified at least to the genus level based on Murray (2006), the foraminifera.eu database (Hesemann, 2015) and the

online database 'World Register of Marine Species' (WoRMS, 2016), while identification of Ostracoda is based on Athersuch et al. (1989).

2.3. AMS radiocarbon dating

For a robust chronological framework, six peat samples of 2 cm thickness were treated with KOH and sieved (200 μm mesh size) to collect macro remains of terrestrial plants for dating. In case of insufficient abundance of macro remains, "fine bulk" containing the organic fraction < 63 μm was used instead. All samples were dated by the AMS (Accelerator Mass Spectrometry) ^{14}C method at the Poznan Radiocarbon Laboratory (Poland). Radiocarbon dates were calibrated with OxCal v4.2.3 (Bronk Ramsey, 2009) using the IntCal13 atmospheric curve (Reimer et al., 2013). Results of individual dates are given as means of the calibrated 2σ uncertainty interval. Sedimentation rates were calculated based on an age depth-model with linear interpolation and by assuming a continuous sedimentation without hiatus.

3. Results

3.1. Lithology

Five lithological units A-E were identified based on lithology, sedimentary structures, organic content and accessory materials such as plant remains and mollusc shells (Fig. 2).

The basal unit E (455.5–283 cm) is 172.5 cm thick and composed of very fine to fine sands and partially intercalated with mm-thick slightly finer-grained layers enriched in organics. Where these layers are present, a horizontal lamination is observed and very rarely broken diatom frustules and sponge spicules as well as phytoliths are found. The colour of the sands changes from light-grey/beige to light brown with a higher organic content in the uppermost 25 cm. Here, quartz grains show clear signs of bleaching.

Lithofacies D (283-248 cm) is represented at the base by a dark-brown to black, highly decomposed peat with abundant wood remains. The uppermost 20 cm of this peat are horizontally laminated with grey silty layers. At the top, the peat changes gradually into an organic-rich mud (lithofacies C, 248–178.5 cm). This unit is composed of a dark to blue-grey, fine to medium silt locally intercalated with mm-thick organic-rich layers. A coarsening upward trend in grain size is observed, although the granulometric trend inverts close to the upper boundary. Occasionally, wood pieces (roots) were found, and smear slides document a high quantity of organic remains, as well as of a variety of diatoms and sponge spicules. At the top of this unit (188.5–193.5 cm) a large, wedge-shaped fragment of eroded peat was deposited. The transition to the overlying lithofacies B (178.5–105.5 cm) is ambiguous. This unit consists of layered, slightly decomposed peat with abundant macro- and microscopic wooden remains. The uppermost lithofacies A (105.5–0 cm) follows above a sharp and irregular erosional contact and consists of a dark to blue-grey silt, faintly laminated within the uppermost 50 cm. Occasionally bivalve shells are found. The sediment top is characterized by burrows and shells of piddocks.

Due to their stratigraphic positions, the peat of lithofacies D represents a basal peat while lithofacies B is an intercalated peat.

3.2. Chronology

The lower part of lithofacies E is most likely of Pleistocene age. The two lowermost palynological samples are characterized by reworked pollen of the thermophilous tree taxa hornbeam and lime (*Carpinus* and *Tilia*, see supplement 1) of interglacial origin (Behre and Lade, 1986), and especially the high *Tilia* values suggest a strong and selective degradation. The organic-rich top of unit E contains pollen typical for Holocene reforestation and soil formation with the thermophilous elements oak and alder (*Quercus*, *Alnus*) following the pioneer trees birch and pine (*Betula*, *Pinus*). The pollen assemblages point to an early Atlantic age (palaeoclimatologically the warmest Holocene pollen zone of northern Europe at ca. 7600 cal. BP). This is supported by an AMS ^{14}C date of fine bulk organic matter at the top of lithofacies E, which results in an age of ca. 7580 cal. BP.

The formation of the basal peat (unit D) started at ca. 6900 cal. BP and continued at least until 6100 cal. BP (Table 1). Disregarding potential peat compression, the peat growth averages 0.4 mm/a and suggests 5960 cal. BP for the top of lithofacies D.

After a short period with deposition of marine mud, a second phase of peat formation started for > 430 years. The top of this intercalated peat (lithofacies B) dates to 5400 cal. BP, giving an average peat-formation rate of 1.4 mm/a and suggesting a basal age for lithofacies B of 5890 cal. BP. When considering the obtained age estimates for the top of the basal peat (lithofacies D) and the base of the intercalated peat (lithofacies B), the first period of marine influence (lithofacies C) lasted approximately 100 years.

3.3. Bulk geochemistry and magnetic susceptibility

The grain-size range recorded within the core varies between clay (< 2 μm) and very coarse sand (0.5–1 mm; Fig. 3). Organic matter (TOC) and carbonates (TIC) are also highly variable along the core. A similar stratigraphic trend of TOC, TS and TN can be observed, and highest values correspond to the peat layers (Fig. 3). The C/N ratios are rather irregular along the core ranging from 10 to 35 (Fig. 3). Magnetic susceptibility is relatively low for most of the core. Higher values occur only from the top of unit D to the base of unit B (Fig. 3).

3.4. Quantitative paleobiological data

The paleobiological records (Fig. 3, Supplements 1, 2) provide valuable information about paleoenvironmental conditions.

Pleistocene sands of lithofacies E are mostly void of microfossils except low concentrations of reworked pollen and palynomorphs as well as shattered diatom frustules in layers slightly enriched in organic matter. Pollen spectra from the organic top of unit E reflect the Holocene reforestation of northern Germany. Both, arboreal pioneer taxa such as *Pinus* and *Betula* as well as tree taxa that established later like *Corylus*, *Quercus* and *Alnus* are present.

Pollen grains archived in the fen peat (lithofacies D) point to regional alder cars (waterlogged forest swamps) and *Quercus* woodlands. Towards the top of the peat, pollen of Chenopodiaceae, a family including salt plants, the marine NPP *Micrhystridium* and linings of Foraminifera point towards in increased marine influence and a diminishing distance to the sea. In addition, the otherwise very rare diatoms are starting to increase at around 270 cm with an assemblage dominated by polyhalob taxa typical for mid to low salt marshes (located between mean tide level and mean high water in a salt marsh environment). Overlying is lithofacies C with silty minerogenic sediments characterized by high Chenopodiaceae values from nearby salt vegetation and redeposited fresh water indicators (*Sphagnum, Pediastrum*) as well as tree pollen of Pleistocene interglacials or interstadials (*Carpinus*). Two agglutinated foraminifera species prevail (i.e., foraminifera shells constructed from sedimentary particles bound together by organic, calcareous or siliceous cement), *Trochammina inflata* (Montagu, 1808) and *Entzia macrescens* (Brady, 1870). Polyhalob diatom species such as *P. sulcata* and *C. belgica* (max. 27%) are present as well as *Diploneis smithii*. Oligohalob species such as *Epithemia* and *Cyclotella baltica* can also be found. With a gradual contact, the following lithofacies B shows the development of a fen peat transitioning from saline (Chenopodiaceae) to fresh water conditions (e.g. Poaceae, *Sparganium*, *Thelypteris*). This unit appears void of zoological microfossils and diatoms. The uppermost lithofacies A is dominated by calcareous species preferring estuarine (mixed fresh and salt water) or brackish conditions (0.5–30 g/l of dissolved salt) of tidal flats. The calcareous *Haynesina germanica* (Ehrenberg, 1840; max. 83%)

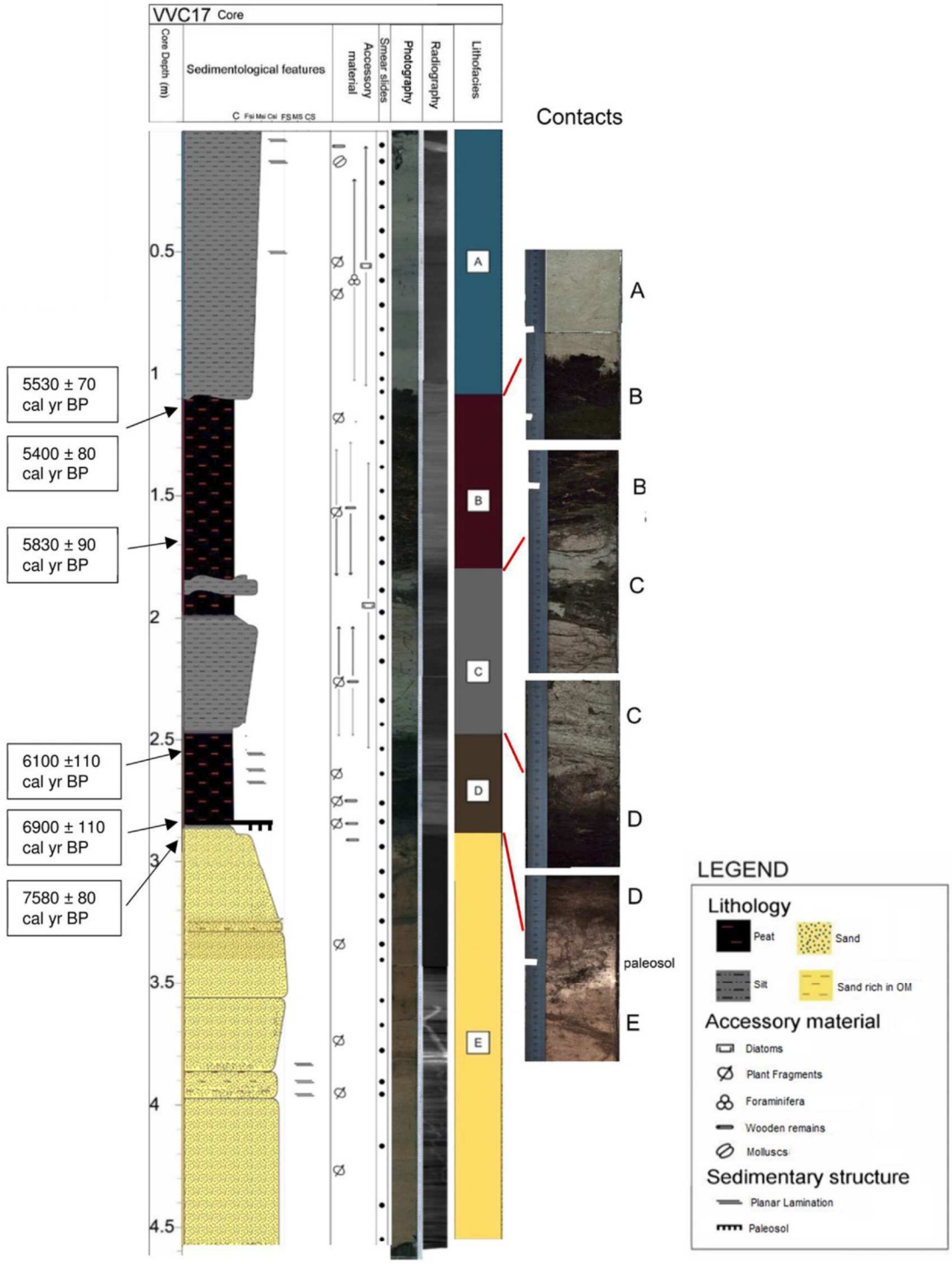

Fig. 2. Stratigraphy of core VVC 17 obtained by integrating visual inspection with smear slide analyses. Additionally, accessory material, photographs, radiographies, and lithofacies are reported. To the left (framed), calibrated radiocarbon ages are provided.

characterizes the foraminifera association accompanied by *Ammonia tepida* (Cushman, 1926), *Cribroelphidium williamsoni* (Haynes, 1973) and the two polyhalob and agglutinated species *E. macrescens* and *T. inflata*. The most abundant ostracods are *Cyprideis torosa* (Jones, 1850) and *Leptocythere* spp. (Sars, 1925; ~60%). In these marine sediments, *Sphagnum* spores as well as small reworked peat fragments indicate a continued erosion of exposed peat layers in the vicinity of the coring location. Chenopodiaceae, foraminifera linings and *Micrhystridium*

Table 1
AMS-radiocarbon dates. For each sample core depths, type and amount of material, uncalibrated (BP) and calibrated age (BC) are reported. All ages are given within the 2 σ (95%) uncertainty range.

Depth (cm below sea level)	Section, Section depth (cm); Composite depth (cm)	Lab. No.	Material dated and sample weight	14C Age (years BP)	δ13C-AMS (‰)	Calibrated age (years cal. BP)			Calibrated age (years BC)		
						min	max	mean	min	max	mean
482.5	sec-3, 7–9; *106.5–108.5*	Poz-94535	*Cladium mariscus* (6.3 mg), Carex flava-type (14.7 mg), Carex spec. (6.5 mg)	4690 ± 40	−27.6 ± 0.2	5320	5480	**5400 ± 80**	3370	3530	**3450 ± 80**
482.5	sec-3, 7–9; *106.5–108.5*	Poz-95124	fine bulk (0.75 g)	4780 ± 40	−27.3 ± 0.5	5460	5600	**5530 ± 70**	3510	3650	**3580 ± 70**
545	sec-3, 70–72; *169.5–171.5*	Poz-95026	fine bulk (3.78 g)	5100 ± 40	−29.6 ± 0.4	5750	5920	**5830 ± 90**	3800	3970	**3890 ± 90**
628.5	sec-2, 28–29; *252.5–254.5*	Poz-94532	*Cladium mariscus* (62 mg)	5320 ± 40	−32.4 ± 0.9	5990	6210	**6100 ± 110**	4040	4260	**4150 ± 110**
657.5	sec-2, 57–59; *281.5–283.5*	Poz-94533	fine bulk (2.85 g)	6050 ± 40	−26.4 ± 0.3	6790	7000	**6900 ± 110**	4840	5060	**4950 ± 110**
662.5	sec-2, 62–64; *286.5–288.5*	Poz-94534	fine bulk (3.23 g)	6710 ± 40	−32.1 ± 0.3	7510	7700	**7580 ± 80**	5560	5710	**5630 ± 80**

increase in the upper 40 cm. An evident turnover between agglutinated and calcareous Foraminifera species occurs as well. The environmental conditions change and *E. macrescens* (max. 61%) dominates the sediments towards the surface followed *by T. inflata* (max. 16%), whereas the number of calcareous taxa clearly decreases (e.g. *H. germanica*, *C. williamsoni*). Polyhalob diatoms are replaced by oligohalob species.

3.5. Geochemistry

In total 18 high-resolution XRF element profiles and specific element log ratios (Fig. 4) were selected to be used as paleoenvironmental proxies. Additionally, the inc/coh ratio was used as an indicator of organic matter content because it was found to be moderately dependent on TOC content (Fig. 5). The sandy lithofacies E is characterized by high signals of silicon (Si) and zirconium (Zr) and corresponding low iron (Fe) and bromine (Br) values. The calcium (Ca) profile shows a decreasing upward trend. This lithofacies shows the highest Si/Ti ratio. The following lithofacies D has similar features compared to the second peat unit, lithofacies B. Both exhibit high sulphur (S), chlorine (Cl) and Br signals as well as an increasing upward trend of potassium (K) and iron/manganese ratio (Fe/Mn). The calcium/strontium (Ca/Sr) ratio shows intermediate values compared to the rest of the core, while zirconium/rubidium (Zr/Rb) displays a great and highly variable trend. On the other hand, a distinct attribute of lithofacies D is a peak in Si, K, Ti, Mn and zinc (Zn) around 260–270 cm core depth as well as an increased signal in Sr. The silty lithofacies C and A present similar elemental trends. In fact, the majority of the element profiles show high steady signals for of Si, Ti, K, Zr, Zn and Rb. The Ca, Mn, Sr, Ca/Sr, Ca/Fe signals are constantly high and reach the maximum values in lithofacies A. In contrast, Fe/Mn ratios are higher in lithofacies C with a pronounced peak at 200 cm core depth.

3.6. Principal component analyses (PCA) and element groups

PCA analyses (Fig. 6) allows the identification of three clusters of elements (Element group 1, 2 and 3) plotting coherently with the identified lithofacies, which indicates that each lithology has a different geochemical signature.

The PC1 axis describes a variance of 47.3%, whereas the variance of PC2 accounts for 36.6%. PC1 mainly opposes the inc/coh ratio (positive values) as an indicator of organic matter content and K, Rb, Ti, Si, Zn, Sr and Zr (negative values) discriminate between organic-rich and clastic sediments. PC2 seems to be mainly controlled by Fe and to a lesser extent by Br, Cl, S, Mn and Ca on the negative side.

3.6.1. Element group 1

The first element group comprises the elements Si and Zr, which are characteristic for coarse grained, siliciclastic sediments (Croudace et al., 2006; Rothwell and Rack, 2006). Consequently, lithofacies E is closely related to this element group in the PCA biplot (Fig. 6). Si is predominantly found as detrital material produced during weathering of quartz and plagioclase, while Zr is primarily related to the heavy mineral zircon. Both elements are considered to be weathering resistant and enriched in coarse sediment fractions.

3.6.2. Element group 2

The second group includes the elements K, Rb, Ti and Zn (Fig. 6), which are characterizing the silty lithofacies C and A. In addition, Rb does not form minerals of its own but is indicative for clay-rich sediments (Cundy et al., 2005). Similarly, K is commonly increased for argillaceous sediments as a function of the clay-mineral content. Likewise, Zn is adsorbed by clay minerals (Wedepohl, 1995). Ti is often used as an indicator for detrital mineral input to the sedimentary record especially for lacustrine environments (Haberzettl et al., 2005; Croudace et al., 2006) and may also substitute Mg or Fe in silicate minerals, leading to enrichment in clay minerals and mica.

Another member of this element group is Ca indicative for carbonates. Due to their chemical similarity, Ca can be replaced by Sr in the crystal lattice of aragonite. Moreover, the data belonging to lithofacies A form a distinct cloud of points reasonably explained by higher values in Ca (carbonate-rich sub-group) with respect to lithofacies C. This is corroborated by TIC values (Fig. 3).

3.6.3. Element group 3

This group includes the elements Fe, Br, Cl, S as well as the inc/coh ratio, which discriminate the organic-rich sediments corresponding to lithofacies D and B (Fig. 6). Especially, the high affinity of Br and Cl to organic matter can be attributed to its ability to adsorb these elements (Thomson et al., 2006). During plant decay, inorganic Cl can be bound to hydrocarbons to form organochlorine compounds. Hence, chlorination of organic compounds during degradation could be the reason that peat horizons are enriched in Cl (Keppler and Biester, 2003). Furthermore, the enrichment of Cl is attributable to the high porosity of peat and could therefore be connected with a higher water content containing Cl in solution. Similarly, Br can be incorporated into organic matter through enzymatic processes related to plant litter decomposition (Leri and Myneni, 2012). For tidal flats and lagoonal sediments Fe and S are generally used as indicator of reducing conditions (Croudace et al., 2006; Kabata-Pendias, 2011). In sediments with increased organic matter content, both elements are linked to the formation of iron sulphides (pyrite) under low-oxygen conditions (Hadler et al., 2018).

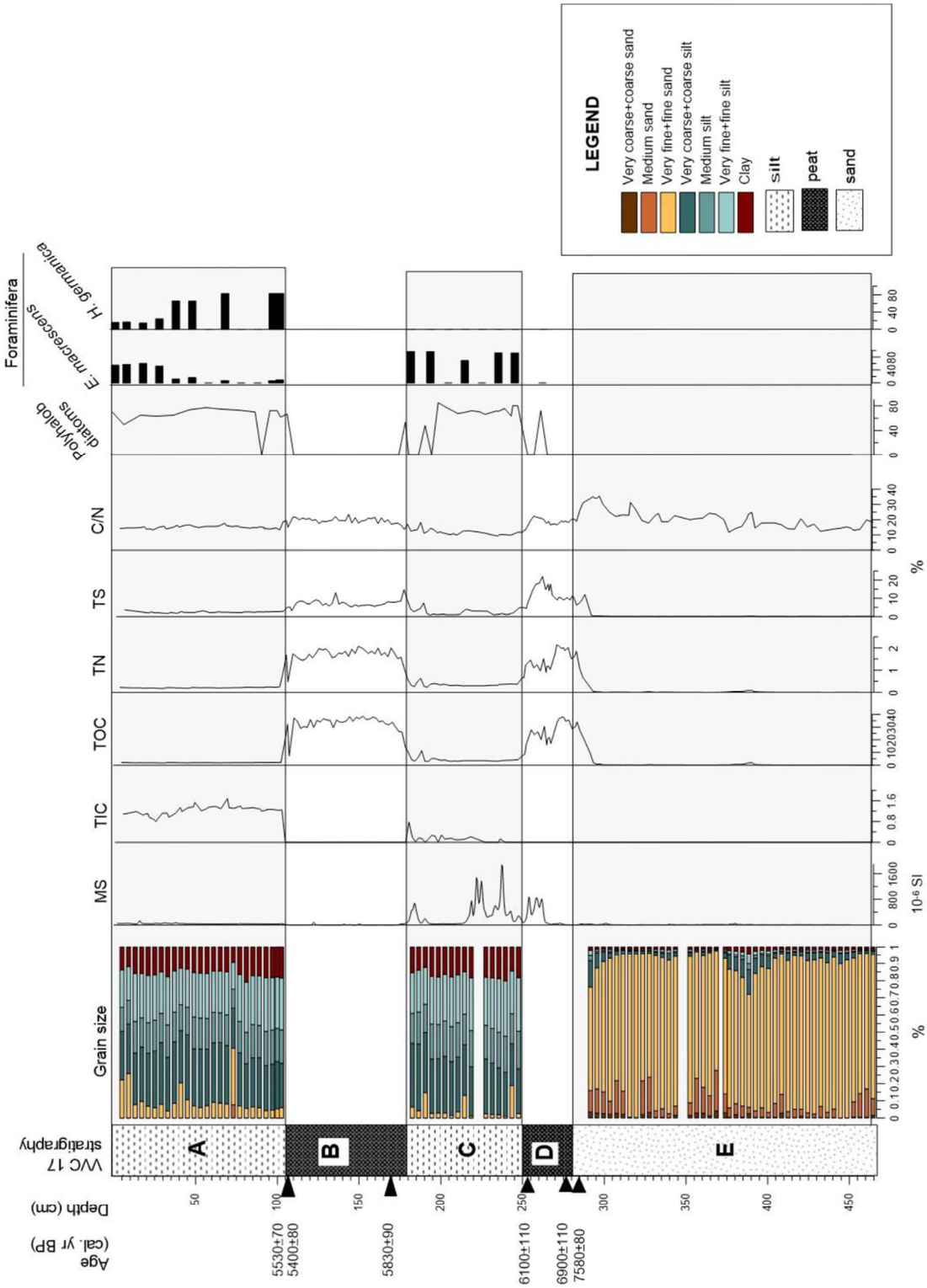

Fig. 3. Stratigraphy of core VVC 17 with radiocarbon ages, grain-size classes, magnetic susceptibility (MS), total inorganic carbon (TIC), total organic carbon (TOC), total nitrogen (TN), total sulphur (TS), carbon/nitrogen ratio (C/N), polyhalob diatom distribution and two environmentally indicative *f*oraminifera species. In peat and sand units there was no reaction with HCl and therefore no carbonate minerals are present. The unrealistic TIC measurements that were obtained for lithofacies E, D and B are regarded as artefacts due to very high TOC concentrations and therefore were set to 0.

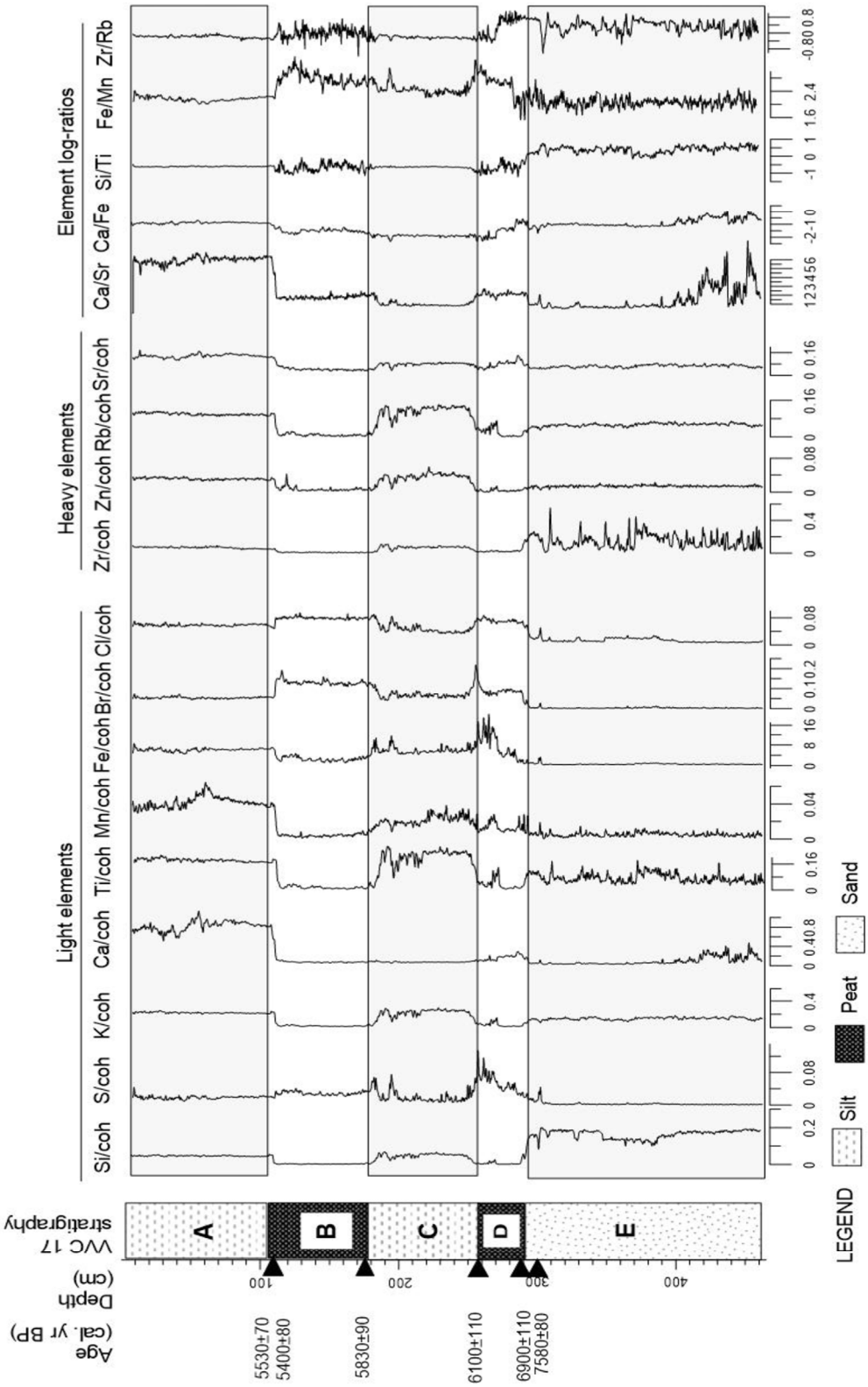

Fig. 4. Stratigraphy of core VVC 17 with XRF scanning results showing selected and normalized elements and element ratios, including ^{14}C-ages.

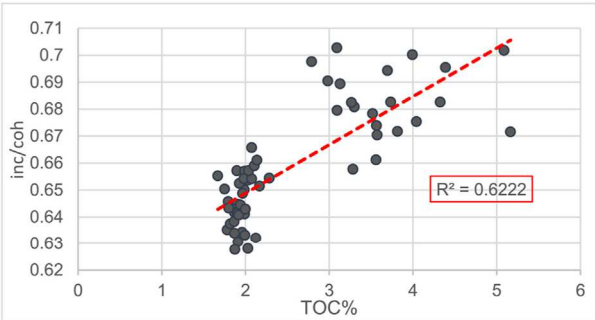

Fig. 5. Scatter plot documenting the correlation between TOC percentage values and inc/coh. The trend line is shown for the whole dataset with the correlation coefficient indicated in the red box. (For interpretation of the references to colour in this figure legend, the reader is referred to the Web version of this article.)

However, a group of data belonging to the uppermost section of lithofacies E and the lowermost section of lithofacies D seems to move away from the general trend of both lithofacies showing positive PC2 and lower PC1 values. This is possibly due to both having a higher affinity to siliciclastic elements such as Si and Zr as well as a high affinity to organic matter (Fig. 6). We define this interval as a paleosol (P in Fig. 6).

4. Discussion

4.1. Facies associations and holocene depositional evolution

Altogether, five Pleistocene to Holocene depositional phases correspond to the described lithofacies (Fig. 2).

4.1.1. Pleistocene sand plain (lithofacies E, > 6900 cal BP)

The origin of the sandy sediments at the core base is ambiguous due to the lack of distinct sedimentary structures and the almost complete absence of microfossils and material suitable for dating. This includes the absence of distinct marine sediments from the Eemian in core VVC17. Only two pollen spectra (Supp. 1) include *Carpinus* and *Tilia* pointing to an interglacial or interstadial origin and therefore possibly to redeposition of Eemian or older material. While the lack of foraminifera and ostracods is explained by decalcification, the sparse occurrence of shattered diatom frustules and sponge spicules suggest, like for the pollen, reworking of sediments most likely by aeolian processes during the Weichselian (e.g. Hoselmann and Streif, 2004; Streif, 2004). A reworking of Saalian till explains high levels of Zr in these sands, as till originates from Scandinavian crystalline basement rocks containing zircon minerals (e.g., gneiss, granite; Schüttenhelm and Laban, 2005). The Si/Ti ratios in lithofacies E are highest due to the coarse grain size (Fig. 4), as also shown by the distinct PCA distribution and separation of both elements (Fig. 6). At around 290 cm core depth high TC, TS and TN percentages paralleled by high Si and Zr counts and a prominent C/N peak indicate degraded organic matter of terrestrial provenience (Figs. 3 and 4; Fujine, 2008), which point to the development of a paleosol. This horizon with a thickness of ca. 7 cm was formed under subaerial conditions when sedimentation ceased creating a quasi-non-depositional period of possibly several millennia. The pollen spectra in this paleosol include tree species (*Corylus, Quercus*) of upland deciduous forests as well as species indicating moister soil conditions (*Alnus*). Soil formation processes include the accumulation of organic matter and an initial bleaching of quartz grains suggesting podzolisation underneath the paleosol. These terrestrial conditions lasted until the initial stages of the Atlantic period.

4.1.2. Fen peatland with increasing marine influence (lithofacies D, ca. 6900–5960 cal. BP)

The development of a fen around 6900 cal. BP is documented by peat characterized by high values of Cl, Br and S (Fig. 4). The local vegetation was a reed characterized by bur-reed (*Sparganium*-type) and marsh fen (*Thelypteris palustris*). The estimated general peat growth-rate of ~0.4 mm/y is lower than the range of values estimated for central Europe (0.5–1.5 mm/y; Bungenstock and Schäfer, 2009), possibly due to high decomposition of organic matter and/or post-depositional compaction.

An increasing marine influence is documented towards the top of the peat by polyhalob diatoms and other marine species (*Micrhystridium*, foraminifera linings; Supp. 1, 2). Their appearances are of allochthonous origin and document deposition during extreme high tides or storm surges. At 265 cm depth, the records of MS and TS increase abruptly, while TC and Fe/Mn decrease. Rising values of K/coh and Ti/coh are caused by a higher content of fine-grained minerogenic matter as the fen peat was influenced by sea water during flooding

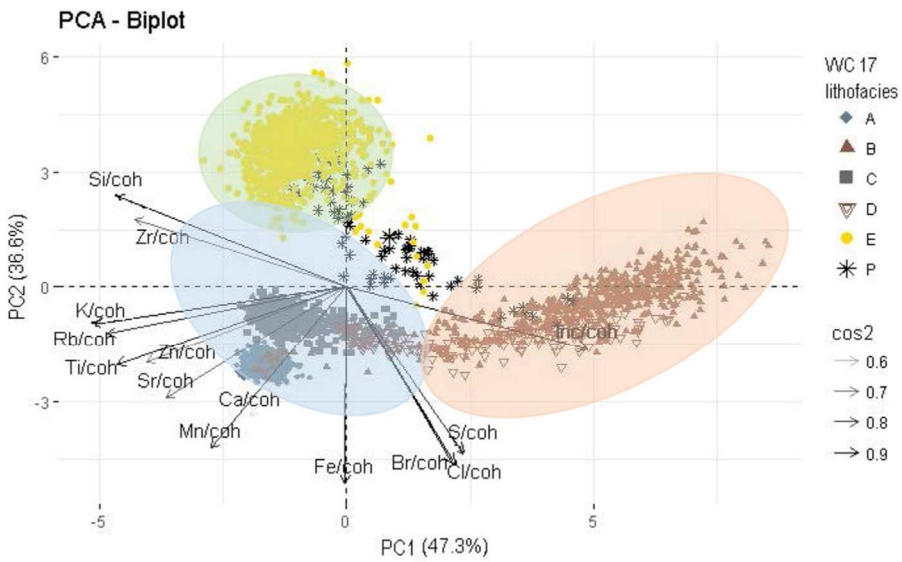

Fig. 6. PCA biplot of coh-normalized elemental data. Samples from different lithofacies (A–E) and the paleosol (P) are shown with different symbols. The colored circles highlight the inferred major element groups 1–3. The squared cosine shows the importance of a component for a given observation. It indicates the contribution of a component to the squared distance of the observation to the origin.

related to storm events.

4.1.3. High salt marsh (lithofacies C, ca. 5960–5890 cal. BP)

A marshland, characterized by silt-sized clastic material with intercalated thin organic-rich horizons (Fig. 2), developed after 6000 cal. BP with fast aggradation rates (~3 mm/a). Low-energy conditions are accompanied by low TOC and marine influence is shown by high values of TIC as well as low C/N ratios (element group 2; Figs. 3, 4 and 6). The change to marine conditions is additionally recorded by dominance of polyhalob diatoms and agglutinated foraminiferal species typical for salt marsh environments (*Trochammina inflata* and *Entzia macrescens*) (Freund et al., 2004; Müller-Navarra et al., 2016; Fig. 3; Supp. 2). Agglutinated species are reliable indicator of a salt marsh because in such environments the biological secretion of calcareous material is impossible due to $CaCO_3$ undersaturation of the water (Alve and Murray, 1995).

The planktonic and semi-planktonic diatom species *Paralia sulcata* and *Cymatosira belgica,* which are abundant in lithofacies C and A, are likely allochthonous, i.e. washed in by tidal waters (see Vos and De Wolf, 1988). In contrast and according to their benthic lifeform, *Diploneis smithii* and *Navicula microdigitoradiata* are most likely autochthonous diatom species typical for brackish environments (Denys, 1991) and provide paleoecological information about the local habitat conditions. Therefore, the obtained salinity classes must be considered with caution. Nevertheless, the allochthonous species document a continuous tidal influence thus excluding closed tidal lagoons with small or no tidal range as depositional environment for lithofacies C and A. This interpretation is additionally supported by the NPP *Micrhystridium,* which has been found in "marine clay" in coastal deposits of The Netherlands (Bakker and van Smeerdijk, 1982; Pals et al., 1980) and similarly could represent an allochthonous sediment component.

However, the occurrence of *Epithemia* and other oligohalob species like *Cyclotella baltica* implies freshwater influx but are most likely also of allochthonous origin. Concerning foraminifers, *Trochammina inflata* and *Entzia macrescens* are usually abundant in high to middle salt marshes (Horton and Edwards, 2006). All these proxies point to the establishment of high salt marsh conditions including a salt-adapted Chenopodiaceae-rich vegetation nearby (Fig. 3). The present MS peaks (Fig. 3) were likely caused by post-depositional formation of diagenic Fe-bearing minerals such as pyrite (Dellwig et al., 2002) under anoxic conditions.

4.1.4. Fen peatland (lithofacies B, ca. 5890–5500 cal. BP)

Prior to 5800 cal. BP the local environment changed from saline to freshwater conditions. The salt marsh was replaced by *Phragmites* fen until ca. 5500 cal. BP. The accumulation of this fen peat took place with an average growth rate of 1.4 mm/yr. Rhizomes of *Phragmites* (Supp. 1; common reed) are macroscopically visible documenting a lower grade of decomposition compared to the basal peat layer. As indicated by increasing C/N and Ca/Sr ratios (Figs. 3 and 4), the marine influence decreased considerably during this peatland phase as expected for such environments. With respect to palynological data (Supp. 1), the common reed (*Phragmites australis*) became accompanied by bur-reed (*Sparganium* spec.) and/or broadleaf cattail (*Typha angustifolia*, part of *Sparganium*-type) and later by sedges (Cyperaceae) and marsh fern (*Thelypteris palustris*). The disappearance of foraminifera and diatoms characteristic of salt marshes (Fig. 3; Supp. 2) is coherent with this regressional trend. Nevertheless, the site was still reached by marine spray (*Micrhystridium*). Chenopodiaceae have a minimum at 150 cm, which may reflect weakest marine influence around 5600 cal. BP.

4.1.5. Tidal flat and transition to low salt marsh (lithofacies A, < 5500 cal. BP)

With an erosional contact at 105.5 cm core depth, a new depositional environment abruptly established after 5500 cal. BP. In comparison to the underlying peat (lithofacies B) most proxies change drastically. In fact, lithological and geochemical features, high Ca values, a C/N around 15 (Fujine, 2008) and relatively low TOC values (element group 2; Figs. 3 and 4) point to the development of a tidal flat. The paleobiological content (Fig. 3; Supp 1, 2) reflects a high marine influence. Pollen and palynomorphs with marine affinity are very abundant (e.g., *Chenopodiaceae*, *Micrhystridium*, *foraminifera linings*) as well as allochthonous, polyhalob diatoms (e.g. *Paralia sulcata*, *Cymatosira belgica*). Calcareous foraminifera species typical of shallow marine (intertidal) conditions (e.g. *Ammonia tepida*, *Haynesina germanica* and *Cribroelphidium williamsoni*; Scheder et al., 2018) coexist with ostracods typical of brackish and back-barrier environments (e.g. *Cyprideis torosa*, *Leptocythere* spp.; Athersuch et al., 1989). The Ca/Sr ratio (Fig. 4) reaches maximum values and validates the abundance of calcareous shells, which is in agreement with oxic conditions testified by stable Fe/Mn. Even though highest Ca/Sr ratios occur when detrital carbonate content is high and biogenic carbonate is low, in fine-grained sediments of mud flats or other shallow near-shore marine environments the absolute Ca values are often higher, consequently showing increased Ca/Sr ratios (Hadler et al., 2018) with increasing marine influence (Freund et al., 2004) like in this case.

Paleobiological indicators change in the topmost 40 cm. Parallel to a decrease in calcareous foraminifera species (e.g. *Haynesina germanica*), a rise in agglutinated species (e.g. *Trochammina inflata*, *Entzia macrescens*) indicates the establishment of a low salt-marsh environment. Further validation is given by the presence of oligohalob diatoms as well as an increase of sand (Fig. 3). However, foraminifers show signs of relocation (scuffed/broken tests). Together with the core location at the margin of a main tidal channel, this suggests massive reworking within the uppermost 40 cm. The recorded salt-marsh fauna could originate from high salt marshes of the surrounding area. Unfortunately, no ^{14}C-dates are available to constrain this unit chronologically. The recent sediment at the top is an erosive surface, inhabited by piddocks and does not reflect modern environmental conditions.

4.2. Transgressive-regressive cycle and comparison with the sea-level curve of the southern North Sea

The first extensive marine transgression accompanied by rising groundwater and leading to the development of basal peat started ca. 7500 cal. BP (Behre, 2007; Meijles et al., 2018) along the coastline of the southern North Sea. This is recorded consistently by the formation of a basal peat on top of a paleosol in core VVC 17 and chronologically constrained to around 7000 cal. BP. According the Behre (2007), mean sea level was then at ca. 700 cm bsl which is in good agreement with the stratigraphic position of the oldest peat at 658 cm bsl.

After ca. 1000 years and with the advancing transgression, marine influence increased, and a high salt marsh established for a ca. 100-year long period (Fig. 7). Around 5830 cal. BP the salt marsh has already been replaced by a second (intercalated) fen peat. This transition represents a short regressional phase which could be indicative of a stable or even decreasing sea level or an accelerated peat growth compensating the sea-level rise. In fact, a period of slow sea-level rise was identified by Behre (2007) around 6000 cal. BP, represented by the first development of wide-spread intercalated peats (corresponding to lithofacies B) in the Wadden Sea area. This is in accordance with e.g. Bungenstock and Schäfer (2009) who identified a relative sea-level stillstand between 6750 and 5300 cal BP. The abrupt deposition of tidal flat sediments (lithofacies A), representing the strongest marine influence of the record, testifies another sea-level rise that occurred ca. 400 years later. Because of potentially significant erosion and therefore the absence of reliable age estimates for the transgression from lithofacies B to A, it is difficult to correlate this sea-level rise to analogues recorded elsewhere in the Wadden Sea area. Nonetheless, studies made in the Jade Bay area (Wartenberg et al., 2013) show an erosional surface related to sea-level rise and transgression dated between 5600 and 4500 cal. BP that could be equivalent to the transgression identified in

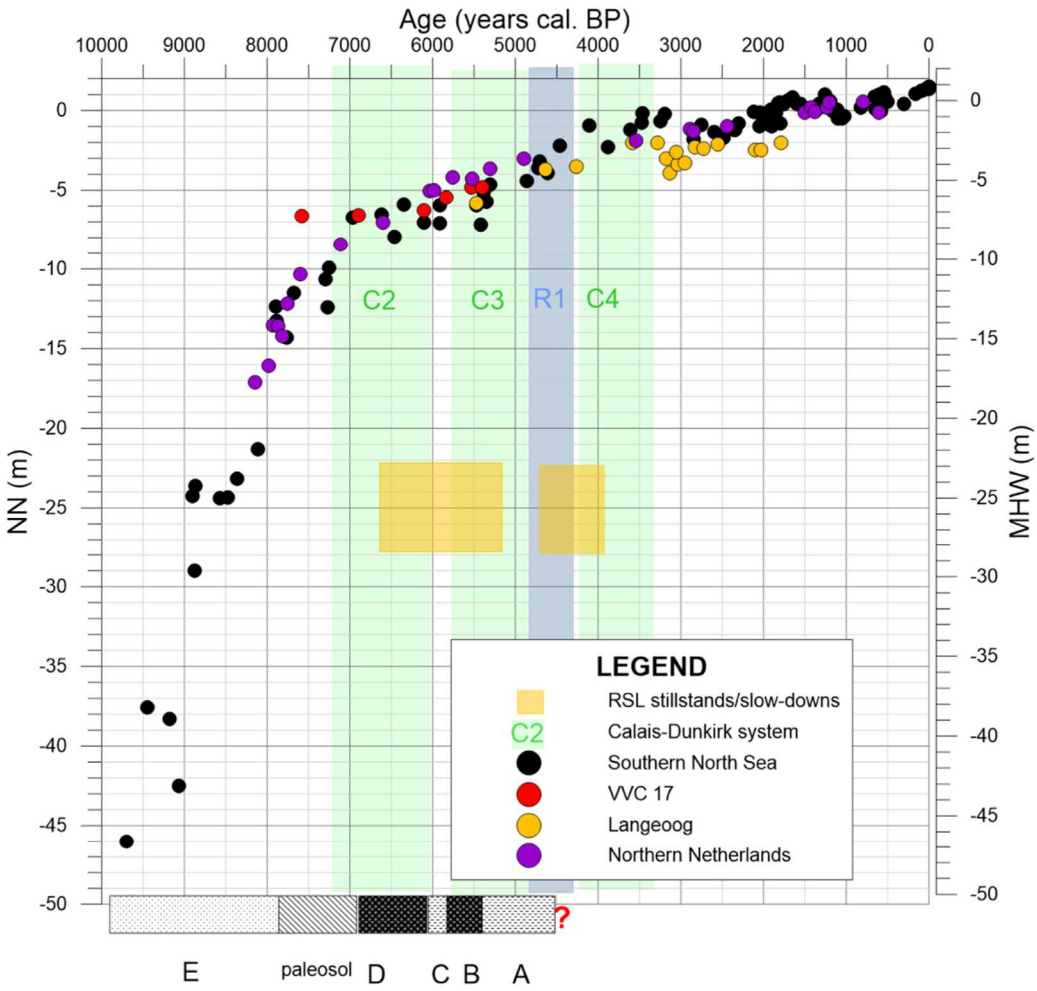

Fig. 7. Sea-level record for the southern North Sea (MHW: mean high water; Behre, 2007), averaged values for the East Frisian Coast at Langeoog (NN: mean tide level; Bungenstock and Schäfer, 2009) and averaged values for the northern Netherlands (relative MSL: mean sea level; Meijles et al., 2018) based on calibrated radiocarbon dates. Calibrated radiocarbon dates of core VVC 17 are plotted in red with relevant transgression phases (Behre, 2007) shaded in green, while sea level stillstands or slow-downs of the sea-level rise (Bungenstock and Schäfer, 2009) are marked in yellow. Shaded in blue is the first Mid-Holocene regression of the German coastal area (R1). (For interpretation of the references to colour in this figure legend, the reader is referred to the Web version of this article.)

VVC 17.

Tidal flat sedimentation continued to the uppermost 40 cm, when the second progradational phase of the system started. It is marked by low salt marsh sediments, possibly caused by a decreased rate of sea-level rise, a sea-level fall, higher sediment supply or by redeposition of reworked material from older salt marshes nearby. Repeated flooding could have caused enhanced sediment deposition which may have resulted in aggradation or even progradation of the coastline, in this case not connected to a drop in sea–level (Bungenstock and Weerts, 2012). Any higher intercalated peat (middle peat layer), known from other parts of the Wadden Sea, deposited during regression phase R1 (Fig. 7; Behre, 2007) or during a sea-level stillstand/slow down (Bungenstock and Schäfer, 2009) is missing at VVC 17. The absence of this middle peat layer and the fact that the core is located in a present-day subtidal area, is related to a hiatus of unknown extent (possibly between 4000 and 5000 years) near the top of the analysed sediment record, which prevents a complete reconstruction of the Holocene depositional history.

5. Summary and conclusions

The multi-proxy facies analysis performed for core VVC 17 makes an important step towards refining and complementing the stratigraphic and paleoenvironmental evolution of the Wadden Sea during the Middle-Holocene on a local scale. Furthermore, this approach offers the opportunity to develop and test the applicability of a variety of paleoenvironmental proxies for investigating coastal tidal environments and allows comparing this dataset with analogue datasets on a more regional scale.

- On top of > 1.5 m of Pleistocene sand, a 3 m-thick fine grained and partly organic-rich succession of Holocene age (older than 7580 cal. BP) is recorded within the backbarrier area between the East Frisian Islands of Juist and Norderney.
- The termination of the basal fen peat deposition is interpreted to reflect the rapid sea-level rise linked to a transgression ranging from 6900 until 5890 cal. BP.
- The Holocene coastal sediments consist of a vertical stack of semi-terrestrial, supra- and intertidal facies (fen peat – high salt marsh –

fen peat – tidal flat – low salt marsh), documenting the occurrence of two small-scale transgressive-regressive cycles. These are possibly related to the discontinuous character of the North Sea relative sea-level curve even though chronologically not in complete accordance with the transgression phases at 7400–6100 and 5900–5000 cal. BP (Behre, 2007) and a sea-level stagnation (6750–5300 cal BP) (Bungenstock and Schäfer, 2009). The facies with the highest marine influence is the tidal flat that developed after 5500 cal. BP. The occurrence of salt marsh deposits at the core top is still a matter of debate and relates to possible reworking and a lack of time control.

- The paleosol of the early Middle-Holocene is the only identified terrestrial surface in this core, which represents a suitable environment for prehistoric people.
- The calibrated radiocarbon ages of VVC 17, when compared to existing sea-level curves for the southern North Sea (Fig. 7; Behre, 2007; Bungenstock and Schäfer, 2009; Meijles et al., 2018), show a relatively good fit both on a local (Bungenstock and Schäfer, 2009) and on a regional scale (Meijles et al., 2018). However, the Behre sea level curve (2007) has been highly debated (Vink et al., 2007; Baeteman et al., 2011; Bungenstock and Weerts, 2012) and should be interpreted with caution. Apparent step like oscillations of the sea-level can also be the result of an interplay between local factors when integrated into one single sea-level curve (Baeteman et al., 2011; Bungenstock and Weerts, 2012). Furthermore, many authors question the reliability of different sea–level index points (especially archaeological index points) used as well as the lack of corrections for sediment compaction (Baeteman et al., 2011) and glacio-isostatic crustal movements (Vink et al., 2007; Baeteman et al., 2011). The oldest date of our core VVC 17 does not reflect sea level changes because it is a sample from a paleosol (the visible outlier in Fig. 7), while the others are more reliable. However, some uncertainties exist due to the possible sediment compaction especially for the three uppermost dates.
- The applied multi-proxy approach (sedimentology, geochemistry, paleobiology) is well suited for paleoenvironmental reconstruction. An essential support was provided by paleobiological analyses, which enabled the reconstruction of marine vs. freshwater influence. Down-core XRF core-scanning data effectively distinguished five lithofacies and PCA analyses document to be an efficient method for lithofacies characterization.
- The Si/Ti ratio is a suitable proxy for shallow-water deposits as suggested by PCA analyses. CNS analyses helped to discriminate the sources of organic matter.

Despite of this, the applicability of other elemental ratios such as Ca/Sr or Fe/Mn have to be studied in more detail and with additional cores from the area to allow more conclusive interpretations. Furthermore, the search for more complete Middle-to Late-Holocene sediment records from the southern North Sea continues in order to reconstruct the regional environmental history of the Wadden Sea in more detail.

Acknowledgments

The present study is part of the The Wadden Sea Archive project (WASA) funded by the „Niedersächsisches Vorab" of the Volkswagen-Stiftung within the funding initiative „Küsten und Meeresforschung in Niedersachsen" of the Ministry for Science and Culture of Lower Saxony, Germany (project VW ZN3197), coordinated by the Lower Saxony Institute for Historical Coastal Research (NIHK). We are grateful for all support from the WASA project members, especially from Kim Peis and Ruggero Capperucci. Finally, special thanks go to Veronica Rossi from Bologna University for her encouragement.

Appendix A. Supplementary data

Supplementary data to this article can be found online at https://doi.org/10.1016/j.ecss.2019.106251.

Horton et al., 2006Szkornik et al., 2006

References

Alve, E., Murray, J.W., 1995. Experiments to determine the origin and palaeoenvironmental significance of agglutinated foraminiferal assemblages. In: In: Kaminski, M.A., Geroch, S., Gasiński, M.A. (Eds.), Proceedings of the Fourth International Workshop on Agglutinated Foraminifera, vol 3. Grzybowski Foundation Special Publication, pp. 1–11.

Armynot du Châtelet, E., Bout-Roumazeilles, V., Riboulleau, A., Trentesaux, A., 2009. Sediment (grain size and clay mineralogy) and organic matter quality control on living benthic foraminifera. Rev. Micropaleontol. 52, 75–84.

Athersuch, J., Horne, D.J., Whittaker, J.E., 1989. Marine and brackish water ostracods (superfamilies Cypridacea and Cytheracea). In: Kermack, D.M., Barnes, R.S.K. (Eds.), Synopses of the British Fauna. The Linnean Society of London & the Estuarine Brackish-Water Sciences Association (No. 43).

Baeteman, C., Waller, M., Kiden, P., 2011. Reconstructing middle to late Holocene sea--level change: a methodological review with particular reference to 'A new Holocene sea-level curve for the southern North Sea'presented by K.-E. Behre. Boreas 40 (4), 557–572.

Bakker, M., van Smeerdijk, D.G., 1982. A palaeoecological study of a late holocene section from 'Het Ilperveld', western Netherlands. In: Review of Palaeobotany and Palynology, vol 36. pp. 95–163 (1-2).

Bazelmans, J., Meier, D., Nieuwhof, A., Spek, T., Vos, P., 2012. Understanding the cultural historical value of the Wadden Sea region. The co-evolution of environment and society in the Wadden Sea area in the Holocene up until early modern times (11,700 BCe1800 AD): an outline. Ocean Coast Manag. 68, 114–126.

Behre, K.-E., 2004. Coastal development, sea-level change and settlement history during the later Holocene in the Clay District of Lower Saxony (Niedersachsen), northern Germany. Quat. Int. 112, 37–53.

Behre, K.-E., 2007. A new Holocene sea-level curve for the southern North Sea. Boreas 36, 82–102.

Behre, K.-E., Lade, U., 1986. Eine Folge von Eem und 4 Weichsel-Interstadialen in Oerel/Niedersachsen und ihr Vegetationsablauf. Eiszeitalt. Ggw. 36, 11–36.

Beug, H.J., 2004. Leitfaden der Pollenbestimmung für Mitteleuropa und angrenzende Gebiete.

Blott, S.J., Pye, K., 2001. GRADISTAT: a grain size distribution and statistics package for the analysis of unconsolidated sediments. Earth Surf. Process. Landforms 26, 1237–1248.

Bronk Ramsey, C., 2009. Bayesian analysis of radiocarbon dates. Radiocarbon 51 (1), 337–360.

Bungenstock, F., Schäfer, A., 2009. The Holocene relative sea-level curve for the tidal basin of the barrier island Langeoog, German Bight, Southern North Sea. Glob. Planet. Chang. 66 (1), 34–51.

Bungenstock, F., Weerts, H.J., 2012. Holocene relative sea-level curves for the German North Sea coast. Int. J. Earth Sci. 101 (4), 1083–1090.

Croudace, I.W., Rindby, A., Rothwell, R.G., 2006. ITRAX: description and evaluation of a new multi-function X-ray core scanner. In: Rothwell, R.G. (Ed.), New Techniques in Sediment Core Analysis. Geological Society of London, Special Publications, pp. 51–63.

Cundy, A.B., Hopkinson, L., Lafite, R., Spencer, K., Taylor, J.A., Ouddane, B., Heppell, C.M., Carey, P.J., Charman, R., Shell, D., Ullyott, S., 2005. Heavy metal distribution and accumulation in two Spartina sp.-dominated macrotidal salt marshes from the Seine estuary (France) and the Medway estuary (U.K.). Appl. Geochem. 20, 1195–1208.

Davis Jr., R.A., Flemming, B., 1995. Stratigraphy of a combined wave-and tide-dominated intertidal sand body: martens Plate, East Frisian Wadden Sea, Germany. In: In: Flemming, B.W., Bartholomä, A. (Eds.), Tidal Signatures in Modern and Ancient Sediments, vol 24. Special Publication, pp. 121–132.

Dellwig, O., Böttcher, M.E., Lipinski, M., Brumsack, H.J., 2002. Trace metals in Holocene coastal peats and their relation to pyrite formation (NW Germany). Chem. Geol. 182 (2–4), 423–442.

Denys, L., 1991. A check-list of the diatoms in the Holocene deposits of the western Belgian coastal plain with a survey of their apparent ecological requirements. I. Introduction, ecological code and complete list. Geol. Surv. Belg. 1991/02–1991246.

Flemming, B.W., 2012. Siliciclastic back-barrier tidal flats. In: Davis Jr.R.A., Dalrymple, R.W. (Eds.), Principles of Tidal Sedimentology. Springer, Dordrecht, pp. 231–267.

Frenzel, P., Boomer, I., 2005. The use of ostracods from marginal marine, brackish waters as bioindicators of modern and Quaternary environmental change. Palaeogeogr. Palaeoclimatol. Palaeoecol. 225, 68–92.

Freund, H., Gerdes, G., Streif, H., Dellwig, O., Watermann, F., 2004. The indicative meaning of diatoms, pollen and botanical macro fossils for the reconstruction of palaeoenvironments and sea-level fluctuations along the coast of Lower Saxony; Germany. Quat. Int. 112, 71–87.

Fujine, K., 2008. International Ocean Discovery Program. FlashEA 1112 Elemental Analyzer. (CHNS): User Guide, 12 pp.

Haberzettl, T., Fey, M., Lücke, A., Maidana, N., Mayr, C., Ohlendorf, C., Schäbitz, F., Schleser, G.H., Wille, M., Zolitschka, B., 2005. Climatically induced lake level changes during the last two millennia as reflected in sediments of Laguna Potrok

Aike, southern Patagonia (Santa Cruz, Argentina). J. Paleolimnol. 33 (3), 283–302.
Hadler, H., Vött, A., Newig, J., Emde, K., Finkler, C., Fischer, P., Willershäuser, T., 2018. Geoarchaeological evidence of marshland destruction in the area of rungholt, present-day Wadden Sea around hallig südfall (North Frisia, Germany), by the grote mandrenke in 1362 AD. Quat. Int.
Hesemann, M., 2015. The foraminifera. eu database: concept and status. Palaeontol. Electron. 18 (3), 1–14.
Horton, B.P., Edwards, R.J., 2006. Quantifying Holocene Sea Level Change Using Intertidal Foraminifera: Lessons from the British Isles, vol 40. Cushman Foundation for Foraminiferal Research Special Publication, pp. 1–97.
Horton, B.P., Corbett, R., Culver, S.J., Edwards, R.J., Hillier, C., 2006. Modern saltmarsh diatom distribution of the Outer Banks, North Carolina, and the development of a transfer function for high resolution reconstructions of sea level. Estuar. Coast Shelf Sci. 69, 381–394.
Hoselmann, C., Streif, H., 2004. Holocene sea-level rise and its effect on the mass balance of coastal deposits. Quat. Int. 112 (1), 89–103.
Jacobs, P., De Batist, M., 1996. Sequence Stratigraphy and Architecture on a Ramp-type Continental Shelf: the Belgian Palaeogene, vol 117. Geological Society, London, Special Publications, pp. 23–48 (1).
Kabata-Pendias, A., 2011. Trace Elements in Soils and Plants, fourth ed. CRC Press, Boca Raton, pp. 505.
Kalbe, L., Werner, H., 1974. Das Sediment des Kummerower Sees. Untersuchungen des Chemismus und der Diatomeenflora. Int. Rev. Hydrobiol. 59 (6), 755–782.
Karle, M., Goldhammer, J., 2018. The Wadden Sea of north-west Germany: an intertidal environment of high archaeological research potential. In: In: Bailey, G.N. (Ed.), Under the Sea: Archaeology and Palaeolandscapes of the Continental Shelf, vol 20. Coastal Research Library, pp. 223–231.
Keppler, F., Biester, H., 2003. Peatlands: a major sink of naturally formed organic chlorine. Chemosphere 52 (2), 451–453.
Krammer, K., Lange-Bertalot, H., 1986-1991. Süßwasserflora von Mitteleuropa. In: Ettl, H., Gerloff, J., Heynig, H., Mollenhauer, D. (Eds.), Bacillariophyceae. Naviculaceae. G. Fisher, Stuttgart. New York 2/1, 1-876; Bacillariaceae, Epithemiaceae, Surirellaceae, 2/2, 1-596; Centrales, Fragilariaceae, Eunotiaceae, 2/3, 1-576; Achnantaceae, 2/4, 1-437.
Lambeck, K., Rouby, H., Purcell, A., Sun, Y., Sambridge, M., 2014. Sea level and global ice volumes from the last glacial maximum to the holocene. Proc. Natl. Acad. Sci. Unit. States Am. 111 (43), 15296–15303.
Lange-Bertalot, H., Witkowski, A., Metzeltin, D., 2000. Iconocgraphia Diatomologica. Volume 7. Diatoms of Marine Coasts I.
Leri, A.C., Myneni, S.C., 2012. Natural organobromine in terrestrial ecosystems. Geochem. Cosmochim. Acta 77, 1–10.
Meijles, E.W., Kiden, P., Streurman, H.J., van der Plicht, J., Vos, P.C., Gehrels, W.R., Kopp, R.E., 2018. Holocene relative mean sea-level changes in the Wadden Sea area, northern Netherlands. J. Quat. Sci. 33 (8), 905–923.
Müller-Navarra, K., Milker, Y., Schmiedl, G., 2016. Natural and anthropogenic influence on the distribution of salt marsh foraminifera in the Bay of Tümlau, German North Sea. J. Foraminifer. Res. 46 (1), 61–74.
Murray, J.W., 2006. Ecology and Applications of Benthic Foraminifera. Cambridge University Press.
Ohlendorf, C., Wennrich, V., Enters, D., 2015. Experiences with XRF-scanning of long sediment records. In: Rothwell, G., Croudace, I.W. (Eds.), Micro-Xrf Studies of Sediment Cores. Springer, Netherlands, pp. 351–372.
Pals, J.P., van Geel, B., Delfos, A., 1980. Paleoecological studies in the Klokkeweel bog near hoogkarspel (prov. of Noord-Holland). In: Review of Palaeobotany and Palynology, vol 30. pp. 371–418 (0).
Reimer, P.J., Bard, E., Bayliss, A., Beck, J.W., Blackwell, P.G., Bronk Ramsey, C., Buck, C.E., Cheng, H., Edwards, R.L., Friedrich, M., Grootes, P.M., 2013. IntCal13 and Marine 13 radiocarbon age calibration curves 0–50,000 years cal BP. Radiocarbon 55 (4), 1869–1887.
Rothwell, R.G., Rack, F.R., 2006. New techniques in sediment core analysis: an introduction. In: In: Rothwell, R.G. (Ed.), New Techniques in Sediment Core Analysis, vol 267. Geological Society of London, Special Publications, pp. 1–29.
Scheder, J., Engel, M., Bungenstock, F., Pint, A., Siegmüller, A., Schwank, S., Brückner, H., 2018. Fossil bog soils ('*dwog* horizons') and their relation to Holocene coastal changes in the Jade Weser region, southern North Sea, Germany. J. Coast. Conserv. 22 (1), 51–69. https://doi.org/10.1007/s11852-017-0502-z.
Schüttenhelm, R.T., Laban, C., 2005. Heavy minerals, provenance and large scale dynamics of seabed sands in the Southern North Sea: baak's (1936) heavy mineral study revisited. Quat. Int. 133, 179–193.
Streif, H., 1990. Das ostfriesische Küstengebiet. Nordsee, Inseln, Watten und Marschen. In: second ed. Sammlung Geologischer Führer, vol 57. Gebrüder Borntraeger, Stuttgart, pp. 376.
Streif, H.J., 2002. The Pleistocene and Holocene development of the southeastern North Sea basin and adjacent coastal areas. In: Wefer, G., Berger, W., Behre, K.-E., Jansen, E. (Eds.), Climate Development and History of the North Atlantic Realm. Springer, Berlin, pp. 387–397.
Streif, H.J., 2004. Sedimentary record of Pleistocene and holocene marine inundations along the north sea coast of lower Saxony, Germany. Quat. Int. 112, 3–28.
Szkornik, K., Gehrels, W.R., Kirby, J.R., 2006. Salt-marsh distribution in Ho Bugt (Denmark) and the development of a transfer function for reconstructing Holocene sea- level changes. Mar. Geol. 235, 137–150.
Thomson, J., Croudace, I.W., Rothwell, R.G., 2006. A geochemical application of the ITRAX scanner to a sediment core containing eastern Mediterranean sapropel units. In: In: Rothwell, R.G. (Ed.), New Techniques in Sediment Core Analysis, vol 267. Geological Society of London, Special Publications, pp. 65–77 (1).
van der Spek, A.J., 2018. The development of the tidal basins in the Dutch Wadden Sea until 2100: the impact of accelerated sea-level rise and subsidence on their sediment budget–a synthesis. Neth. J. Geosci. 97 (3), 71–78.
van Geel, B., Aptroot, A., 2006. Fossil ascomycetes in Quaternary deposits. Nova Hedwigia 82 (3–4), 313–329.
Vink, A., Steffen, H., Reinhardt, L., Kaufmann, G., 2007. Holocene relative sea-level change, isostatic subsidence and the radial viscosity structure of the mantle of northwest Europe (Belgium, The Netherlands, Germany, southern North Sea). Quat. Sci. Rev. 26 (25–28), 3249–3275.
Vos, P.C., De Wolf, H., 1988. Methodological aspects of paleo-ecological diatom research in coastal areas of the Netherlands. Geol. Mijnb. 67, 31–40.
Vos, P.C., van Kesteren, W.P., 2000. The long-term evolution of intertidal mudflats in the northern Netherlands during the Holocene; natural and anthropogenic processes. Cont. Shelf Res. 20 (12–13), 1687–1710.
Wartenberg, W., Vött, A., Freund, H., Hadler, H., Frechen, M., Willershäuser, T., Schnaidt, S., Fischer, P., Obrocki, L., 2013. Evidence of isochronic transgressive surfaces within the Jade Bay tidal flat area, southern German North Sea coast–Holocene event horizons of regional interest. Z. Geomorphol. - Suppl. 57 (4), 229–256.
Wedepohl, K.H., 1995. The composition of the continental crust. Geochem. Cosmochim. Acta 59 (7), 1217–1232.
Weltje, G.J., Tjallingii, R., 2008. Calibration of XRF core scanners for quantitative geochemical logging of sediment cores: theory and application. Earth Planet. Sci. Lett. 274, 423–438.
WoRMS, E.B., 2016. World Register of Marine Species.
Ziemann, H., 1971. Die Wirkung des Salzgehaltes auf die Diatomeenflora als Grundlage für eine biologische Analyse und Klassifikation der Binnengewässer. Limnologica 8 (2), 505–525.
Ziemann, H., Schulz, C.-J., 1999. Methods for biological assessment of salt-loaded running waters– fundamentals, current positions and perspectives. Limnologica 41, 90–95.

Supplementary material – Bulian et al. (2019) Estuarine, Coastal and Shelf Science 225, 106251

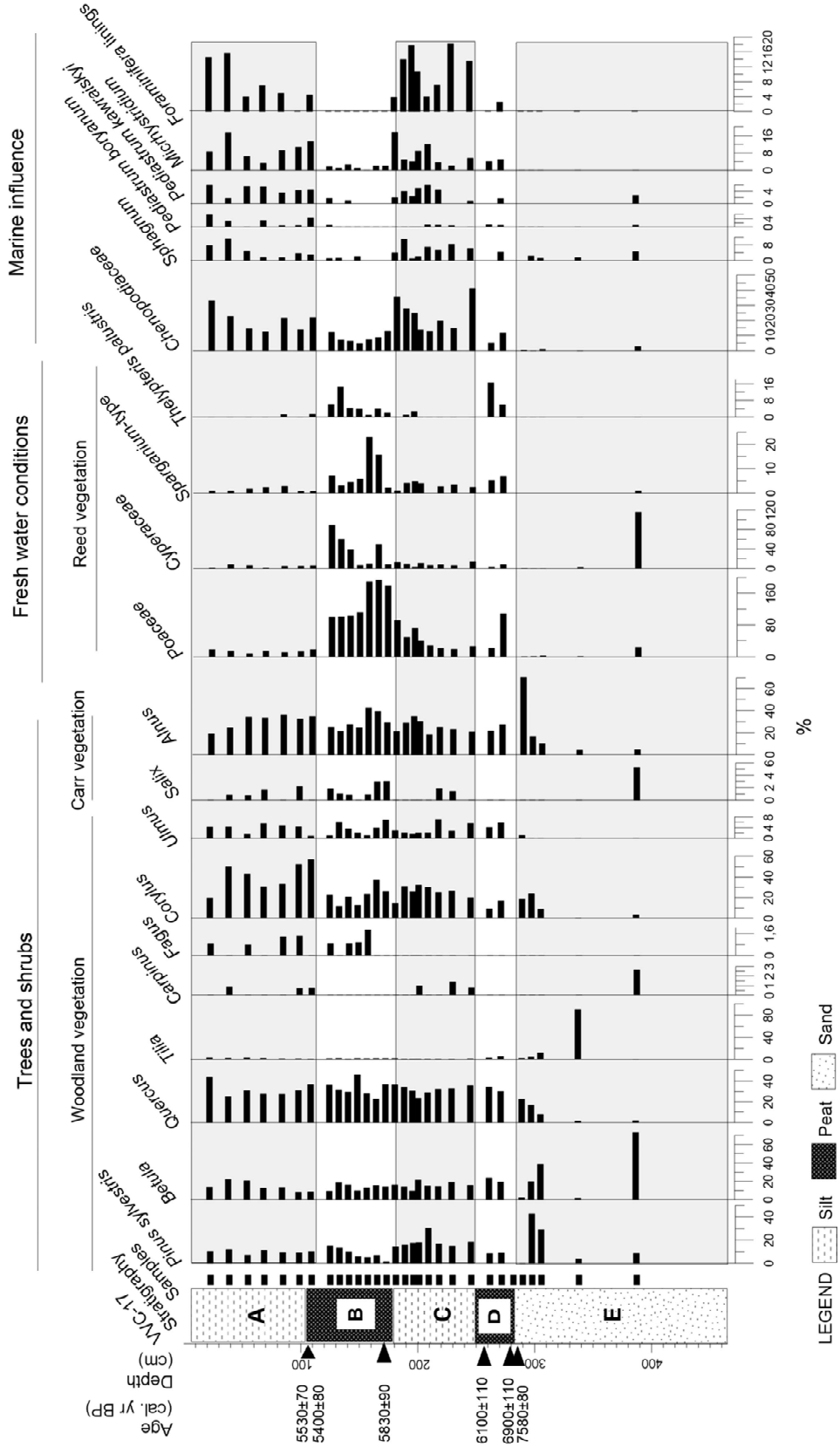

Fig. 3.S1 Pollen and non-pollen palynomorph diagram of selected taxa for core VVC 17 including ^{14}C-ages and lithofacies A-E. All percentages refer to an arboreal sum without Corylus, Myrica and Ericaceae. The fresh water green algae (Pediastrum) and Sphagnum spores are mostly reworked.

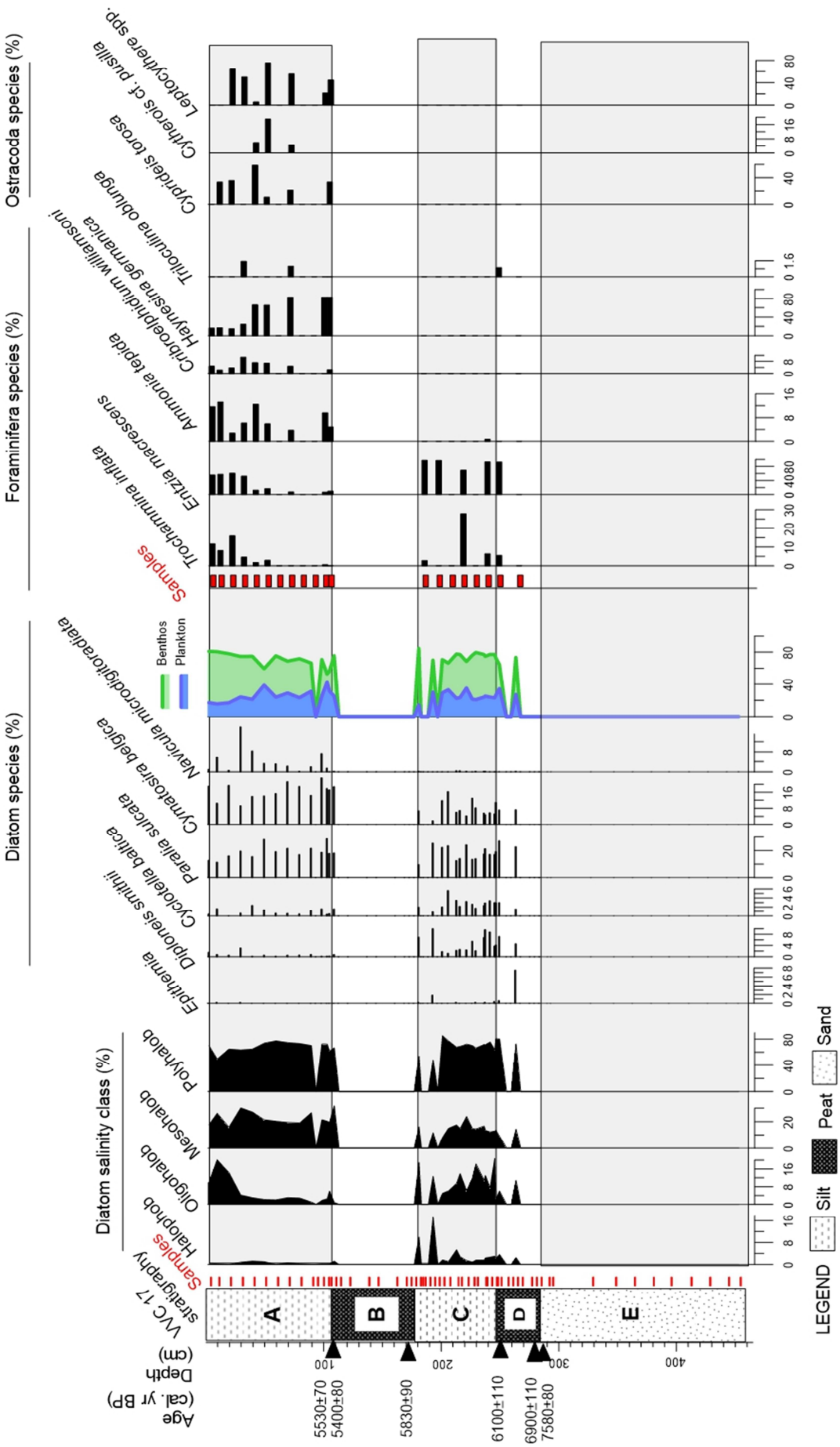

Fig. 3.S2 Diatom, foraminifer and ostracod diagram for core VVC 17, including ^{14}C-ages and lithofacies A-E.

Chapter 4

4 Microfauna- and sedimentology-based facies analysis for palaeolandscape reconstruction in the back-barrier area of Norderney (NW Germany)

Annastasia Elschner[1], Juliane Scheder[2,3], Friederike Bungenstock[3], Alexander Bartholomä[4], Thorsten M Becker[3], Ruggero M Capperucci[4], Dirk Enters[3], Martina Karle [3,4], Frank Schlütz[3], Achim Wehrmann[4], Gösta Hoffmann[1,5]

[1] Institute of Geoscience – Geology, Bonn University, Nussallee 8, 53115 Bonn, Germany

[2] Institute of Geography, University of Cologne, Albertus-Magnus-Platz, 50923 Cologne, Germany

[3] Lower Saxony Institute for Historical Coastal Research, Viktoriastraße 26/28, 26382 Wilhelmshaven, Germany

[4] Marine Research Department, Senckenberg am Meer, Südstrand 40, 26382 Wilhelmshaven, Germany

[5] Institute for Neotectonics and Natural Hazards, RWTH Aachen University, Lochnerstraße 4–20, 52056 Aachen, Germany

Abstract

Palaeolandscape reconstructions at the German North Sea coast are essential for the understanding of coastal changes and dynamic landscape-forming processes. This study contributes to reconstructing Holocene coastal changes in the back-barrier area of the East Frisian island of Norderney and draws conclusions on the local palaeogeography. Five sediment cores were analysed in terms of sedimentology (grain-size distribution), geochemistry (TOC, TIC, N, C/N), microfauna (foraminifers and ostracods) and 13 radiocarbon dates. In order to identify driving environmental factors and support the facies interpretation, multivariate statistics (PCA) were carried out. Additional cores from the surrounding area (WASA Project and 'Landesamt für Bergbau, Energie und Geologie' (LBEG) Hannover) enabled correlation of the investigated cores over a transect of ~6 km, showing six depositional environments, which can be used for landscape reconstruction. Deposition starts with periglacial (aeolian and glaciofluvial) Pleistocene sediments, with subsequent pedogenesis followed by swamp conditions that develop into a salt marsh. The overlying tidal-flat sediments are partially cut by (fossil and recent) channel deposits. A hiatus at the base of the tidal-flat deposits that spans some 3000 years hints at their reworking caused by a combination of antrophogenic coastal protection measures and the impact of storms. Furthermore, based on the profile correlation and the age data, a widespread salt-marsh area with a minimum age of ~4000 cal BP is defined for the 'Hohes Riff' in the southwestern back-barrier of Norderney Island.

Keywords

Foraminifera, Holocene coastal change, multi-proxy approach, North Sea coast, Ostracoda

Published in *Netherlands Journal of Geosciences* 100 (2021), e4
https://doi.org/10.1017/njg.2020.16

Netherlands Journal of Geosciences

www.cambridge.org/njg

Original Article

Cite this article: Elschner A, Scheder J, Bungenstock F, Bartholomä A, Becker TM, Capperucci RM, Enters D, Karle M, Schlütz F, Wehrmann A, and Hoffmann G. Microfauna- and sedimentology-based facies analysis for palaeolandscape reconstruction in the back-barrier area of Norderney (NW Germany). *Netherlands Journal of Geosciences*, Volume 100, e4. https://doi.org/10.1017/njg.2020.16

Received: 7 May 2020
Revised: 14 October 2020
Accepted: 15 October 2020

Keywords:
foraminifera; Holocene coastal change; multi-proxy approach; North Sea coast; Ostracoda

Author for correspondence: G. Hoffman, Email: g.hoffman@uni-bonn.de

© The Author(s), 2021. Published by Cambridge University Press. This is an Open Access article, distributed under the terms of the Creative Commons Attribution-NonCommercial-NoDerivatives licence (http://creativecommons.org/licenses/by-nc-nd/4.0/), which permits non-commercial re-use, distribution, and reproduction in any medium, provided the original work is unaltered and is properly cited. The written permission of Cambridge University Press must be obtained for commercial re-use or in order to create a derivative work.

CAMBRIDGE UNIVERSITY PRESS

Microfauna- and sedimentology-based facies analysis for palaeolandscape reconstruction in the back-barrier area of Norderney (NW Germany)

Annastasia Elschner[1], Juliane Scheder[2,3], Friederike Bungenstock[3], Alexander Bartholomä[4], Thorsten M Becker[3], Ruggero M Capperucci[4], Dirk Enters[3], Martina Karle[3,4], Frank Schlütz[3], Achim Wehrmann[4] and Gösta Hoffmann[1,5]

[1]Institute of Geoscience – Geology, Bonn University, Nussallee 8, 53115 Bonn, Germany; [2]Institute of Geography, University of Cologne, Albertus-Magnus-Platz, 50923 Cologne, Germany; [3]Lower Saxony Institute for Historical Coastal Research, Viktoriastraße 26/28, 26382 Wilhelmshaven, Germany; [4]Marine Research Department, Senckenberg am Meer, Südstrand 40, 26382 Wilhelmshaven, Germany and [5]Institute for Neotectonics and Natural Hazards, RWTH Aachen University, Lochnerstraße 4-20, 52056 Aachen, Germany

Abstract

Palaeolandscape reconstructions at the German North Sea coast are essential for the understanding of coastal changes and dynamic landscape-forming processes. This study contributes to reconstructing Holocene coastal changes in the back-barrier area of the East Frisian island of Norderney and draws conclusions on the local palaeogeography. Five sediment cores were analysed in terms of sedimentology (grain-size distribution), geochemistry (TOC, TIC, N, C/N), microfauna (foraminifers and ostracods) and 13 radiocarbon dates. In order to identify driving environmental factors and support the facies interpretation, multivariate statistics (PCA) were carried out. Additional cores from the surrounding area (WASA Project and 'Landesamt für Bergbau, Energie und Geologie' (LBEG) Hannover) enabled correlation of the investigated cores over a transect of ~6 km, showing six depositional environments, which can be used for landscape reconstruction. Deposition starts with periglacial (aeolian and glaciofluvial) Pleistocene sediments, with subsequent pedogenesis followed by swamp conditions that develop into a salt marsh. The overlying tidal-flat sediments are partially cut by (fossil and recent) channel deposits. A hiatus at the base of the tidal-flat deposits that spans some 3000 years hints at their reworking caused by a combination of antrophogenic coastal protection measures and the impact of storms. Furthermore, based on the profile correlation and the age data, a widespread salt-marsh area with a minimum age of ~4000 cal BP is defined for the 'Hohes Riff' in the southwestern back-barrier of Norderney Island.

Introduction

Coastal zones are preferred areas of human settlement (Small & Nicholls, 2003). However, they are also highly dynamic zones where sea-level variations lead to changes in coastal configuration. The relative sea level (RSL) at any given coastal site depends on climatically induced global changes as well as local factors that lead to vertical movement of the lithosphere including tectonics, compaction and glacio-isostatic adjustment. These changes act on different timescales and result in transgressions and regressions. Natural hazards such astsunamis or storm surges may cause severe changes to the coastal geomorphology.

The project WASA (Wadden Sea Archive) focuses on the analysis of marine sediment archives and aims to reconstruct the Holocene transgression history of the German North Sea coast (see Bittmann et al., 2020). The approach is interdisciplinary and combines archaeological with geological data. A challenging task is to detect former land surfaces and subsequently map potential areas for past human settlements.

The German North Sea coast is a highly dynamic environment with a very wide intertidal area consisting of tidal flats, wetlands and channels. Barrier islands separate the so-called Wadden Sea from the open North Sea. From a sedimentological point of view, the various environments result in different facies. Due to tidal currents and a widely branched net of tidal channels, areas of sediment accumulation are located next to areas of erosion. The Wadden Sea is a classic example of Walther's Law (López, 2014), where the sediment profiles reflect lateral changes in the environment. However, the depositional environment is also characterised by extremely small-scale facies changes. Therefore, the lateral correlation of sediment profiles is

Downloaded from https://www.cambridge.org/core. IP address: 88.130.158.217, on 13 Mar 2021 at 22:28:39, subject to the Cambridge Core terms of use, available at https://www.cambridge.org/core/terms. https://doi.org/10.1017/njg.2020.16

challenging. Reconstruction of former landscapes is further complicated by post-depositional processes including sediment remobilisation, bioturbation and compaction.

This study primarily aims at reconstructing palaeolandscape changes as a base for identifying former land surfaces. These surfaces can be upper salt marshes or soils. WASA integrates several disciplines for detailed analysis of cores and core transects, which enable reliable definition of different facies. The combination of sedimentological and microfaunal analyses is a powerful tool to improve the initial macroscopic facies analysis and to provide detailed information about the depositional environment. Palaeolandscapes are reconstructed based on this information and analysed for chronology, triggers and development in the sense of sedimentation processes, transgressive or regressive contacts, characteristic hiatuses and the spatial extent of erosional surfaces. This study focuses on a west–east transect in the back-barrier of Norderney to test our approach for profile correlation and to better understand the vertical and lateral facies succession.

Secondly, this study aims at defining vertical and lateral segments within a profile section with a continuous and quiet sedimentation (Wartenberg et al., 2013). These may serve for suggestions on sampling for further studies on RSL evolution in the Norderney tidal basin. Although the Holocene RSL history is generally understood (Streif, 2004; Behre, 2007), especially spatial variations of the continuing glacio-isostatic adjustment call for RSL reconstructions based on dense datasets with a close regional context (Vink et al., 2007; Bungenstock & Weerts, 2010, 2012).

Study area

Geological setting

Norderney island and its back-barrier are part of the back-barrier island system of the southern North Sea (Fig. 1) and located within the UNESCO World Heritage 'Wattenmeer' in Germany. Today, the Wadden Sea can be divided into different landscapes that also prevailed during the transgression after the Last Glacial Maximum (LGM). These include barrier islands, tidal flats, coastal marshlands and *Geest* (Streif, 1998).

The sedimentary record is directly related to the Holocene sea-level rise. After the LGM ~21 ka BP, a strong eustatic sea-level rise (Clark et al., 2009) started as a consequence of the melting of the Fennoscandian and Laurentide ice sheets. The increase in free water as well as the glacio-isostatic adjustment led to a sea-level rise of 110 to 130 m which resulted in a lateral shift of the North Sea coast of *c.*600 km to the south (Kiden et al., 2002; Behre, 2004; Streif, 2004).

The East Frisian Islands have formed since ~7–6 ka BP (Flemming, 2002), when sea-level rise slowly decelerated. With continuing RSL rise and prevalent current direction they have continuously migrated southeastward. The tidal flats also formed after the deceleration of the RSL rise around 6–7 ka BP when the North Sea reached the position of the present-day Wadden Sea (e.g. Flemming, 2002; Streif, 2004; Behre, 2007). The tidal range increased when the southern and northern North Sea merged and as a consequence the tidal flats expanded. Subsequently, Holocene peat deposits and siliciclastic sediments accumulated on top of the Pleistocene sands, reaching thicknesses of up to 25 m (Streif, 2004). Peat layers intercalated in the marine sediments of the Holocene sequence are interpreted as temporary changes of rates of RSL rise and accelerated sediment supply causing regressive phases in the sense of a coastal progradation (Freund & Streif, 2000; Streif, 2004). The tidal-flat sediments consist 90% of reworked Pleistocene sediments, and only 10% of recently transported fluvial material (Hoselmann & Streif, 1997).

The marshlands are defined as the terrestrial area bordering the sea (Streif, 1998). Two different types of marshland are distinguished: the salt marshes and the diked areas (Streif, 1990). The salt marshes formed on nutrient-rich silt deposits above the mean high tide level. They are inundated and supplied with sediments only during spring-tide and storm-surge events.

In the Netherlands, human interference with the coastline started in the late Iron Age/Roman period. The development of the Wadden Sea is subject to intense anthropogenic influences, at latest since the construction of a continuous dyke system along the Frisian coast in the 13th century. This leads to a strong reworking of the tidal-flat sediments (Van der Spek, 1996), a process known as Wadden Sea Squeeze, which results in the loss of mudflats (Reineck & Siefert, 1980; Flemming & Nyandwi, 1994; Mai & Bartholomä, 2000). The long-term consequences of these influences are not conceivable in detail but will affect the stability, persistence and preservation of this unique UNESCO World Heritage Site.

Study site

Norderney is one of the East Frisian barrier islands of the German North Sea coast, lying *c.*4.5 km north of the mainland. The East Frisian barrier islands build an island chain in a mesotidal regime protecting the back-barrier tidal flats and the mainland from the direct influence of waves and storm surges. The tidal range at Norderney is 2.5 m (BSH, 2019). The tidal flats exhibit a shore-normal energy gradient resulting in an overall succession from sand flats in the north, to mixed flats and finally mudflats in the south directly bordering the mainland coast (Nyandwi & Flemming, 1995). The analysed ~6 km long west–east transect is situated in the back-barrier of Norderney. In the west, it starts at the main tidal inlet, 'Norderneyer Seegat', crossing the sandbank 'Hohes Riff' to the northeast up to the 'Norderneyer Wattfahrwasser' directly south of the island (Fig. 1). According to the maps by Homeier (1964), the positions of the 'Norderneyer Seegat' and the 'Hohes Riff' were relatively stable during the previous 400 years.

Methods

Fieldwork

Five sediment cores were collected in different environments. The investigated sediment cores (N77, N49, VC13, N44, N45) were obtained as part of the WASA project, using different coring techniques. Tidal-channel cores were conducted from the research vessel MS *Burchana* using a vibrocorer VGK-6 (VC-6000, med consultans GmbH) and plastic liners with 10 cm diameter, whereas tidal-flat cores were conducted using a vibrocorer (Wacker Neuson IE high-frequency vibrator head and generator) and aluminium liners with 8 cm diameter.

The geographic position of the drill sites was determined by a differential GPS with a cm-range accuracy. The elevation data were obtained with reference to the German standard elevation zero (NHN).

Opening, photographic documentation and macroscopic core description after Preuss et al. (1991) was performed at the Lower Saxony Institute for Historical Coastal Research in Wilhelmshaven, Germany, and the Institute of Geography of the University of Bremen, Germany. Samples for sedimentological

Downloaded from https://www.cambridge.org/core. IP address: 88.130.158.217, on 13 Mar 2021 at 22:28:39, subject to the Cambridge Core terms of use, available at https://www.cambridge.org/core/terms. https://doi.org/10.1017/njg.2020.16

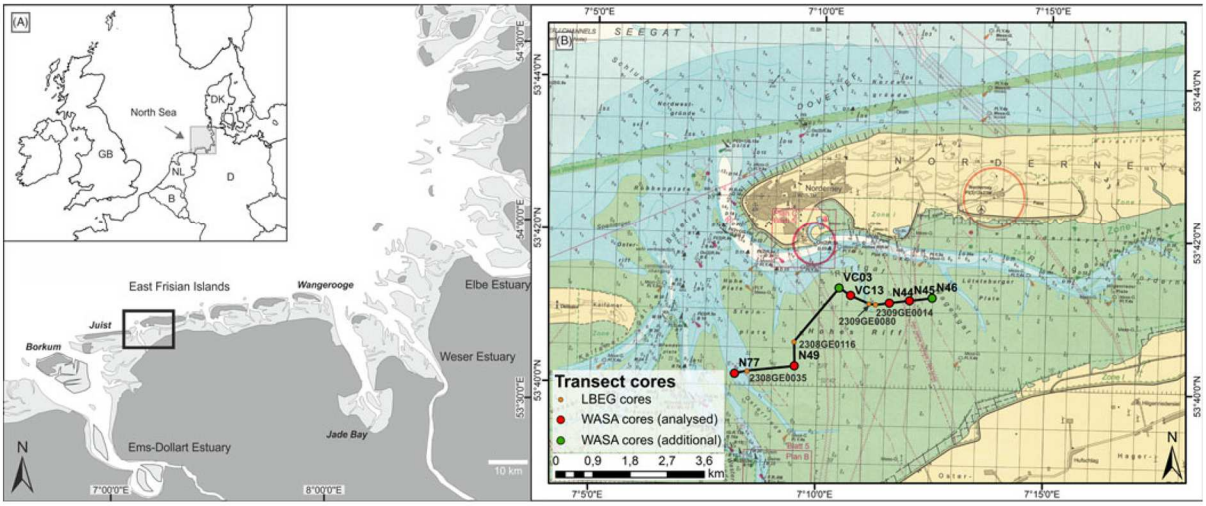

Fig. 1. Study area. (A) Overview of the North Sea coast with framed study area; (B) Investigated transect in the back-barrier of Norderney with investigated cores (red), additional WASA cores (green) and archive cores (orange). Map source: BMS (2016).

and microfaunal analyses were taken along a 10 or 20 cm grid, including some additional samples for smaller-scale layers.

Laboratory analyses

In order to determine depositional processes, sedimentological, geochemical and microfaunal investigations were conducted for 84 samples from the five sediment cores. A special focus was laid on the identification of microfauna associations enabling conclusions on ecological conditions, thus supporting or adjusting facies interpretation. Sedimentological and geochemical analysis concentrated on the grain-size distribution and on nitrogen (N) and carbon content (total organic carbon = TOC, total inorganic carbon = TIC). These analyses helped to further classify the facies. Multivariate statistics (PCA) were performed to support the interpretation and identify controlling environmental factors.

For sedimentological and geochemical investigations, the sample material was dried at 40°C and carefully pestled by hand. For grain-size analysis, carbonate was removed by adding hydrochloric acid (HCl, 10%) and the organic components were removed using hydrogen peroxide (H_2O_2, 15%) (Blume et al., 2011). In order to prevent aggregation, sample material was treated with sodium pyrophosphate ($Na_4P_2O_7$; 46 g l^{-1}). The grain-size distribution was measured for the fraction between 0.04 µm and 2 mm using a laser particle size analyser (Beckmann Coulter LS13320; laser beam 780 nm) applying the Fraunhofer optical mode (Eshel et al., 2004). The grain-size distribution provides important information on hydro-energetic levels and the depositional environment. Furthermore, microfaunal associations can be related to the grain-size distribution, since different species prefer different substrates (Blott & Pye, 2001; Frenzel et al., 2010).

The concentrations of N, TOC (accounting for *c*.50% of the organic matter) and total carbon (TC) within the samples were measured after grinding the samples using an elemental analyser (elementar, Vario EL Cube). For TOC measurements, carbonates were removed by the addition of HCl (10%) (Pribyl, 2010). This enabled the determination of TIC, accounting for *c*.12% of the calcium carbonate ($CaCO_3$), from the difference of TC and TOC (Bernard et al., 1995). Finally, the C/N ratio was derived providing information about the origin of organic matter (Last & Smol, 2002; Khan et al., 2015).

Microfauna samples were carefully shaken overnight, using a dispersant (sodium pyrophosphate; $Na_4P_2O_7$; 46 g l^{-1}) to prevent clay adhesion, and washed through sieves (63 and 100 µm) in order to isolate microfossils (>100 µm) from fine-grained sediment. Where possible, 100 individuals were counted dry, however, accepting a minimum of 40 individuals for samples with very low abundance (cf. Scheder et al., 2019). Analysed and residual material was weighed to enable extrapolation and calculation of microfaunal concentration. Species determination followed taxonomic descriptions and illustrations in Athersuch et al. (1989), Gehrels & Newman (2004), Horton & Edwards (2006), Murray (2006) and Frenzel et al. (2010). The replacement of *Elphidium excavatum* by *Cribroelphidium excavatum* (Terquem, 1875) as well as the replacement of *Pontocythere elongata* by *Cushmanidea elongata* (Brady, 1868) was adopted according to the online database WORMS. Due to problematic discrimination and low counts of individuals of (*Cribro-*)*Elphidium* (e.g. *Elphidium cuvillieri* and *Cribroelphidium gunteri*), these species were grouped under *Elphidium* spp. for counting. Furthermore, occurring species of *Leptocythere* were grouped under *Leptocythere* spp. for counting, due to the problematic discrimination of juvenile individuals.

Radiocarbon (^{14}C) age determination

A chronological framework is provided by 13 age determinations originating from the sediment cores N77, N49, VC13 and N44 (Table 1). The ^{14}C age determinations (accelerator mass spectrometry (AMS)) were performed by the Poznań Radiocarbon Laboratory (Poland). The results were calibrated with the software CALIB (Version 7.1) using the calibration curves IntCal13 and Marine13 (Reimer et al., 2013). According to measurements of Enters et al. (2020) the ΔR value for reservoir correction of ages originating from *in situ* shell material was presumed 74 ± 16 ^{14}C years.

Downloaded from https://www.cambridge.org/core. IP address: 88.130.158.217, on 13 Mar 2021 at 22:28:39, subject to the Cambridge Core terms of use, available at https://www.cambridge.org/core/terms. https://doi.org/10.1017/njg.2020.16

Table 1. Radiocarbon ages calibrated with IntCal13, dataset 1 (for northern hemisphere terrestrial ^{14}C dates) and Marine13 (for mollusc dating, sample Poz-97990) with reservoir correction (delta R 74 ± 16) after Enters et al. (2020).

Core	Depth (m NHN)	Lab. No.	Dated material[a]	Conventional ^{14}C age and uncertainty (^{14}C a BP)	Calibrated age, 95% probability (cal a BP)[b]
N49	−2.99	Poz-97990	*Barnea candida* (in living position)	1350 ± 30	905–733
	−3.07	Poz-106641	fine bulk	3940 ± 35	4515–4255
	−3.29	Poz-115426	fine bulk	4645 ± 30	5465–5311
	−3.29	Poz-115164	*Phragmites australis*	3795 ± 35	4346–4010
	−4.27	Poz-106643	charred stem and rhizome	4205 ± 30	4845–4628
VC13	−2.93	Poz-115133	fine bulk	3660 ± 30	4084–3899
	−3.72	Poz-115134	*Cladium mariscus*	4100 ± 35	4814–4449
N44	−2.915	Poz-115136	*Phragmites australis*	3330 ± 30	3637–3477
	−2.915	Poz-115163	charred stem remains	3335 ± 35	3682–3475
	−3.185	Poz-112307	*Schoenoplectus*, *Potentilla anserine*	3580 ± 35	3980–3729
N77	−3.38	Poz-112521	charred stem remains	4690 ± 35	5577–5319
	−3.66	Poz-112311	*Cladium mariscus*	5025 ± 35	5892–5661
	−4.38	Poz-115167	*Calluna vulgaris*, *Erica tetralix*	6160 ± 40	7166–6949

[a]*Ph. australis, C. vulgaris* and *E. tetralix* vegetative remains, *C. mariscus, Schoenoplectus* and *P. anserina* fruits and seeds.
[b]Exact age data after calibration.

Data processing

Measures for univariate statistical grain size were calculated by means of the Excel tool GRADISTAT (Version 4.0) (Blott & Pye, 2001), after Folk & Ward (1957). A correlation analysis (Spearman's rs) allowed detection of relationships between the different parameters (sand amount, mean grain size, TOC, TIC and C/N) and of possible autocorrelations. Microfauna distributions and environmental parameters were analysed by means of multivariate statistics (principal component analysis (PCA)) in order to find driving environmental factors and support the facies interpretation. PCA was only performed on samples with a complete dataset of all three analyses using the software PAST (v. 3.2.1) (Hammer et al., 2001).

Results and interpretation

Lithological units

Six lithological units (A–F) were identified based on foraminifer and ostracod associations, visual features in the sediment cores, grain-size distribution and TOC, TIC and N content. However, not all units are present in all sediment cores (Figs. 3 and 4 further below; Supplementary Figs S1–S3 (in the Supplementary Material available online at https://doi.org/10.1017/njg.2020.16)). Nine foraminifer taxa and 11 ostracod taxa were identified (Fig. 2; Supplementary Table S1 (in the Supplementary Material available online at https://doi.org/10.1017/njg.2020.16)).

Unit A: Pleistocene deposits

Unit A is characterised by moderately well to well-sorted fine sand and was exclusively documented in N77 (7.75–4.95 m below NHN) (Fig. 3). TOC, TIC and N measurements are below the detection limit. Therefore, the C/N ratio is not regarded as significant as it varies around transitional values between aquatic and terrestrial environments (e.g. Last & Smol, 2002; Khan et al., 2015). The entire unit is void of microfauna, which indicates a terrestrial environment. Since the study area was subject to periglacial conditions, with accumulation of aeolian and glaciofluvial sands (cf. Streif, 2004), Unit A is assumed to represent Pleistocene/*Geest* deposit.

Unit B: palaeosol

Unit B is characterised by moderately well-sorted fine sand and also occurs exclusively in core N77 (4.95–4.41 m below NHN). Macroscopic core description shows dark laminae which seem richer in organic matter than Unit A. However, TOC contents are below the detection limit, permitting verification of higher organic contents. Since N also remains below the detection limit, the C/N ratio, indicating a terrestrial origin of the organic matter (Last & Smol, 2002; Khan et al., 2015), is again not significant. Observations of Bulian et al. (2019) from a core in the vicinity show signs of pedogenesis for a comparable layer. Together with the macroscopic core description, this leads to the assumption that Unit B represents a palaeosol at the base of the Holocene sedimentary sequence (Holocene base).

Unit C: peat

Unit C is characterised by dark brown organic deposits containing layers of clastic material with moderately well-sorted fine sand and poorly sorted sandy mud. It was documented in four cores (N77: 4.41–3.68 m below NHN; VC13: 3.76–3.73 m below NHN; N44: 3.786–3.24 m below NHN; and N49: C-1: 4.42–4.17 m; C-2: 3.37–3.0 m below NHN). Since no sample material was available from Unit C in VC13, the identification here is based on the macroscopic core description. TOC contents increase in all cores, representing the maximum (between ~30% and ~40%) of the respective

Downloaded from https://www.cambridge.org/core. IP address: 88.130.158.217, on 13 Mar 2021 at 22:28:39, subject to the Cambridge Core terms of use, available at https://www.cambridge.org/core/terms. https://doi.org/10.1017/njg.2020.16

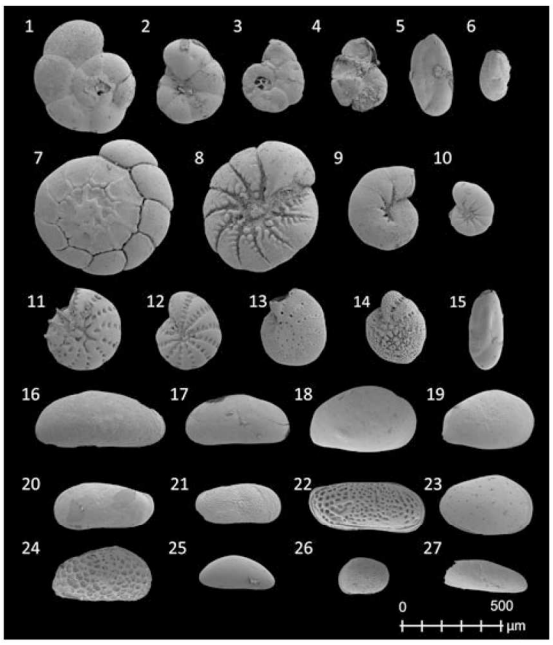

Fig. 2. Scanning electron microscope (SEM) images of frequently documented foraminifera (1–15) and ostracod (16–27). 1–2: *Trochammina inflata* (Montagu, 1808); 3–4: *Entzia macrescens* (Brady, 1870); 5–6: *Miliammina fusca* (Brady, 1870); 7–8: *Ammonia tepida* (Cushman, 1926); 9–10: *Haynesina germanica* (Ehrenberg, 1840); 11–12: *Cribroelphidium williamsoni* (Haynes, 1973); 13: *Elphidium cuvillieri* (Levy, 1966); 14: *Cribroelphidium gunteri* (Cole, 1931); 15: *Triloculina oblonga* (Montagu, 1803); 16: *Cushmanidea elongata* (Brady, 1868); 17: *Cushmanidea elongata* (Brady, 1868), juvenile, 18–19: *Cyprideis torosa* (Jones, 1850), juvenile; 20: *Leptocythere lacertosa* (Hirschmann, 1912), juvenile; 21: *Leptocythere castanea* (Sars, 1866), juvenile; 22: *Leptocythere pellucida* (Baird, 1850); 23: *Loxoconcha elliptica* (Brady, 1868), juvenile; 24: *Urocythereis britannica* (Athersuch, 1977), juvenile; 25: *Cytherois cf. pusilla* (Sars, 1928), juvenile; 26: *Hirschmannia viridis* (Mueller, 1785), juvenile; 27: *Sahnicythere retroflexa* (Klie, 1936), juvenile.

core. A similar pattern is documented for N contents (maximum values around 1.6%). For C-2 (N49) both values increase but do not reach similarly high values. TIC is considerably low except for N77 and N49 (C-2), where it increases to ~35% and ~10%. C/N ratios and the lack of microfauna point to a semi-terrestrial environment in most samples. Together, these results indicate the formation of a peat, with high organic contents due to decaying vegetation and low carbonate contents resulting from decalcification processes associated with peat formation (Bungenstock 2005; Scheder et al., 2018). The locally higher TIC values (N77 and N49 C-2) may indicate an increased marine influence. For N77 this is in accordance with several intercalated fine-grained layers indicating episodic marine inundations. For N49 (C-2), the slightly increased TIC content possibly results from bioturbation at the erosive contact (Bird, 2008). The foraminifers occurring in C-1 (N49) are mainly characterised by agglutinated *Trochammina inflata* (Montagu, 1808), *Entzia macrescens* (Brady, 1870) and *Miliammina fusca* (Brady, 1870). These typical salt-marsh species were either introduced by relocation or by post-depositional bioturbation (Athersuch et al., 1989; Murray, 2006) or alternatively, they indicate a transition to the overlying deposit. The fen peat in N49 (C-1), VC13 and N44 formed directly on top of the *Geest* deposits and is therefore referred to as basal peat. Samples from N77, N49 (C-1) and N44 provided ^{14}C ages for the upper parts of the basal peat (Table 1); in the west (N77) it dates to 7170–6950 cal BP (bottom) and 5890–5660 cal BP (top), whereas towards the east (N49) it dates to 4850–4630 cal BP and 3980–3730 cal BP (N44). The bottom of the second peat in N49 (C-2) dates to 4350–4010 cal BP and the top shows an age of 4520–4260 cal BP directly below the erosional contact.

Unit D: salt-marsh deposits

Unit D is characterised by poorly sorted sandy mud to muddy sand and was documented in four cores (N77: 3.68–3.32 m below NHN; N49: 4.17–3.37 m below NHN; VC13: 3.73–2.87 m below NHN; and N44: 3.24–2.895 m below NHN). The geochemical parameters vary strongly between the cores. While TIC, TOC and N values in N49 are very low, TOC and N values in N77 decrease but are still considerably high, whereas no TIC is documented. Furthermore, in VC13, TOC and N show high values, whereas TIC strongly decreases upwards. N44 shows a reversed pattern (increasing TIC, decreasing TOC and N. C/N ratios vary between >5 and ~20, indicating a transitional environment between terrestrial and aquatic conditions (cf. Last & Smol, 2002; Khan et al., 2015). However, the presence of salt-marsh foraminifers, which are almost exclusively *T. inflata* and *E. macrescens*, indicates a more aquatic environment. Unit D is identified as salt-marsh deposit based on the documented C/N ratios, the microfaunal association and the typical poorly sorted, fine-grained sediments (Bakker et al., 2003). The lack of microfauna in N77 is interpreted as a very low inundation frequency resulting from the distance from the coastline which defines the upper limit of the high salt marsh. An alternative explanation is that microfauna was destroyed after the deposition of the layer or dissolved by humic acids of plant decomposition (Bungenstock, 2005; Scheder et al., 2018). The top of the salt-marsh deposits in VC13 and N44 is erosive. Salt-marsh samples from N77 (top), VC13 (bottom and top) and N44 (top) were dated (Table 1), providing the oldest age of 5580–5320 cal BP in the west (N77). The base of Unit D in VC13 dates to 4810–4450 cal BP, and the top dates to 4080–3900 cal BP, whereas the top in N44 shows ages of 3680–3480 cal BP and 3980–3730 cal BP.

Unit E: channel deposits

Unit E is characterised by (very) poorly sorted muddy sand and was documented in three cores (N77: 3.32–2.98 m below NHN; N44: 2.895–2.245 m below NHN; and N45: 6.21–2.70 m below NHN). TOC, TIC and N values are considerably low in all samples and the low C/N ratios indicate an aquatic environment. The poor sorting, with sand as main grain-size component, and the low nutrient contents point to a marine channel with low energy levels, where fine-grained sediments are deposited due to meandering (Zepp, 2017). The microfauna supports this interpretation, as occurring salt-marsh species (N77) indicate relocation (Horton & Edwards, 2006; Murray, 2006) and were possibly redistributed by the typical erosion–accumulation pattern of meandering channels (cf. Zepp, 2017). The microfauna concentration in N44 is generally high, with lower abundances in the sandier (higher-energy) parts. The layer shows very great diversity, with shallow marine species clearly dominating. As such were identified mainly *Ammonia tepida* (Cushman, 1926) and *Haynesina germanica* (Ehrenberg, 1840), accompanied by *Cribroelphidium williamsoni* (Haynes, 1973), *Leptocythere* (Sars, 1925) and taxa of lower abundance (Athersuch et al., 1989; Horton & Edwards, 2006; Murray, 2006; Frenzel et al., 2010). This dominance of shallow marine

Downloaded from https://www.cambridge.org/core. IP address: 88.130.158.217, on 13 Mar 2021 at 22:28:39, subject to the Cambridge Core terms of use, available at https://www.cambridge.org/core/terms. https://doi.org/10.1017/njg.2020.16

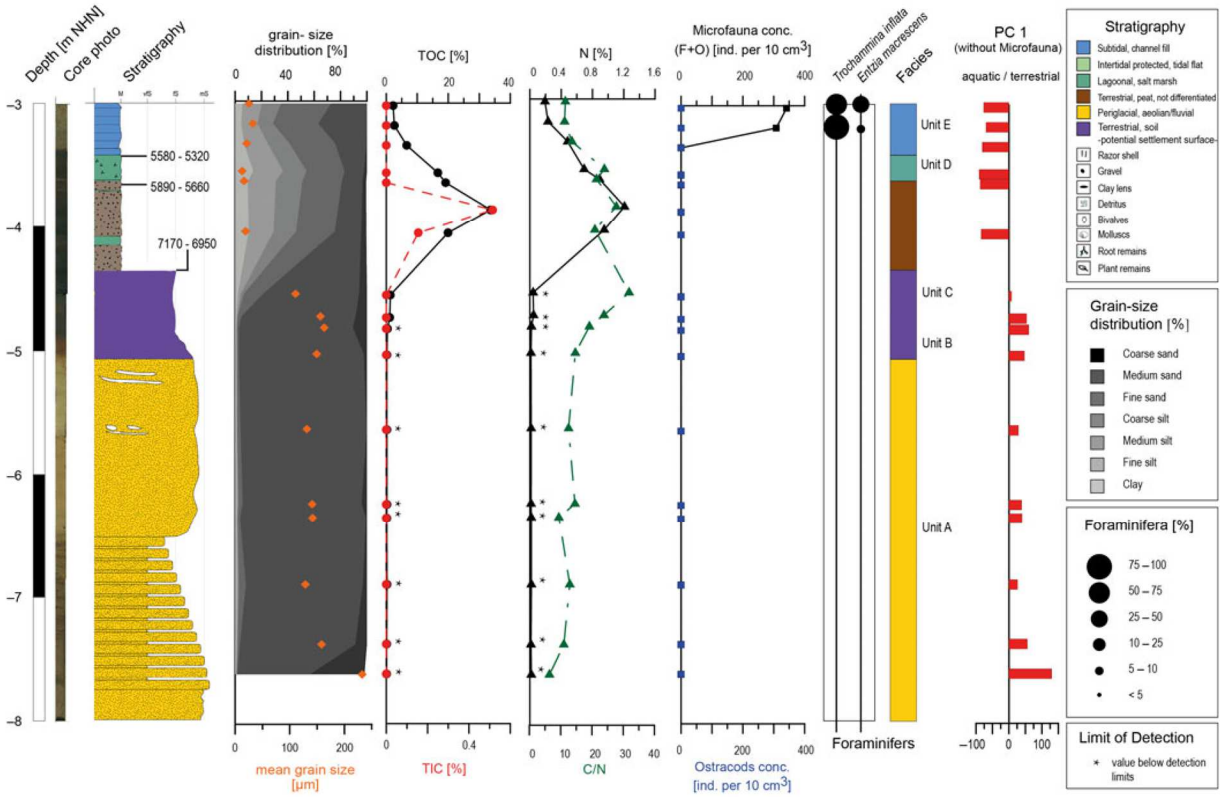

Fig. 3. Sedimentological, geochemical and microfaunal results of N77, including the most relevant component of the PCA.

species supports the interpretation that Unit E represents a low-energy channel.

Unit F: tidal-flat deposits

Unit F is characterised by poorly sorted muddy sand gradually changing upwards to very well-sorted fine sand and was documented in four cores (N49: 3.0–0.98 m below NHN; VC13: 2.87–0.73 m below NHN; N44: 2.245–0.795 m below NHN; and N45: 2.70–0.53 m below NHN). The top of this unit represents the sediment surface in these cores. For N49 and N44, only microfaunal data are available, in addition to the macroscopic description, due to lack of material. The good sorting and the high dominance of fine sand indicate a higher energy level compared to Units C–D (Wartenberg et al., 2013). Unit F exhibits subunits in all sediment cores, which are characterised by coarser-grained deposits, indicating a short-term high-energy event, such as a storm surge (Wartenberg et al., 2013). TOC and N lie at considerably low levels and are below the detection limit in VC13. The C/N ratio varies but mainly indicates aquatic conditions (N45). The present mollusc fragments and the intercalated coarser layers support this interpretation. The microfauna concentration in Unit F varies between <100 and ~8000 Ind./10 cm^3 (individuals per 10 cm^3), which is possibly connected to variations in grain-size distribution representing energy levels, and TOC and N contents representing nutrient availability. One peak is documented for the microfauna concentration at the base of Unit F in VC13, which is interpreted as reworking due to the erosive contact between units D and E. *A. tepida* mainly dominates over *H. germanica*. This indicates a lower salinity, as *A. tepida* has its optimum at lower salinities (Murray, 2006). *H. germanica* dominates over *A. tepida* only in the uppermost samples of N44 and VC13, indicating an increasing salinity. Besides these two most common species, shallow marine foraminifer and ostracod taxa occur. All this leads to the interpretation of Unit F as a tidal-flat environment. The very few documented salt-marsh foraminifers are interpreted as introduced by the tidal current. The articulated bivalve *Barnea candida* (Linnaeus, 1758) in living position is documented directly at the erosional contact between the tidal flat and the underlying peat in N49 (Fig. 4). It is positioned inside its borehole and dates to 910–730 cal BP.

Evaluation and interpretation of the fossil data

In order to find variables accounting for as much of the variance in the dataset as possible (Davis, 1986; Harper, 1999), the foraminifer and osctracod associations as well as the environmental parameters were analysed by means of a PCA. This analysis should enable the identification of driving environmental factors and support the facies interpretation.

After the calculation of Spearman's correlation coefficients, parameters showing auto- or very high correlations were excluded from the dataset. Very rare (<5%) taxa of foraminifers and ostracods were also excluded. Subsequently, the PCA was performed separately for each sediment core as well as jointly for all sediment cores, including the parameters sand amount, TOC, TIC, C/N and the microfaunal associations. The results (Figs 5–7; Supplementary Figs S4–S7 (in the Supplementary Material available online at

Downloaded from https://www.cambridge.org/core. IP address: 88.130.158.217, on 13 Mar 2021 at 22:28:39, subject to the Cambridge Core terms of use, available at https://www.cambridge.org/core/terms. https://doi.org/10.1017/njg.2020.16

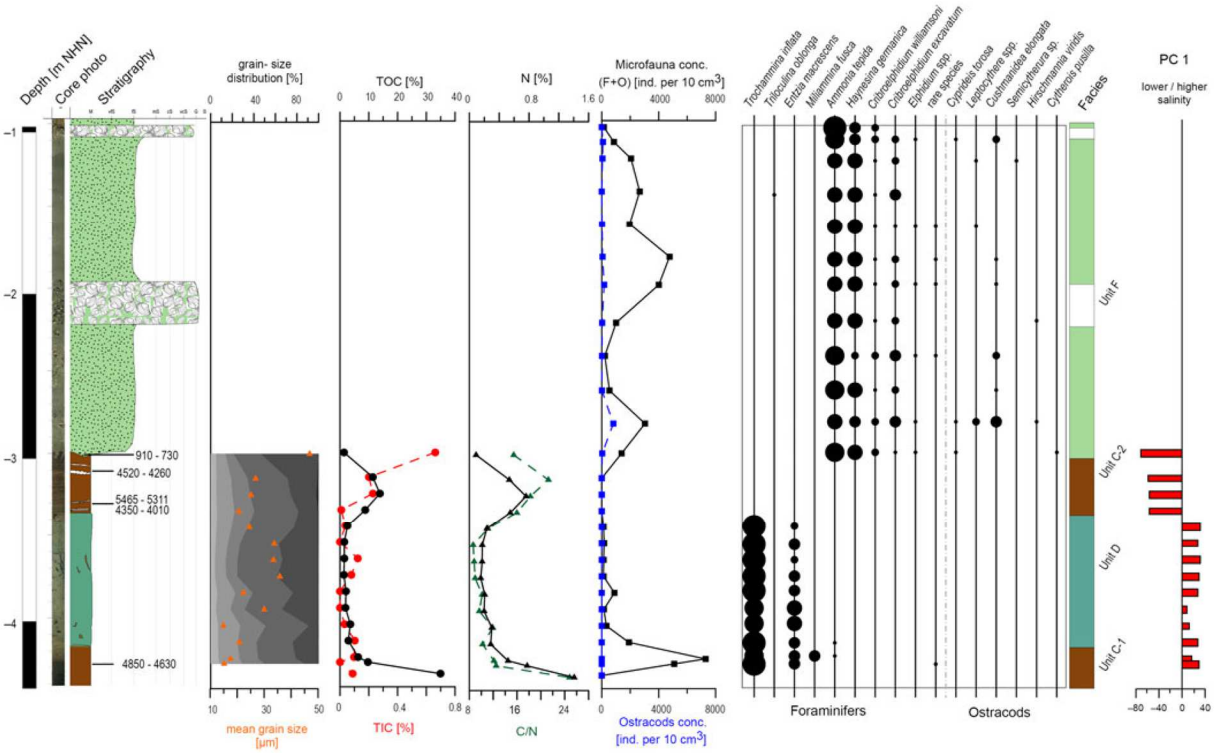

Fig. 4. Sedimentological, geochemical and microfaunal results of N49, including the most relevant component of the PCA. For the colour legend see Figure 3.

https://doi.org/10.1017/njg.2020.16)) confirm the identified units based on the revealed sample groupings. In all PCAs, PC 1 and 2 are the most relevant components, whereas PC 3 shows variances of less than 10%.

For N77, the PCA was carried out without microfauna, as there were only two samples containing the latter (Fig. 5). PC 1 (98.7%) opposes samples with higher TIC contents (negative values) and those with TIC values below the detection limit (positive values) suggesting that PC 1 represents a factor driven by marine influence possibly connected to water depth (Bird, 2008). This component shows a very high variance, which makes PC 2 (0.9%) insignificant. Nevertheless, it is clearly opposing TOC content (positive values) and sand amount (negative values). Since the deposition of organic matter is strongly dependent on hydrodynamic levels, a grain-size factor is assumed for PC 2 (Khan et al., 2015). The different sample groupings (Fig. 5) are mainly associated to the identified units (A, C, D and E), whereas the salt-marsh samples (Unit D) form the most distinct group.

For N49, two PCAs were carried out, one including the lower half of the core with all performed analyses, and one for the upper half with exclusively microfauna (Fig. 6; Supplementary Fig. S4 (in the Supplementary Material available online at https://doi.org/10.1017/njg.2020.16)). In both cases, PC 1 does not outnumber PC 2 as intensely as in N77. For the lower core (Fig. 6), PC 1 (77.6%) opposes all salt-marsh samples together with the typical salt-marsh species (positive values) and mainly peat and shallow marine species (negative values) indicating a marine-influence factor, whereby the peat samples distort the results here. Comparison of the ecological preferences of the opposed species leads to the assumption that PC 1 represents salinity (Murray, 2006). PC 2 (13.8%) opposes sand amount (positive values) and TOC content (negative values), again suggesting a grain-size component. However, due to the preference of *A. tepida* and *H. germanica* for rather fine-grained material, which hints at reworking effects, uncertainties remain. Again, the groupings reflect the previously defined units (C, D and F). For the upper half (Supplementary Fig. S4 (in the Supplementary Material available online at https://doi.org/10.1017/njg.2020.16)), PC 1 (63.2%) opposes *A. tepida* and *H. germanica*, which hints at the salinity. This is based on the fact that *A. tepida* dominating over *H. germanica* indicates a lower salinity (Murray, 2006). PC 2 (32%) is much stronger than in the lower core half and opposes the two mentioned species and all other taxa, especially *C. williamsoni*. Since the latter prefers substrates with clay- and mud contents <60%, whereas *A. tepida* and *H. germanica* prefer clay- and mud contents >80% (Murray, 2006), this component is interpreted to represent the grain size. Only one group is visible in the PCA plot (Supplementary Fig. S4 (in the Supplementary Material available online at https://doi.org/10.1017/njg.2020.16)) apparently associated to *H. germanica*, suggesting an influence of slightly increased salinity for this part of the tidal-flat deposits (Murray, 2006). Considering both partial PCAs, salinity plays a major role for the complete core, whereas the grain size is more important in the upper than in the lower half.

The PCA plots of the other cores are documented in Supplementary Figures S5–S7 (in the Supplementary Material available online at https://doi.org/10.1017/njg.2020.16). For VC13, PC 1 (76.8%) is interpreted as a water-depth factor, whereas PC 2 (12.3%) represents the general marine influence. N44 is influenced by the grain size as the first component (PC 1; 63.9%) and

Downloaded from https://www.cambridge.org/core. IP address: 88.130.158.217, on 13 Mar 2021 at 22:28:39, subject to the Cambridge Core terms of use, available at https://www.cambridge.org/core/terms. https://doi.org/10.1017/njg.2020.16

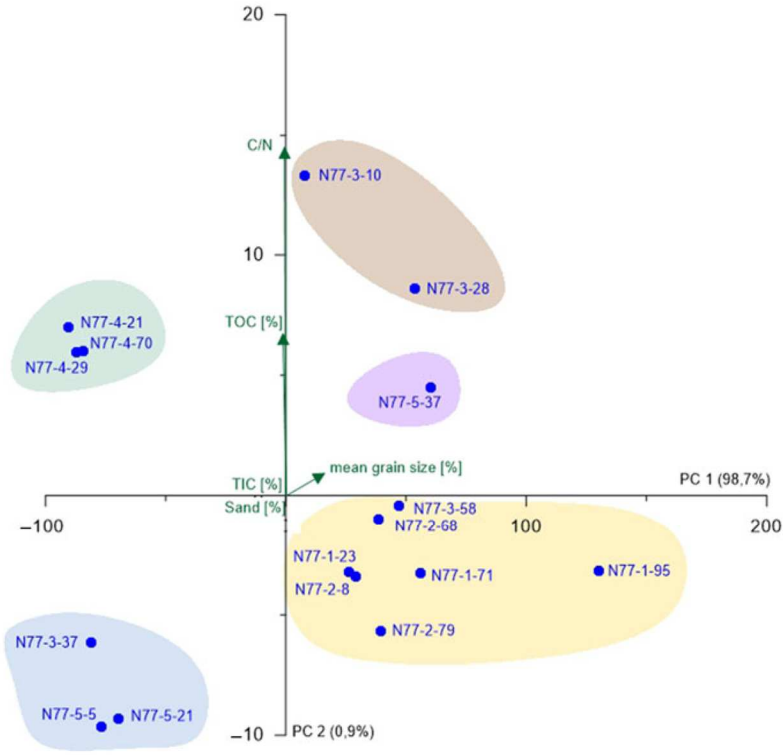

Fig. 5. PCA biplot of N77 showing the two most relevant axes (PC 1 and PC 2). Colours of sample groupings relate to the colour legend in Figure 3; green arrows represent environmental parameters and blue points represent samples.

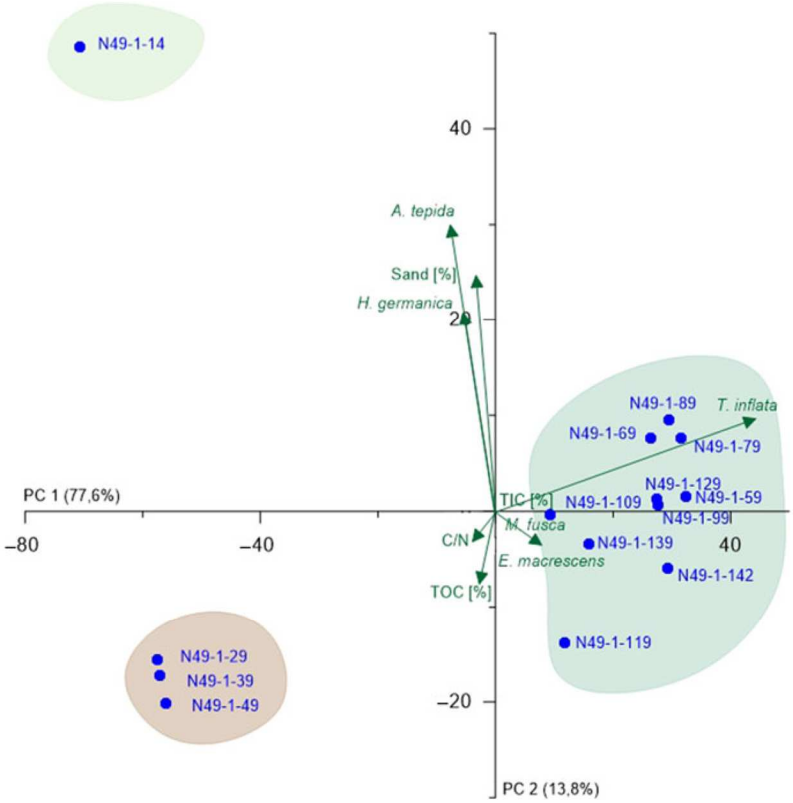

Fig. 6. PCA biplot of N49 (lower part) showing the two most relevant axes (PC 1 and PC 2). Colours of sample groupings relate to the colour legend in Figure 3; green arrows represent microfaunal taxa and environmental parameters, and blue points represent samples.

Downloaded from https://www.cambridge.org/core. IP address: 88.130.158.217, on 13 Mar 2021 at 22:28:39, subject to the Cambridge Core terms of use, available at https://www.cambridge.org/core/terms. https://doi.org/10.1017/njg.2020.16

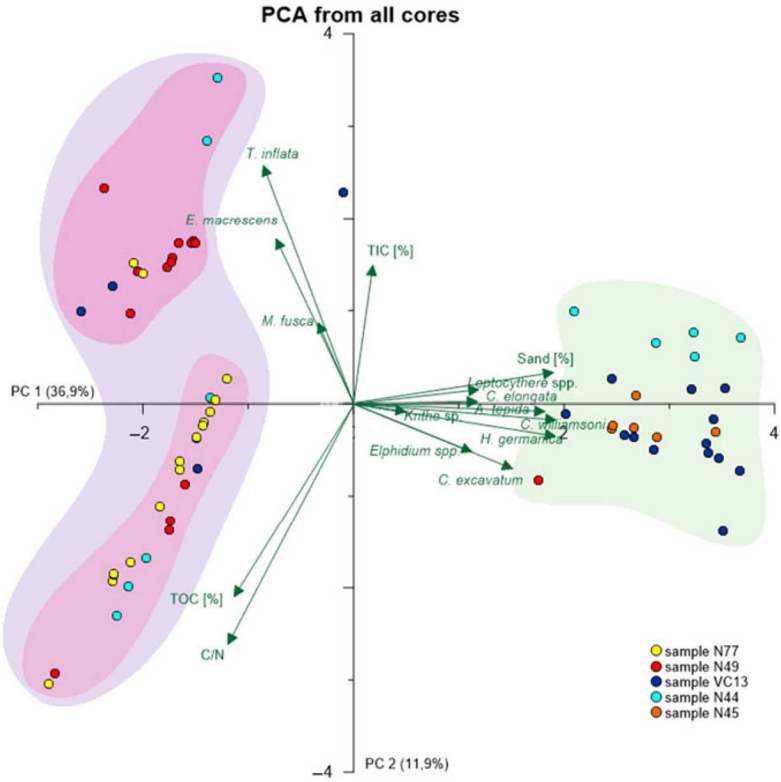

Fig. 7. PCA biplot of all cores, showing the two most relevant axes (PC 1 and PC 2). Colours of sample groupings relate to the colour legend in Figure 3; green arrows represent microfaunal taxa and environmental parameters, and coloured points represent samples.

the marine influence as the second (PC 2; 23.1%). N45 is mainly driven by the grain size (PC 1; 87.0%) and to a lesser extent by water depth and/or salinity (PC 2; 8.7%). The joint PCA (Fig. 7) is highly influenced by the presence or absence of microfauna, leading to a relatively good separation of shallow-marine (Units E and F), mainly supratidal to semi-terrestrial (Units C and D) and mainly semi-terrestrial to terrestrial (Units A, B and C) environments (Fig. 7). PC 1 (36.9%) is likely related to the grain size due to the strong approximation of the sand amount to the first axis. PC 2 (11.9%) opposes salt-marsh species (and samples) and TIC content with TOC content and more terrestrial samples suggesting a general marine-influence factor.

Correlation

The analysed cores were complemented by two additional WASA cores (VC03 and N46) and four archive cores of the LBEG (2308GE0035, 2308GE116, 2309GE0080, 2309GE0014), in order to enable the correlation of the layers identified and their respective facies. The transect reaches from the '*Norderneyer Seegatt*' at the western tip of Norderney 6 km to the east directly south of the Norderney island tidal channel (Fig. 8). Since only one core reaches the Pleistocene deposits, the Holocene base was modelled based on the geological coastal map of the LBEG (2019), accessed through the '*NIBIS® Kartenserver*'.

The integration of the LBEG cores in our stratigraphic cross-section requires critical analysis of the archive core descriptions. The descriptions are often not detailed enough for a reliable landscape reconstruction, as the LBEG cores were conducted for different purposes, e.g. engineering or hydrogeology, and by different processors. Therefore, facies interpretations were reviewed based on the knowledge gained from the WASA cores (cf. Scheder et al., 2019). With that, integrating them in the profile section helps to obtain a more precise picture of facies successions in the study area.

The sedimentation history in the study area can be reconstructed starting with the deposition of late Pleistocene sands. These were documented in the western part of the study area (N77) and identified based on the grain-size distribution and the lack of organic and inorganic carbon as well as missing microfauna. The latter indicates a non-aquatic habitat, supporting the interpretation as late Pleistocene. We assign the last glacial period, locally known as Weichselian. The study area was subject to periglacial conditions where aeolian and glaciofluvial processes dominated (Streif, 2004). The top of these deposits shows higher C/N ratios pointing to terrestrial conditions (Khan et al., 2015), but inconclusively as the counts of C and N are low (N77, chapter 4). The terrestrial origin is clear in VVC17, as decomposition of organic matter indicates the formation of a palaeosol on top of the aeolian and glaciofluvial sands (Bulian et al., 2019).

Subsequently, a fen peat developed, marking the base of the Holocene sequence. The dating results indicate spatial differences in peat formation and a time-transgressive development. In the western part, peat formation started ~7500 cal BP and lasted for ~1500 years (VVC17), whereas to the east, peat formation is documented with an age of ~4700 cal BP in the upper part of the basal peat in N49. This is regarded as a minimum age, as the base of the peat was not reached. The time-transgressive nature of the peat

Downloaded from https://www.cambridge.org/core. IP address: 88.130.158.217, on 13 Mar 2021 at 22:28:39, subject to the Cambridge Core terms of use, available at https://www.cambridge.org/core/terms. https://doi.org/10.1017/njg.2020.16

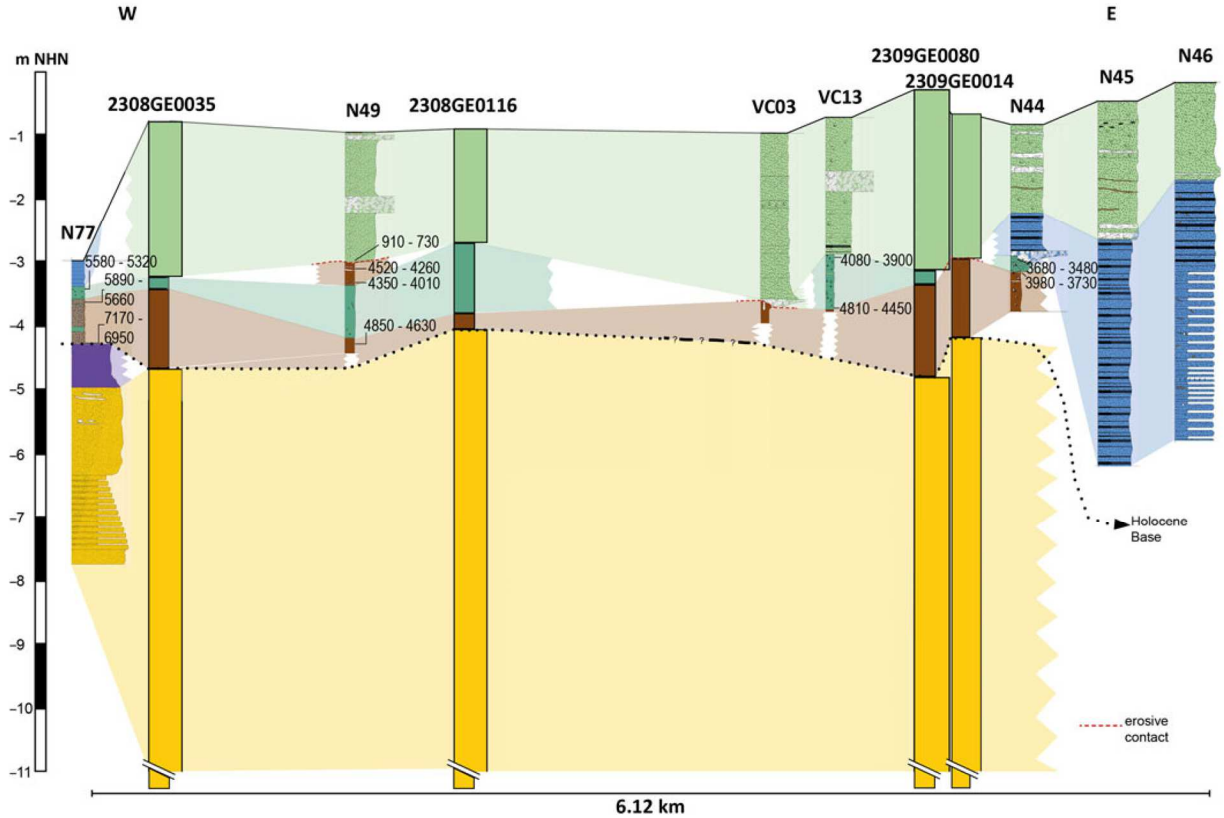

Fig. 8. Stratigraphic cross-section of the five investigated cores, the two additional WASA cores and the four LBEG cores. For the colour legend see Figure 3. Ages are given in cal a BP (rounded to decades; for exact ages see Table 1).

formation reflects the rising groundwater level associated with the RSL rise (e.g. Vink et al., 2007; Baeteman et al., 2011). Furthermore, the area became protected ~6–7 ka BP by the developing barrier island, maintaining sheltered conditions for peat growth during a rising RSL (Freund & Streif, 2000; Flemming, 2002; Bungenstock & Schäfer, 2009). Foraminifers and marine diatoms in the upper parts of the peat suggest an increasing marine influence.

The increasing marine influence resulted in the development of a salt marsh burying the basal peat. This interpretation is based on the microfaunal association, consisting of typical salt-marsh species, especially *T. inflata* and *E. macrescens*. The grain-size distribution indicates a low-energy environment, and C/N ratios vary between aquatic and semi-terrestrial conditions (Horton and Edwards, 2006; Khan et al., 2015). The ^{14}C age data prove the initiation of salt-marsh formation ~6000 cal BP in the west (N77), whereas to the east it started to develop after ~4700 cal BP. This is explained by the palaeogeographic situation of the forming barrier island, which provided shelter for the more easterly part, leading to a delay in salt-marsh formation. However, an influence of relocation of the dated material in N77 (Table 1) has to be considered. Since the salt-marsh deposits documented in the adjacent core VVC17 (Bulian et al., 2019) are of approximately the same age but are situated ~2 m deeper than in N77, a correlation of both layers is difficult, supporting the assumption of relocation in N77.

An intercalated peat in the west was documented in core VVC17, with peat growth dated from ~5900 to 5300 cal BP. It remains undetermined whether this indicates a regression (Baeteman 1999; Bungenstock & Weerts, 2010, 2012).

An additional intercalated peat developed ~4300 cal BP on top of the salt marsh, documented in core N49). The top is characterised by an erosive contact. Erosional contacts are documented in three cores further east (VC03, VC13 after ~3900 cal BP and N44 after ~3600 cal BP), indicating a hiatus.

During that time, the main channel had already shifted to the western part of the study area, following the southeastward migration of the barrier islands (e.g. Flemming, 2002; Streif, 2004). Salt-marsh species in the top layer of VVC17 indicate reworking and erosion, which appears as tidal-flat facies. East of the main channel, a tidal-flat environment developed as the result of rising RSL. Further to the east, this tidal flat was cut by another tidal channel, which was either infilled subsequently or shifted its location. An intercalated coarse-grained layer with abundant macrofaunal remains, which is correlated over three cores (N49, VC03 VC13), cuts the tidal-flat deposit laterally. We interpret this layer to represent either a high-energy event or a period of increased storm activity. The dating results prove a deposition after ~3600 cal BP. The overlying deposits show further coarse-grained layers, which indicates that higher dynamic conditions established in the back-barrier tidal flat, lasting until today.

Downloaded from https://www.cambridge.org/core. IP address: 88.130.158.217, on 13 Mar 2021 at 22:28:39, subject to the Cambridge Core terms of use, available at https://www.cambridge.org/core/terms. https://doi.org/10.1017/njg.2020.16

Discussion

Assumptions on the spatial extent of palaeo-salt marshes

Palaeogeographic maps for different time periods during the Holocene RSL rise, with a landward- as well as seaward-shifted coastline, are an important reference for models of coastal protection, future long-term coastal development and archaeological sites. Especially for archaeological research, the salt marshes play an important role. Whereas the lower parts, the pioneer zones, were not appropriate for settling, the highly silted-up parts of the upper salt marshes with their high biological productivity were very attractive for habitation (Vos & Knol, 2015; Nieuwhof & Vos, 2018).

Existing approaches for landscape reconstruction on the German North Sea coast are mainly based on the so-called 'Küstenprofilkarten' derived from the descriptions of the archive core data published by the LBEG (Streif, 1998, 2004; Goldhammer & Karle, 2015; Karle et al., 2017). These reconstructions do not show any, or show only small, rims or patches of salt-marsh areas. Possibly, this is because salt-marsh deposits are not always clearly detectable in the cores and are deficiently described, especially in cores taken for engineering purposes. We assume that salt marshes exhibited a much wider spatial extent compared to the traditionally mapped areas, which are based on the archive core data (Vos & Knol, 2015; Karle, 2020; Vos et al., 2020;).

The anthropogenic influence on the present-day coastal landscape is very strong. Even before embankment, ditches connected the sea to the hinterland and drainage lowered the peat areas. Due to the dyke system, the coastline is static, with the consequences of Wadden Sea Squeeze (Flemming & Nyandwi, 1994), intense reworking of the tidal flats (Van der Spek, 1996) and the loss of mudflats (Reineck & Siefert, 1980; Mai & Bartholomä, 2000). A small coastal transition zone with salt marshes exists only as a remnant in the protected areas of the national park. The inner-dyke landscape is even more artificial. This impedes imagination of a former coastal landscape, as there is no modern analogue. This is especially true for the brackish and lagoonal deposits described in the archive cores and several publications (e.g. Streif, 2004; Bungenstock & Schäfer, 2009; Wartenberg & Freund, 2012; Karle et al., 2017). Streif (1990) describes widely distributed brackish areas with low tidal ranges as transition between marine environments and river-, lake- and swamp-dominated environments. For areas of the Unterems, the Krummhörn (western East Frisia) and Wilhelmshaven, even lagoonal deposits were documented by Streif (1971), Barckhausen & Streif (1978) and Barckhausen (1984). They describe clayey to silty deposits with up to 5% fine sand, which show very low to no carbonate content. The deposits exhibit a horizontal layering, with plant debris and Fe-sulphide aggregates. Both the brackish and the lagoonal sediments are deposited in a subaquatic, microtidal and low-saline environment (Streif, 1990). However, predictions on changing tidal range during the Holocene RSL rise in the southern North Sea consistently show increases in tidal range since the early Holocene. The major changes occurred prior to 6 ka BP, and only minor (cm-scale) to no changes occurred subsequently (Shennan et al., 2000; Van der Molen & De Swart, 2001). This is in contrast to the deposition of microtidal-induced brackish and lagoonal deposits as described before. Therefore, it may be assumed that the brackish/lagoonal sediments were deposited locally and are typical of protected areas like the Ems–Dollart region or Jade Bay. There, the brackish and lagoonal environment is mainly controlled by the palaeogeographical situation, including bays and the transition to rivers and swamps, and not under direct influence of the tides.

However, several authors apply the brackish/lagoonal core description to take account of sediments deposited in a less dynamic environment close to a terrestrial environment (LBEG core descriptions; Streif 2004; Bungenstock & Schäfer 2009; Karle et al., 2017). Wartenberg et al. (2013) classify the brackish/lagoonal deposits as *quiet reach sediments*. This facies allows both direct access to the open sea and a lagoon-type isolated palaeogeographical situation. In this way, depositional processes are described independently from a lagoonal landscape situation *sensu stricto*. Tidal–marine as well as limnic–terrestrial conditions may occur and locally salt marshes form (Wartenberg et al., 2013). As salt marshes are part of the supratidal area, stagnant water in ponds was present.

For the presented west–east transect in the back-barrier of Norderney, the fine-grained sediments showing a quiet-reach deposition in between and on top of the peat layers are clearly identified as salt-marsh deposits. They were deposited within a timespan between ~4500 cal BP and ~3300 cal BP in the largest part of the transect. The latter allows the correlation of these salt-marsh deposits over up to 5 km. A landscape reconstruction for this area, therefore, shows a wide and stable rim of salt marshes along the former coastline. This wide distribution defines them as a characteristic element of the palaeolandscape.

For the coast of the northern Netherlands, geoarchaeological research has revealed that salt marshes were inhabited after having reached a minimum thickness of 80 cm and an elevation with less than ~50 days of inundation per year (Vos, 1999; Vos & Gerrets, 2004). The habitation of the salt-marsh region in the Netherlands started around 2700 cal BP (Taayke, 2016) directly on the high marshes and later on salt-marsh ridges or levees that had reached the level of only a middle marsh (Vos, 1999, 2015; Vos & Gerrets, 2004). Due to the higher tidal range in the tidal basin of Norderney, for this area a thickness of *c.*1 m for salt marshes can be expected to enable settlement or at least human activity. Applying this information on the presented core transect, the western part of the sand plate 'Hohes Riff' (from N77 in the west to VC13, only interrupted in VC03 by strong erosion) has the potential for buried settlement remains with a minimum age of ~4000 cal BP. So far, no settlements of this age are known in the marshland areas of the German North Sea coast. The oldest known marshland settlement is Rodenkirchen, situated in the river marshes of the Weser and dating to ~3000 cal BP (Strahl, 2005). Therefore, further mapping of the extent of internal structure of the salt-marsh deposits in the back-barrier area of Norderney could give further information on the potential for human activity.

What triggers landscape change? Sea-level rise versus single events versus anthropogenic influence?

The sedimentary record shows an erosional contact on top of the peat and salt-marsh deposits of N49, VC03 and VC13. It extends over more than 3 km and is followed by a drastic change in depositional environment, suggesting a significant hiatus. In all three cores, the top of the peat is eroded and boreholes of *B. candida* are documented in the topmost part of the peat. In N49 an articulated adult individual of *B. candida* was documented inside its borehole. The adult species digs *c.*15 cm into soft substrates such as peat (Richter & Rumohr 1976; National Museum Wales, 2016). It

Downloaded from https://www.cambridge.org/core. IP address: 88.130.158.217, on 13 Mar 2021 at 22:28:39, subject to the Cambridge Core terms of use, available at https://www.cambridge.org/core/terms. https://doi.org/10.1017/njg.2020.16

typically occurs from the lower intertidal to shallow subtidal environments (Tebble, 1976; Hayward & Ryland, 1990). Therefore, the peat must have been exposed to an intertidal to subtidal environment. This could be generally the case due to (a) the autocompaction of the peat (Long et al., 2006) or, what we assume here, (b) the erosion of peat material. Furthermore, the drowned peat surface should have been free of deposition for at least some years before it was covered with tidal-flat sediments, as *B. candida* needs ~2.5 to 3 years until it reaches its full size within the borehole (Richter & Rumohr, 1976).

Overall, Holocene RSL rise is the most important driver for landscape change along the coast of the southern North Sea. Nevertheless, questions about other processes possibly changing the landscape on a local, regional, short-term or enduring scale arise. For the last ~2000 years, Streif (1990) and Wildvang (1911) describe an increasing loss of lagoonal environments, which finally disappeared with the first continuous dyke system in the 13th century. This is concordant with studies on intense reworking of the tidal flats connected to the beginning of dyke construction (e.g. Van der Spek, 1996). Studies based on comparison of nautical charts and aerial photographs document a reworking of the back-barrier tidal flats by migrating channels of more than 50% within 50 years (Trusheim, 1929; Lüders, 1934; Reineck & Siefert, 1980; Van der Spek, 1996). Depending on the size of the channels, reworking cuts down to depths of more than 20 m (Van der Spek, 1996). However, since the channels do not migrate over the entire back-barrier tidal flat, their catchment area is relatively stable. For the back-barrier area of Spiekeroog, Tilch (2003) showed that between 1866 and 1935 significant erosional deepening related to dyke construction on the mainland took place, but no significant lateral enlargement of the channel systems was documented. Nevertheless, over millennial-scale timespans, reworking over wider areas can be expected relative to the migration of the islands and the shift of the tidal-flat watersheds. In addition, intensified reworking has to be expected during storm surges. Tilch (2003) documented vertical erosion of 16 cm for the northern rim of the Janssand, the sandbank between Langeoog and Spiekeroog, during the summer season of 2001, whereas in the centre of the sandbank the same amount was accumulated. This suggests only proximal sediment transport. For more protected sandbanks, Tilch (2003) reported erosion and accumulation rates in the order of 5 cm. Therefore, the intensified reworking of the tidal flats since the beginning of dyke building could be responsible for the abrupt change from semi-terrestrial to intertidal deposits within the investigated sedimentary record. In this case, the erosional contact might date to ~700 cal BP, indicating a hiatus of more than 3000 years. This is in distinct concordance with the age of the dated piddock, *B. candida*, with an age of 905–733 cal BP.

From historical time, the high impact of storm surges is well known (e.g. Streif, 1990). Their impact is a consequence of coastal-protection measures and especially documented on the mainland. With the first continuous dyke system in the 13th century, sedimentation associated with RSL rise was interrupted for the hinterland. Additionally, the hinterland was drained, resulting in subsidence as the sediments compacted, creating accommodation space. In case of dyke breaches during storm surges, these two factors enabled intense flooding, severe destruction and therefore sustainable change in coastal geomorphology. The consequences of the historical storm surges at the mainland are well documented in historical reports, such as in church registers and documentation of land reclamation by dyking (Homeier, 1964, 1969; Behre, 1999). Furthermore, the impact of storm surges on the tidal flats is expected to be higher than in pre-dyke times, due to the static coastline and lack of inundation space at the mainland. Hence, a high impact of erosion and reworking connected to storm surges is expected in the transition zones of palaeolandscapes as well as in the tidal flats.

Conclusion and outlook

The multi-proxy investigations of the presented sedimentary record are a reliable approach for the reconstruction of the Holocene landscape evolution of the tidal basin of Norderney, leading to specific identifications of six different facies units. The investigations show that microfauna-based core analysis provides robust data for profile correlation, which is needed to better understand palaeolandscape changes as well as syn- and post-depositional processes influencing deposition. This is crucial for the definition of reliable RSL index points (Bungenstock et al., 2020). The clear identification of salt-marsh deposits and their correlation within the transect suggests a much wider expansion of salt marshes along the southern North Sea coast than predicted so far. We conclude that the sand plate 'Hohes Riff' has the potential for buried settlement remains with a minimum age of ~4000 cal BP. Moreover, the clear definition of Unit D as salt marsh, the thickness of Unit D in several cores and its spatial extent provide promising conditions for the application of a microfauna-based transfer function for RSL reconstruction (J Scheder et al., unpublished information).

Furthermore, our results show that an understanding of the impact of future sea-level rise requires precise analyses of underlying processes, as the North Sea coast is highly dynamic. Processes responsible for large-scale changes in coastal geomorphology include global and local factors, and, as well as RSL changes, storm intensity and frequency and the anthropogenic influence by coastal protection measures are key elements in coastal development. Summarising, the depositional succession of the transect is the result of multicausal processes. Besides the Holocene RSL rise, the anthropogenic influence and the impact of storms or a combination of both have significantly changed the facies succession within the geological record documenting, in this case, a low resilience of landscape. Yet, the working hypothesis that the peat surface, initially, was not immediately exposed to new sedimentation hints at the erosional impact of a storm. Hence, palaeolandscape change is not only triggered by Holocene RSL changes but also by single events with an impact too severe for the landscape to withstand or to heal. Nevertheless, further investigations are necessary, in order to better understand reasons for the significant and widespread hiatus documented in the transect, as it cannot be clarified whether it was caused by a single or several storm surges or by possibly intensified reworking since the beginning of dyke building.

Supplementary material. To view supplementary material for this article, please visit https://doi.org/10.1017/njg.2020.16

Acknowledgements. The reported research is part of the WASA project (The Wadden Sea as an archive of landscape evolution, climate change and settlement history: exploration – analysis – predictive modelling), funded by the 'Niedersächsisches Vorab' of the VolkswagenStiftung within the funding initiative 'Küsten und Meeresforschung in Niedersachsen' of the Ministry for Science and Culture of Lower Saxony, Germany (project VW ZN3197). We gratefully acknowledge Dr Anna Pint (University of Cologne) and apl. Prof. Dr Peter Frenzel (Friedrich Schiller University Jena) for their help concerning the determination of ostracod species and questions connected to ecological interpretation. We further acknowledge the skilful work of Hanna Cieszynski who

Downloaded from https://www.cambridge.org/core. IP address: 88.130.158.217, on 13 Mar 2021 at 22:28:39, subject to the Cambridge Core terms of use, available at https://www.cambridge.org/core/terms. https://doi.org/10.1017/njg.2020.16

obtained the SEM images. We thank Peter Vos and an anonymous reviewer for constructive comments that helped to improve the initial manuscript. This paper is a contribution to the IGCP project 639 'Sea-level change from minutes to millennia'.

References

Athersuch, J., Horne, D.J. & Whittaker, J.E., 1989. Marine and brackish water ostracods. (Superfamilies Cypridacea and Cytheracea). Published for the Linnean Society of London and the Estuarine and Brackish-water Sciences Association by E.J. Brill: 183 pp.

Baeteman, C., 1999. The Holocene depositional history of the Ijzer palaeovalley (Western Belgian coastal plain) with reference to the factors controlling the formation of intercalated peat beds. Geologica Belgica **2**: 39–72.

Baeteman, C., Waller, M. & Kiden, P., 2011. Reconstructing middle to late Holocene sea-level change: a methodological review with particular reference to 'A new Holocene sea-level curve for the southern North Sea' presented by K.-E. Behre. Boreas **40**(4): 557–572.

Bakker, J.P., Bos, D., Stahl, J., Vries, D.Y. & Jensen, A., 2003. Biodiversität und Landnutzung in Salzwiesen. Nova Acta Leopoldina NF **87**: 163–194.

Barckhausen, J., 1984. Geologische Karte von Niedersachsen 1:25000, Erläuterungen Blatt 2609 Emden. Landesamt für Bergbau, Energie und Geologie (Hannover): 109 pp.

Barckhausen, J. & Streif, H., 1978. Geologische Karte von Niedersachsen 1:25000, Erläuterungen Blatt 2608 Emden West. Landesamt für Bergbau, Energie und Geologie (Hannover): 80 pp.

Behre, K.-E., 1999. Die Veränderungen der niedersächsischen Küstenlinien in den letzten 3000 Jahren und ihre Ursachen. Probleme der Küstenforschung im südlichen Nordseegebiet **26**: 9–33.

Behre, K.-E., 2004. Coastal development, sea-level change and settlement history during the later Holocene in the Clay District of Lower Saxony (Niedersachsen), northern Germany. Quaternary International **112**: 37–53.

Behre, K.-E., 2007. A new Holocene sea-level curve for the southern North Sea. Boreas **36**: 82–102.

Bernard, B.B., Bernard, H. & Brooks, J.M., 1995. Determination of total Carbon, total organic Carbon and inorganic Carbon in sediments. TDI-Brooks International/B&B Laboratories Inc. College Station (Texas): 1–5.

Bird, E.C.F., 2008. Coastal geomorphology: an introduction. John Wiley & Sons Ltd (Chichester): 436 pp.

Bittmann, F., Capperucci, R., Bartholomä, A., Becker, T., Bungenstock, F., Enters, D., Karle, M., Siegmüller, A., Wehrmann, A., Wurpts, A. & Zolitschka, B., 2020. Drowned paleo-landscapes: current archaeological and natural scientific research in the Wadden Sea and the North Sea basin. Netherlands Journal of Geosciences / Geologie en Mijnbouw (this issue).

Blott, S.J. & Pye, K., 2001. GRADISTAT: a grain size distribution and statistics package for the analysis of unconsolidated sediments. Earth Surface Processes and Landforms **26**: 1237–1248.

Blume, H.-P., Stahr, K. & Leinweber, P., 2011. Bodenkundliches Praktikum. Eine Einführung in pedologisches Arbeiten für Ökologen, insbesondere Land- und Forstwirte, und für Geowissenschaftler. Spektrum Akademischer Verlag (Heidelberg): 272 pp.

BSH, Bundesamt für Seeschifffahrt und Hydrographie, 2019. Gezeitenkalender – Hoch- und Niedrigwasserzeiten für die Deutsch Bucht und deren Flussgebiete. Bundesamt für Seeschifffahrt und Hydrographie (Hamburg).

BMS, Bundesamt für Seeschifffahrt und Hydrographie, 2016. Ostfriesland-Amtliche Karten für die Klein- und Sportschifffahrt, 3015, Blatt 6.

Bulian, F., Enters, D., Schlütz, F., Scheder, J., Blume, K., Zolitschka, B. & Bittmann, F., 2019. Multi-proxy reconstruction of Holocene paleoenvironments from a sediment core retrieved from the Wadden Sea near Norderney, East Frisia, Germany. Estuarine, Coastal and Shelf Science **225**: 106251.

Bungenstock, F., 2005. Der holozäne Meerespiegelanstieg südlich der ostfriesischen Insel Langeoog, südliche Nordsee, hochfrequente Meerespiegelbewegungen während der letzten 6000 Jahre. PhD thesis, University of Bonn (Bonn): 130 pp. https://tinyurl.com/y6qw7p2e.

Bungenstock, F. & Schäfer, A., 2009. The Holocene relative sea-level curve for the tidal basin of the barrier island Langeoog, German Bight, Southern North Sea. Global and Planetary Change **66**(1): 34–51.

Bungenstock, F. & Weerts, H.J.T., 2010. The high-resolution Holocene sea-level curve for Northwest Germany: global signals, local effects or data-artefacts? International Journal of Earth Sciences **99**: 1687–1706.

Bungenstock, F. & Weerts, H.T.J., 2012. Holocene relative sea-level curves for the German North Sea coast. International Journal of Earth Sciences **101**: 1083–1090.

Bungenstock, F., Freund, H., Mauz, B. & Bartholomä, A., 2020. Holocene relative sea level data for the Eastfrisian barrier coast (NW Germany). Netherlands Journal of Geosciences / Geologie en Mijnbouw (this issue).

Clark, P.U., Dyke, A.S., Shakun, J.D., Carlson, A.E., Clark, J., Wohlfarth, B., Mitrovica, J.X., Hostetler, S.W. & McCabe, A.M., 2009. The Last Glacial Maximum. Science **325**: 710–714.

Davis, J.C., 1986. Statistics and data analysis in geology, 2nd ed. John Wiley & Sons (New York): 639 pp.

Enters, D., Haynert, K., Wehrmann, A., Freund, H. & Schlütz, F., 2020. A new ΔR for the southern North Sea and its application in coastal research. Netherlands Journal of Geosciences / Geologie en Mijnbouw (this issue).

Eshel, G., Levy, G.J., Mingelgrin, U. & Singer, M.J., 2004. Critical evaluation of the use of laser diffraction for particle-size distribution analysis. Soil Science Society of America Journal **68**: 736–743.

Flemming, B.W., 2002. Effects of climate and human interventions on the evolution of the Wadden Sea depositional system (southern North Sea). In: Wefer, G., Berger, W.H., Behre, K.-E. & Jansen, E. (eds): Climate development and history of the North Atlantic realm. Springer (Berlin/Heidelberg): 399–413.

Flemming, B.W. & Nyandwi, N., 1994. Land reclamation as a cause of fine-grained sediment depletion in backbarrier tidal flats (southern North Sea). Netherlands Journal of Aquatic Ecology **28**: 299–307.

Folk, R.L. & Ward, W.C., 1957. Brazos River bar (Texas); a study in the significance of grain size parameters. Journal of Sedimentary Research **27**: 3–26.

Frenzel, P., Keyser, D. & Viehberg, F.A., 2010. An illustrated key and (palaeo) ecological primer for Post-glacial to Recent Ostracoda (Crustacea) of the Baltic Sea. Boreas **19**: 153.

Freund, H. & Streif, H., 2000. Natürliche Pegelmarken für Meeresspiegelschwankungen der letzten 2000 Jahre im Bereich der Insel Juist. Petermanns Geographische Mitteilungen **143**: 34–45.

Gehrels, W.R. & Newman, S.W.G., 2004. Salt-marsh foraminifera in Ho Bugt, western Denmark, and their use as sea-level indicators. Geografisk Tidsskrift/Danish Journal of Geography **104**: 97–106.

Goldhammer, J. & Karle, M., 2015. Geoarchaeological research in the Wadden Sea area of Lower Saxony. Settlement and Coastal Research in the Southern North Sea Region (SCN) **38**: 59–70.

Hammer, O., Harper, D.A.T. & Ryan, P.D., 2001. PAST: Paleontological Statistics Software Package for Education and Data Analysis. Palaeontologia Electronica **4**(1): 1–9.

Harper, D.A.T. (ed.), 1999. Numerical palaeobiology. computer-based modelling and analysis of fossils and their distributions. John Wiley & Sons (Chichester): 468 pp.

Hayward, P.J. & Ryland, J.S., 1990. The marine fauna of the British Isles and North-West Europe. Molluscs and Chordates 2. Oxford University Press (Oxford): 386 pp.

Homeier, H., 1964: Niedersächsische Küste. Historische Karte 1 : 50.000, Nr. 5 Osterems mit Memmert bis Mitte Norderney. 4 Karten mit Beiheft. Forschungsstelle Norderney der Niedersächsischen Wasserwirtschaftsverwaltung (Norderney).

Homeier, H., 1969. Der Gestaltwandel an der ostfriesischen Küste im Laufe der Jahrhunderte – Ein Jahrtausend ostfriesischer Deichgeschichte. Ostfriesland im Schutz des Deiches **2**: 1–75.

Horton, B.P. & Edwards, R.J., 2006. Quantifying Holocene sea level change using intertidal foraminifera: lessons from the British Isles. Cushman Foundation for Foraminiferal Research, Special Publication **40**: 97 pp.

Hoselmann, C. & Streif, H., 1997. Bilanzierung der holozänen Sedimentakkumulation im niedersächsischen Küstenraum. Zeitschrift der Deutschen Geologischen Gesellschaft **148**: 431–445.

Downloaded from https://www.cambridge.org/core. IP address: 88.130.158.217, on 13 Mar 2021 at 22:28:39, subject to the Cambridge Core terms of use, available at https://www.cambridge.org/core/terms. https://doi.org/10.1017/njg.2020.16

Karle, M., 2020. Changing the scene: Holocene coastal development in northwestern Germany. Netherlands Journal of Geosciences / Geologie en Mijnbouw (this issue).

Karle, M., Frechen, M. & Wehrmann, A., 2017. Holocene coastal lowland evolution: reconstruction of land-sea transitions in response to sea-level changes (Jade Bay, southern North Sea, Germany). German Journal of Geology (ZDGG) **168**(1): 21–38.

Khan, N., Vans, C.H. & Horton, B.P., 2015. Stable carbon isotope and C/N geochemistry of coastal wetland sediments as a sea-level indicator. In: I. Shennan, A.J. Long & B.P. Horton (eds): Handbook of seal-level research. John Wiley & Sons, Ltd (Chichester): 295–311.

Kiden, P., Denys, L. & Johnston, P., 2002. Late Quaternary sea-level change and isostatic and tectonic land movements along the Belgian-Dutch North Sea coast: geological data and model results. Journal of Quaternary Science **17**: 535–546.

Landesamt für Bergbau, Energie und Geologie (LBEG), 2019. NIBIS® Kartenserver. https://nibis.lbeg.de/cardomap3, 07.10.2019.

Last, W.M. & Smol, J.P. (eds), 2002. Tracking environmental change using lake sediments: basin analysis, coring, and chronological techniques. Springer Science & Business Media (Berlin): 548 pp.

Long, A.J., Waller, M.P. & Stupples, P., 2006. Driving mechanisms of coastal change: peat compaction and the destruction of late Holocene coastal wetlands. Marine Geology **225**: 63–84.

López G.I., 2014. Walther's Law of Facies. In: Rink W. & Thompson J. (eds): Encyclopedia of scientific dating methods. Springer (Dordrecht): 957–958.

Lüders, K., 1934. Über das Wandern der Priele. Abhandlungen des Naturwissenschaftlichen Vereins zu Bremen **29**(1/2): 19–32.

Mai, S. & Bartholomä, A., 2000. The missing mud flats of the Wadden Sea: a reconstruction of sediments and accommodation space lost in the wake of land reclamation. Proceedings in Marine Science **2**: 257–272.

Murray, J.W., 2006. Ecology and applications of benthic foraminifera. Cambridge University Press (Cambridge/New York): 426 pp.

National Museum Wales, 2016. Marine bivalve shells of the British Isles. https://naturalhistory.museumwales.ac.uk/BritishBivalves.

Nieuwhof, A. & Vos, P.C., 2018. New data from terp excavations on sea-level index points and salt marsh sedimentation rates in the eastern part of the Dutch Wadden Sea. Netherlands Journal of Geosciences / Geologie en Mijnbouw **97**(1–29): 31–43.

Nyandwi, N. & Flemming, B.W., 1995. A hydraulic model for the shore-normal energy gradient in the East Frisian Wadden Sea (Southern North Sea). Senckenbergiana Maritima **25**(4/6): 163–171.

Preuss, H., Vinken, R. & Voss, H.-H., 1991. Symbolschlüssel Geologie – Symbole für die Dokumentation und automatische Datenverarbeitung geologischer Feld- und Aufschlußdaten. Niedersächsisches Landesamt für Bodenforschung (Hannover): 328 pp.

Pribyl, D.W., 2010. A critical review of the conventional SOC to SOM conversion factor. Geoderma **156**: 75–83.

Reimer, P.J., Bard, E., Bayliss, A., Beck, J.W., Blackwell, P.G., Ramsey, C.B., Buck, C.E., Cheng, H., Edwards, R.L., Friedrich, M., Grootes, P.M., Guilderson, T.P., Haflidason, H., Hajdas, I., Hatté, C., Heaton, T.K., Hoffmann, D.L., Hogg, A.G., Hughen, K.A., Kaiser, K.F., Kromer, B., Manning, S.W., Niu, M., Reimer, R.W., Richards, D.A., Scott, E.M., Southon, J.R., Staff, R.A., Turnex, C.S.M. & van der Plicht, J., 2013. IntCal13 and Marine13 radiocarbon age calibration curves 0–50,000 years cal BP. Radiocarbon **55**: 1869–1887.

Reineck, H.-E. & Siefert, W., 1980. Faktoren der Schlickbildung im Sahlenburger und Neuwerker Watt. Die Küste **35**: 26–51.

Richter, W. & Rumohr, H., 1976. Untersuchungen an *Barnea candida* (L.): Ihr Beitrag zur submarinen Geschiebemergelabrasion in der Kieler Bucht. Kieler Meeresforschungen **3**: 82–86.

Scheder, J., Engel, M., Bungenstock, F., Pint, A., Siegmüller, A., Schwank, S. & Brückner, H., 2018. Fossil bog soils ('dwog horizons') and their relation to Holocene coastal changes in the Jade Weser region, southern North Sea, Germany. Journal of Coastal Conservation **22**: 51–69.

Scheder, J., Frenzel, P., Bungenstock, F., Engel, M., Brückner, H. & Pint, A., 2019. Vertical and lateral distribution of Foraminifera and Ostracoda in the East Frisian Wadden Sea – developing a transfer function for relative sea-level change. Geologica Belgica **22**(3–4): 99–110.

Shennan, I., Lambeck, K., Flather, R., Horton, B., McArthur, J., Innes, J., Lloyd, J., Rutherford, M. & Wingfield, R., 2000. Modelling western North Sea palaeogeographies and tidal changes during the Holocene. In: I. Shennan & J. Andrews (eds): Holocene land-ocean interaction and environmental change around the North Sea. Geological Society (London), Special Publications **166**: 299–319.

Small, C. & Nicholls, R. J., 2003. A global analysis of human settlement in coastal zones. Journal of Coastal Research **19**: 584–599.

Strahl, E., 2005. Die jungbronzezeitliche Siedlung Rodenkirchen-Hahnenknooper Mühle, Ldkr. Wesermarsch – Erste Bauern in der deutschen Marsch. In: M. Fansa (ed.): Kulturlandschaft Marsch. Natur, Geschichte, Gegenwart. Vorträge anlässlich des Symposiums in Oldenburg vom 3. bis 5. Juni 2004. Schriftenreihe des Landesmuseums für Natur und Mensch 33, 52–59. Oldenburg.

Streif, H., 1971. Stratigraphie und Faziesentwicklung im Küstengebiet von Woltzeten in Ostfreisland. Beihefte geologisches Jahrbuch **119**: 59 pp.

Streif, H., 1990. Sammlung Geologischer Führer 57. Das ostfriesische Küstengebiet – Nordsee, Inseln, Watten und Marschen. Gebr. Borntraeger (Berlin/Stuttgart): 376 pp.

Streif, H., 1998. Die Geologische Küstenkarte von Niedersachsen 1 : 25.000 – eine neue Planungsgrundlage für die Küstenregion. Zeitschrift für angewandte Geologie **4**: 183–194.

Streif, H., 2004. Sedimentary record of Pleistocene and Holocene marine inundations along the North Sea coast of Lower Saxony, Germany. Quaternary International **112**: 3–28.

Taayke, E., 2016. Het Norrd-Nederlandse kustgebied in de vroege ijertied. In: Nieuwhof, A. (ed.): Van Wierhuizen tot Achlum. Honderd jaar archeologisch onderzoek in terpene en wierden, Vereniging voor Terpenonderzoek (Groningen): 69–82.

Tebble, N., 1976. British bivalve sea shells: a handbook for identification. HM Stationery Office (Edinburgh): 212 pp.

Tilch, E., 2003. Oszillation von Wattflächen und deren fossils Erhaltungspotential (Spiekerooger Rückseitenwatt, Südliche Nordsee). Berichte, Fachbereich Geowissenschaften, Universität Bremen **222**: 137 pp.

Trusheim, F., 1929. Zur Bildungsgeschwindigkeit geschichteter Sedimente im Wattenmeer, besonders solcher mit schräger Parallelschichtung. Senkenbergiana **11**: 47–56.

Van der Molen, J. & De Swart, H.E., 2001. Holocene tidal conditions and tide-induced sand transport in the Southern North Sea. Journal of Geophysical Research **106**(C5): 9339–9362.

Van der Spek, A., 1996. Holocene depositional sequences in the Dutch Wadden Sea south of the island of Ameland. Mededelingen Rijks Geologische Dienst **57**: 41–68.

Vink, A., Steffen, H., Reinhardt, L. & Kaufmann, G., 2007. Holocene relative sea-level change, isostatic subsidence and the radial viscosity structure of the mantle of northwest Europe (Belgium, the Netherlands, Germany, southern North Sea). Quaternary Science Reviews **26**: 3249–3275.

Vos, P.C, 1999. The Subatlantic evolution of the coastal area around the Wijnaldum. Tjitsma terp. In: Besteman, J.C. ***et al.*** (eds): The excavation near Wijnaldum. Reports on Friesland in Roman and Medieval Times 1. University of Amsterdam (Amsterdam): 33–73.

Vos, P., 2015. Origin of the Dutch landscape. Long-term landscape evolution of the Netherlands during the Holocene, described and visualized in national, regional and local palaeogeographical map series. Barkhuis (Groningen): 359 pp.

Vos, P.C. & Gerrets, D.A., 2004. Archaeology, a major tool in the reconstruction of the coastal evolution of Westergo (the Northern Netherlands). Quaternary International **133–134**: 61–75.

Vos, P.S. & Knol, E., 2015. Holocene landscape reconstruction of the Wadden Sea area between Marsdiep and Weser. Netherlands Journal of Geosciences / Geologie en Mijnbouw **94**(2): 157–183.

Vos, P.S., van der Meulen, M., Weerts, H.J. & Bazelmans, J., 2020: Atlas of the Holocene Netherlands. Amsterdam University Press (Amsterdam): 96 pp.

Downloaded from https://www.cambridge.org/core. IP address: 88.130.158.217, on 13 Mar 2021 at 22:28:39, subject to the Cambridge Core terms of use, available at https://www.cambridge.org/core/terms. https://doi.org/10.1017/njg.2020.16

Wartenberg, W. & Freund, H., 2012. Late Pleistocene and Holocene sedimentary record within the Jade Bay, Lower Saxony, Northwest Germany: new aspects for the palaeo-ecological record. Quaternary International **251**: 31–41.

Wartenberg, W., Vött, A., Freund, H., Hadler, H., Freche, M., Willershäuser, T., Schnaidt, S., Fischer, P. & Obrocki, L., 2013. Evidence of isochronic transgressive surface within the Jade Bay tidal flat area, southern German North Sea coast – Holocene event horizons of regional interest. Zeitschrift für Geomorphologie Supplementary Issues **57**: 229–256.

Wildvang, D., 1911. Eine prähistorische Katastrophe an der deutschen Nordseeküste und ihr Einfluß auf die spätere Gestaltung der Alluviallandschaft zwischen der Ley und dem Dollart. Haynel (Emden/Borkum): 67 pp.

Zepp, H., 2017. Geomorphologie. Schöningh (Paderborn): 402 pp.

Downloaded from https://www.cambridge.org/core. IP address: 88.130.158.217, on 13 Mar 2021 at 22:28:39, subject to the Cambridge Core terms of use, available at https://www.cambridge.org/core/terms. https://doi.org/10.1017/njg.2020.16

Supplementary material – Elschner et al. (2021) Netherlands Journal of Geosciences

4.S1. Microfauna – taxa and ecological information

Tab. 4.S1 Abundant foraminifer and ostracod species and their ecological characteristics (for visual information and distributions see Fig 4.2–Fig, 4.4 [main article] and Fig. 4.S1–Fig. 4.S3 [supplement]).

Foraminifers

Ammonia tepida (Cushman, 1926)				
Order	**Superfamily**	**Family**	**Subfamily**	**Genus**
Rotaliida	Rotalioidea	Ammoniidae	Ammoniinae	*Ammonia*
Ecology: sheltered, shallow marine, often slightly brackish, intertidal environments, may extend onto low and mid marshes (Murray 2006)				

Cribroelphidium excavatum (Terquem, 1875)				
Order	**Superfamily**	**Family**	**Subfamily**	**Genus**
Rotaliina	Rotalioidea	Elphidiidae	Elphidiinae	*Cribroelphidium*
Ecology: intertidal to subtidal, estuaries, lagoons, continental shelf and slope, sediments with highly variable sand, mud and TOC contents, salinity 15–31 psu (Murray, 2006)				

Cribroelphidium williamsoni (Haynes, 1973)				
Order	**Superfamily**	**Family**	**Subfamily**	**Genus**
Rotaliina	Rotalioidea	Elphidiidae	Elphidiinae	*Cribroelphidium*
Ecology: shallow parts of intertidal mud flats, estuaries, lagoons and sea-bound parts of salt marshes (Murray 2006); mainly less than 20 cm water depth, found in 0.1 to 0.5 m water depth and between 8 and 19 psu on mud to medium sand, also within the phytal zone, brackish water species, mainly temperate climate (Lehmann, 2000)				

Elphidium spp. (Montfort, 1808)				
Order	**Superfamily**	**Family**	**Subfamily**	**Genus**
Rotaliida	Rotalioidea	Elphidiidae	Elphidiinae	*Elphidium*
Ecology: braskish to hyper-saline salt marshes, lagoonal to marine, muddy to sandy substrate (Murray, 2006)				

Haynesina germanica (Ehrenberg, 1840)			
Order	**Superfamily**	**Family**	**Genus**
Rotaliina	Rotalioidea	Haynesinidae	*Haynesina*
Ecology: middle and low marshes, tidal flats (Horton and Edwards 2006); shallow marine, intertidal environments, may extend onto low and mid marshes (Murray 2006)			

Entzia macrescens (Brady, 1870)					
Order	**Suborder**	**Superfamily**	**Family**	**Subfamily**	**Genus**
Lituolida	Trochamminina	Trochamminoidea	Trochamminidae	Jadamininae	*Entzia*
Ecology: Euryhaline species, land-bound parts of salt marshes, sand flats also, in 0.1 to 0.3 m water depth and 8.5 to 19 psu on mud to medium sand and within the phytalzone of the southern Baltic; extremely euryhaline (Lehmann 2000); controlled more by substrate than salinity (Murray 2006)					

– Continued on next page –

Miliammina fusca (Brady, 1870)				
Order	**Suborder**	**Superfamily**	**Family**	**Genus**
Miliolida	Miliolina	Miliolacea	Miliamminidae	*Entzia*
Ecology: salt marshes and lagoons, brackish (Murray, 2006)				

Triloculina oblonga (Montagu, 1803)					
Order	**Suborder**	**Superfamily**	**Family**	**Subfamily**	**Genus**
Miliolida	Miliolina	Milioloidea	Hauerinidae	Miliolinellinae	*Triloculina*
Ecology: Salt marshes (Lehmann 2000)					

Trochammina inflata (Montagu, 1808)					
Order	**Suborder**	**Family**		**Subfamily**	**Genus**
Lituolida	Trochamminina	Trochamminoidea	Trochamminidae	Trochamminina	*Trochammina*
Ecology: Euryhaline brackish water species, shallow water, typical for salt marshes (Lehmann, 2000); high and middle marsh environments (Horton and Edwards 2006)					

4.S2. Laboratory results of sediment cores

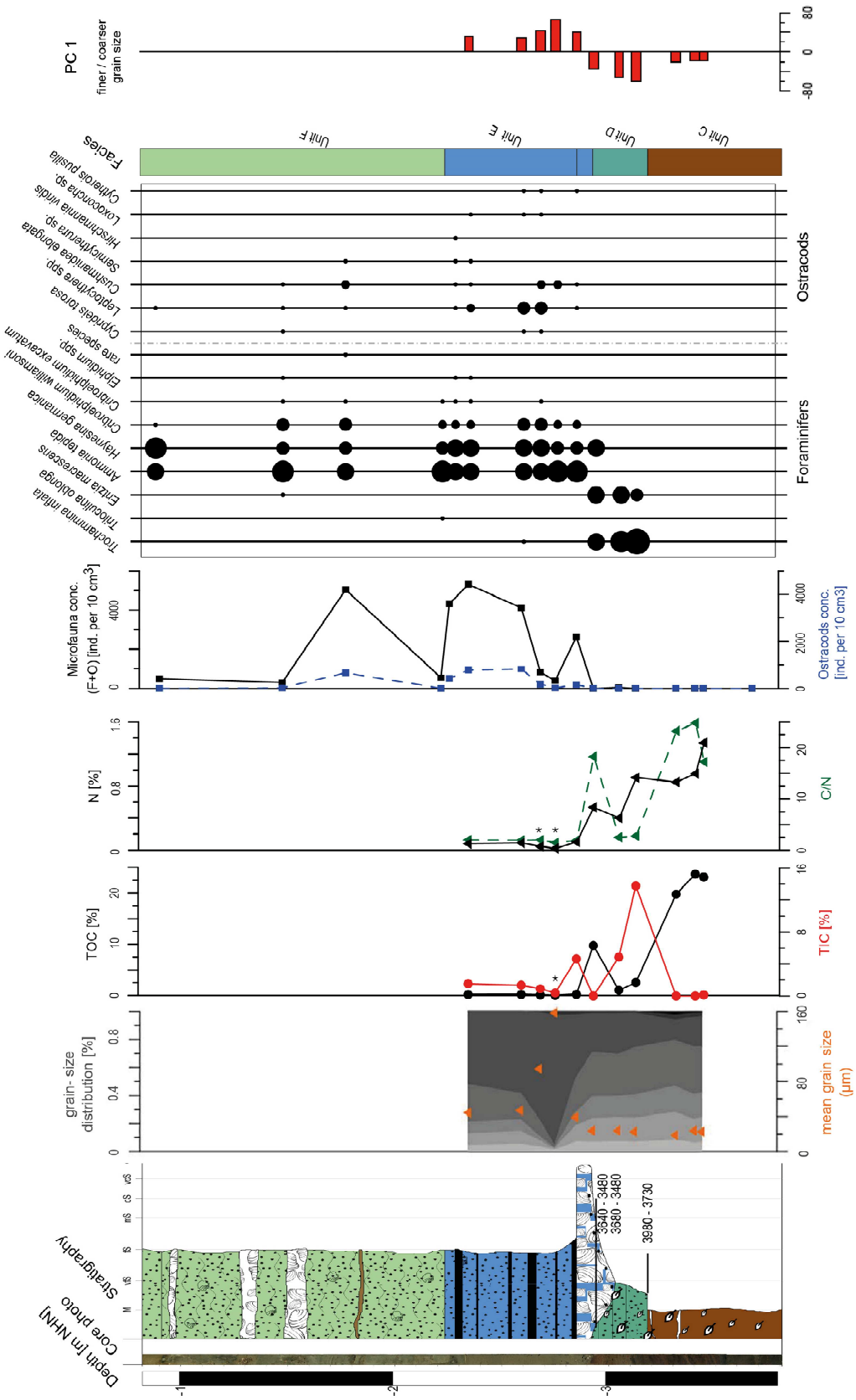

Fig. 4.S1 Sedimentological, geochemical and microfaunal results of N44, including the most relevant component of the PCA (only lower part including all analyses). For colour legend see Fig. 4.3 (main article).

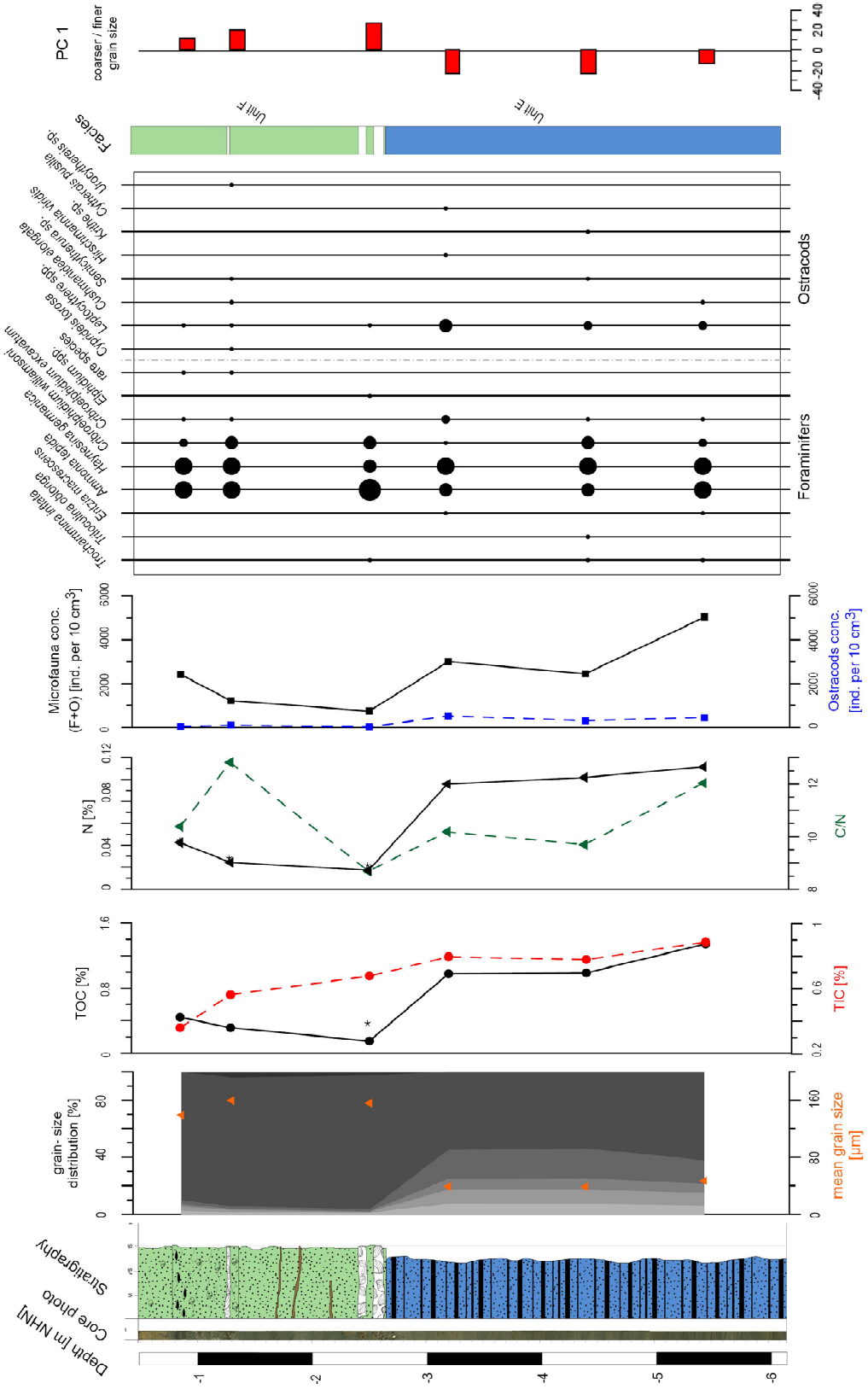

Fig. 4.S2 Sedimentological, geochemical and microfaunal results of N45, including the most relevant component of the PCA. For colour legend see Fig. 4.3 (main article).

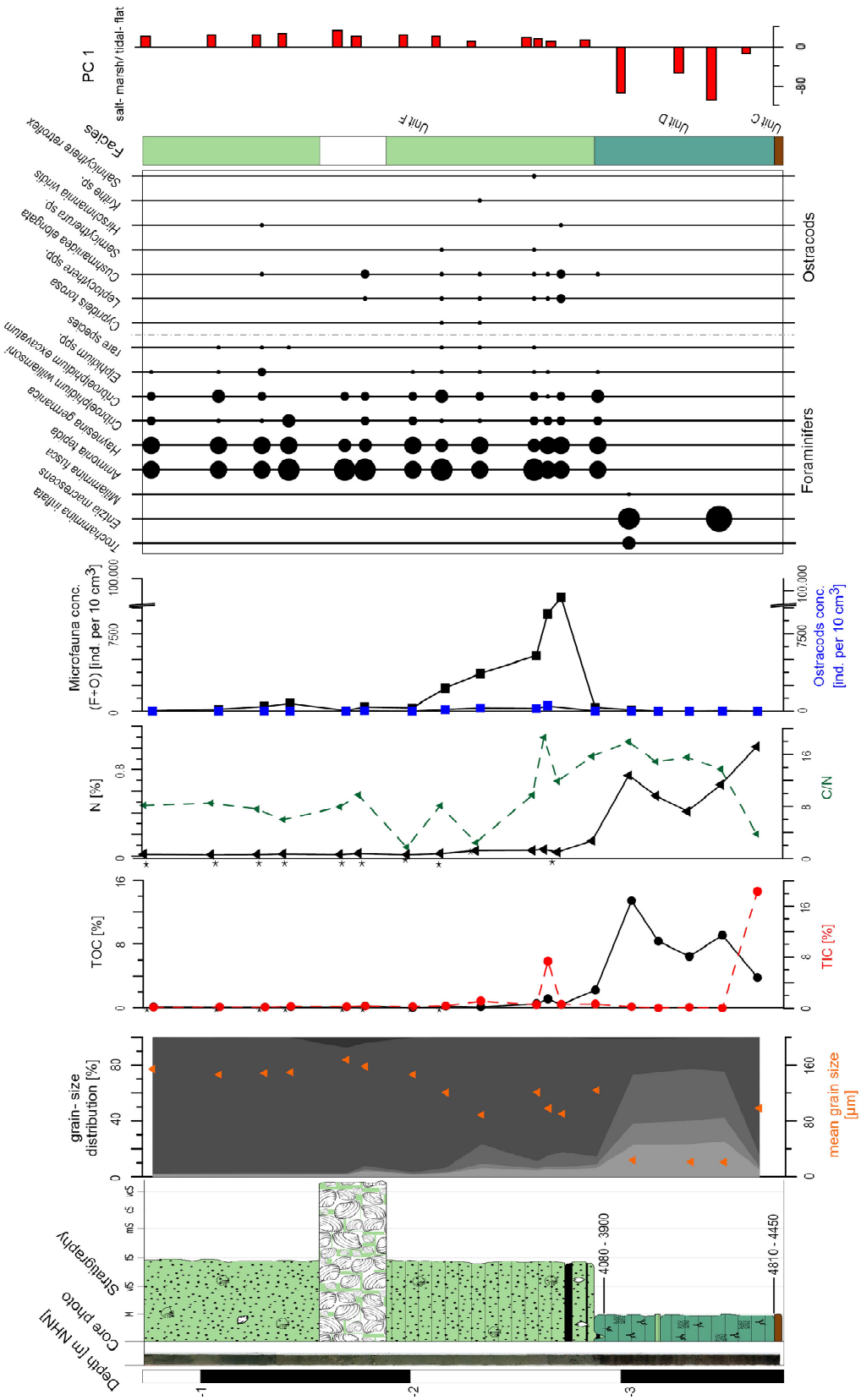

Fig. 4.S3 Sedimentological, geochemical and microfaunal results of VC13, including the most relevant component of the PCA. For colour legend see Fig. 4.3 (main article).

4.S3. Multivariate Statistics

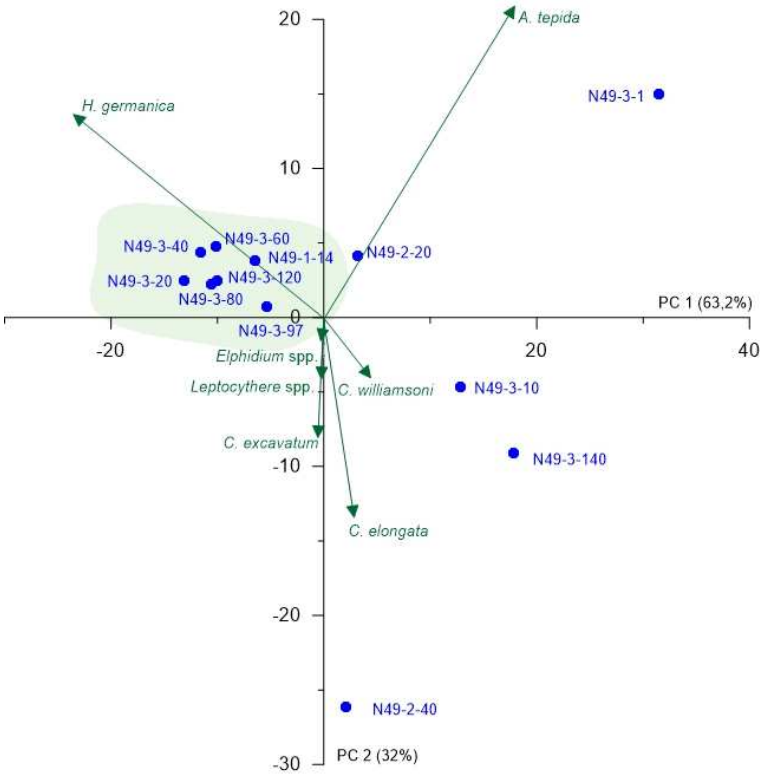

Fig. 4.S4 PCA biplot of N49 (upper part of the core, Unit F) showing the two most relevant axes (PC 1 and PC 2). Colours of sample groupings relate to the colour legend in Fig. 4.3 (main article); green arrows represent microfaunal taxa and environmental parameters and blue points represent samples.

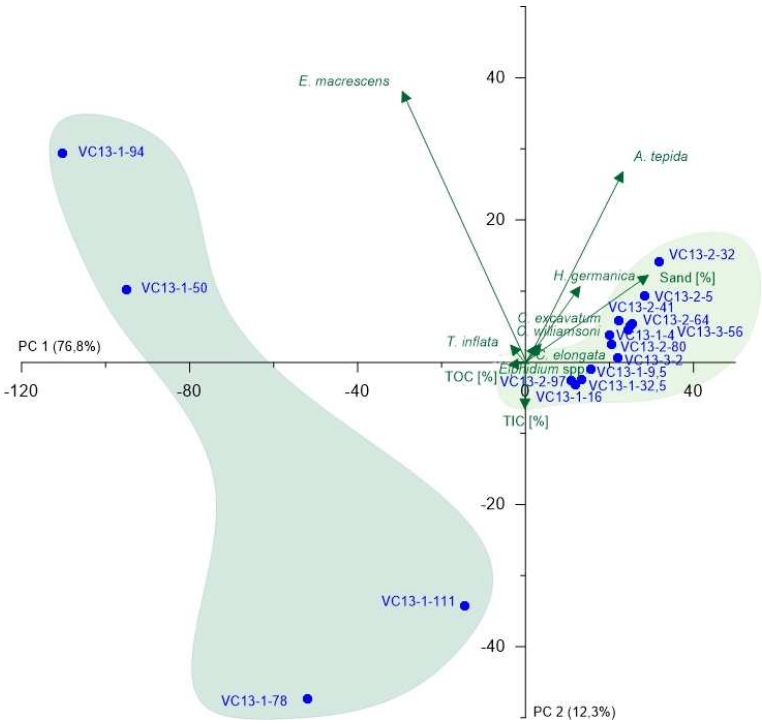

Fig. 4.S5 PCA biplot of VC13 showing the two most relevant axes (PC 1 and PC 2). Colours of sample groupings relate to the colour legend in Fig. 4.3 (main article); green arrows represent microfaunal taxa and environmental parameters and blue points represent samples.

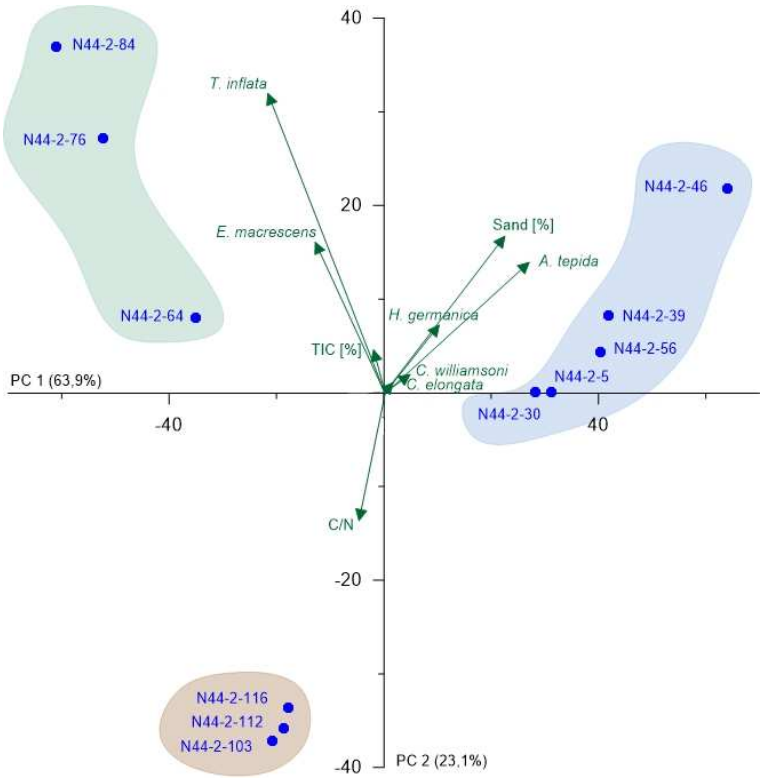

Fig. 4.S6 PCA biplot of N44 (lower part of the core with all available data) showing the two most relevant axes (PC 1 and PC 2). Colours of sample groupings relate to the colour legend in Fig. 4.3 (main article); green arrows represent microfaunal taxa and environmental parameters and blue points represent samples.

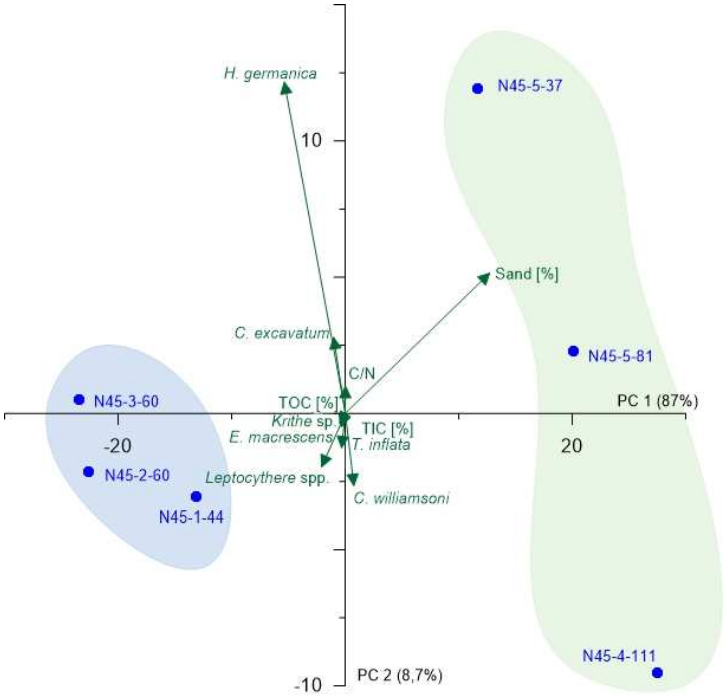

Fig. 4.S7 PCA biplot of N45 showing the two most relevant axes (PC 1 and PC 2). Colours of sample groupings relate to the colour legend in Fig. 4.3 (main article); green arrows represent microfaunal taxa and environmental parameters and blue points represent samples.

4.S4. Underlying data

Tab. 4.S2 Grain-size data of all investigated cores.

Section Sample number	Depth NHN [m]	Coarse sand [%]	Medium sand [%]	Fine sand [%]	Coarse silt [%]	Medium silt [%]	Fine silt [%]	Clay [%]	mean grain size [µm]
N77-5-5	-3.02	0.0	0.0	27.3	38.0	14.5	14.8	5.5	25.2
N77-5-21	-3.18	0.0	0.2	36.8	34.3	11.9	12.3	4.6	32.5
N77-5-37	-3.34	0.0	0.4	23.9	34.6	16.3	18.1	6.8	21.3
N77-4-21	-3.56	0.0	2.3	14.7	28.9	17.9	22.7	13.6	13.0
N77-4-29	-3.64	0.5	2.8	15.7	30.0	20.1	21.4	9.5	16.4
N77-4 70	-4.05	0.5	3.9	20.0	29.4	17.0	19.0	10.3	19.0
N77-3-10	-4.55	0.0	5.9	72.9	14.6	2.2	2.2	2.1	110.6
N77-3-28	-4.73	0.0	8.6	86.7	2.8	0.3	0.5	1.1	156.1
N77-3-37	-4.82	0.0	10.7	86.5	1.4	0.2	0.3	0.9	163.0
N77-3-58	-5.03	0.0	2.5	94.8	1.2	0.2	0.4	1.0	149.3
N77-2-8	-5.63	0.0	0.3	95.6	2.5	0.2	0.3	1.1	131.4
N77-2-68	-6.23	0.0	4.0	90.3	3.1	0.5	0.8	1.3	141.0
N77-2-79	-6.34	0.0	0.7	95.6	1.7	0.3	0.5	1.2	141.8
N77-1-23	-6.88	0.0	3.1	88.7	5.4	0.6	0.8	1.4	128.5
N77-1 71	-7.36	0.0	8.8	87.5	1.6	0.3	0.6	1.2	158.2
N77-1-95	-7.60	1.9	41.5	55.0	0.4	0.1	0.3	0.8	232.5
N49-1-14	-2.97	0.0	0.0	53.5	25.2	7.7	8.5	5.1	46.9
N49-1-29	-3.12	0.0	1.2	27.4	37.1	15.3	13.9	5.1	26.8
N49-1-39	-3.22	0.5	1.8	23.6	37.6	16.5	14.9	5.1	25.1
N49-1-49	-3.32	0.0	0.7	18.1	40.8	18.5	16.2	5.7	20.6
N49-1-59	-3.42	0.0	0.5	22.1	43.0	15.2	13.9	5.3	24.5
N49-1-69	-3.52	0.0	0.4	36.4	36.0	11.2	11.5	4.5	33.7
N49-1-79	-3.62	0.0	0.1	33.5	41.6	11.1	9.8	3.9	33.4
N49-1-89	-3.72	0.0	0.2	38.0	37.2	10.3	10.3	3.9	35.8
N49-1-99	-3.82	0.0	0.0	23.8	37.3	16.1	16.8	6.0	22.3
N49-1-109	-3.92	0.0	0.4	33.5	34.8	13.1	13.4	4.8	30.0
N49-1-119	-4.02	0.0	0.0	9.1	40.0	23.4	20.8	6.7	14.9
N49-1-129	-4.12	0.0	0.0	24.1	33.5	17.4	18.3	6.7	20.8
N49-1-139	-4.22	0.0	0.0	20.9	35.2	17.4	19.3	7.2	17.5
N49-1-142	-4.25	0.0	0.0	12.9	37.5	20.3	21.1	8.1	15.1
VC13-3-2	-0.75	0.0	0.5	97.3	0.8	0.1	0.3	0.9	154.7
VC13-3-34	-1.07	0.0	0.2	97.4	1.0	0.2	0.4	1.0	146.7
VC13-3-56	-1.29	0.0	0.2	97.3	1.0	0.2	0.4	1.0	149.0
VC13-2-5	-1.42	0.0	0.3	97.2	1.0	0.2	0.4	0.9	150.2
VC13-2-32	-1.69	0.0	7.3	90.3	0.7	0.2	0.5	1.0	168.1
VC13-2-41	-1.78	0.0	3.7	88.4	2.8	1.3	1.9	1.9	158.5
VC13-2-64	-2.01	0.0	0.4	96.7	1.2	0.3	0.5	1.0	146.8
VC13-2-80	-2.17	0.0	0.0	93.4	3.7	0.6	0.9	1.4	120.8
VC13-2-97	-2.34	0.0	0.1	76.7	13.8	3.1	3.6	2.7	88.8
VC13-1-4	-2.61	0.0	0.1	89.0	4.8	1.6	2.2	2.2	121.1

– Continued on next page –

Section Sample number	Depth NHN [m]	Coarse sand [%]	Medium sand [%]	Fine sand [%]	Coarse silt [%]	Medium silt [%]	Fine silt [%]	Clay [%]	mean grain size [µm]
VC13-1-9,5	-2.66	0.0	0.0	84.4	8.0	2.0	2.8	2.7	98.1
VC13-1-16	-2.73	0.0	0.0	82.2	10.9	1.9	2.5	2.5	90.5
VC13-1-32,5	-2.89	0.0	1.2	84.3	5.6	2.4	3.4	3.0	124.1
VC13-1-50	-3.07	0.0	1.4	25.3	34.9	15.8	16.0	6.6	23.6
VC13-1-78	-3.35	0.0	0.5	21.9	37.7	16.6	16.6	6.7	21.3
VC13-1-94	-3.51	0.0	0.5	23.9	33.6	16.8	18.1	7.2	21.0
VC13-1 111	-3.68	0.0	0.0	84.9	8.0	1.9	2.6	2.5	98.4
N44-2 5	-2.36	0.0	0.0	52.3	26.7	8.3	8.3	4.4	44.4
N44-2 30	-2.61	0.0	0.0	58.3	18.8	8.3	9.2	5.3	46.7
N44-2 39	-2.70	0.0	0.7	77.0	11.7	3.0	4.1	3.5	94.1
N44-2 46	-2.77	0.0	3.0	92.7	1.7	0.6	0.9	1.2	158.1
N44-2 56	-2.87	0.0	2.5	45.5	24.1	9.5	11.5	6.9	38.9
N44-2 64	-2.95	0.0	1.8	27.2	31.8	15.6	17.1	6.5	24.2
N44-2 76	-3.07	0.0	1.6	28.8	30.0	15.2	17.3	7.0	24.1
N44-2 84	-3.15	0.0	1.1	24.9	33.4	16.7	17.3	6.6	22.4
N44-2 103	-3.34	2.6	3.9	14.2	32.7	18.7	19.8	8.2	19.0
N44-2 112	-3.43	1.4	3.0	21.1	33.7	17.9	16.8	6.2	23.4
N44-2 116	-3.47	1.1	2.7	21.5	32.8	17.4	17.9	6.6	22.0
N45-5-37	-0.87	0.0	0.3	89.8	3.0	1.7	2.8	2.4	139.1
N45-5-81	-1.31	0.0	3.8	90.8	1.9	0.7	1.3	1.6	159.8
N45-4-111	-2.52	0.0	2.6	94.0	1.3	0.4	0.6	1.1	156.2
N45-3-60	-3.21	0.0	0.0	54.7	20.5	7.4	10.1	7.3	38.8
N45-2-60	-4.41	0.0	0.0	53.7	21.2	7.6	10.2	7.4	38.5
N45-1-44	-5.45	0.0	0.0	62.1	16.6	6.5	8.8	5.9	46.7

Tab. 4.S3 Geochemical data of all investigated cores.

Section Sample number	Depth NHN [m]	TC [%]	TOC [%]	TIC [%]	TN [%]	C/N	
N77-5-5	-3.02	2.17	2.21	0.00	0.19	11.52	Below
N77-5-21	-3.18	2.58	2.61	0.00	0.23	11.27	detection limit
N77-5-37	-3.34	6.50	6.59	0.00	0.48	13.63	
N77-4-21	-3.56	16.63	16.64	0.00	0.69	24.00	
N77-4-29	-3.64	18.81	19.14	0.00	0.89	21.50	
N77-4 51	-3.86	34.15	33.64	0.51	1.21	27.82	
N77-4 70	-4.05	20.08	19.92	0.15	0.95	20.97	
N77-3-10	-4.55	1.11	1.31	0.00	0.04	31.88	
N77-3-28	-4.73	0.99	1.11	0.00	0.05	23.87	
N77-3-37	-4.82	0.25	0.38	0.00	0.02	19.21	
N77-3-58	-5.03	0.10	0.20	0.00	0.01	14.72	
N77-2-8	-5.63	0.07	0.20	0.00	0.02	12.56	
N77-2-68	-6.23	0.12	0.22	0.00	0.01	14.60	

– Continued on next page –

Section Sample number	Depth NHN [m]	TC [%]	TOC [%]	TIC [%]	TN [%]	C/N
N77-2-79	-6.34	0.12	0.17	0.00	0.02	9.43
N77-1-23	-6.88	0.20	0.24	0.00	0.02	12.95
N77-1 71	-7.36	0.10	0.15	0.00	0.01	11.03
N77-1-95	-7.60	0.07	0.12	0.00	0.02	6.43
N49-1-14	-2.97	2.05	1.39	0.66	0.09	15.44
N49-1-29	-3.12	11.61	11.41	0.20	0.54	21.27
N49-1-39	-3.22	14.10	13.87	0.23	0.76	18.23
N49-1-49	-3.32	8.78	8.77	0.01	0.55	15.97
N49-1-59	-3.42	2.64	2.60	0.04	0.23	11.09
N49-1-69	-3.52	1.49	1.49	0.00	0.17	8.64
N49-1-79	-3.62	1.62	1.50	0.12	0.17	8.80
N49-1-89	-3.72	1.45	1.37	0.08	0.15	8.97
N49-1-99	-3.82	2.04	2.08	0.00	0.21	10.14
N49-1-109	-3.92	1.85	1.90	0.00	0.20	9.67
N49-1-119	-4.02	3.62	3.59	0.03	0.30	11.92
N49-1-129	-4.12	3.03	2.92	0.10	0.29	10.23
N49-1-139	-4.22	6.39	6.29	0.10	0.52	12.12
N49-1-142	-4.25	9.66	9.69	0.00	0.78	12.49
N49-1 149	-4.32	35.02	34.93	0.09	1.41	24.83
VC13-3-2	-0.75	0.33	0.15	0.18	0.02	8.17
VC13-3-34	-1.07	0.36	0.12	0.24	0.01	8.52
VC13-3-56	-1.29	0.32	0.12	0.21	0.02	7.61
VC13-2-5	-1.42	0.46	0.12	0.33	0.02	5.98
VC13-2-32	-1.69	0.43	0.12	0.31	0.02	7.94
VC13-2-41	-1.78	0.60	0.25	0.35	0.03	9.77
VC13-2-64	-2.01	0.33	0.02	0.31	0.01	1.72
VC13-2-80	-2.17	0.62	0.20	0.42	0.02	8.11
VC13-2-97	-2.34	1.29	0.12	1.16	0.05	2.44
VC13-1-4	-2.61	1.11	0.51	0.59	0.05	9.78
VC13-1-9,5	-2.66	8.51	1.13	7.38	0.06	18.65
VC13-1-16	-2.73	1.06	0.42	0.64	0.04	11.90
VC13-1-32,5	-2.89	2.91	2.21	0.70	0.14	15.75
VC13-1-50	-3.07	13.68	13.41	0.27	0.75	17.98
VC13-1-63	-3.20	8.41	8.33	0.07	0.56	14.94
VC13-1-78	-3.35	6.63	6.44	0.18	0.41	15.60
VC13-1-94	-3.51	9.14	9.08	0.05	0.66	13.76
VC13-1 111	-3.68	22.12	3.80	18.33	1.01	3.75
N44-2 5	-2.36	1.68	0.16	1.52	0.08	1.99
N44-2 30	-2.61	1.51	0.17	1.34	0.09	1.94
N44-2 39	-2.70	0.98	0.09	0.89	0.04	1.98
N44-2 46	-2.77	0.40	0.03	0.37	0.02	1.44
N44-2 56	-2.87	4.84	0.19	4.64	0.10	1.92

– Continued on next page –

Section Sample number	Depth NHN [m]	TC [%]	TOC [%]	TIC [%]	TN [%]	C/N
N44-2 64	-2.95	9.57	9.74	0.00	0.53	18.24
N44-2 76	-3.07	5.85	1.00	4.85	0.40	2.49
N44-2 84	-3.15	16.26	2.51	13.75	0.91	2.77
N44-2 103	-3.34	19.70	19.74	0.00	0.85	23.25
N44-2 112	-3.43	23.66	23.69	0.00	0.96	24.79
N44-2 116	-3.47	23.22	23.08	0.14	1.34	17.21
N45-5-37	-0.87	0.80	0.44	0.36	0.04	10.38
N45-5-81	-1.31	0.88	0.31	0.56	0.02	12.82
N45-4-111	-2.52	0.83	0.15	0.68	0.02	8.68
N45-3-60	-3.21	1.77	0.98	0.80	0.10	10.18
N45-2-60	-4.41	1.77	0.99	0.78	0.10	9.69
N45-1-44	-5.45	2.23	1.34	0.89	0.11	12.03

Tab. 4.S4 Foraminifer and ostracod counts of all investigated cores

		Foraminifers										Ostracods								
Section sample number	**Depth NHN [m]**	*Trochammina inflata*	*Triloculina oblonga*	*Entzia macrescens*	*Miliammina fusca*	*Ammonia tepida*	*Haynesina germanica*	*Cribroelphidium williamsoni*	*Cribroelphidium excavatum*	*Elphidium* spp.	*Cyprideis torosa*	*Leptocythere* spp.	*Cushmanidea elongata*	*Semicytherura* sp.	*Hirschmannia viridis*	*Krithe* sp.	*Loxoconcha* sp.	*Sahnicythere retroflexa*	*Cytherois pusilla*	*Urocythereis* sp.
N77-5-5	-3.02	65	0	42	0	0	0	0	0	0	0	0	0	0	0	0	0	0	0	0
N77-5-21	-3.18	99	0	8	0	0	0	0	0	0	0	0	0	0	0	0	0	0	0	0
N77-5-37	-3.34	0	0	0	0	0	0	0	0	0	0	0	0	0	0	0	0	0	0	0
N77-4-21	-3.56	0	0	0	0	0	0	0	0	0	0	0	0	0	0	0	0	0	0	0
N77-4-29	-3.64	0	0	0	0	0	0	0	0	0	0	0	0	0	0	0	0	0	0	0
N77-4-51	-3.86	0	0	0	0	0	0	0	0	0	0	0	0	0	0	0	0	0	0	0
N77-4-70	-4.05	0	0	0	0	0	0	0	0	0	0	0	0	0	0	0	0	0	0	0
N77-3-10	-4.55	0	0	0	0	0	0	0	0	0	0	0	0	0	0	0	0	0	0	0
N77-3-28	-4.73	0	0	0	0	0	0	0	0	0	0	0	0	0	0	0	0	0	0	0
N77-3-37	-4.82	0	0	0	0	0	0	0	0	0	0	0	0	0	0	0	0	0	0	0
N77-3-58	-5.03	0	0	0	0	0	0	0	0	0	0	0	0	0	0	0	0	0	0	0
N77-2-8	-5.63	0	0	0	0	0	0	0	0	0	0	0	0	0	0	0	0	0	0	0
N77-2-68	-6.23	0	0	0	0	0	0	0	0	0	0	0	0	0	0	0	0	0	0	0
N77-2-79	-6.34	0	0	0	0	0	0	0	0	0	0	0	0	0	0	0	0	0	0	0
N77-1-23	-6.88	0	0	0	0	0	0	0	0	0	0	0	0	0	0	0	0	0	0	0
N77-1-71	-7.36	0	0	0	0	0	0	0	0	0	0	0	0	0	0	0	0	0	0	0
N77-1-95	-7.60	0	0	0	0	0	0	0	0	0	0	0	0	0	0	0	0	0	0	0
N49-3-1	-0.99	0	0	0	0	48	6	5	0	0	0	0	0	0	0	0	0	0	0	0
N49-3-10	-1.08	0	0	0	0	54	15	6	9	1	2	0	7	0	0	0	0	0	0	0
N49-3-20	-1.18	0	0	0	0	40	34	3	7	0	0	1	0	1	0	0	0	0	0	0

– Continued on next page –

Section sample number	Depth NHN [m]	Foraminifers										Ostracods								
		Trochammina inflata	*Triloculina oblonga*	*Entzia macrescens*	*Miliammina fusca*	*Ammonia tepida*	*Haynesina germanica*	*Cribroelphidium williamsoni*	*Cribroelphidium excavatum*	*Elphidium* spp.	*Cyprideis torosa*	*Leptocythere* spp.	*Cushmanidea elongata*	*Semicytherura* sp.	*Hirschmannia virdis*	*Krithe* sp.	*Loxoconcha* sp.	*Sahnicythere retroflexa*	*Cytherois pusilla*	*Urocythereis* sp.
N49-3-40	-1.38	0	1	0	0	40	31	2	9	0	0	0	0	0	0	0	0	0	0	0
N49-3-60	-1.58	0	0	0	0	46	37	3	4	3	0	1	0	0	0	0	0	0	0	0
N49-3-80	-1.78	0	0	0	0	42	32	2	8	0	0	0	1	0	0	0	0	0	0	0
N49-3-97	-1.95	0	0	0	0	49	32	3	5	4	0	0	4	0	0	0	0	0	0	0
N49-3-120	-2.18	0	0	0	0	42	32	2	6	0	0	0	0	0	2	0	0	0	0	0
N49-3-140	-2.38	0	0	0	0	48	8	7	13	1	0	0	5	0	0	0	0	0	0	0
N49-2-20	-2.59	0	0	0	0	44	21	3	7	0	0	0	1	0	0	0	0	0	0	0
N49-2-40	-2.79	0	0	0	0	29	12	8	9	2	2	5	13	0	2	0	0	0	0	0
N49-1-14	-2.97	0	0	0	0	45	31	6	4	1	1	0	0	0	0	0	0	0	1	0
N49-1-29	-3.12	0	0	0	0	0	0	0	0	0	0	0	0	0	0	0	0	0	0	0
N49-1-39	-3.22	0	0	0	0	0	0	0	0	0	0	0	0	0	0	0	0	0	0	0
N49-1-49	-3.32	0	0	0	0	0	0	0	0	0	0	0	0	0	0	0	0	0	0	0
N49-1-59	-3.42	92	0	10	0	0	0	0	0	0	0	0	0	0	0	0	0	0	0	0
N49-1-69	-3.52	92	0	18	0	0	0	0	0	0	0	0	0	0	0	0	0	0	0	0
N49-1-79	-3.62	91	0	10	0	0	0	0	0	0	0	0	0	0	0	0	0	0	0	0
N49-1-89	-3.72	95	0	13	0	0	0	0	0	0	0	0	0	0	0	0	0	0	0	0
N49-1-99	-3.82	86	0	16	0	0	0	0	0	0	0	0	0	0	0	0	0	0	0	0
N49-1-109	-3.92	63	0	39	0	0	0	0	0	0	0	0	0	0	0	0	0	0	0	0
N49-1-119	-4.02	63	0	37	0	0	0	0	0	0	0	0	0	0	0	0	0	0	0	0
N49-1-129	-4.12	104	0	18	0	1	0	0	0	0	0	0	0	0	0	0	0	0	0	0
N49-1-139	-4.22	75	0	12	15	1	0	0	0	0	0	0	0	0	0	0	0	0	0	0
N49-1-142	-4.25	89	0	13	0	0	0	0	0	0	0	0	0	0	0	0	0	0	0	0

– Continued on next page –

		Foraminifers										Ostracods								
Ection sample number	**Depth NHN [m]**	*Trochammina inflata*	*Triloculina oblonga*	*Entzia macrescens*	*Miliammina fusca*	*Ammonia tepida*	*Haynesina germanica*	*Cribroelphidium williamsoni*	*Cribroelphidium excavatum*	*Elphidium* spp.	*Cyprideis torosa*	*Leptocythere* spp.	*Cushmanidea elongata*	*Semicytherura* sp.	*Hirschmannia virdis*	*Krithe* sp.	*Loxoconcha* sp.	*Sahnicythere retroflexa*	*Cytherois pusilla*	*Urocythereis* sp.
N49-1 149	-4.32	0	0	0	0	0	0	0	0	0	0	0	0	0	0	0	0	0	0	0
VC13-3-02	-0.75	0	0	0	0	15	18	3	4	2	0	0	0	0	0	0	0	0	0	0
VC13-3-34	-1.07	0	0	0	0	39	25	3	11	1	0	0	0	0	0	0	0	0	0	0
VC13-3-56	-1.29	0	0	0	0	52	34	5	6	6	0	0	1	0	1	0	0	0	0	0
VC13-2-5	-1.42	0	0	0	0	58	28	12	0	0	0	0	0	0	0	0	0	0	0	0
VC13-2-32	-1.69	0	0	0	0	36	11	0	4	0	0	0	0	0	0	0	0	0	0	0
VC13-2-41	-1.78	0	0	0	0	61	16	9	7	0	0	2	8	0	0	0	0	0	0	0
VC13-2-64	-2.01	0	0	0	0	48	33	8	7	2	0	0	0	0	0	0	0	0	0	0
VC13-2-80	-2.17	0	0	0	0	54	23	5	14	3	2	2	2	2	0	0	0	0	0	0
VC13-2-97	-2.34	0	0	0	0	42	28	4	9	1	1	2	4	0	0	1	0	0	0	0
VC13-1-4	-2.61	0	0	0	0	53	24	7	8	1	0	1	1	1	0	0	0	2	0	0
VC13-1-9,5	-2.66	0	0	0	0	46	45	6	4	2	0	5	1	0	0	0	0	0	0	0
VC13-1-16	-2.73	0	0	0	0	38	28	5	9	0	0	5	6	0	1	0	0	0	0	0
VC13-1-32,5	-2.89	0	0	0	0	32	23	6	14	2	0	0	2	0	0	0	0	0	0	0
VC13-1-50	-3.07	26	0	83	5	0	0	0	0	0	0	0	0	0	0	0	0	0	0	0
VC13-1-63	-3.20	0	0	0	0	0	0	0	0	0	0	0	0	0	0	0	0	0	0	0
VC13-1-78	-3.35	0	0	0	0	0	0	0	0	0	0	0	0	0	0	0	0	0	0	0
VC13-1-94	-3.51	0	0	36	0	0	0	0	0	0	0	0	0	0	0	0	0	0	0	0
VC13-1-111	-3.68	0	0	0	0	0	0	0	0	0	0	0	0	0	0	0	0	0	0	0
N44-3-13	-0.90	0	0	0	0	39	53	3	0	0	0	1	0	0	0	0	0	0	0	0
N44-3-71	-1.48	0	0	1	0	57	23	10	1	1	2	1	3	0	0	0	0	0	0	0
N44-3-101	-1.78	0	0	0	0	49	24	15	3	0	0	4	7	3	0	0	0	0	0	0

– Continued on next page –

		Foraminifers										Ostracods								
Ection sample number	**Depth NHN [m]**	*Trochammina inflata*	*Triloculina oblonga*	*Entzia macrescens*	*Miliammina fusca*	*Ammonia tepida*	*Haynesina germanica*	*Cribroelphidium williamsoni*	*Cribroelphidium excavatum*	*Elphidium* spp.	*Cyprideis torosa*	*Leptocythere* spp.	*Cushmanidea elongata*	*Semicytherura* sp.	*Hirschmannia virdis*	*Krithe* sp.	*Loxoconcha* sp.	*Sahnicythere retroflexa*	*Cytherois pusilla*	*Urocythereis* sp.
N44-3-146	-2.23	0	1	0	0	75	19	6	1	0	0	0	0	0	0	0	0	0	0	0
N44-3-150	-2.27	0	0	0	0	39	39	10	3	1	0	4	2	2	2	0	0	0	0	0
N44-2-5	-2.36	0	0	0	0	50	35	11	1	2	0	8	5	3	0	0	1	0	0	0
N44-2-30	-2.61	1	0	0	0	33	30	16	0	0	2	15	0	0	0	0	1	0	2	0
N44-2-39	-2.70	0	0	0	0	41	26	11	1	0	2	11	6	0	0	0	1	0	1	0
N44-2-46	-2.77	0	0	0	0	63	23	7	0	0	0	0	5	0	0	0	0	0	0	0
N44-2-56	-2.87	0	0	0	0	70	21	8	0	0	0	4	1	0	0	0	0	0	1	0
N44-2-64	-2.95	3	0	4	0	0	3	0	0	0	0	0	0	0	0	0	0	0	0	0
N44-2-76	-3.07	22	0	21	0	0	0	0	0	0	0	0	0	0	0	0	0	0	0	0
N44-2-84	-3.15	26	0	6	0	0	0	0	0	0	0	0	0	0	0	0	0	0	0	0
N44-2-103	-3.34	0	0	0	0	0	0	0	0	0	0	0	0	0	0	0	0	0	0	0
N44-2-112	-3.43	0	0	0	0	0	0	0	0	0	0	0	0	0	0	0	0	0	0	0
N44-2-116	-3.47	0	0	0	0	0	0	0	0	0	0	0	0	0	0	0	0	0	0	0
N44-2-139	-3.70	0	0	0	0	0	0	0	0	0	0	0	0	0	0	0	0	0	0	0
N45-5-37	-0.87	0	0	0	0	42	47	9	5	0	0	2	0	0	0	0	0	0	0	0
N45-5-81	-1.31	0	0	0	0	42	33	13	5	0	1	5	1	1	0	0	0	0	0	1
N45-4-111	-2.52	1	0	0	0	67	20	13	0	1	0	4	0	0	0	0	0	0	0	0
N45-3-60	-3.21	0	0	1	0	24	46	4	8	0	0	14	0	0	1	0	0	0	2	0
N45-2-60	-4.41	2	1	0	0	19	44	14	4	0	0	7	0	2	0	3	0	0	0	0
N45-1-44	-5.45	3	0	3	0	32	41	10	4	0	0	8	1	0	0	0	0	0	0	0

Chapter 5

5 Vertical and lateral distribution of Foraminifera and Ostracoda in the East Frisian Wadden Sea – developing a transfer function for relative sea-level change

Juliane Scheder[1,2], Peter Frenzel[3], Friederike Bungenstock[1], Max Engel[2,4], Helmut Brückner[2] & Anna Pint[2]

[1] *Lower Saxony Institute for Historical Coastal Research, Viktoriastraße 26/28, 26382 Wilhelmshaven, Germany*
[2] *Institute of Geography, University of Cologne, Albertus-Magnus-Platz, 50923 Köln, Germany*
[3] *Institute of Geosciences, Friedrich Schiller University Jena, Burgweg 11, 07749 Jena, Germany*
[4] *Geological Survey of Belgium, Royal Belgian Institute of Natural Sciences, Jennerstraat 13, 1000 Brussels, Belgium*

Abstract

In light of rising sea levels and increased storm surge hazards, detailed information on relative sea-level (RSL) histories and local controlling mechanisms is required to support future projections and to better pre-pare for future coastal-protection challenges. This study contributes to deciphering Holocene RSL changes at the German North Sea coast in high resolution by developing a transfer function for RSL change. Recent associations of Foraminifera and Ostracoda from low intertidal to supratidal settings of the barrier island of Spiekeroog in combination with environmental parameters (granulometry, C/N, total organic carbon, salini-ty) were investigated and quantified in elevation steps of 15 cm in order to generate a first transfer function (TF) of Holocene RSL change. In a future step, the TF can be applied to the stratigraphic record. Our data show a clear vertical zonation of foraminifer and ostracod taxa between the middle salt marsh and the tidal flat with very few individuals in the sand flat area, suggesting removal by the tidal current or poor preserva-tion. Multivariate statistics identify the elevation, corresponding to the inundation frequency, as main driving factor. The smallest vertical error (49 cm) is associated with an entirely new approach of combining Foram-inifera and Ostracoda for a TF. Advantages of the TF over classical RSL indicators such as basal and inter-calated peats – beside the relatively narrow indicative meaning – include the possible application to a wide range of intertidal facies and that the resulting RSL curve does not depend on compaction-prone peats.

Keywords

North Sea, Holocene, microfauna, ecology, relative sea-level history, Spiekeroog, back-barrier tidal flats, Germany

Published in *Geologica Belgica 22/3-4* (2019) 99–110.
https://doi.org/10.20341/gb.2019.007

GEOLOGICA BELGICA (2019) 22/3-4: 99-110

Vertical and lateral distribution of Foraminifera and Ostracoda in the East Frisian Wadden Sea – developing a transfer function for relative sea-level change

Juliane SCHEDER[1,2,*], Peter FRENZEL[3], Friederike BUNGENSTOCK[1], Max ENGEL[2,4], Helmut BRÜCKNER[2] & Anna PINT[2]

[1] *Lower Saxony Institute for Historical Coastal Research, Viktoriastraße 26/28, 26382 Wilhelmshaven, Germany.*
[2] *Institute of Geography, University of Cologne, Albertus-Magnus-Platz, 50923 Köln, Germany.*
[3] *Institute of Geosciences, Friedrich Schiller University Jena, Burgweg 11, 07749 Jena, Germany.*
[4] *Geological Survey of Belgium, Royal Belgian Institute of Natural Sciences, Jennerstraat 13, 1000 Brussels, Belgium.*
** corresponding author: scheder@nihk.de; schederj@uni-koeln.de.*

ABSTRACT. In light of rising sea levels and increased storm surge hazards, detailed information on relative sea-level (RSL) histories and local controlling mechanisms is required to support future projections and to better prepare for future coastal-protection challenges. This study contributes to deciphering Holocene RSL changes at the German North Sea coast in high resolution by developing a transfer function for RSL change. Recent associations of Foraminifera and Ostracoda from low intertidal to supratidal settings of the barrier island of Spiekeroog in combination with environmental parameters (granulometry, C/N, total organic carbon, salinity) were investigated and quantified in elevation steps of 15 cm in order to generate a first transfer function (TF) of Holocene RSL change. In a future step, the TF can be applied to the stratigraphic record. Our data show a clear vertical zonation of foraminifer and ostracod taxa between the middle salt marsh and the tidal flat with very few individuals in the sand flat area, suggesting removal by the tidal current or poor preservation. Multivariate statistics identify the elevation, corresponding to the inundation frequency, as main driving factor. The smallest vertical error (49 cm) is associated with an entirely new approach of combining Foraminifera and Ostracoda for a TF. Advantages of the TF over classical RSL indicators such as basal and intercalated peats – beside the relatively narrow indicative meaning – include the possible application to a wide range of intertidal facies and that the resulting RSL curve does not depend on compaction-prone peats.

KEYWORDS: North Sea, Holocene, microfauna, ecology, relative sea-level history, Spiekeroog, back-barrier tidal flats, Germany.

1. Introduction

Relative sea-level (RSL) reconstructions are essential for understanding past and recent coastal processes and represent a crucial framework for future predictions of sea-level rise (Woodroffe & Murray-Wallace, 2012). This information is urgently needed for all fields of coastal zone management and the mitigation of coastal hazards – in particular in light of rising sea levels and a future increase of storm surge levels (Weisse et al., 2012; Rahmstorf, 2017) –, as well as in the fields of basic coastal research (e.g. geomorphology, sedimentology, palaeoclimatology, geoarchaeology) (Overpeck et al., 2006; Nicholls & Cazenave, 2010). The reconstruction of Holocene RSL changes along the German North Sea coast, until now, is mostly based on basal and intercalated peats (e.g. Behre & Streif, 1980; Behre, 2007) and shows rather coarse vertical resolution. Several authors have expressed the need for more precise quantitative data (Vink et al., 2007; Bungenstock & Schäfer, 2009; Bungenstock & Weerts, 2010, 2012; Baeteman et al., 2011; Meijles et al., 2018).

A high-resolution reconstruction of past local RSL changes can be achieved by means of analysis of fossil salt-marsh Foraminifera, shell-bearing protists, which create very specific assemblages in the sedimentary record based on habitat conditions. A dense dataset of taxa distribution along a vertical transect of local modern intertidal environments can be used to develop a transfer function (TF), which models the relation between elevations of sample points and relative abundances of foraminifer species over time. Such a TF may permit inferences of palaeo-water depths with a centimetre-scale precision (Leorri et al., 2010; Kemp et al., 2012; Edwards & Wright, 2015), but typically within ~10–15% of the tidal range, leading to a decimetre-scale precision for mesotidal environments (Barlow et al., 2013). The use of salt-marsh Foraminifera for local RSL reconstructions has been established during the last two decades especially in North America, Denmark and on the British Isles (e.g. Scott et al., 2001; Gehrels & Newman, 2004; Gehrels et al., 2002; Pedersen et al., 2009; Engelhart & Horton, 2012; Kemp et al., 2013), but so far, applications are lacking for the southern part of the German Bight. Besides Foraminifera, Ostracoda, small crustaceans with a bivalved calcified carapace, occur within the same sediment fractions in the wider study area (Scheder et al., 2018). We assume that Ostracoda may provide additional information for more detailed reconstructions for the lower intertidal and uppermost subtidal. For the first time in palaeo-sea-level research, we combine Foraminifera and Ostracoda for a RSL TF (relative sea-level transfer function).

This study presents the vertical zonation of recent living and dead Foraminifera and Ostracoda along a cross-shore profile in the back-barrier tidal flat of the East Frisian barrier island of Spiekeroog as an initial step of a transfer function-based RSL reconstruction. Foraminifera and Ostracoda distribution is interpreted in light of tidal influence and sedimentary environments and translated into a first RSL TF. Research hypotheses are:

A vertical and lateral zonation of associations of foraminifers and ostracods mainly depends on elevation, hence, the duration of water cover.

The additional use of ostracods for TF development leads to an improvement compared to the common procedure of using exclusively foraminifers.

A foraminifer and ostracod based TF provides a more precise vertical resolution of sea-level index points than so far used at the German North Sea coast.

2. Study area

The study area is situated at the southern coast of Spiekeroog (Fig. 1), one of the East Frisian barrier islands, which developed after around 6–7 ka BP (kiloyears before present, i.e. before AD 1950) when the post-glacial sea-level rise decelerated (Behre, 1987; Freund & Streif, 1999; Flemming, 2002; Bungenstock & Schäfer, 2009). Due to ongoing RSL rise and prevalent longshore current directions, the barrier islands have shifted over several kilometres in a south-easterly direction since their formation (Streif, 1990; Flemming, 2002), reaching their recent position about 2000 years ago (Freund & Streif, 2000). Diurnal tides (mean tidal range = 2.7 m; BSH 2018) fill and empty the back-barrier mesotidal prism of Spiekeroog through the two tidal inlets Otzumer Balje and Harle. The tidal flat merges towards the island and transforms into a well-developed salt marsh. The area is characterised by a humid tempered climate (Cfb after latest Köppen-Geiger classification; Kottek et al., 2006; Beck et al., 2018) with mean winter temperatures between 2.9 and 5.7 °C and mean summer temperatures between 15.8 and 18.3 °C (weather station Wangerland-Hooksiel, survey duration: 2014–2019). The

https://doi.org/10.20341/gb.2019.007

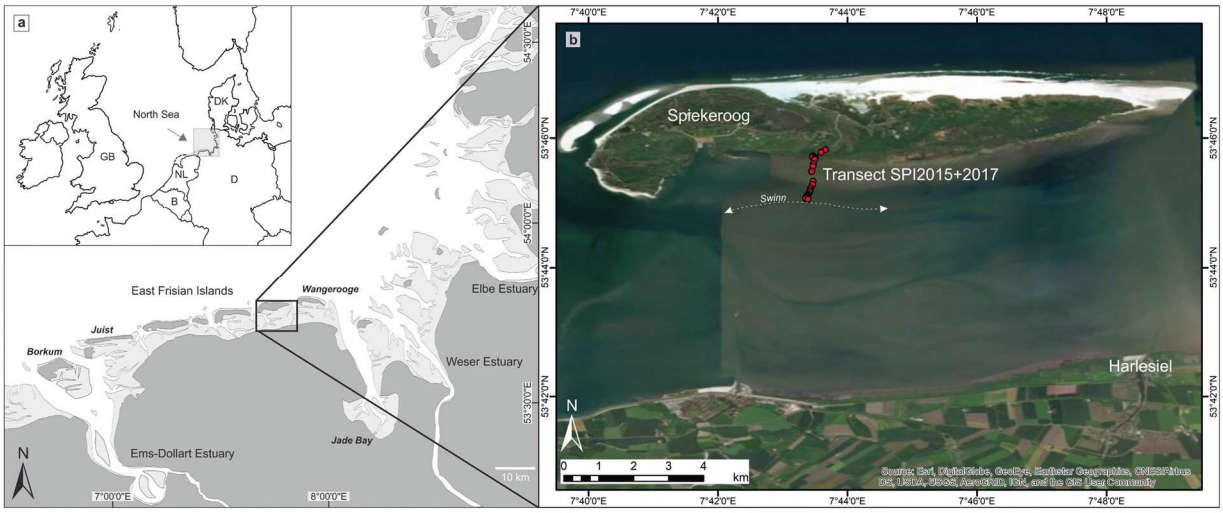

Figure 1. Overview of the study area. a: The southern North Sea coast with the East Frisian Islands (Spiekeroog is framed). b: The back-barrier area of Spiekeroog with the investigated surface transect at the southern coast of the island reaching from the salt marsh to the nearest tidal channel 'Swinn' (map source: Esri, Digital Globe, GeoEye, Earthstar Geographics, CNES/Airbus DS, USDA, USGS, Aerogrid, IGN, and the GIS User Community).

salinity lies around 30 psu (practical salinity units) close to the main tidal channel (southeast of the island) and a little lower towards the mainland. After occasional freshwater input (e.g. heavy rainfall events), the salinity can decrease to less than 25 psu (Kaiser & Niemeyer, 1999; Reuter et al., 2009).

Due to the shore-normal energy gradient (cf. Nyandwi & Flemming, 1995), an offshore-coarsening trend in grain sizes is observed. This general trend can be locally interrupted by tidal channels, depressions or old channel fillings (Bungenstock et al., 2002), whereas the barrier islands do not disturb it. Thus, there is no shoreward fining trend in grain size in the southern salt marshes of the island. Therefore, sampling in the opposite direction from the island's salt marshes down to the low water line in the back-barrier tidal flat generally results in sampling from sand flats to finer-grained mixed flats. The investigated transect (c. 1180 m in N-S direction, directly bordering the national park area) covers the natural salt marsh and adjacent back-barrier tidal flat of the island reaching the nearest tidal channel 'Swinn' in the south (Figs 1 and 2). The vegetation above and along the transect shows a more or less characteristic pattern from the high to middle salt marsh (sea lavender [*Limonium vulgare*]) crossing the 'Andel' Zone (lower salt marsh; andel grass [*Puccinellia maritima*], salt bush [*Atriplex halimus*]) and the Glasswort Zone (pioneer zone; cord grass [*Spartina anglica*], glasswort [*Salicornia europaea*]) down to the Seagrass Zone (tidal flat; seagrass [*Zostera*]) (e.g. Streif, 1990; Gerlach, 1999).

3. Methods

3.1. Field work

Twenty-three samples were taken during low tide (nineteen in December 2015 [neap-tide situation, 9–10 °C, dry weather], additional four in July 2017 [spring-tide situation, 15–20 °C, c. 1 mm of rainfall before sampling]) along a transect reaching from shallow subtidal (tidal channel levee) to supratidal (salt marsh) areas (Fig. 2) at the southern coast of Spiekeroog. Samples were taken in steps of 15 cm elevation difference with steel sampling rings (Eijkelkamp; diameter: 5 cm) comprising the uppermost 5 cm of the sediment surface. In order to distinguish living from dead individuals, samples were conserved with rose Bengal-coloured Ethanol (Walton, 1952; Edwards & Wright, 2015). At each sampling point, additional surface samples were taken for sedimentological analyses and, water coverage provided, water samples were taken in centrifuge tubes for salinity measurements in the laboratory. Elevation measurements at each sampling point were conducted using a differential global navigation satellite system (DGNSS; Topcon Hiper Pro). By anchoring the measured grid to the trigonometric point 2212 052 00 of the 'Landesamt für Geoinformation und Landesvermessung Niedersachsen' (LGLN) in the Spiekeroog salt marsh, the setup provides a vertical and lateral accuracy of ±2 cm. Since the 2017 transect is slightly shifted in N-S direction, samples had to be projected onto the 2015 surface profile (Fig. 3).

3.2. Laboratory analyses

All microfaunal samples were carefully shaken overnight with a dispersant (sodium pyrophosphate; $Na_4P_2O_7$; 46 g/l) to prevent adhesion of clay particles and afterwards washed through sieves, separating them into >63 µm and >100 µm fractions. For three representative samples the latter was split into eight aliquots per sample using a wet splitter after Scott & Hermelin (1993). From these aliquots a maximum of 200–300 individuals were counted wet in order to avoid drying of organic components and damaging of agglutinated Foraminifera (e.g. de Rijk, 1995; Edwards & Wright, 2015; Milker et al., 2016; Müller-Navarra et al., 2016). No species sensitive to drying were found in these samples and no damaging of tests could be observed after drying extracted individuals. Therefore, the remaining samples were air-dried, split with a micro splitter (ripple divider) and counted dry. The proportion of dry-counted material was weighed in order to enable extrapolation of microfaunal concentration per sample. Foraminiferal species were identified based on taxonomic descriptions and illustrations in Gehrels & Newman (2004), Horton & Edwards (2006) and Murray (2006), whereas identification of ostracod species followed the descriptions in Athersuch et al. (1989) and Frenzel et al. (2010). Because of the problem of discriminating juvenile individuals of *Leptocythere*, those species were grouped under *Leptocythere* spp. for counting. Discrimination of living and dead individuals was based on staining for foraminifers (at least one chamber stained = living; not stained = dead) and on well preserved soft parts in ostracods. The replacement of the genus *Jadammina* by *Entzia* is based on Filipescu & Kaminski (2011), who regard *Entzia* as a senior synonym of *Jadammina*. Foraminifer and ostracod associations were combined into a basic population for statistical analysis (100% = foraminifers + ostracods). After testing the detailed vertical distribution of living individuals for three representative samples, showing significant numbers of living individuals within the upper 3 cm, these were combined for microfaunal investigation and the lower 2 cm were discarded.

Samples for sedimentological and geochemical analyses were dried at 40 °C and carefully pestled by hand. For grain-size analysis, carbonates were dissolved with hydrochloric acid (HCl; 10%) and organic matter removed using hydrogen peroxide (H_2O_2; 15%). In order to prevent aggregation, samples were treated with sodium pyrophosphate ($Na_4P_2O_7$; 46 g/l). The

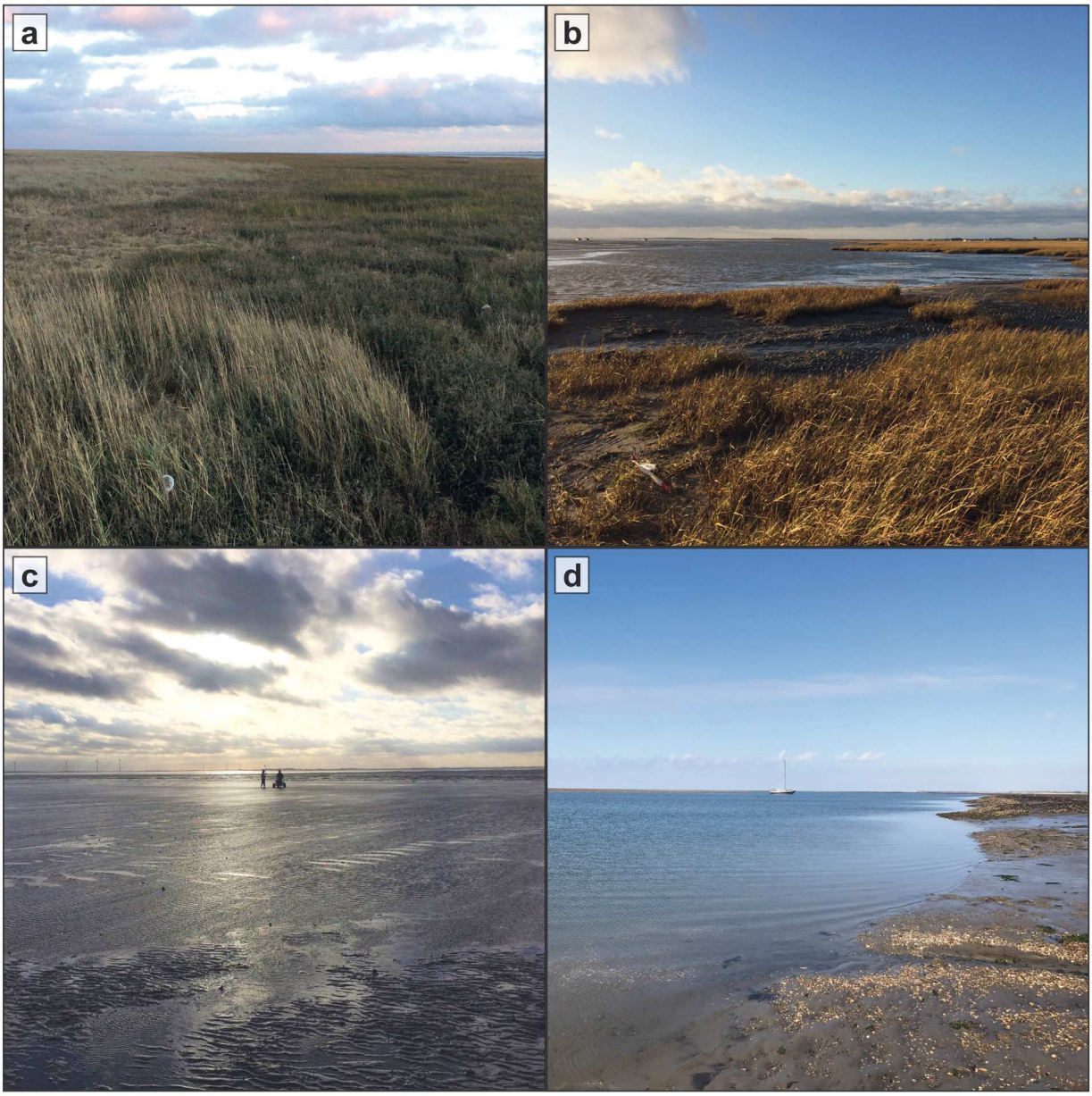

Figure 2. Photographic documentation of the study area during low tide. a: transition between middle and lower salt marsh (view towards SE); b: transition between salt marsh (pioneer zone) and sand flat (view towards W); c: view from the sand flat to the mixed flat (view towards S); d: margin of the tidal channel 'Swinn' (view towards SW).

grain-size distribution was determined on the <2 mm fraction using a laser particle size analyser (Beckman Coulter LS 13320) with a laser beam (780 nm) applying the Fraunhofer optical mode (Eshel et al., 2004). Since different species of Foraminifera and Ostracoda often prefer different substrates (cf. Frenzel et al., 2010), the microfaunal associations can be related to grain-size distribution.

The organic content was determined by measuring the concentration of total organic carbon (TOC, constituting c. 50% of the organic matter). This was accomplished using an elemental analyser (elementar, Vario EL Cube), which enabled simultaneous measurements of nitrogen (N) and the determination of total inorganic carbon (TIC). The derived C/N ratio can provide information about the aquatic or terrestrial origin of organic matter (e.g. Last & Smol, 2001).

The salinity was measured under laboratory conditions using a conductivity meter CO310 (VWR). Since the measurement was conducted with a delay of several months, the results are expected to be influenced by evaporation within the closed vessels. However, this should be consistent between all samples, so a general trend can be inferred.

3.3. Data processing

The calculation of univariate statistical grain-size measures after Folk & Ward (1957) was carried out using GRADISTAT software (Blott & Pye, 2001). As preparation of the data set for multivariate analyses, Pearson correlation coefficients were calculated between the environmental parameters (sand amount, mean grain size, TOC, TIC, N, C/N, elevation) and microfaunal data in order to detect possible auto-correlations. The distributions of foraminifer and ostracod taxa as well as standardised environmental parameters were analysed by means of multivariate statistics (PCA, CCA, DCA) in order to evaluate driving environmental parameters and test whether species show unimodal or linear response along the main environmental gradient. Both correlation and multivariate statistics were performed using the software PAST (v. 3.21; Hammer et al., 2001). Afterwards, the TF was developed from the training data using the software C2 (v. 1.7.7; Juggins, 2007). According to the gradient length revealed by the DCA (3.3 standard deviation [SD]), a more unimodal species-environment relation can be expected (Birks, 1995; Lepš & Šmilauer, 2003), wherefore

modelling was conducted using the weighted averaging-partial least squares (WA-PLS) method. To avoid overfitting, a maximum of three components was modelled (cf. Kemp & Telford, 2015). Bootstrapping cross-validation (1000 cycles) was used to evaluate the TF performance based on the coefficient of determination (R^2_{boot}), providing an estimation of the grade of the linear relationship between observed and estimated elevations in the training set, and the root mean squared error of prediction (RMSEP), enabling the evaluation of the general predictive capability of the TF (Milker et al., 2017). The most appropriate of the three modelled components was chosen based on the lowest RMSEP and highest R^2_{Boot}. Visual presentation of the data was accomplished by means of the software Grapher (v. 8.0.278) and the drawing application CorelDRAW X8 (v.18.1.0.690).

4. Results of microfaunal, sedimentological and geochemical investigations

The investigated transect reaches from 53°45'42.27" N, 7°43'27.76" E (1.51 m NHN [m above *Normalhöhennull* = standard elevation zero referring to gauge Amsterdam]) in the north to 53°45'2.32" N, 7°43'23.49" E (-1.31 m NHN) in the south (Fig. 3). The separation of six zones (Zones A–F) was carried out based on qualitative interpretation of sedimentary (in particular grain-size distribution, TOC) and microfaunal (in particular foraminiferal abundance and composition) data in combination with field observations (Figs 3 and 4). Zone boundaries were defined in between two samples by considering the mean elevation between them. Foraminifer and ostracod species are always mentioned in ranking order concerning their abundances. In total, eight foraminifer and three ostracod taxa (Plate 1) were identified in both living and dead fauna. In general, much less living than dead individuals occur and microfaunal densities vary strongly between zero and 2500 ind./10 cm³ (individuals per 10 cm³) throughout the transect.

Zone A (middle salt marsh), comprising the northernmost three samples (c. 1.51–1.13 m NHN; samples 1, 2 and 3) is characterised by very poorly sorted sandy mud in the upper and muddy sand in the lower part. The vegetation is characterised by *Limonium vulgare* (sea lavender) and *Puccinellia maritima* (andel grass). TOC and TIC values show opposite trends with TOC decreasing and TIC increasing towards lower elevations. The N content and the C/N ratio both decrease towards lower elevations. No water cover was present. The microfaunal composition is characterised by high diversity and high abundance (up to c. 2200 individuals/10 cm³). Foraminifers are dominated by *Triloculina oblonga* (Montagu, 1803) in the upper and *Ammonia tepida* (Cushman, 1926) in the lower part, followed by *Haynesina germanica* (Ehrenberg, 1840), *Cribroelphidium williamsoni* (Haynes, 1973) and the agglutinated species *Trochammina inflata* (Montagu, 1803), *Miliamina fusca* (Brady, 1870) and *Entzia macrescens* (Brady, 1870). A few individuals of *Spirillina* sp. could also be observed. Ostracods are dominated by *Leptocythere* spp., represented by *L. pellucida* (Baird, 1850), *L. castanea* (Sars, 1866) and *L. lacertosa* (Hirschmann, 1912), followed by *Cytherois pusilla* (Sars, 1928) and *Cyprideis torosa* (Jones, 1850). However, ostracods show a much lower abundance than foraminifers. Living individuals are barely present. The microfaunal concentration increases towards the following zone (Zone B) from c. 600 ind./10 cm³ in the uppermost sample (1) to c. 2300 ind./10 cm³ in the lowest sample (3). Most shells seem to be well preserved (transparent) and only a few show slight signs of degradation (opaque/white colour). Only *E. macrescens* repeatedly exhibits collapsed chambers, which could have happened during sample treatment, after drying of the individuals or even prior to sampling due to their very lightly agglutinated tests (e.g. Murray, 2006; Filipescu & Kaminski, 2011).

Zone B (lower salt marsh), comprising three adjacent samples (c. 1.06–0.86 m NHN; samples 4, 5 and 6), is characterised by very poorly sorted sandy mud with an increasing sand amount towards lower elevations. The vegetation is composed of *Atriplex portulacoides* (salt bush), *Puccinellia maritima* (andel grass) and *Spartina anglica* (cord grass). The highest TOC and second highest TIC values of the whole transect occur in this zone as well as the highest values for N. Water coverage is partially given by small pools near the sampling points with a salinity of 27.5 psu in the upper part of Zone B. This zone, with abundances of up to c. 600 individuals/10 cm³, is further defined by the presence of *T. inflata*, *E. macrescens* and *M. fusca*. *E. macrescens* dominates the upper part (sample 20), while *T. inflata* dominates the lower part (sample 5), both followed by the hyaline foraminifer species *T. oblonga*, *A. tepida*, *H. germanica* and *C. williamsoni*. Ostracods are only present in the lower part of the zone, dominated by *Leptocythere* and accompanied by *C. pusilla*. Only ~11–22% of all present foraminifers, but half of the ostracods were identified as 'living'. However, compared to the amount of foraminifers, ostracods only show very low abundances. Sample 5 taken from a small salt-marsh pool (0.72 m NHN, laterally belonging to the lower salt marsh) stands out in Zone B and represents Subzone B1. It is characterised by a much higher sand amount (sandy mud), higher TIC, lower TOC and N values as well as a lower C/N ratio than in the rest of Zone B. The salinity also decreases to the lowest value of the complete transect. The microfaunal composition changes in this subzone with a slightly higher amount of living Foraminifera (~25%). Foraminifera are dominated by *H. germanica* followed by *A. tepida* and *C. williamsoni*, accompanied by only a few individuals of *T. oblonga* and only one specimen of *T. inflata*. Ostracoda are strongly dominated by dead (~25%) and living (~43%) individuals of *C. torosa*, accompanied by *Leptocythere* and *C. pusilla*. This sample shows the highest amount of ostracods throughout the complete transect. Within the complete zone (including B1), the microfaunal concentration decreases towards Zone C from c. 500 ind./10 cm³ to c. 100 ind./10 cm³. Only very few shells seem slightly degraded, whereas the major part is well preserved.

Zone C (pioneer zone; c. 0.86–0.48 m NHN) comprises three samples (7, 8 and 9) and represents a transition to Zone D, i.e. a transition from the salt marsh to the tidal flat. It is characterised by moderately to well sorted sand. *Spartina anglica* (cord grass) dominates the vegetation of this zone. No TIC and almost no TOC and N were documented. The C/N ratio first decreases before increasing to the highest value throughout the transect in the last sample of this zone. Water coverage in this zone occurred mainly in the lower part, which is the border between salt marsh and sand flat, due to the neap tide situation at the sampling day in 2015. The salinity is higher than in Zone B. The amount of microfauna (mainly foraminifers) is much lower than in Zone B, even though the uppermost sample still shows a moderate concentration of individuals. It is strongly dominated (62%) by living individuals of *C. williamsoni* followed by *H. germanica* and *A. tepida* accompanied by only one individual each of *T. inflata* and *T. oblonga*. In terms of Ostracoda, only six individuals of *Leptocythere* occurred in the lower two samples. The microfaunal concentration strongly decreases with decreasing elevation with c. 120 ind./10 cm³ in the upper sample (7) and only 4–6 ind./10 cm³ in the lower two samples. Most of the shells are well preserved and only very few seem slightly degraded.

Zone D (sand flat; c. 0.48–-0.30 m NHN) comprises six samples (10–15) and is the widest zone of the transect with a length of ~750 m. It is characterised by moderately well to well sorted sand with a coarsening trend towards lower elevations (medium sand increasing from c. 40 to c. 52%, fine sand decreasing from c. 51 to 38%). No vegetation was present in 2015 (winter), while occasional carpets of algae characterised the zone in 2017 (summer). TIC values are negligible as well as the only slightly higher TOC and N values. The C/N ratio is at a quite constant level (6–7). Water coverage occurred in the form of small puddles or micro-channels in a higher number in 2015 than in 2017. All samples are situated within these water-covered areas. The salinity shows only slight variations (0.6 psu). There are very few foraminifers in this zone (0–30 ind./10 cm³), dominated by living *C. williamsoni* in the upper part, where *A. tepida* is also present, and by dead *H. germanica* in the central part. The lower part of the zone comprises even fewer individuals while ostracods are completely absent. The few foraminifers observed in this zone show signs of degradation, except for the living individuals of *C. williamsoni*, which are well preserved.

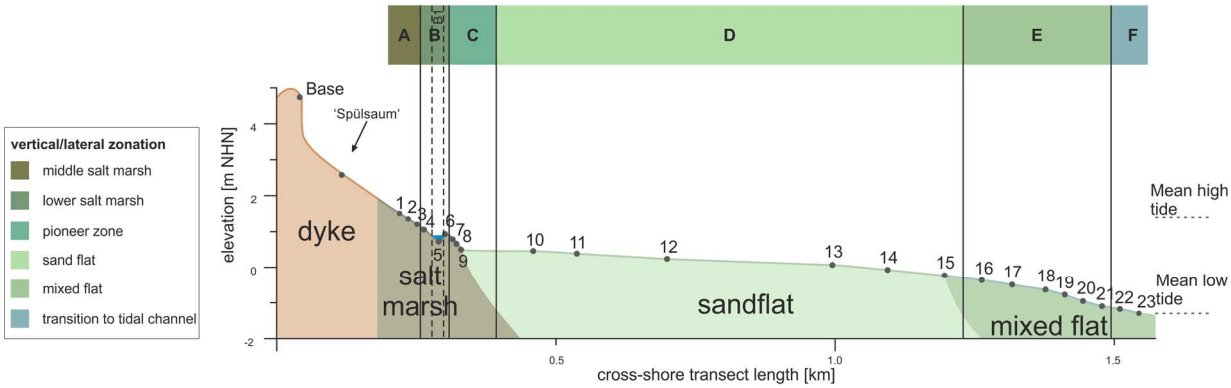

Figure 3. Elevation profile of the investigated surface transect showing sampling points, landscape units observed in the field as well as the identified zonation.

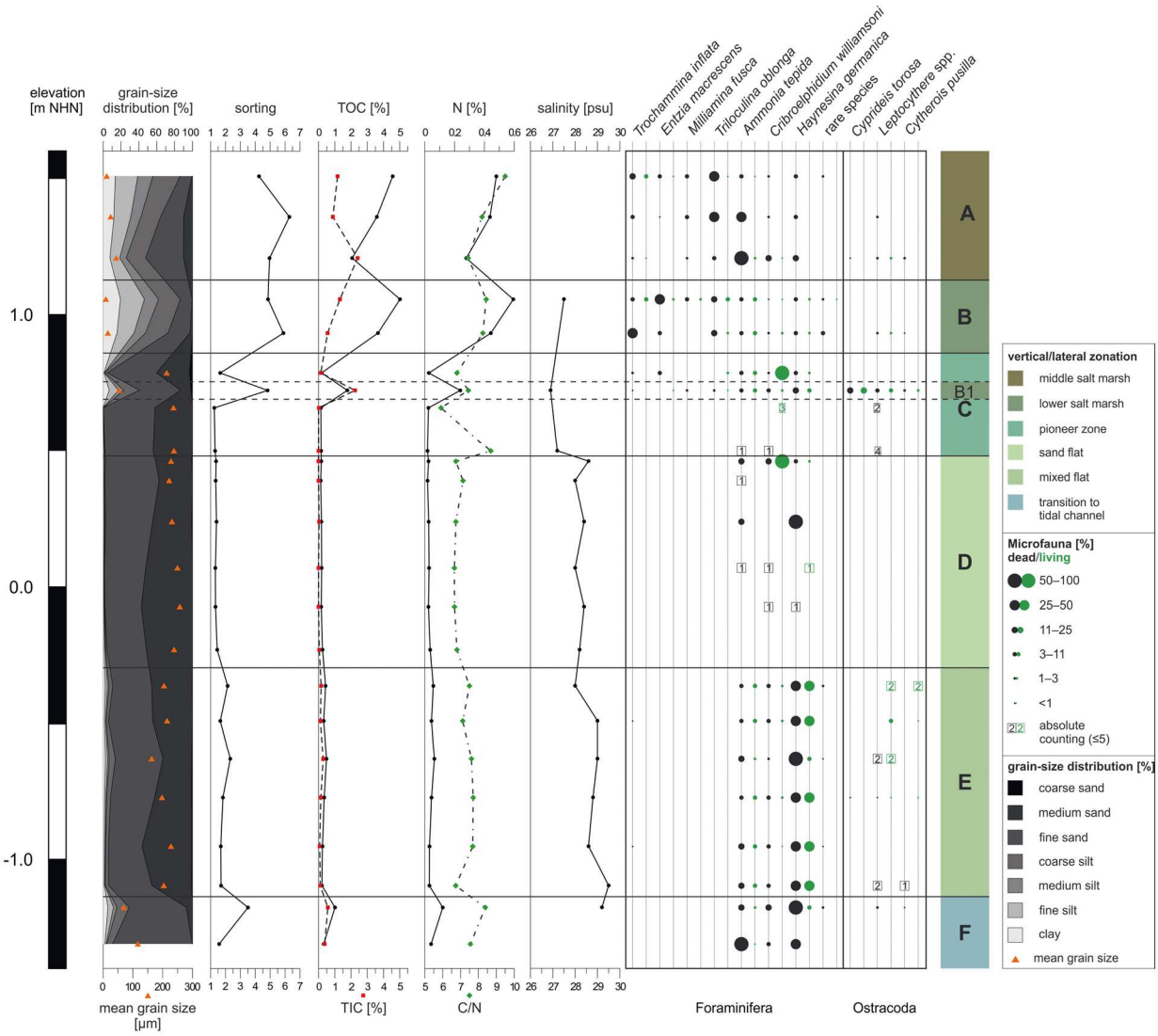

Figure 4. Microfaunal, sedimentological and geochemical results of the investigated surface transect in relation to the elevation. From left to right: grain-size distribution and mean grain size; sorting of the sediments, content of organic (TOC) and inorganic (TIC) carbon; nitrogen (N) content and ratio of organic carbon and nitrogen (C/N); salinity trend measured for sampling points with present water coverage; foraminifer and ostracod species association; identified lateral and vertical zones.

In Zone E (mixed flat; c. -0.30–-1.14 m NHN), comprising six samples (16–21), silt and clay reappear (Fig. 4). It is characterised by a poorly to moderately sorted muddy sand to pure sand. No vegetation is present. In this zone, for the first time, occasional molluscs induce slight bioturbation of the upper centimetres of the sediment. TIC, TOC, N and the C/N ratio show slight variations compared to Zone D. Water coverage occurred in the form of small puddles or micro-channels and the salinity increases from the upper to the lower part by 1.5 psu, resulting in the highest value of the transect (29.5 psu). Besides the grain-size distribution, the most striking change is the reappearance of microfauna with generally increasing concentrations towards lower elevations (from c. 50 to c. 900 ind./10 cm³). It is dominated by *H. germanica* (living and dead) followed by *A. tepida*, *C. williamsoni* and two individuals of *T. inflata*. The highest abundance of ostracods (20 individuals) occurs in sample 17 dominated by living *Leptocythere* (like in the

rest of Zone E). While *C. pusilla* and *C. torosa* are also present, some juvenile ostracod individuals remain indeterminable (8 out of 49 in total). Preservation of shells is mainly good and only very few individuals seem slightly degraded.

Zone F (transition to tidal channel; c. -1.14 m NHN until at least -1.31 m NHN) comprises two samples (22 and 23). With first increasing and then decreasing silt and clay amounts, it is characterised by poorly to moderately sorted muddy sand. In 2015, no vegetation was present, while in 2017 algae remains were visible along the levee of the tidal channel. Furthermore, the levee was characterised by many mollusc shells (Fig. 2d). In the upper sample, TIC, TOC and N show a slight increase of 0.09–0.8%, while the C/N ratio increases by ~1.6 and only the salinity shows a slight decrease of 0.3 psu. In the lower sample 23, all values are more similar to Zone E. Due to the lack of water cover, no salinity was measured for the lowest sample, but the salinity of the shallow water of the adjacent tidal channel was 29.3 psu. The foraminiferal composition is similar to that of Zone E, although the amount of living individuals decreases with decreasing elevation, as does the microfaunal concentration (from c. 2500 to c. 1000 ind./10 cm³). Towards the lowermost sample (23), a shift in the dominance between the two most abundant tidal flat foraminifer species of the transect – *H. germanica* and *A. tepida* – is observed; *C. williamsoni* occurs as well. Ostracods are only present in the upper sample represented by dead *Leptocythere* and *C. pusilla*. Approximately half of the shells or tests are well preserved, while the rest appears to be slightly degraded.

5. Results of statistical analyses

5.1. Driving environmental factors

The Pearson correlation shows that *T. oblonga* is highly correlated with the sand amount, N and TOC (and these factors are also highly correlated with each other). The sand amount and the N content were therefore excluded for the downstream statistical analyses. Since TIC seems to be rather insignificant throughout the transect and TOC is also connected to the grain size, we also excluded TIC for the multivariate statistics. Furthermore, *Spirillina* sp. is highly correlated with *M. fusca*, the latter being slightly more frequent. Therefore, the rare *Spirillina* sp. was also excluded. In order to find variables, which account for as much of the variance in our dataset as possible (Davis, 1986; Harper, 1999), a principle component analysis (PCA) was performed. In order to receive statistically relevant results, only samples with a minimum of 40 individuals counted were considered, thus excluding almost all sand flat samples between c. 0.39 and -0.29 m NHN. The most relevant axes for our modern dataset are PC 1 and 2 (biplot in Fig. 5).

PC 1, with an explained variance of 53.48%, contrasts *T. oblonga* and *C. williamsoni* along with all agglutinated foraminifer species with *H. germanica*. This includes all salt marsh and transitional samples on the negative and all tidal flat samples on the positive side leading to the conclusion of PC 1 describing a 'salt marsh versus tidal flat' factor, which could be related to the duration of water cover, i.e. the elevation. PC 2, describing a variance of 26.09%, opposes mainly *T. oblonga* (associated with the salt marsh samples) and *C. williamsoni* (associated with the transitional samples of the pioneer zone and sand flat). Since *C. williamsoni* tolerates higher salinities than most salt marsh species (Murray, 2006), PC 2 could relate to the salinity, which does not seem to have much of an influence on the tidal flat samples. The two samples of Zone F (transition to the tidal channel; samples 22 and 23 marked in yellow in Fig. 5) seem to be 'misplaced' by the PCA, since sample 22 is associated with the tidal flat group, whereas sample 23 is situated at the 'salt marsh' side of PC 1 and associated to *A. tepida*. This may be explained by the position at the margin of the tidal channel and related higher-dynamic conditions, to which *A. tepida* seems to be better adapted.

As shown by the PCA, the elevation seems to have a strong influence on foraminifer and ostracod distribution. In order to test if it is the main driving environmental factor, a canonical correspondence analysis (CCA) was carried out including the microfaunal data and the remaining parameters elevation, TOC and C/N. The CCA biplot (Fig. 6) shows the first axis, describing a variance of 63.73%, with highest scores for TOC and elevation (in ranking order). The latter exhibits the highest score for the second axis, which describes a variance of 28.52%. The C/N ratio seems rather irrelevant for both axes with the lowest scores for both. The different species exhibit different relations to the depicted environmental parameters. Since the second axis is mainly described by the elevation, the foraminifer species *A. tepida* and *C. williamsoni* and all three ostracod species show the highest relation to this parameter, whereas the salt marsh foraminifers *T. oblonga*, *M. fusca* and *T. inflata* are highly related to TOC, mainly describing the first axis. This indicates that the foraminifer and ostracod distribution is mainly influenced by the organic content and the inundation frequency related to elevation. Since the elevation is related to both axes and the TOC content shows quite high correlation values concerning the elevation (~0.75), a strong influence of the elevation, related to water depth and inundation frequency, can be assumed.

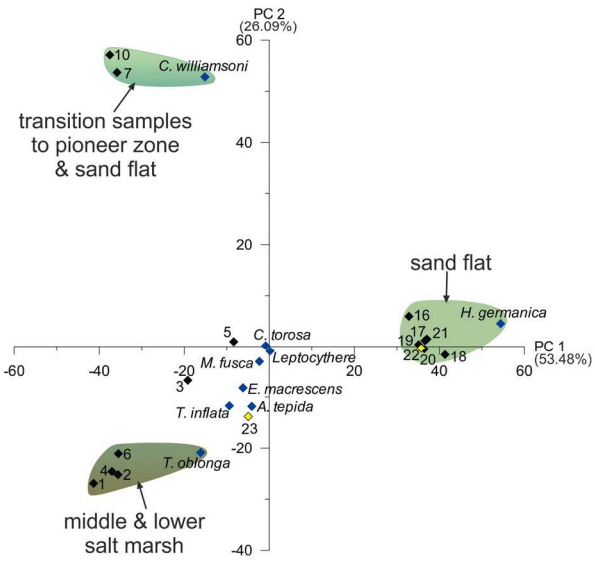

Figure 5. PCA biplots of the investigated surface transect with identified groupings (for colour legend of facies zones see fig. 3). Black diamonds represent samples (two outliers marked in yellow), blue diamonds represent microfaunal taxa.

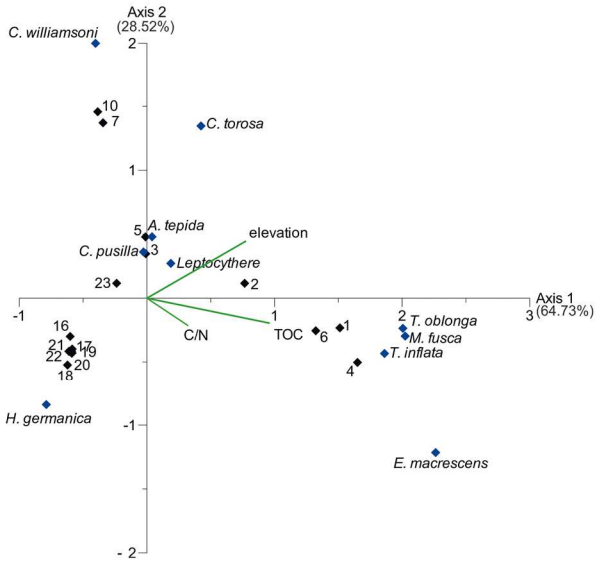

Figure 6. CCA biplot of the investigated surface transect. Black diamonds represent samples, blue diamonds represent microfaunal taxa. The three remaining environmental factors (elevation, TOC and C/N) are visualised by green lines. TOC and elevation have the highest scores for axes 1 and 2, identifying them as the main influence on the dataset.

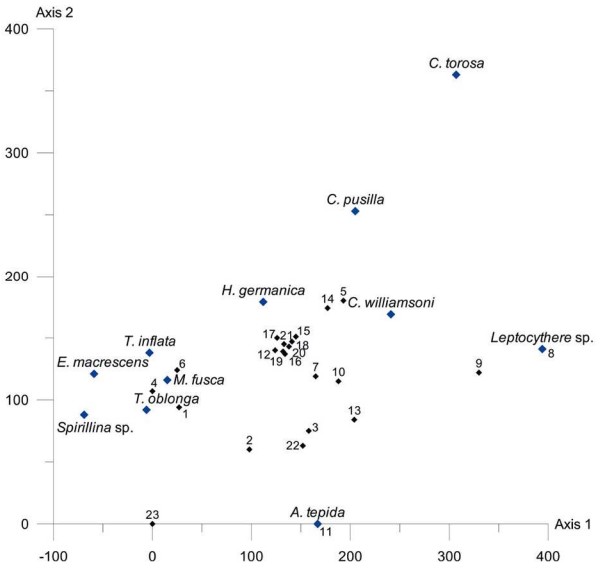

Figure 7. DCA plot showing the length of the environmental gradient (x=330, i.e. 3.3 pointing to unimodal species distributions). Samples are represented by black, species by blue diamonds.

A detrended correspondence analysis (DCA) was carried out in order to test the species-environment relationship. Since PCA and CCA confirmed the elevation (i.e. inundation frequency) as the strongest driving factor, we included only the elevation and the microfaunal data for the DCA. As the DCA plot (Fig. 7) shows, the length of the environmental gradient was determined as 3.3 SD, which indicates a rather unimodal species response (e.g. Birks, 1995; Lepš & Šmilauer, 2003).

5.2. Transfer function (TF) development and testing

Since living associations of foraminifers and ostracods can be affected by seasonal differences and the 2015 and 2017 samples were taken during different seasons – in fact showing differences in the densities of living individuals (Fig. 4) – only the dead assemblages were used for the TF development. Those represent the result of habitat preferences and connected taphonomic changes averaged over several years (e.g. Murray, 2000).

Two different models were developed for the TF (Fig. 8): Model I using exclusively foraminifers, representing the most commonly applied procedure, and Model II including the ostracods. Again, only samples with a minimum of 40 individuals were considered. For both models, component 2 seems to be the most suitable (lowest RMSEP and highest R^2) and is presented here. Since during the initial modelling, sample 23, once again, turned out to be an outlier, it was excluded from the dataset reducing the investigated elevation gradient to a vertical distance of 2.69 m (+1.51 to -1.18 m NHN). Since samples were taken during different tidal situations (neap and spring tide), the description of the RMSEP is related to the mean tidal range instead of the mean spring tidal range.

Model I shows an R^2_{boot} of 0.82 and an RMSEP of 54.2 cm, which accounts for 20.2% of the elevation gradient (and 20.1% of the mean tidal range). There is no visible trend of the TF over- or underestimating samples in relation to their observed elevation and structures of residuals are also not noticeable (Fig. 8).

Model II shows a slightly better R^2_{boot} of 0.84 and with 49.1 cm also a better RMSEP accounting for only 18.3% of the total elevation gradient (and 18.2% of the mean tidal range). Again, there is neither a clear trend of over- or underestimation related to the observed elevation nor are there visible structures of the residuals (Fig. 8).

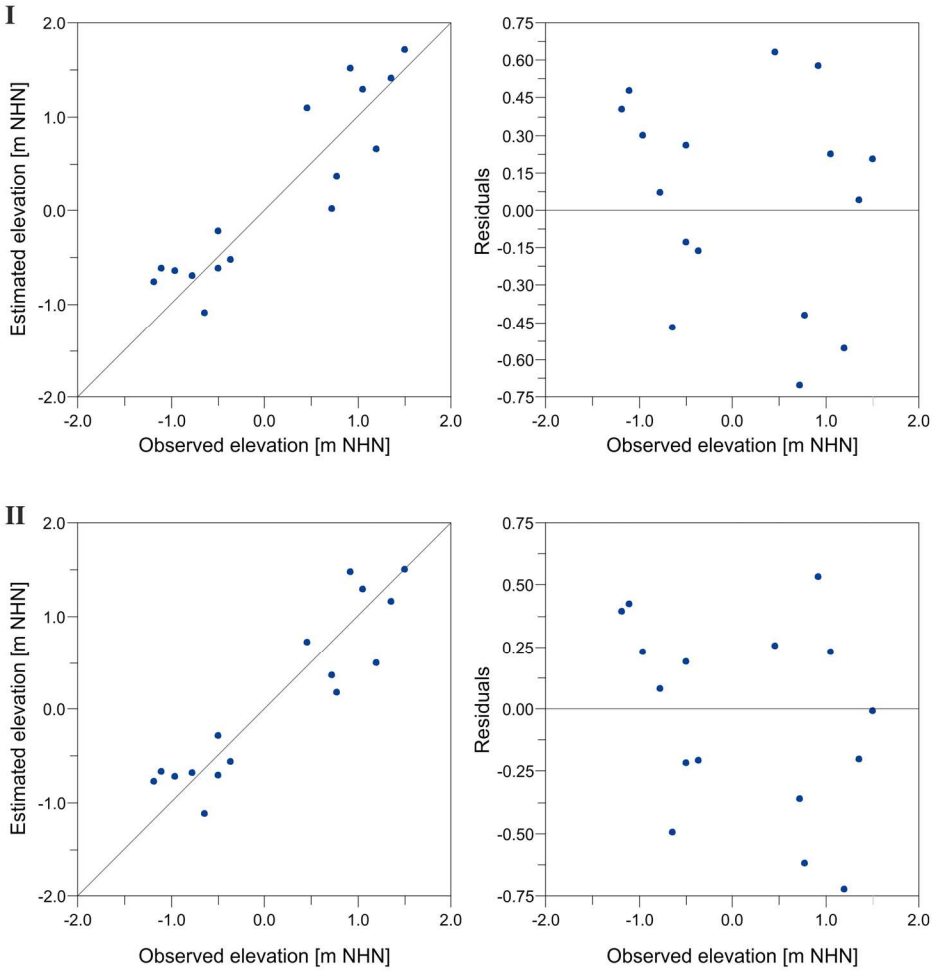

Figure 8. Results of testing the transfer function (TF) by bootstrapping cross validation (1000 cycles). Diagrams depict estimated vs. observed elevation (left diagrams) and deviation of each sample from the observed elevation (right diagrams) for both Model I based on dead Foraminifera alone (top) and Model II based on dead Foraminifera and Ostracoda combined (bottom).

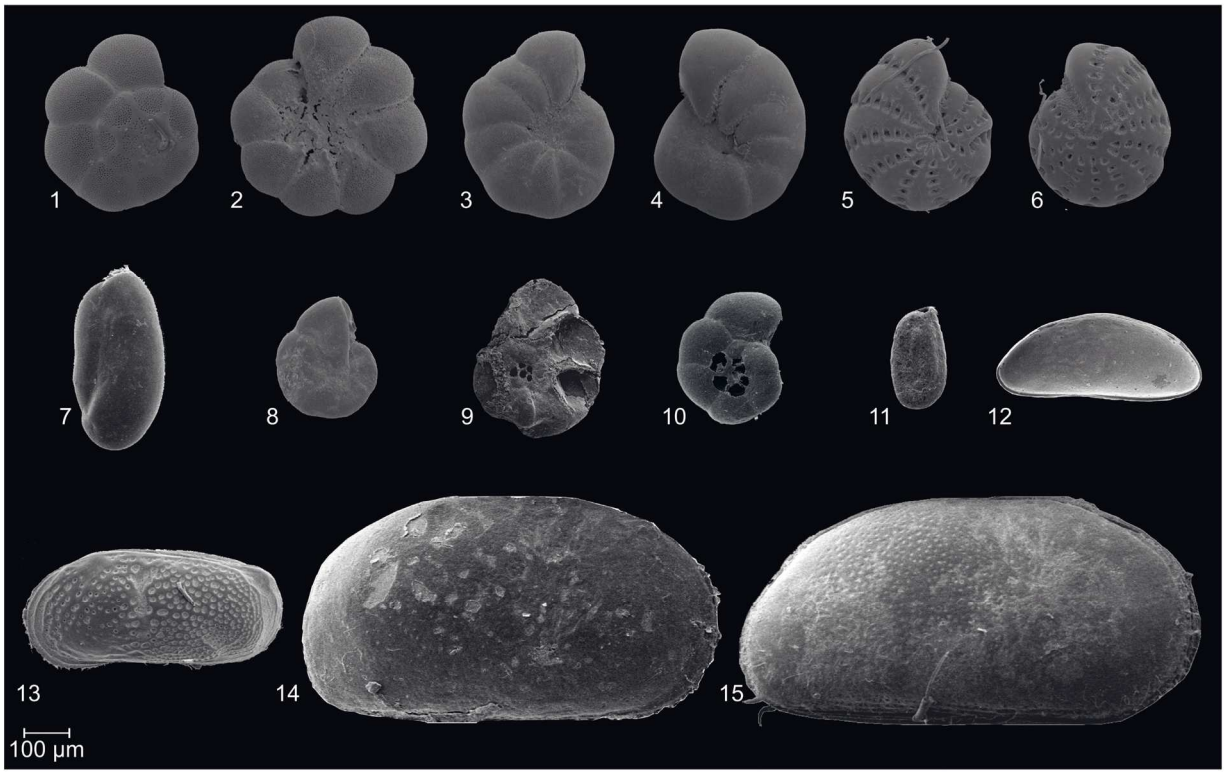

Plate 1. SEM images of frequently documented foraminifer (1–11) and ostracod (12–15) species. 1, 2: *Ammonia tepida* (Cushman, 1926); 3, 4: *Haynesina germanica* (Ehrenberg, 1840); 5, 6: *Cribroelphidium williamsoni* (Haynes, 1973); 7: *Triloculina oblonga* (Montagu, 1803); 8, 9: *Entzia macrescens* (Brady, 1870); 10: *Trochammina inflata* (Montagu, 1803); 11: *Miliammina fusca* (Brady, 1870); 12: *Cytherois pusilla* (Sars, 1928); 13: *Leptocythere pellucida* (Baird, 1850); 14, 15: *Cyprideis torosa* (Jones, 1850).

6. Discussion and evaluation of the modern training set

6.1. General observations

In general, higher amounts of fine-grained sediments, TIC, TOC and N correlate very well with the presence of microfauna, whereas areas of coarser-grained sediments and constantly low TIC, TOC and N contents correspond to areas of low abundance or even complete absence. The C/N ratio, lying between 4 and 10 throughout the complete transect, indicates that all organic matter originates from aquatic sources (e.g. Last & Smol, 2001). In accordance with our expectations, the salinity shows a general rising trend from the salt marsh to the tidal channel and increasing water cover and depths (Kaiser & Niemeyer, 1999; Flöser et al., 2011).

6.2. Living vs. dead fauna

Comparing the living and dead associations, we notice differences along the transect. The remarkably lower percentages of living than dead individuals occurring in the middle salt marsh (Zone A) suggest a quite good preservation of tests without significant dissolution effects. Furthermore, a part of the observed foraminifers and ostracods could be allochthonous and introduced during spring tides or storm surges (cf. de Rijk & Troelstra, 1999).

In the lower salt marsh (Zone B), especially in the salt-marsh pool (Subzone B1), the discrepancy between living and dead individuals is smaller, indicating either a poorer preservation of empty tests or better living conditions, mostly due to the higher frequency of water coverage at this elevation. Moreover, the permanently covered salt-marsh pool provides good living conditions with new, probably oxygen-rich water inundating during high tide and provided by rainfall combined with bioturbation (roots) and diffusion (cf. de Rijk & Troelstra, 1999; Berkeley et al., 2007). Furthermore, its surrounding is sheltered by the vegetation of the lower salt marsh enabling permanent water coverage, which results in the quite high number of living foraminifers and ostracods, especially *C. torosa* (e.g. Athersuch et al., 1989; Murray, 2006). Probably, a combination of better living conditions (higher numbers of living individuals) and poorer preservation led to the observations for this zone.

In the pioneer zone (Zone C), a clear dominance of living *C. williamsoni* is observed, whereas the dead fauna is more diverse. Since *C. williamsoni* prefers sediments with <60% mud/silt content (Murray, 2006), this pattern correlates well with the abruptly increased sand amount in this zone, also reflecting the higher dynamics in the transition area between salt marsh and tidal flat (Nyandwi & Flemming, 1995). Due to a higher energy level, dead individuals could, once again, be introduced by the tidal current. The situation is similar in the upper part of the sand flat (Zone D), where the transition sample again is strongly dominated by living *C. williamsoni*. However, since the rest of the sand flat shows only one living and a few dead individuals, dynamics seem to get too intense towards the lower parts of the sand flat for the survival of foraminifers or tests underlie *post-mortem* removal by currents (Hofker, 1977). Another reason for the very low occurrence of microfauna may be the very low (organic and inorganic) carbon content in the sand flat. Processes of early diagenesis (Berkeley et al., 2007) could influence the test preservation through changed saturation rates of calcium carbonate ($CaCO_3$) causing the dissolution of tests (Sanders, 2003).

A completely different situation is documented in the mixed flat (Zone E). Foraminifers show a similar pattern in both living and dead associations indicating a good fossilisation potential (cf. Smith, 1987). Ostracods show higher abundances of living individuals in the upper part and of dead ones in the lower part suggesting that they experience *post-mortem* transport towards the tidal channel (e.g. Edwards & Horton, 2000; Frenzel & Boomer, 2005). In the transition area to the tidal channel (Zone F), living individuals are very few compared to dead ones, which may be due to the current of the channel complicating the settlement of foraminifers as well as ostracods (e.g. Hofker, 1977; Murray, 2006). However, since dead shells are easier to be carried away by the current, this could again suggest a very good preservation of empty tests. Still, it needs to be taken into account that a certain part of the observed dead individuals is probably introduced by the tidal current. The few dead ostracods could have been transported from the adjacent mixed flat.

6.3. Evaluation of the transfer function (TF)

Adding the ostracod data to our training set improves sea-level estimations for the higher elevation stations only. The reason for this result is the higher abundance of ostracods in these samples from the tidal pond and surroundings. Thus, more detailed data would likely improve the performance of the TF. We would expect a similar outcome for the deeper stations as well but this needs samples with higher ostracod counts, a target for future studies.

Although the inclusion of ostracods clearly improves the TF performance and an RMSEP of 18.3% seems acceptable (Barlow et al., 2013), a vertical error of ~49 cm, leading to a total error range of the indicative meaning of ~1 m, is still comparably large (Edwards & Wright, 2015). Since other studies of similar environments focus only on the vegetated marsh (e.g. Edwards & Horton, 2000; Gehrels & Newman, 2004; Kemp et al., 2013; Müller-Navarra et al., 2017), the relatively high vertical error could be related to the high environmental gradient (2.69 m; approx. the mean tidal range of Spiekeroog). However, the tidal flat needs to be included in the TF, since the sediment cores dedicated to the future TF application cover large sections of tidal flat and salt marsh deposits. In general, it has to be noted that the exclusion of the sand-flat samples with <40 individuals leads to a lack of information about estimates within the elevation range of these samples (from 0.39 to -0.29 m NHN), which may lead to a deteriorated predictive ability for equivalent palaeo-elevations. We expect that a higher number of training samples will result in a better TF performance as most studies base their TF on a minimum of 40 samples, resulting in smaller error ranges (e.g. Kemp et al., 2012; Müller-Navarra et al., 2016, 2017; Milker et al., 2017). In a next step we will, therefore, increase the total number of samples in order to fill the elevation gap created by the weak sand flat samples.

6.4. Transfer function (TF) vs. peat-based reconstruction

The vertical error range (~1 m) of Model II of our TF is significantly smaller than the one of existing peat-based RSL reconstructions of up to 3–5 m (e.g. Long et al., 2006; Bungenstock & Schäfer, 2009; Bungenstock & Weerts, 2010, 2012; Baeteman et al., 2011). Reasons for the better performance of the TF include:

The TF provides a direct relation to the sea level, whereas peat has an indirect relation to the sea level. However, the indicative meaning of peat is still not universally defined (e.g. Baeteman, 1999; van de Plassche et al., 2005; Bungenstock & Schäfer, 2009; Wolters et al., 2010). Moreover, basal peat cannot always be used as sea-level index point. For example, for the early Holocene, Wolters et al. (2010) document a basal peat, which cannot be linked to sea level, as sea level was ~17 m lower, when peat growth started. They state that sea level-independent paludification in special topographic conditions is well known as described by e.g. Jelgersma, 1961; Lange & Menke, 1967; Baeteman, 1999. However, widespread intercalated peat layers are, in general, used as RSL index points, but close investigation of formation processes is essential (Bungenstock & Schäfer, 2009; Bungenstock & Weerts, 2010).

Post-depositional compaction results in high uncertainty for peat-based RSL reconstructions and significantly affects intercalated peats and the upper parts of basal peats. Horton & Shennan (2009) found average compaction rates of 0.4±0.3 mm/yr for peats buried in Holocene sequences along the east coast of England. The TF, however, can be applied to a wide range of intertidal facies and sequences comprising large amounts of compaction-prone peat can be avoided.

The microfossil-based TF also helps to avoid uncertainties imposed by relocated peat, which is ripped off at peat cliffs in so-called '*Dargen*' and transported over wide areas (e.g., Pliny the Elder (Naturalis Historia, XVI, 5-6) in Herrmann, 1988; Streif, 1990; Behre & Kučan, 1999; van Dijk et al., 2019) potentially resulting in age inversions in Holocene stratigraphies and invalid RSL indication.

Finally, the microfossil-based TF is a promising tool to derive RSL information from the uppermost part of the Holocene sequence in the wider region covering the last 2000 years, where peats are usually rare.

6.5. Method evaluation

As a few additional samples were taken during the summer, whereas the main transect was sampled during winter time, differences in the living microfauna between these samples could be well explained by seasonal differences. However, since only dead individuals were used for the TF development, in order to capture information over a longer time period (Murray, 2000), this is not expected to influence the outcome of our study.

Concerning the sampling thickness, most studies dealing with microfaunal surface distributions only use the uppermost 1 cm of the surface sediments (e.g. Kemp et al., 2012; Korsun et al., 2014; Shaw et al., 2016; Müller-Navarra et al., 2016, 2017). However, due to the high dynamics in the meso-tidal Wadden Sea and expected infaunal foraminifer taxa down to a depth of up to 5 cm (Hofker, 1977), we decided for deeper sampling. By investigating down to a depth of 3 cm, we account for most of the potential habitats of living individuals in order to better represent the modern conditions in our analysis. Given the dm-scale accuracy of the TF, the error imposed by the vertical integration of 3 cm is negligible for future RSL reconstructions. This sampling depth will, however, require undisturbed fossil inter- and supratidal layers with a minimum thickness of 3 cm for the future application of the TF.

Many of the studies applying Foraminifera to sea-level problems pick the individuals wet in order to prevent drying of organic components and potential damaging of agglutinated taxa (e.g. de Rijk, 1995; Edwards & Wright, 2015; Milker et al., 2016; Müller-Navarra et al., 2016, 2017), whereas in the present study most of the samples were picked dry. However, since we did not observe any significant effects of drying on species associations or preservation of agglutinated taxa, which is similar to observations of, e.g., Schönfeld et al. (2013), we assess our results to be comparable with those of previous studies.

7. Conclusion and outlook

The investigated surface transect in the back-barrier salt marsh and tidal flat of the island of Spiekeroog shows a clear vertical as well as lateral zonation of both foraminifers and ostracods. While environmental factors like the hydro-energetic level (reflected by grain-size distribution), the food availability (organic carbon) and the $CaCO_3$ saturation (inorganic carbon) influence this zonation, the major influence is given through the water depth or the duration of water cover (connected to the elevation). Hence, our surface transect shows a good potential for the establishment of a relative sea-level transfer function (RSL TF). The common TF model, using only dead foraminifer associations, was improved by ~5 cm (vertical error), resulting in an improvement of the error range of ~10 cm, by including dead ostracod associations. The improved TF provides an R^2_{Boot} of 0.84 and a vertical error of 49.1 cm accounting for 18.3% of the investigated elevation gradient of ~2.7 m, which is the approximate tidal range of Spiekeroog (BSH, 2018). Even though this vertical error is already lower than the one associated with previously used RSL index points such as basal or intercalated peats, a clear demand for higher resolutions and lower error ranges remains (e.g. Vink et al., 2007; Bungenstock & Schäfer, 2009; Bungenstock & Weerts, 2010, 2012; Baeteman et al., 2011). Thus, further improvements of our TF will be attempted in the near future by integrating additional modern local samples in order to expand the modern training set. Further improvements could probably be accomplished by narrowing the environmental gradient or by combining the dataset with existing data from North Frisia collected by Müller-Navarra et al. (2017) in order to develop a regional TF. In a final step, the RSL TF will be applied to Holocene sedimentary records already recovered by the WASA (Wadden Sea Archive) project (Bittmann, 2019).

8. Acknowledgements

The research reported here is part of the WASA project (*The Wadden Sea as an archive of landscape evolution, climate change and settlement history: exploration – analysis – predictive*

modelling) funded by the "Niedersächsisches Vorab" of the VolkswagenStiftung within the funding initiative "Küsten und Meeresforschung in Niedersachsen" of the Ministry for Science and Culture of Lower Saxony, Germany (project VW ZN3197). We gratefully acknowledge Dr. Yvonne Milker (University of Hamburg) for her help regarding statistical analyses and interpretations. The head of the WASA project, Dr. Felix Bittmann (Lower Saxony Institute for Historical Coastal Research), is acknowledged for proofreading and valuable comments on the manuscript. We also appreciate the very constructive and helpful comments by Dr. Simon Engelhart and one anonymous reviewer. Sampling and analyses of most of the samples were carried out during the funding period of the Start-up Honours Grant 2016A of the Graduate School of Geosciences, University of Cologne, awarded to J.S. This research is a contribution to IGCP Project 639 '*Sea Level Change from Minutes to Millennia*'.

9. References

Athersuch, J., Horne, D.J. & Whittaker, J.E., 1989. Marine and brackish water ostracods (superfamilies Cypridacea and Cytheracea): keys and notes for the identification of the species. Brill, Leiden, Synopses of the British fauna, 43, 343 p.

Baeteman, C., 1999. The Holocene depositional history if the Ijzer palaeo-valley (western Belgian coastal plain) with reference to the factors controlling the formation of intercalated peat beds. Geologica Belgica, 2, 39–72.

Baeteman, C., Waller, M. & Kiden, P., 2011. Reconstructing middle to late Holocene sea-level change: A methodological review with particular reference to 'A new Holocene sea-level curve for the southern North Sea' presented by K.-E. Behre. Boreas, 40, 557–572. https://doi.org/10.1111/j.1502-3885.2011.00207.x

Barlow, N.L.M., Shennan, I., Long, A.J., Gehrels, W.R., Saher, M.H., Woodroffe, S.A. & Hiller, C., 2013. Salt marshes as late Holocene tide gauges. Global and Planetary Change, 106, 90–110. https://doi.org/10.1016/j.gloplacha.2013.03.003

Beck, H.E., Zimmermann, N.E., McVicar, T.R., Vergopolan, N., Berg, A. & Wood, E.F., 2018. Present and future Köppen-Geiger climate classification maps at 1-km resolution. Scientific Data, 5, 180214. https://doi.org/10.1038/sdata.2018.214

Beets, D.J. & Van der Spek, A.J.F., 2000. The Holocene evolution of the barrier and the back-barrier basins of Belgium and The Netherlands as a function of late Weichselian morphology, relative sea-level rise and sediment supply. Netherlands Journal of Geosciences, 79(1), 3–16. https://doi.org/10.1017/S0016774600021533

Behre, K.-E., 1987. Meeresspiegelbewegungen und Siedlungsgeschichte in den Nordseemarschen. Holzberg-Verlag, Oldenburg, Vorträge der Oldenburgischen Landschaft, 17, 47 p.

Behre, K.-E., 2007. A new Holocene sea-level curve for the southern North Sea. Boreas, 36, 82–102. https://doi.org/10.1080/03009480600923386

Behre, K.-E. & Kučan, D., 1999. Neue Untersuchungen am Außendeichsmoor bei Sehestedt am Jadebusen. Probleme der Küstenforschung im südlichen Nordseegebiet, 26, 35–64.

Behre, K.-E. & Streif, H., 1980. Kriterien zu Meeresspiegel- und darauf bezogene Grundwasserabsenkungen. E&G Quaternary Science Journal, 30, 153–160. https://doi.org/10.3285/eg.30.1.12

Berkeley, A., Perry, C.T., Smithers, S.G., Horton, B.P. & Taylor, K.G., 2007. A review of the ecological and taphonomic controls on foraminiferal assemblage development in intertidal environments. Earth-Science Reviews, 83, 205–230. https://doi.org/10.1016/j.earscirev.2007.04.003

Birks, H.J.B., 1995. Quantitative palaeoenvironmental reconstructions. In Maddy, D. & Brew, J.S. (eds), Statistical Modelling of Quaternary Science Data. Quarternary Research Association, Cambridge, Technical Guide 5. 161–254.

Bittmann, F., 2019. Das Wattenmeer als Archiv zur Landschaftsentwicklung, Klimaänderung und Siedlungsgeschichte. Nachrichten des Marschenrats zur Förderung der Forschung im Küstengebiet der Nordsee, 56, 25–27.

Blott, S.J. & Pye, K., 2001. Gradistat: A grain size distribution and statistics package for the analysis of unconsolidated sediments. Earth Surface Processes and Landforms, 26, 1237–1248. https://doi.org/10.1002/esp.261

Bundesamt für Seeschifffahrt und Hydrographie (BSH), 2018. Gezeitenkalender 2018: Hoch- und Niedrigwasserzeiten für die Deutsche Bucht und deren Flussgebiete. Bundesamt für Seeschifffahrt und Hydrographie, Hamburg, 136 p.

Bungenstock, F. & Schäfer, A., 2009. The Holocene relative sea-level curve for the tidal basin of the barrier island Langeoog, German Bight, Southern North Sea. Global and Planetary Change, 33, 34–51. https://doi.org/10.1016/j.gloplacha.2008.07.007

Bungenstock, F. & Weerts, H.J.T., 2010. The high-resolution Holocene sea-level curve for Northwest Germany: global signals, local effects or data-artefacts? International Journal of Earth Sciences, 99, 1687–1706. https://doi.org/10.1007/s00531-009-0493-6

Bungenstock, F. & Weerts, H.J.T., 2012. Holocene relative sea-level curves for the German North Sea coast. International Journal of Earth Sciences, 101, 1083–1090. https://doi.org/10.1007/s00531-011-0698-3

Bungenstock, F., Wehrmann, A., Hertweck, G. & Schäfer, A., 2002. Modification of current systems and bedforms during the tidal cycle on tidal flats of the barrier island Baltrum, Southern North Sea. Zentralblatt für Geologie und Paläontologie, Teil I, 2001, 283–295.

Davis, J.C., 1986. Statistics and Data Analysis in Geology. John Wiley & Sons, New York, 656 p.

de Rijk, S., 1995. Salinity control on the distribution of salt marsh foraminifera (Great Marshes, Massachusetts). Journal of Foraminiferal Research, 25, 156–166. https://doi.org/10.2113/gsjfr.25.2.156

de Rijk, S. & Troelstra, S., 1999. The application of a foraminiferal actuo-facies model to salt-marsh cores. Palaeogeography, Palaeoclimatology, Palaeoecology, 149, 59–66. https://doi.org/10.1016/S0031-0182(98)00192-8

Edwards, R.J. & Horton, B.P., 2000. Reconstructing relative sea-level change using UK salt-marsh foraminifera. Marine Geology, 169, 41–56. https://doi.org/10.1016/S0025-3227(00)00078-5

Edwards, R. & Wright, A., 2015. Foraminifera. In Shennan, I., Long, A.J. & Horton, B.P. (eds), Handbook of Sea-Level Research. AGU/Wiley, Hoboken, 191–217. https://doi.org/10.1002/9781118452547.ch13

Engelhart, S.E. & Horton, B.P., 2012. Holocene sea level database for the Atlantic coast of the United States. Quaternary Science Reviews, 54, 12–25. https://doi.org/10.1016/j.quascirev.2011.09.013

Eshel, G., Levy, G.J., Mingelgrin, U. & Singer, M.J., 2004. Critical evaluation of the use of laser diffraction for particle-size distribution analysis. Soil Science Society of America Journal, 68, 736–743. https://doi.org/10.2136/sssaj2004.7360

Filipescu, S. & Kaminski, M.A., 2011. Re-discovering Entzia, an agglutinated foraminifer from the Transylvanian salt marshes. In Kaminski, M.A. & Filipescu, S. (eds), Proceedings of the Eighth International Workshop on Agglutinated Foraminifera. Grzybowski Foundation Special Publication, 16, 29–35.

Flemming, B.W., 2002. Effects of climate and human interventions on the evolution of the Wadden Sea depositional system (southern North Sea). In Wefer, G., Berger, W., Behre, K.-E. & Janssen, E. (eds), Climate Development and History of the North Atlantic Realm. Springer, Berlin, 399–413. https://doi.org/10.1007/978-3-662-04965-5_26

Flöser, G., Burchard, H. & Riethmüller, R., 2011. Observational evidence for estuarine circulation in the German Wadden Sea. Continental Shelf Research, 31, 1633–1639. https://doi.org/10.1016/j.csr.2011.03.014

Folk, R.L. & Ward ,W.C., 1957. Brazos River Bar: a study in the significance of grain size parameters. Journal of Sedimentary Research, 27, 3–26. https://doi.org/10.1306/74D70646-2B21-11D7-8648000102C1865D

Frenzel, P. & Boomer, I., 2005. The use of ostracods from marginal marine, brackish waters as bioindicators of modern and Quaternary environmental change. Palaeogeography, Palaeoclimatology, Palaeoecology, 225, 68–92. https://doi.org/10.1016/j.palaeo.2004.02.051

Frenzel, P., Keyser, D. & Viehberg, F.A., 2010. An illustrated key and (palaeo) ecological primer for Postglacial to Recent Ostracoda (Crustacea) of the Baltic Sea. Boreas, 39/3, 567–575. https://doi.org/10.1111/j.1502-3885.2009.00135.x

Freund, H. & Streif, H., 1999. Natürliche Pegelmarken für Meeresspiegelschwankungen der letzten 2000 Jahre im Bereich der Insel Juist. Petermanns Geographische Mitteilungen, 143, 34–45.

Freund, H. & Streif, H., 2000. Natural sea-level indicators recording the fluctuations of the mean high tide level in the southern North Sea. Wadden Sea Newsletter, 2, 16–18.

Gehrels, W. R. & Newman, S.W., 2004. Salt-marsh foraminifera in Ho Bugt, western Denmark, and their use as sea-level indicators. Geografisk Tidsskrift – Danish Journal of Geography, 104/1, 97–106. https://doi.org/10.1080/00167223.2004.10649507

Gehrels, W.R., Belknap, D.F., Black, S. & Newnham, R.M., 2002. Rapid sea-level rise in the Gulf of Maine, USA, since AD 1800. The Holocene, 12/4, 383–389. https://doi.org/10.1191/0959683602hl555ft

Gerlach, A., 1999. Pflanzengesellschaften auf Spülsäumen. In Henke, S., Roy, M. & Andrae, C. (eds), Umweltatlas Wattenmeer. Band 2, Wattenmeer zwischen Elb- und Emsmündung. Ulmer, Stuttgart, 58–59.

Hammer, Ø., Harper, D.A.T. & Ryan, P.D, 2001. PAST: Palaeontological statistics software package for education and data analysis. Palaeontologica Electronica, 4/1, article 4.

Harper, D.A.T. (ed.), 1999. Numerical Palaeobiology. John Wiley & Sons, Chichester, 468 p.

Herrmann, J. (ed.), 1988. Griechische und lateinische Quellen zur Frühgeschichte Mitteleuropas bis zur Mitte des 1. Jahrtausends u.Z. 1, von Homer bis Plutarch. Akademie Verlag, Berlin, 657 p.

Hofker, J., 1977. The foraminifera of Dutch tidal flats and salt marshes. Netherlands Journal of Sea Research, 11, 223–296. https://doi.org/10.1016/0077-7579(77)90009-6

Horton, B.P & Edwards, R.J, 2006. Quantifying Holocene Sea Level Chance Using Intertidal Foraminifera: Lessons from the British Isles. Cushman Foundation for Foraminiferal Research, Special Publication, 40, 97 p.

Horton, B.P. & Shennan, I., 2009. Compaction of Holocene strata and the implications for relative sea-level change on the east coast of England. Geology, 37, 1083–1086. https://doi.org/10.1130/G30042A.1

Jelgersma, S., 1961. Holocene sea level changes in the Netherlands. Mededelingen van de Geologische Stichting, C(7), 1–100.

Juggins, S., 2007. C2 Version 1.5: software for ecological and palaeoecological data analysis and visualisation. University of Newcastle, Newcastle upon Tyne.

Kaiser, R. & Niemeyer, H.D., 1999. Wasser-Beschaffenheit. In Henke, S., Roy, M. & Andrae, C. (eds), Umweltatlas Wattenmeer. Band 2, Wattenmeer zwischen Elb- und Emsmündung. Ulmer, Stuttgart, 32–33.

Kemp, A.C. & Telford, R.J., 2015. Transfer functions. In Shennan, I., Long, A.J. & Horton, B.P. (eds), Handbook of Sea-Level Research. AGU/Wiley, Hoboken, 191–217. https://doi.org/10.1002/9781118452547.ch31

Kemp, A.C., Horton, B.P., Vann, D.R., Engelhart, S.E., Grand, C.A., Vane, C.H., Nikitina, D. & Anisfeld, S.C., 2012. Quantitative vertical zonation of salt-marsh foraminifera for reconstructing former sea level; an example from New Jersey, USA. Quaternary Science Reviews, 54, 26–39. https://doi.org/10.1016/j.quascirev.2011.09.014

Kemp, A.C., Telford, R.J., Horton, B.P., Anisfeld, S.C. & Sommerfield, C.K., 2013. Reconstructing Holocene sea level using salt-marsh foraminifera and transfer functions: lessons from New Jersey, USA. Journal of Quaternary Science, 28/6, 617–629. https://doi.org/10.1002/jqs.2657

Korsun, S., Hald, M., Golikova, E., Yudina, A., Kuznetsov, I., Mikhailov, D. & Knyazeva, O., 2014. Intertidal foraminiferal fauna and the distribution of Elphidiidae at Chupa Inlet, western White Sea. Marine Biology Research, 10/2, 153–166. https://doi.org/10.1080/17451000.2013.814786

Kottek, M., Grieser, J., Beck, C., Rudolf, B. & Rubel, F., 2006. World map of the Köppen-Geiger climate classification updated. Meteorologische Zeitschrift, 15, 259–263. https://doi.org/10.1127/0941-2948/2006/0130

Lange, W. & Menke, B., 1967. Beiträge zur frühpostglazialen erd- und vegetationsgeschichtlichen Entwicklung im Eidergebiet, insbesondere zur Flußgeschichte und zur Genese des sogenannten Basistorfs. Meyniana, 17, 29–44. https://doi.org/10.2312/meyniana.1967.17.29

Last, W.M. & Smol, J.P. (eds), 2001. Tracking Environmental Change Using Lake Sediments. Volume 2, Physical and Geochemical Methods. Kluwer Academic Publishers, Dordrecht, 504 p. https://doi.org/10.1007/0-306-47670-3

Leorri, E., Gehrels, W.R., Horton, B.P., Fatela, F. & Cearreta, A., 2010. Distribution of foraminifera in salt marshes along the Atlantic coast of SW Europe: Tools to reconstruct past sea-level variations. Quaternary International, 221/1-2, 104–115. https://doi.org/10.1016/j.quaint.2009.10.033

Lepš, J. & Šmilauer, P. 2003. Multivariate Analysis of Ecological Data using CANOCO. Cambridge University Press, New York, 284 p.

Long, A.J., Waller, M..P, Stupples, P., 2006. Driving mechanisms of coastal change: peat compaction and the destruction of late Holocene coastal wetlands. Marine Geology 225, 63–84. https://doi.org/10.1016/j.margeo.2005.09.004

Meijles, E.W., Kiden, P., Steurman, H.-J., van der Plicht, J., Vos, P.S., Gehrels, W.R. & Kopp, R.E., 2018. Holocene relative mean sea-level changes in the Wadden Sea area, northern Netherlands. Journal of Quaternary Science, 33/8, 905–923. https://doi.org/10.1002/jqs.3068

Milker, Y., Nelson, A.R., Horton, B.P., Engelhart, S.E., Bradley, L.A. & Witter, R.C., 2016. Differences in coastal subsidence in southern Oregon (USA) during at least six prehistoric megathrust earthquakes. Quaternary Science Reviews, 142, 143–163. https://doi.org/10.1016/j.quascirev.2016.04.017

Milker, Y., Weinkauf, M.F.G., Titschack, J., Freiwald, A., Krüger, S., Jorissen, F.J. & Schmiedl, G., 2017. Testing the applicability of a benthic foraminiferal-based transfer function for the reconstruction of paleowater depth changes in Rhodes (Greece) during the early Pleistocene. PLoS ONE, 12/11, e0188447. https://doi.org/10.1371/journal.pone.0188447

Müller-Navarra, K., Milker, Y. & Schmiedl, G., 2016. Natural and anthropogenic influence on the distribution of salt marsh foraminifera in the Bay of Tümlau, German North Sea. Journal of Foraminiferal Research, 46/1, 61–74. https://doi.org/10.2113/gsjfr.46.1.61

Müller-Navarra, K., Milker, Y. & Schmiedl, G., 2017. Applicability of transfer functions for relative sea-level reconstructions in the southern North Sea coastal region based on salt-marsh foraminifera. Marine Micropaleontology, 135, 15–31. https://doi.org/10.1016/j.marmicro.2017.06.003

Murray, J.W., 2000. The enigma of the continued use of total assemblages in ecological studies of benthic Foraminifera. Journal of Foraminiferal Research, 30/3, 224–245. https://doi.org/10.2113/0300244

Murray, J.W., 2006. Ecology and Applications of Benthic Foraminifera. Cambridge University Press, Cambridge, 440 p.

Nicholls, R.J. & Cazenave, A., 2010. Sea-level rise and its impact on coastal zones. Science, 328, 1517–1520. https://doi.org/10.1126/science.1185782

Nyandwi, N. & Flemming, B.W., 1995. A hydraulic model for the shore-normal energy gradient in the East Frisian Wadden Sea (southern North Sea). Senckenbergiana maritima, 25, 163–172.

Overpeck, J.T., Otto-Bliesner, B.L., Miller, G.H., Muhs, D.R., Alley, R.B. & Kiehl, J.T., 2006. Paleoclimatic evidence for future ice-sheet instability and rapid sea-level rise. Science, 311, 1747–1750. https://doi.org/10.1126/science.1115159

Pedersen, J.B.T., Svinth, S. & Bartholdy, J., 2009. Holocene evolution of a drowned melt-water valley in the Danish Wadden Sea. Quaternary Research, 72/1, 68–79. https://doi.org/10.1016/j.yqres.2009.02.006

Rahmstorf, S., 2017. Rising hazard of storm-surge flooding. Proceedings of the National Academy of Sciences of the United States of America, 114, 11806–11808. https://doi.org/10.1073/pnas.1715895114

Reuter, R., Badewien, T.H., Bartholomä, A., Braun, A., Lübben, A. & Rullkötter, J., 2009. A hydographic time series station in the Wadden Sea (southern North Sea). Ocean Dynamics, 59, 195–211. https://doi.org/10.1007/s10236-009-0196-3

Sanders, D., 2003. Syndepositional dissolution of calcium carbonate in neritic carbonate environments: geological recognition, processes, potential significance. Journal of African Earth Sciences, 36/3, 99–134. https://doi.org/10.1016/S0899-5362(03)00027-7

Scheder, J., Engel, M., Bungenstock, F., Pint, A., Siegmüller, A., Schwank, S. & Brückner, H., 2018. Fossil bog soils (dwog horizons) and their relation to Holocene coastal changes in the Jade-Weser Region. Journal of Coastal Conservation, 22, 51–69. https://doi.org/10.1007/s11852-017-0502-z

Schönfeld, J., Golikova, E., Korsun, S. & Spezzaferri, S., 2013. The Helgoland Experiment – assessing the influence of methodologies on Recent benthic foraminiferal assemblage composition. Journal of Micropalaeontology, 32, 161–182. https://doi.org/10.1144/jmpaleo2012-022

Scott, D.B. & Hermelin, J.O.R., 1993. A device for precision splitting of micropaleontological samples in liquid suspension. Journal of Paleontology, 67/1, 151–154. https://doi.org/10.1017/S0022336000021302

Scott, D.B., Medioli, F.S. & Schafer, C.T., 2001. Monitoring in Coastal Environments Using Foraminifera and Thecamoebian Indicators. Cambridge University Press, Cambridge, 192 p.

Shaw, T.A., Kirby, J.R., Holgate, S., Tutman, P. & Plater A.J., 2016. Contemporary salt-marsh foraminiferal distribution from the Adriatic coast of Croatia and its potential for sea-level studies. Journal of Foraminiferal Research, 46/3, 314–332. https://doi.org/10.2113/gsjfr.46.3.314

Smith, R.K., 1987. Fossilization potential on modern shallow-water benthic foraminiferal assemblages. Journal of Foraminiferal Research, 17/2, 117–122. https://doi.org/10.2113/gsjfr.17.2.117

Streif, H., 1990. Das ostfriesische Küstengebiet: Nordsee, Inseln, Watten und Marschen. Gebr. Borntraeger, Berlin, Sammlung Geologischer Führer, 57, 376 p.

van de Plassche, O., Bohncke, S.J.P., Makaske, B. & van der Plicht, J., 2005. Water-level changes in the Flevo area, central Netherlands (5300-1500 BC): implications for relative mean sea-level rise in the Western Netherlands. Quaternary International, 133-134, 77–93. https://doi.org/10.1016/j.quaint.2004.10.009

van Dijk, G., Fritz, C., Straathof, N., van de Riet, B., Hogeweg, N., Harpenslager, S.F., Roelofs, J.G.M., Behre, K.-E. & Lamerset, L.P.M., 2019. Biogeochemical characteristics of the last floating coastal bog remnant in Europe, the Sehestedt Bog. Wetlands, 39, 227–238. https://doi.org/10.1007/s13157-018-1089-3

Vink, A., Steffen, H., Reinhardt, L. & Kaufmann, G., 2007. Holocene relative sea-level change, isostatic subsidence and the radial viscosity of the mantle of northwest Europe (Belgium, the Netherlands, Germany, southern North Sea). Quaternary Science Reviews, 26, 3249–3275. https://doi.org/10.1016/j.quascirev.2007.07.014

Walton, W.R., 1952. Techniques for recognition of living Foraminifera. Contribution Cushman Foundation of Foraminiferal Research, 3, 56–60.

Weisse, R., von Storch, H., Niemeyer, H.D. & Knaack, H., 2012. Changing North Sea storm surge climate: An increasing hazard? Ocean and Coastal Management, 68, 58–68. https://doi.org/10.1016/j.ocecoaman.2011.09.005

Wolters, S., Zeiler, M. & Bungenstock, F., 2010. Early Holocene environmental history of sunken landscapes: pollen, plant macrofossil and geochemical analyses from the Borkum Riffgrund, southern North Sea. International Journal of Earth Sciences, 99, 1707–1719. https://doi.org/10.1007/s00531-009-0477-6

Woodroffe, C.D. & Murray-Wallace, C.V., 2012. Sea-level rise and coastal change: the past as a guide to the future. Quaternary Science Reviews, 54, 4–11. https://doi.org/10.1016/j.quascirev.2012.05.009

Manuscript received 21.12.2018, accepted in revised form 28.06.2019, available online 03.09.2019.

Chapter 6

6 Unravelling Holocene relative sea-level change in the southern North Sea using an improved microfauna-based transfer function

Juliane Scheder[1,2], Friederike Bungenstock[2], Kristin Haynert[3], Anna Pint[1], Frank Schlütz[2], Peter Frenzel[4], Achim Wehrmann[3], Helmut Brückner[1] & Max Engel[1,5,6]

[1] *Institute of Geography, University of Cologne, Albertus-Magnus-Platz, 50923 Köln, Germany.*
[2] *Lower Saxony Institute for Historical Coastal Research, Viktoriastraße 26/28, 26382 Wilhelmshaven, Germany*
[3] *Marine Research Departments, Senckenberg am Meer, Südstrand 40, 26382 Wilhelmshaven, Germany*
[4] *Institute of Geosciences, Friedrich Schiller University Jena, Burgweg 11, 07749 Jena, Germany*
[5] *Geological Survey of Belgium, Royal Belgian Institute of Natural Sciences, Jennerstraat 13, 1000 Brussels, Belgium*
[6] *Institute of Geography, Heidelberg University, Im Neuenheimer Feld 348, 69120 Heidelberg, Germany*

Abstract

Considering climate change and associated rising sea levels, detailed reconstructions of relative sea-level (RSL) histories and information on controlling processes are essential, in order to manage coastal-protection challenges. This study contributes to unravelling Holocene RSL change on the East Frisian North Sea coast in high resolution and with smaller error ranges than previously published investigations. For the first time, an improved transfer function (vertical error: 29.7 cm ≙ ~11% of the mean tidal range) for RSL change based on a combined training set of benthic foraminifers and ostracods from the tidal basin of Spiekeroog is applied. The resulting RSL curve for the Norderney tidal basin shows a deceleration in RSL rise between 6000 and 5000 cal BP and the smallest error range (~1 m), resulting from the good suitability of salt-marsh layers, between 5000 and 4000 cal BP. Even though compaction cannot be excluded and is hard to quantify for the present record, the RSL curve provides smaller error bands than most peat-based curves for the southern North Sea and allows conclusions on possible palaeo-tidal changes as well as verification of regional differences in glacial isostatic subsidence.

Keywords

coastal change, multi-proxy approach, Northern Germany, Foraminifera, Ostracoda

The results of this chapter were recently submitted to *Journal of Quaternary Science* (manuscript number: JQS-20-0040).

6.1 Introduction

Detailed field-based reconstructions of the relative sea level (RSL) are crucial for the understanding of coastal change, for improving glacial isostatic adjustment (GIA) models and for the implementation of future predictions of RSL rise, which are necessary for coastal zone and hazard management (Weisse et al., 2012; Woodroffe and Murray-Wallace, 2012; Rahmstorf, 2017). Due to local effects (peat compaction, tidal range, GIA), RSL curves only have local to regional validity (Kiden et al., 2002; Bungenstock and Schäfer, 2009; Bungenstock and Weerts, 2012; Meijles et al., 2018). Since existing RSL reconstructions from the North Sea region based on basal and intercalated peats (e.g. Behre, 2007; Bungenstock and Schäfer, 2009) show rather high vertical error ranges of several metres, the necessity of more precise data has been widely expressed (Vink et al., 2007; Bungenstock and Schäfer, 2009; Bungenstock and Weerts, 2010, 2012; Baeteman et al., 2011; Meijles et al., 2018). Therefore, in a first step, a preliminary transfer function (TF) for RSL change, based on foraminifers and ostracods, providing a vertical error range of ±49.1 cm (18.2% of the mean tidal range), was developed for the East Frisian islands (Scheder et al., 2019). Such a TF models the modern relation between relative species abundances and sample elevations and allows implications on palaeo-water depths with a decimetre-scale precision for mesotidal environments (~10–15% of the tidal range) (Leorri et al., 2010; Kemp et al., 2012; Barlow et al., 2013; Edwards and Wright, 2015).

This study presents new foraminifer and ostracod data from a surface transect on the southern coast of the East Frisian island of Spiekeroog, which are combined with the existing TF data (Scheder et al., 2019), in order to improve the TF performance and reduce the vertical error. The resulting final TF is applied to seven sediment cores located in the back-barrier area of Norderney, which were analysed for microfaunal, sedimentological and geochemical characteristics (Bittmann, 2019; Bulian et al., 2019). Research hypotheses are:

- The performance of the existing TF can be improved by including additional modern sample data, leading to a smaller vertical error.
- The Holocene sediment cores from Norderney show the same microfaunal species composition as the modern samples from Spiekeroog.
- The first ever application of a microfossil-based TF to Holocene sediment cores of the East Frisian North Sea coast leads to a RSL curve with higher resolution and lower error ranges than the existing peat-based RSL curves.
- Microfossil-based transfer functions help to better quantify regional differences in GIA and other factors influencing RSL in the southern North Sea region.

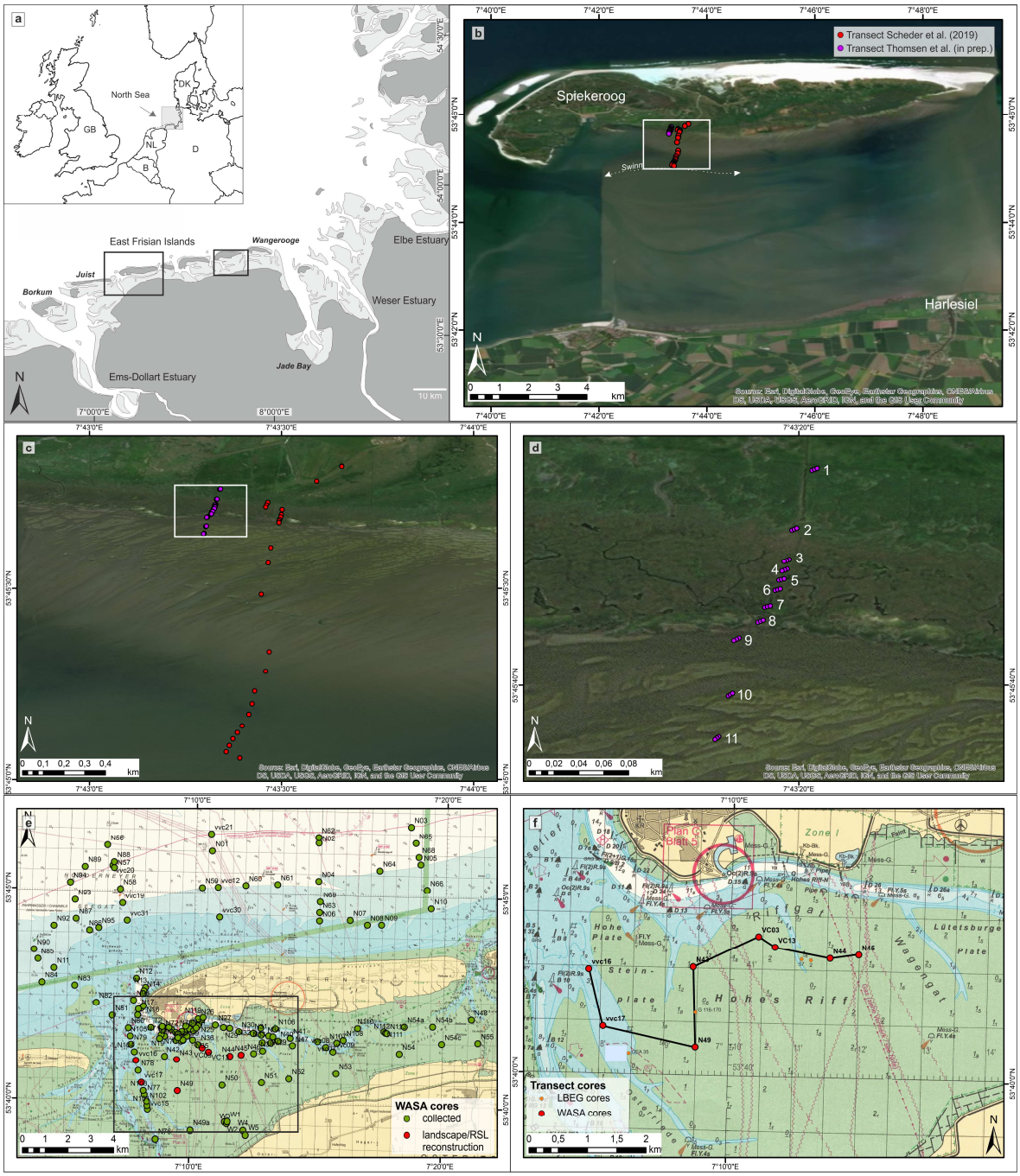

Fig. 6.1 Study area. a: Overview map of the North Sea with Spiekeroog and Norderney framed; b: overview of Spiekeroog with the transect investigated by Scheder et al. (2019) and the additional transect of modern microfauna; c: detail image showing the location of both transects in the salt marsh and tidal flat; d: detail of the additional transect; e: overview of Norderney with all WASA cores (cores for TF application are marked in red); f: detail of the cores used for TF application and RSL reconstruction. WASA = *The Wadden Sea as an archive of landscape evolution, climate change and settlement history*. Map sources: b-d: Esri, Digital Globe, GeoEye, Earthstar Geographics, CNES/Airbus DS, USDA, USGS, Aerogrid, IGN, and the GIS User Community; e-f: Bundesamt für Seeschifffahrt und Hydrographie, 2016.

The East Frisian barrier islands are situated in the southern North Sea, off the coast of NW Germany; they have formed since the deceleration of the post-glacial sea-level rise around 6–7 ka BP (kiloyears before present, i.e. before AD 1950) (Freund and Streif, 2000; Flemming, 2002; Bungenstock and Schäfer, 2009). Their south-eastward shift of several kilometres since then is driven by the prevailing longshore current and ongoing RSL rise

(Streif, 1990; Flemming, 2002). The two study areas (Fig. 6.1a) investigated here are the tidal basins of Spiekeroog (Fig. 6.1b–d) and Norderney (Fig. 6.1e–f). Spiekeroog is limited by the two tidal inlets Otzumer Balje and Harle, channeling water of semi-diurnal tides (mean tidal range = 2.7 m; BSH, 2018). Norderney is situated between the two tidal inlets Norderneyer Seegat and Wichter Ee with a mean tidal range of 2.5 m (BSH, 2018). Both islands are characterised by intertidal back-barrier tidal flats, which transform into supratidal salt marshes onshore. A humid temperate climate (Cfb after Köppen-Geiger classification) prevails in the complete area (Kottek et al., 2006; Beck et al., 2018).

The investigated transect of surface sediment samples (c. 230 m in N-S direction, c. 180 m west of the transect by Scheder et al., 2019) covers the natural salt marsh and c. 100 m of the adjacent tidal flat (Fig. 6.1b–d). The natural salt marsh in the back-barrier of Spiekeroog consists of the upper salt marsh and the lower salt marsh, based on different shore height, inundation frequency and hydro-morphological parameters (van Wijnen and Bakker, 2001). The lower salt marsh is dominated by *Elytrigia atherica*, *Puccinellia maritima* and *Atriplex portulacoides*. Halophytic plants such as *Salicornia* spp. and *Spartina anglica* predominantly colonise the pioneer zone (Bakker, 2014). In contrast to the salt marsh, the adjacent tidal flat is characterised by marine resources such as marine detritus, micro- and macrophyto-benthos (Flemming et al., 1994; Flemming and Ziegler, 1995).

The investigated sediment cores are located along a transect (c. 7000 m in an overall E-W direction) in the back-barrier tidal flat of Norderney, starting in the west at the inner margin of the tidal inlet ‘Norderneyer Seegatt’, reaching across the sand flat ‘Hohes Riff’ and crossing a smaller tidal channel.

6.2 Methods

6.2.1 Field work

Modern samples

The additional samples were collected along the 11 transect stations from the surface sediment (0–1 cm) using a soil corer (Ø 10 cm). On each transect station, three replicates were taken resulting in 33 samples. The sediment samples were transferred into Kautex™ wide-neck containers, preserved with Rose Bengal ethanol (94%) solution (2 g/l) to stain the protoplasm in all living foraminifers and to differentiate between living specimens and dead/empty tests according to Walton (1952), Lutze and Altenbach (1991) and Edwards and Wright (2015). The samples were stored for three weeks until further processing in the laboratory. For biochemical analysis, data for oxygen and TOC (total organic carbon) were measured at each transect station. Replicates (3n) of oxygen were determined with a Fibox

4 oxygen meter (PreSens – Precision Sensing GmbH) in the surface sediment from 0–1 cm. Additional samples for TOC analysis were taken from the surface sediment (<2 cm) and frozen at –20 °C until measurement. Elevation of the 11 transect stations was determined using a differential GPS (DGNSS Stonex S9) with real-time correction service. The applied sampling method only slightly differs from that of the existing dataset (Scheder et al., 2019), in particular concerning the sample thickness (3 cm for existing dataset, 1 cm for additional samples). However, due to negligible variability of species associations within the upper 3 cm (Scheder et al., 2019), the results are expected to be comparable.

Core drillings

On the tidal flats, cores were retrieved using a vibrocorer (Wacker Neuson IE high-frequency vibrator head and generator) and aluminium tubes (8 cm diameter, 6 m length), whereas tidal-channel cores were drilled from the research vessel *MS BURCHANA* using a vibrocorer VKG-6 (VC-6000, med consultans GmbH) and plastic liners (10 cm diameter, 5 m length). Opening and macroscopic core description after Preuß et al. (1991) was conducted either at the Lower Saxony Institute for Historical Coastal Research (Wilhelmshaven, Germany) or the Institute of Geography of the University of Bremen (Germany). Sampling mainly followed 10- or 20-cm intervals with additional samples in smaller-scale layers of interest.

Additional information for correlation was taken from archive core data provided by the 'Landesamt für Bergbau, Energie und Geologie' (LBEG, Hannover, Germany).

6.2.2 Laboratory analyses

Modern samples

Samples were washed with tap water and first passed through a 2000-µm screen, in order to remove macrophyto- and macrozoobenthos. Subsequently, the samples were washed through a 63-µm sieve and dried at 60 °C for at least 24 h. The 63-µm fraction was split by using a microsplitter and analysed for living and dead individuals. Living individuals (= with Rose Bengal stained protoplasm and preserved soft parts in ostracods) and dead/empty tests (= without stained protoplasm and empty ostracod valves) were picked, sorted by species and counted under a stereo microscope (Leica MZ12). Tests were mounted in Plummer cell slides with glue (Rahman, 2018) and ostracod valves were stored in Fema cells. Determination of foraminifer species followed the descriptions in Frenzel et al. (2005), Müller-Navarra et al. (2016) and the foraminifera.eu database (Hesemann, 2015), whereas ostracod taxa were determined based on Athersuch et al. (1989) and Frenzel et al. (2010).

TOC samples were measured using the CHNS elemental analyser “vario EL cube” (ELEMENTAR Analysensysteme GmbH Heraeus, Langenselbold, Germany). Prior to analysis, carbonates were removed by treatment with HCl (10%). The precision of the measurement was <0.2% (for detailed description see Lange et al., 2018).

Core drillings

Microfaunal, sedimentological and geochemical investigations were performed for 139 samples from seven cores (for details see 6.S1.1 [suppl.]) for facies interpretation (see also Elschner et al., 2021). VVC17 was analysed as described in Bulian et al. (2019).

The chronological framework is based on AMS-^{14}C dating on peats (Bulian et al., 2019), *in-situ* bivalves and foraminifer tests. ^{14}C dating were performed by the Poznan Radiocarbon Laboratory (Poland) and Beta Analytic Inc. (USA). Calibration and age-depth modelling was accomplished using R software (rbacon, v. 2.3.9.1, Blaauw and Christen, 2019), calibration curves IntCal13 and Marine13 (Reimer et al., 2013) and reservoir correction after Enters et al. (2021) (Tab. 6.1).

6.2.3 Data processing

In order to analyse the influence of oxygen and TOC on the density of intertidal foraminifers, a redundancy analyses (RDA) was performed using the software CANOCO 5 (Microcomputer Power, Ithaca, USA, 2012). Microfaunal data of the preliminary TF (Scheder et al., 2019) were combined with the additional foraminifer and ostracod data (dead assemblages). All measured elevations were transformed to the most recent vertical datum (DHHN2016; ‘*Deutsches Haupthöhennetz*’), also leading to slight elevation adjustments of the existing transect. Pearson and Spearman’s correlation coefficients were calculated showing no auto-correlations between taxa. In order to verify elevation, connected to the inundation frequency, as the main driving factor of species composition and that the unimodal response along the main environmental gradient does not change after adding the new samples, principle component analysis (PCA) and detrended correspondence analysis (DCA) were performed. Correlation and multivariate statistics were accomplished using the software PAST (v.3.2.1) (Hammer et al., 2001). The gradient length indicated by the DCA (3.86 standard deviation [SD]) suggests a more unimodal species-environment relation (Birks, 1995; Lepš and Šmilauer, 2003). Therefore, the final TF was modelled using the weighted averaging-partial least squares (WA-PLS) method with a maximum of three components, in order to avoid overfitting (Kemp and Telford, 2015) using the software C2 (v. 1.7.7) (Juggins, 2007). The TF performance was evaluated by bootstrapping cross-validation (1000 cycles) based on the coefficient of determination (R^2_{boot}), estimating the quality of the linear relationship between observed and estimated elevations, and the root mean

square error of prediction (RMSEP), facilitating the assessment of the general predictive capability of the TF (Milker et al., 2017). The appropriate component was chosen based on the lowest RMSEP and highest R^2_{boot}.

Core data were processed and evaluated similar to the modern dataset (Scheder et al., 2019) (for more detail, see 6.S1.2 [suppl.]). Where possible, facies identified from the cores were correlated in a cross section, in order to get an understanding of their spatial extent. Only supra- and intertidal layers, identified based on the core investigations, were used for the application of the TF.

6.3 Results of the modern samples

Back-barrier foraminifers from Spiekeroog followed a typical horizontal zonation (Tab. 6.S2.1, [suppl.]). Accordingly, agglutinated species (*Deuterammina balkwilli* [Brönnimann & Whittaker, 1983], *Jadammina macrescens* [as synonym for *Entzia macrescens* (Brady, 1870)], *Miliammina fusca* [Brady, 1870], *Trochammina inflata* [Montagu, 1808]) and miliolid calcareous species (*Cornuspira involvens* [Reuss, 1850] and *Triloculina oblonga* [Montagu, 1803]) tend to have a higher abundance in vegetated supra- and intertidal environments with higher elevation (salt marsh). In comparison, hyaline calcareous species (*Ammonia tepida* [Cushman, 1926], *Haynesina germanica* [Ehrenberg, 1840], *Elphidium* spp. [Montfor, 1808]) occur with higher abundances in lower intertidal and subtidal elevations (tidal flat). Ostracods follow the same zonation but exhibit a transition zone between the vegetated salt marsh and the lower elevations of the tidal flat. The vegetated salt marsh and most of the pioneer zone are almost exclusively characterised by high abundances of *Leptocythere* (Sars, 1925), especially *L. lacertosa* (Hirschmann, 1912). The transition zone between pioneer zone and tidal flat shows the highest abundances (mainly *Leptocythere* and *Cytherois fischeri* [Sars, 1866]) and the tidal flat shows additional *Semicytherura striata* (Sars, 1866).

Environmental parameters such as oxygen concentration and TOC play a major role for the distribution of foraminifers. Along the transect, the mean oxygen concentration increases from 178.3±27.79 µmol/l in the upper salt marsh to 229.9±58.07 µmol/l in the lower salt marsh and 224.1±54.84 µmol/l in the tidal flat, whereas the TOC-content decreases from 6.1±0.95% to 3.2±1.92% and 0.3±0.10%, respectively (Tab. 6.S2.2 and Tab. 6.S2.3 [suppl.]). Accordingly, the abundance of agglutinated and miliolid species correlates with higher TOC in vegetated intertidal environments and is less impacted by oxygen (Fig. 6.2).

In contrast to that, the abundance of hyaline species correlates with oxygen in subtidal elevations and is less impacted by TOC (Fig. 6.2).

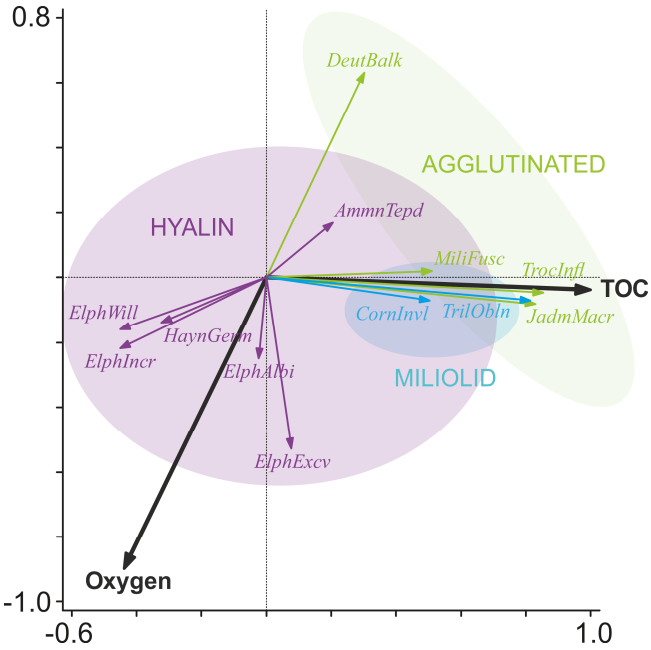

Fig. 6.2 Redundancy analysis (RDA) of supra- to intertidal foraminifers in relation to oxygen and TOC. Eigenvalues of axis 1 = 0.3746 and axis 2 = 0.0427. Full species names of agglutinated species: *DeutBalk* = *Deuterammina balkwilli*, *JadmMacr* = *Jadammina macrescens* (= *Entzia macrescens*), *MiliFusc* = *Miliammina fusca*, *TrocInfl* = *Trochammina inflata;* miliolid species: *CornInvl* = *Cornuspira involvens*, *TrilObln* = *Triloculina oblonga;* hyaline species: *AmmnTepd* = *Ammonia tepida*, *HaynGerm* = *Haynesina germanica*, *ElphAlbi*, *ElphExc*, *ElphIncr*, *ElphWill* = *Elphidium* spp. (*Elphidium albiumbilicatum*, *Elphidium excavatum*, *Elphidium incertum*, *Elphidium williamsoni* [as synonym for *Cribroelphidium williamsoni*]).

6.4 Results and interpretation of the statistical analyses

6.4.1 The combined modern training set

After comparing the new samples with the previous samples of the preliminary TF (Scheder et al., 2019), the rare foraminifer previously determined as *Spirillina* sp. could be re-identified as *Cornuspira involvens* (Reuss, 1850) based on the determinations of the additional modern samples. Identification of the other taxa remains unchanged. In the combined dataset, both Pearson and Spearman's correlation show no (auto-) correlations between foraminifer and ostracod taxa. Thus, all taxa were included in the following PCA. This was performed in order to find variables accounting for as much of the variance in the combined dataset as possible (Davis, 1986; Harper, 1999) using samples with a minimum of 40 individuals. The PCA (Fig. 6.3) reveals two components with variances >10 %.

The most significant axis is PC 1 (31.99%), opposing salt-marsh foraminifers and associated samples (positive values) and shallow-water species and associated tidal flat samples (negative values) suggesting a salt-marsh vs. tidal-flat component. This could be related to salinity, organic content and hydro-energetic levels, which are all connected through the

duration of water cover or inundation frequency (Scheder et al., 2019). PC 1 is therefore interpreted to represent the elevation, meaning that the combined dataset can be used for the development of the final TF.

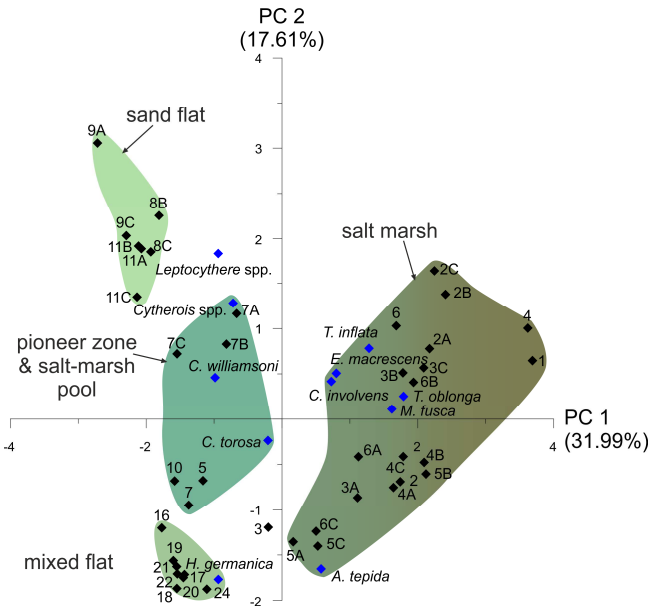

Fig. 6.3 PCA biplot showing the two most relevant axes. Black diamonds represent samples, blue diamonds represent foraminifer and ostracod taxa. Colour shades correspond to facies colours used also for core drawings (suppl. Figs. 6.S2.2–6.S2.8) and for the stratigraphic cross section (Fig. 6.5).

PC 2 (17.61%) opposes euryhaline species with tolerances of dysoxic conditions (e.g. *Ammonia tepida*) (negative values) and species less tolerant of dysoxic conditions (e.g. *Trochammina inflata*) (positive values) (Murray, 2006). Dysoxic conditions may relate to finer-grained substrates, whereas oxic conditions are associated with sand-dominated substrates. PC 2 may therefore relate to the oxygen availability or the substrate.

6.4.2 Final transfer function (TF)

In order to cover information over longer time periods and avoid seasonal influences, only the dead assemblages were used for the development of the TF, since those average the result of habitat preferences and related taphonomic changes over several seasons and years (Murray, 2000).

As performed for the preliminary TF (Scheder et al., 2019), two models were developed (Fig. 6.4): Model I exclusively considers foraminifers (commonly applied approach) and Model II additionally considers the ostracods. For both, the third of the three modelled components is the most suitable (lowest RMSEP and highest R^2). During initial modelling, sample 1A (highest elevation) proved to be an outlier and was therefore excluded from the dataset, resulting in an elevation gradient of ~2.71 m in vertical distance (+1.506 to -1.206 m NHN [m above *Normalhöhennull* = standard elevation zero referring to gauge Amsterdam]).

This is comparable to the mean tidal range of Spiekeroog (2.70 m). Since samples were taken during different tidal situations (spring and neap tide), the RMSEP is related to the mean tidal range.

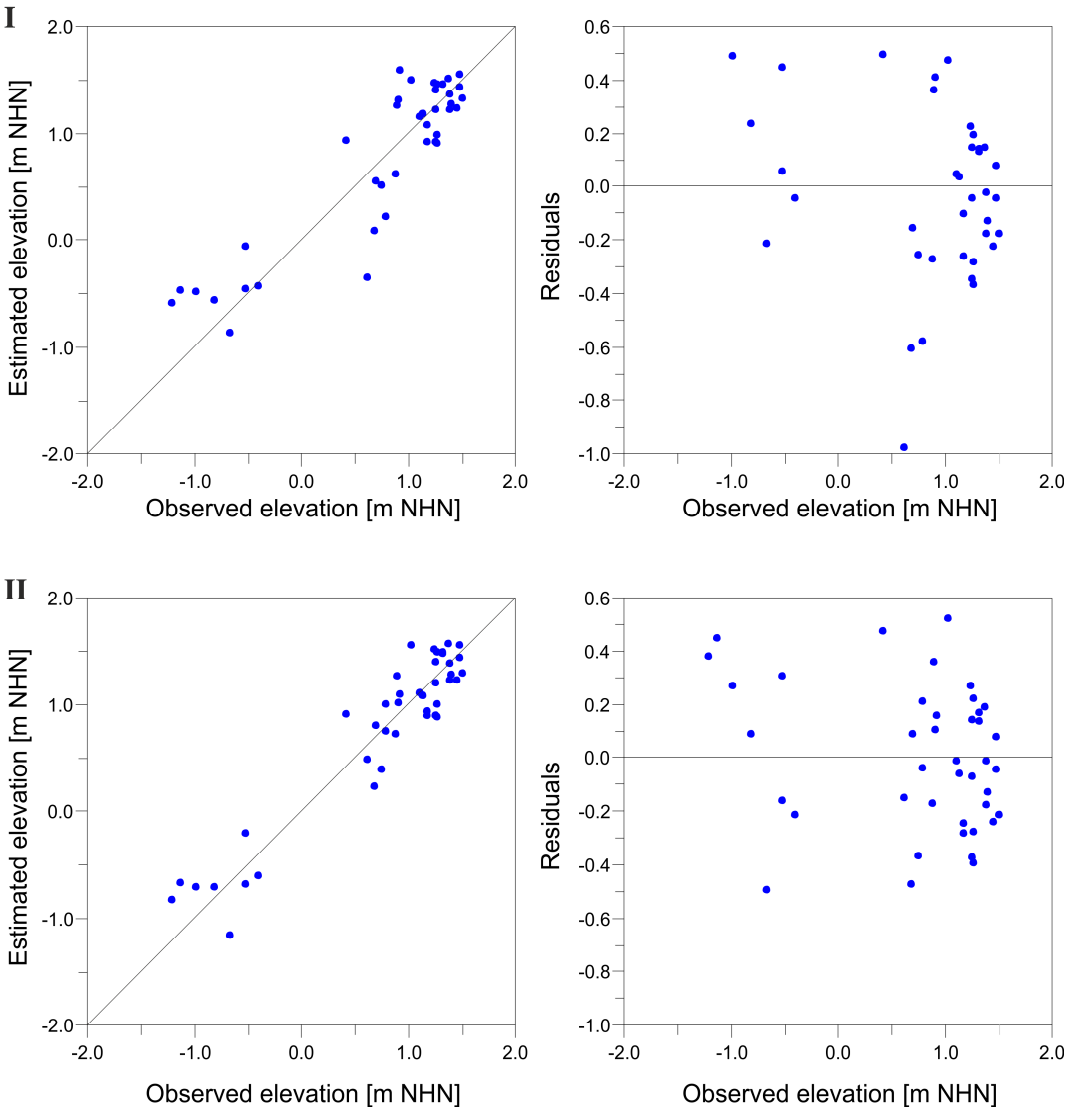

Fig. 6.4 Testing of the transfer function (TF) by bootstrapping cross-validation (1000 cycles). Diagrams show estimated vs. observed elevation (left) and deviation of samples from the observed elevation (right) for both Model I (dead foraminifers) and Model II (combined associations of dead foraminifers and ostracods).

Model I shows an R^2_{boot} of 0.81 and an RMSEP of 37.8 cm, which accounts for 13.92% of the elevation gradient (13.98% of the mean tidal range). No clear trend in the TF over- or underestimating samples related to their observed elevation is visible and no structures of residuals can be documented (Fig. 6.4). However, underestimation seems to be higher than overestimation.

Model II delivers an R^2_{boot} of 0.89 and an RMSEP of only 29.7 cm, accounting for 10.98% of the elevation gradient (11.02% of the mean tidal range). The residuals show reduced underestimation compared to Model I, indicating an improved precision (Fig. 6.4).

6.5 Results and interpretation of the Holocene sediment cores

The facies of the investigated sediment cores are depicted along a W-E transect, which also includes information of four archive cores (Fig. 6.5). For detailed sedimentological, geochemical and microfaunal results of the investigated cores, see Figs. 6.S2.2–6.S2.8 (suppl.; for VVC17 see Bulian et al., 2019). Detailed information on ^{14}C dating is given in Tab. 6.1.

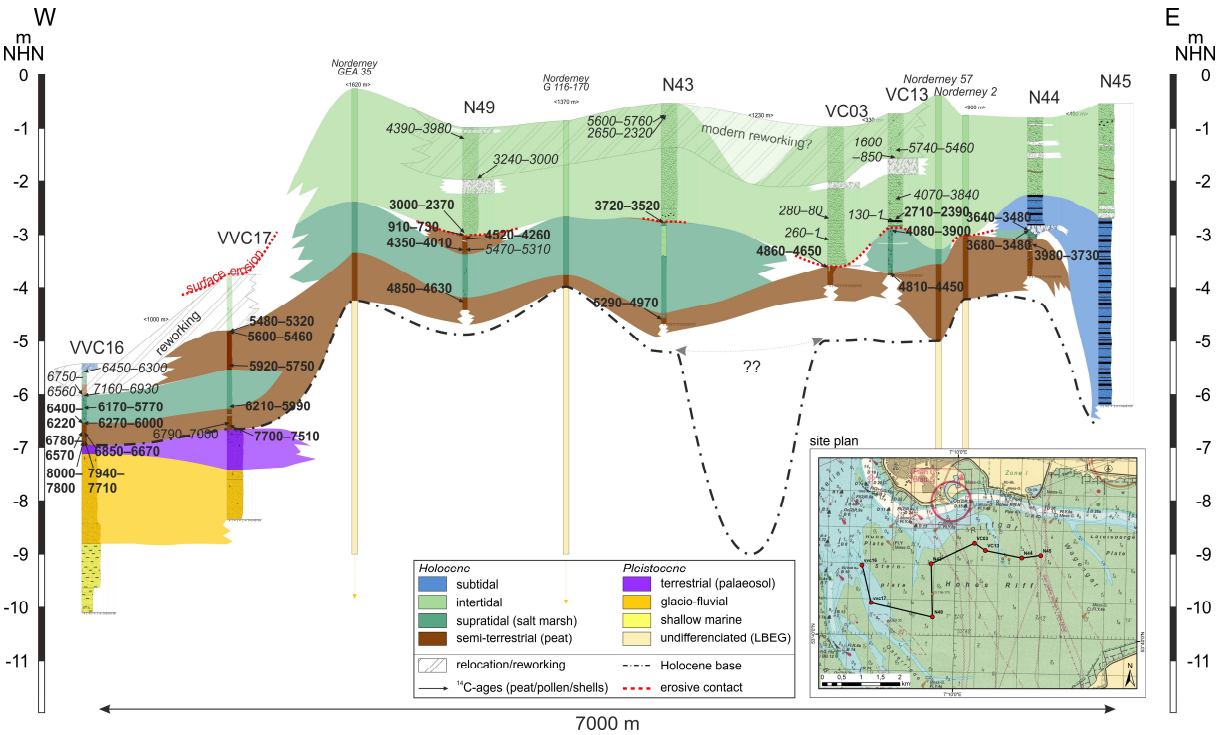

Fig. 6.5 Stratigraphic cross section of the cores investigated by Elschner et al. (2021), additional WASA and archive core data including radiocarbon data from peats, bivalve shells and foraminifer tests. Ages written in italics were excluded due to reworking, whereas ages written in bold were deemed reliable.

The investigated sedimentary record in the study area starts with Eemian marine highstand sediments documented in the most western core (VVC16). During the following Weichselian glaciation, the area was subject to periglacial conditions and the accumulation of aeolian and glacio-fluvial sands (Streif, 2004), showing initial pedogenesis (palaeosol in Fig. 6.5). The upper boundary of these deposits marks the Holocene base, which in the eastern part was modelled based on information from archive core data.

Around 7–8 ka BP, a basal peat started to develop first in the west (VVC16 and 17), driven by rising groundwater levels and the tidal-channel situation during the post-glacial transgression (Bungenstock and Schäfer, 2009). In the east (N43, VC03, VC13, N44–45), the basal peat formed later due to the higher topography. The area slowly started to become protected by early-barrier island formation, which was initiated during the deceleration of the sea-level rise around 6–7 ka BP (Freund and Streif, 2000; Flemming, 2002; Bungenstock and Schäfer, 2009).

Tab. 6.1 AMS ^{14}C data chart

Core	Depth [m NHN]	Lab. no.	Dated material	Conventional ^{14}C age & uncertainty [^{14}C a BP]	Calibration		Calibrated age, 95% probability [cal yrs. BP]
					Data-set(1)	Delta R(2)	
VVC16	-5.65	Poz-94979	fine bulk	5600±40	1		6453–6299
	-5.80	Poz-94630	*Carex, Hydrocotyle*	5850±35	1		6745–6561
	-5.975	Poz-94641	charred Ericaceae	6140±40	1		7163–6930
	-6.31	Poz-94642	charred grasses	5190±40	1		6171–5773
	-6.52	Poz-94976	fine bulk	5515±35	1		6399–6223
	-6.52	Poz-94631	*Cladium mariscus*	5350±35	1		6271–6002
	-6.72	Poz-94633	*Carex*, *Hydrocotyle*, *Ranunculus repens*	5870±35	1		6783–6569
	-6.72	Poz-94634	charred Ericaceae and grasses	5930±35	1		6850–6667
	-6.9	Poz-94978	fine bulk	7000±50	1		7938–7712
	-6.9	Poz-94643	charred Ericaceae and grasses	7080±50	1		8000–7796
VVC17	-4.82	Poz-94535	*Cladium mariscus, Carex flava-type*	4690±40	1		5480–5320
	-4.82	Poz-95124	fine bulk	4780±40	1		5600–5460
	-5.45	Poz-95026	fine bulk	5100±40	1		5920–5750
	-6.235	Poz-94532	*Cladium mariscus*	5320±40	1		6210–5990
	-6.525	Poz-94533	fine bulk	6050±40	1		7000–6790
	-6.575	Poz-94534	fine bulk	6710±40	1		7700–7510
N49	-1.18	Poz-120122	*Ammonia* group	4200±70	2	74±16	4393–3978
	-1.95	Beta-554300	*Ammonia* group	3370±30	2	74±16	3243–3005
	-2.97	Poz-120123	*Ammonia* group	3030±120	2	74±16	3005–2365
	-2.99	Poz-97990	*Barnea candida* (in living position)	1350±30	2	74±16	905–733
	-3.07	Poz-106641	fine bulk	3940±35	1		4515–4255
	-3.29	Poz-115426	fine bulk	4645±30	1		5465–5311
	-3.29	Poz-115164	*Phragmites australis*	3795±35	1		4346–4010
	-4.27	Poz-106643	stem, rhizome	4205±30	1		4845–4628
N43	-0.8	Poz-120120	*Ammonia* group	5590±40	2	74±16	5995–5755
	-0.8	Poz-120121	*Haynesina germanica*	2810±50	2	74±16	2650–2324
	-2.775	Poz-106624	charred plant remains	3385±35	1		3717–3515
	-4.625	Poz-106640	*Cladium mariscus*	4470±35	1		5289–4974
VC03	-2.7	Poz-93522	*Cerastoderma edule* (articulated)	630±30	2	74±16	278–78
	-3.085	Poz-95925	*Cerastoderma edule* (articulated)	600±30	2	74±16	260–1
	-3.64	Poz-116736	charred stem remains (Poaceae)	4235±35	1		4863–4645
VC13	-1.415	Poz-120125	*Ammonia* group	5320±60	2	74±16	5741–5462
	-1.55	Poz-93524	*Mya arenaria* (in living position)	127.84±0.38*	2	74±16	1598–584
	-2.335	Beta-554302	*Ammonia* group	4030±30	2	74±16	4065–3841
	-2.725	Poz-120126	*Ammonia* group	2890±50	2	74±16	2711–2390
	-2.735	Poz-93523	*Mytilus edulis*	560±30	2	74±16	228–1
	-2.93	Poz-115133	fine bulk	3660±30	1		4084–3899
	-3.72	Poz-115134	*Cladium mariscus*	4100±35	1		4814–4449
N44	-2.915	Poz-115136	*Phragmites australis*	3330±30	1		3637–3477
	-2.915	Poz-115163	charred stem remains	3335±35	1		3682–3475
	-3.185	Poz-112307	*Schoenoplectus, Potentilla anserina*	3580±35	1		3980–3729

(1) 1: IntCal13 (for northern hemisphere terrestrial ^{14}C dates; 2: Marine13 (for marine ^{14}C dates)
(2) Delta R value and uncertainty used for reservoir correction of marine ^{14}C dates after Enters et al. (2021).
* pMC modern; dated botanical plant material are seeds and fruits from identified taxa, for Ericaceae twigs and leafs, vegetative remains of Phragmites or unclear identity.

When sea level had almost reached the position of VVC16 and VVC17 around 6000 cal BP, a salt marsh formed, enabling the settlement of typical salt-marsh foraminifers (e.g. *Entzia*

macrescens and *Trochammina inflata*) and salt-tolerant plants, indicated by higher organic contents and low C/N ratios (Last and Smol, 2001).

In VVC17, after the salt-marsh phase, peat growth continued simultaneously with basal peat formation in the eastern part, verifying that the peat of that age and depth is sea-level related. The intercalated salt-marsh deposits are probably due to the ingressing sea along the main channels, which caused regular flooding of the peat and subsequent salt-marsh formation. Caused by the high sediment supply in the vicinity of the tidal channels, finally, peat was able to re-establish (cf. Baeteman, 1999). N49 shows another similar intercalated peat at -3 m NHN, which has an upper erosional contact and is not documented in the other cores. The peat could have formed locally, explaining its absence in the adjacent cores. However, the erosional contacts described in N43, VC03 and VC13 may indicate that this peat has been eroded in these cores. Furthermore, LBEG maps ('Profiltypenkarte', 'NIBIS® Kartenserver', https://nibis.lbeg.de/cardomap3/) show intercalated peats in this area, which is why a more extensive peat formation and subsequent erosion is more likely. ^{14}C dating of the intercalated peat in N49 shows age inversions. The base was dated to 5465–5311 cal BP (bulk sample), being older than the basal peat of this core (4845–4628 cal BP). A second sample at the same depth was dated to 4346–4010 cal BP (*Phragmites australis*) and the upper part to 4515–4255 cal BP. For the base of the intercalated peat, the youngest age gained from individual plant remains was preferred over the older bulk sample (Hatté and Jull, 2007). Regarding the age of the peat top, interpreted as a fen peat, possible incorporation of older ^{14}C from groundwater has to be considered, leading to a slight age overestimation.

The second peat as well as second salt marsh documented in VVC16 show approximately the same age as the underlying sequence of peat and salt marsh. This may suggest the upper sequence to be proximally relocated during a storm event, known from the so called '*Dargen*' (Streif, 1990; Behre and Kučan, 1999; van Dijk et al., 2019).

After this phase, sea-level rise continued and with the southeastward migrating barrier island the main channel shifted to the western part of the study area (VVC16 and VVC17). This channel led to subtidal deposition on top of VVC 16 but also to erosion and relocation in VVC17. The latter shows relevant numbers (>10%) of dominant typical salt-marsh foraminifers within the upper part of the layer that appears as tidal-flat deposits and is situated at the top of the core (Bulian et al., 2019). This can only be explained by the introduction of salt-marsh deposits from a fossil layer eroded nearby by channel migration after an initial tidal-flat phase. In the back-barrier area, a tidal flat developed, which in the east was first cut by a smaller channel (N44 and 45) that was subsequently filled. ^{14}C dating of molluscs and foraminifer shells in four cores (N43, N49, VC03, VC13) suggests a hiatus at the base

of the tidal-flat sediments as well as sediment reworking within this unit. The hiatus is well documented in the chronostratigraphy of N49, where the top of the intercalated peat layer is dated to 4515–4255 cal BP, with potential minor overestimation as mentioned earlier, followed by an erosive contact with a borehole of an articulated bivalve (*Barnea candida*) dated to 905–733 cal BP. Reworking is indicated by age data above this hiatus with age inversions in all four cores (Fig. 6.5) and very young ages derived from molluscs (278–78 and 260–1 cal BP) at depths of -2.7 to -3.1 m NHN (VC03). We expect two different reworking layers, separated by the marker horizon of an undisturbed storm deposit, which can be correlated between all reworking-affected cores, except for N43. Intense reworking of the tidal-flat facies is mainly connected to dyke construction, with first continuous dyke systems around AD 1300, and may amount to around 50% of the tidal-flat deposits within 50 years (Trusheim, 1929; Lüders, 1934; Reineck and Siefert, 1980; van der Spek, 1996; Gerdes et al., 2003; Bungenstock and Schäfer, 2009). Depending on the size of the channels, reworking may cut down to more than -20 m (van der Spek, 1996). The catchment area of the channels is relatively stable and they do not migrate over the entire back-barrier tidal flat. For the back-barrier area of Spiekeroog, Tilch (2003) showed that between 1866 and 1935 no significant lateral enlargement of the channel system took place, in contrast to significant erosional deepening related to dyke construction on the mainland. Nevertheless, over longer time scales, reworking over wider areas can be expected concordant to the migration of the islands and the shift of the tidal-flat water sheds, intensified during storm surges. Tilch (2003) documented vertical erosion of 16 cm for the northern rim of the Janssand, the sandy tidal flat between Langeoog and Spiekeroog, during the summer season of 2001 alone, whereas in the centre of the sandbank accumulation of the same amount was documented. For more protected sandbanks, erosion and accumulation rates in the order of 5 cm are reported (Tilch, 2003). Due to the position of the erosive contact in N49 and VC03 (especially here, the hiatus lies deeper than in the other cores) and the reconstructed subsurface structure (Fig. 6.5), we expect these cores to be influenced by migrating tidal channels probably causing the deeper scouring. In N43 and VC13, the erosive contact lies higher and the subsurface does not show channel-like structures, which is why reworking after the hiatus is expected to be less intense, at least for the lower part of the tidal-flat deposits. However, the relocated bivalves at this depth in VC13 may indicate that this is only valid for N43. Still, due to their similar pattern, the hiatus in N43 should be similar to VC13 (~1500 years) and the hiatus in VC03 should be similar to N49 (~3500 years). The more recent reworking processes on top of the storm-surge layer may relate to the diurnal tides as well as to the tidal channel that exists between N43 and VC03. The fact that the foraminifer tests in these affected deposits do not show significant signs of relocation (opacity, signs of abrasion) indicates only proximal transport (Hofker, 1977).

6.6 Discussion

6.6.1 Evaluation of sample material for TF application

Samples from non-marine Pleistocene deposits and peat facies were excluded for the application of the RSL TF. Furthermore, deposits with indications for reworking, i.e. most tidal-flat samples, were excluded, since their taphocoenoses may not adequately reflect RSL during deposition. Only the lowest samples of the base of the tidal-flat deposits of N43 and VVC17 were included due to the expected lower intensity of reworking (see section 6.5).

The final TF was applied to 38 (out of originally 139) samples from seven sediment cores. Since Model II of the final TF provides the best vertical error (RMSEP) and correlation (R^2_{boot}), only this model was used for the final RSL reconstructions. Therefore, the combined data of foraminifers and ostracods (total=100%) of each core were integrated. The TF provides the palaeo-elevation of each sample relative to the palaeo-sea level. It was converted to an absolute elevation (m NHN) using the following equation, in order to reflect the palaeo-sea level; the result was plotted against the time (Fig. 6.6).

$$SL_p = d_s + e_p$$

SL_p: palaeo-sea level [m NHN]
d_s: depth of fossil sample [m NHN]
e_p: palaeo-elevation of fossil sample relative to palaeo-sea level [m]

6.6.2 The resulting RSL curve

The resulting RSL curve (Fig. 6.6) shows the phase of the transition from faster sea-level rise to the decelerated rise with rates of ~0.5 m per century until ~5700 cal BP followed by a gap that matches documented basal-peat formations in the area of the East Frisian coast and the deceleration of sea-level rise (Freund and Streif, 2000; Streif, 2004; Bungenstock and Schäfer, 2009). The following phase between 5000 and ~3700 cal BP shows the first distinct deceleration of the sea-level rise to ~0.16 m per century. Here, the reconstruction shows four outliers (from VC03, VVC17 and VC13), which represent samples from above the erosive contact. Here, conditions must have been too turbulent for a certain time, due to stronger tidal currents or a location closer to the channel, before the re-establishment of short-term calmer conditions. The two samples from VC03 and VC13 were taken from within a mollusc borehole inside the peat, indicating that the ages of these samples might be overestimated by the age-depth models. Therefore, these outlier samples are not expected to be reliable and were not integrated into the error band. The next phase is characterised by a stagnation between ~3700 and ~1700 cal BP. There is no peat formation documented for

the study area during this time, but Bungenstock and Schäfer (2009) report a regressive signal for the tidal basin of Langeoog for approximately this time, which is why a stagnation phase seems plausible here. However, this part of the curve remains uncertain resulting from the hiatus at the base of the tidal-flat deposits as well as the subsequent reworking. Since the length of this hiatus had to be estimated for N43, we can only assume the temporal position of the samples within the curve, which would imply a RSL rise of almost 4 m within the last 2000 years. This is not in accordance with any existing reconstructions for the southern North Sea coast (e.g. Denys and Baeteman, 1995; De Groot et al., 1996; Streif, 2004; Bungenstock and Schäfer, 2009; Meijles et al., 2018). Therefore, the two samples from N43 are discarded for further investigations, cutting the curve at ~2500 cal BP (Fig. 6.7). Furthermore, the vertical position of the sample from on top of the intercalated peat (VVC17) could be influenced by compaction of the peat, which is hard to quantify at this point. Hence, this data point might underestimate the RSL, which is why this phase is marked in the figures (hatching). Changes after ~1700 cal BP cannot be reconstructed due to the exclusion of all remaining tidal-flat samples.

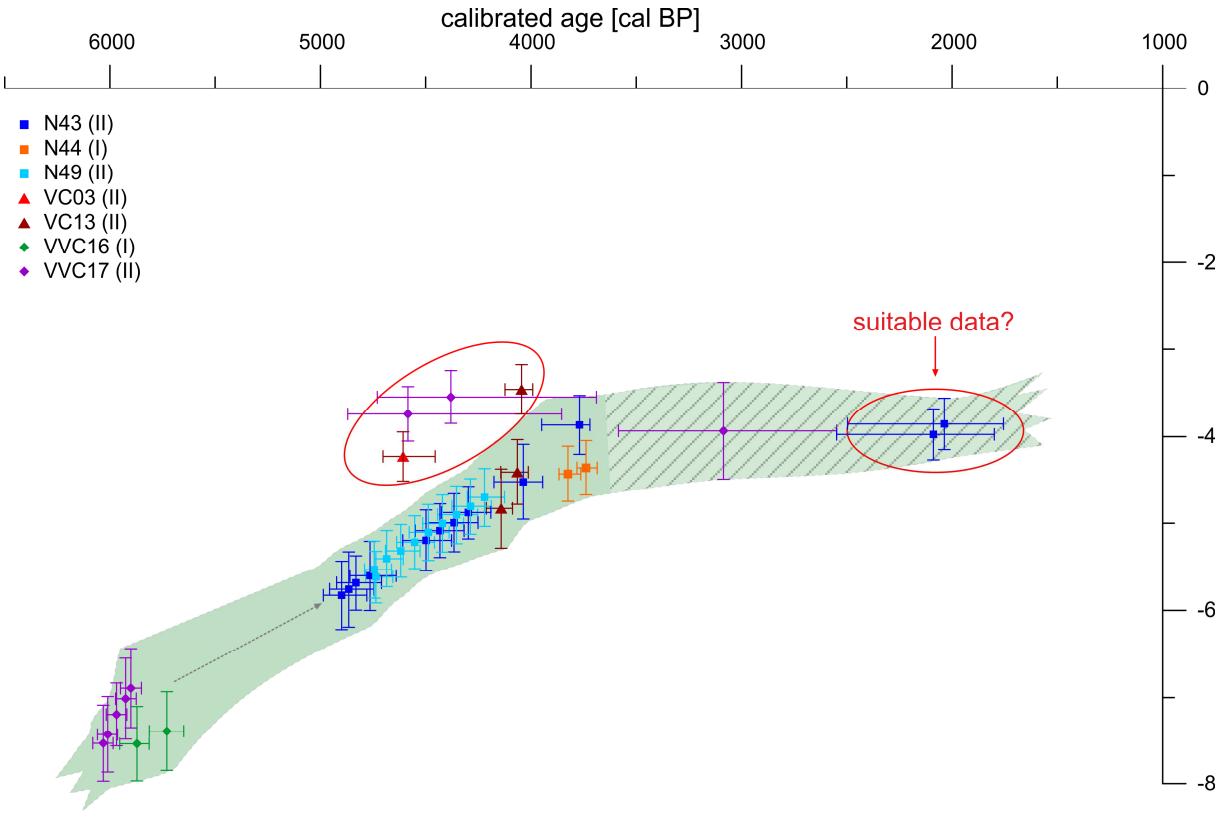

Fig. 6.6 RSL envelope curve based on the application of the final TF on samples from seven WASA cores in the back-barrier area of Norderney. Ages are given in calibrated years BP and palaeo-RSL is related to present-day NHN. The phase still affected by main uncertainties is crosshatched.

Concerning the error band, a smaller error (~1 m) is noticeable for the phase between ~5000 and ~4000 cal BP even though originating from several cores. This phase is reconstructed

from salt-marsh layers, confirming that also in the Wadden Sea these layers are most suitable for TF application.

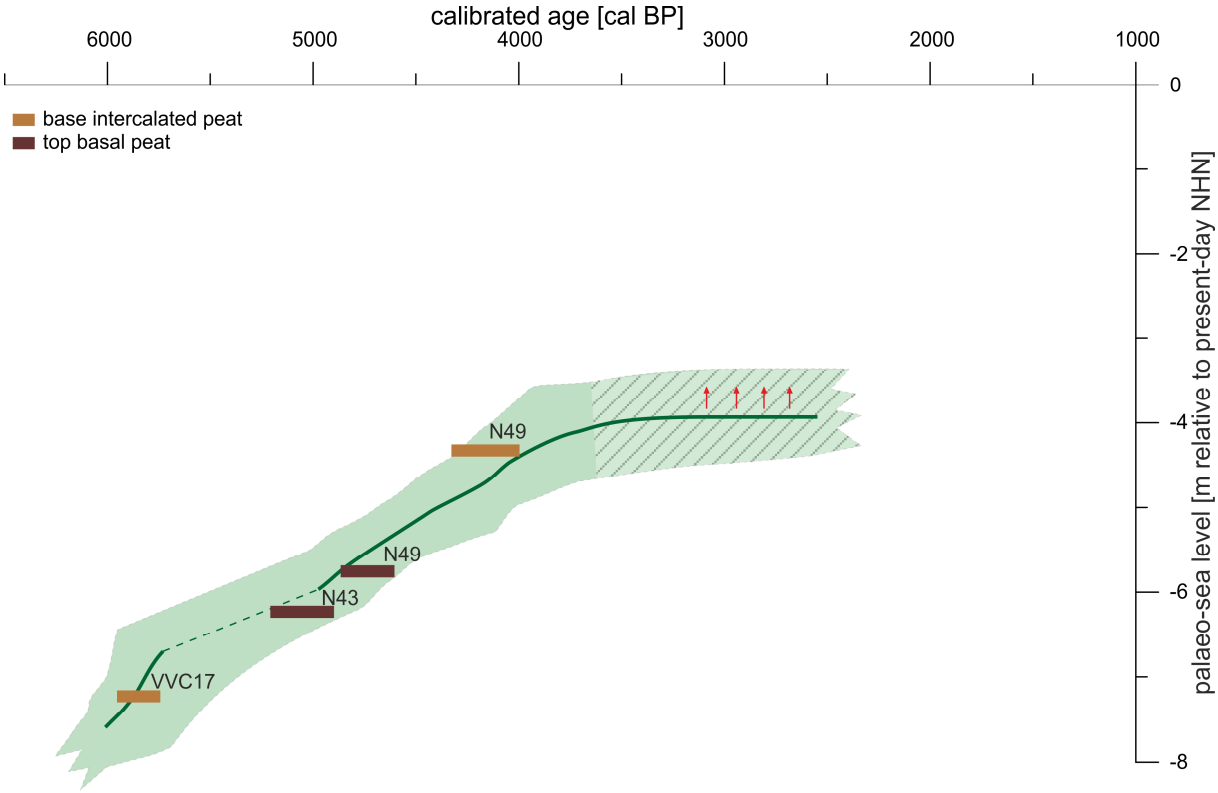

Fig. 6.7 Simplified depiction of the RSL curve for Norderney combined with available sea-level related peat data from three different WASA cores along the investigated transect. Ages are given in calibrated years BP and palaeo-RSL is related to present-day NHN. The phase still affected by main uncertainties is crosshatched.

In order to fill the gap between ~5700 and ~5000 cal BP, we included available peat data in the RSL curve (Fig. 6.7). Only those peat layers were used, for which sea-level induced growth is unequivocal, i.e. the base of the intercalated peat in VVC17, which correlates with the basal peat further east, as well as the intercalated peat base in N49. The data of the basal peats (N43 and N49) originate from the top of the peat. In general, the peats lie within the error band of the curve but their depths could not be corrected for compaction, since only the top of the basal peat is known. Since on tidal coasts, the basal peat forms at or slightly above mean high water (MHW) (Vink et al., 2007; Weerts, 2013), this could suggest an impact of peat auto-compaction by decomposition or post-depositional compaction of at least ~0.7 m. This could also (partially) have impacted the overlying sediments. The same is valid for the intercalated peats (VVC17 and N49) also indicating an influence of compaction either by decomposition or by sediment and water load of at least ~0.9 m (VVC17) and ~0.3 m (N49). This could have resulted in a positive feedback effect of enhanced accommodation space, which led to increased intertidal sedimentation (Long et al., 2006). Hence, a slightly underestimated course of the present curve due to these compaction effects remains possible. In this case, the third phase of the curve might be doubly influenced by compaction, resulting in its lower course.

6.6.3 Evaluation of the reconstructed RSL development

In order to evaluate the validity and trans-regional significance of the RSL curve, a comparison with existing curves is shown in Fig. 6.8. The presented data lie below most of the existing curves probably confirming regional differences.

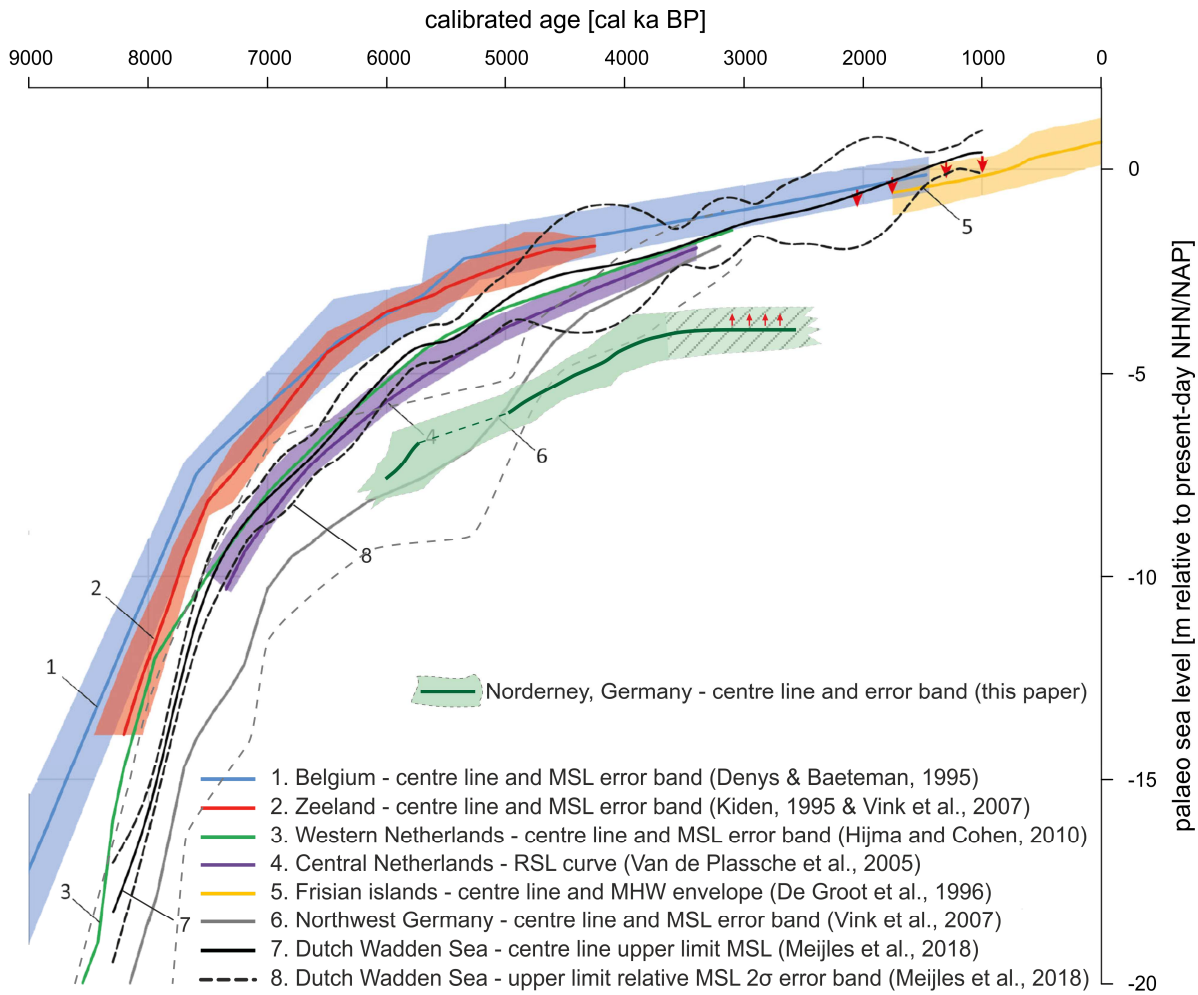

Fig. 6.8 Compilation of RSL curves established along the North Sea coast of Belgium, the Netherlands and Germany. Our data are plotted on top of the existing curves, in order to detect differences and similarities. The phase still affected by main uncertainties is crosshatched. Design *modified after* Meijles et al. (2018).

Considering the differences to Belgium and Zeeland, the present curve shows a generally lower course but a similar trend and decreasing difference towards younger times. During the first phase (~6100–5700 BP), the present reconstruction lies ~3.5–4 m lower than the ones from Belgium and Zeeland, whereas in the second phase (~5000–3700 cal BP), the difference becomes smaller towards the end of the phase (3.8–2.8 m). The third phase (~2500–1700 cal BP) shows again increasing differences (2.8–3.2 m). The general discrepancy could be explained by northwards increasing glacial-isostatic subsidence due to the position relative to the NW-ESE orientated glacial forebulge (Kiden et al., 2002; Meijles et al., 2018). The decreasing differences from the first to the second phase may relate to slowly decreasing subsidence rates over time (cf. Kiden et al., 2002; Vink et al., 2007). However,

the discrepancies could also result from a combination of differences in GIA and compaction of the basal peat. Interpretation of the third-phase advocates caution due to uncertainties associated with potential compaction of the underlying intercalated peat combined with a possible compaction of the basal peat. If a trend similar to the Belgian curve (Denys and Baeteman, 1995) would be assumed, a compaction of ~0.5 m could be indicated for the present data during the third phase.

The discrepancies of the present curve to curves from the central and western Netherlands (van de Plassche et al., 2005; Hijma and Cohen, 2010) as well as from the Dutch Wadden Sea (Meijles et al., 2018) are smaller; ~2.6–1.5 m in the first phase and ~2.8–1.7 m in the second phase. The third phase is again characterised by increasing discrepancies (~1.7–2.9 m). The general trend of the present curve is most similar to the curve from the Flevo area using the base of basal peats as sea-level index points (van de Plassche et al., 2005). Hence, compaction most likely has no impact on that curve. However, since the Flevo area is situated in the basin of the Ijsselmeer, it can be influenced by the flood-basin effect, which could have reduced the local mean high water (MHW) level resulting in smaller discrepancies with the present curve (van de Plassche, 1982; Meijles et al., 2018). The study area of Norderney represents a more open coast, which is why the flood-basin effect is less intense. Due to the generally similar trend of the present reconstruction and all three mentioned curves, the elevation differences could again be explained by the different GIA rates (Meijles et al., 2018). However, the curves should approximate with time (cf. Steffen et al., 2006), whereas the present data depart from all curves in the third phase. Since the sample representing this phase (VVC17) only exhibits a very low proportion of salt-marsh foraminifers (<3.5%), reworking is expected to be still weak and not to have that much of an impact on the curve, even though this cannot be entirely excluded. Most likely, this implies a high influence of compaction for the youngest part of the curve.

Apart from the third phase, the curve shows overlaps with the curve for northwest Germany (Vink et al., 2007). In the first phase (~6100–5700 cal BP), the presented data plot above the existing curve (~0.4–0.9 m) departing from each other over time, but completely within the error band, and in the second phase (~5000–3700 cal BP) the data plot below the existing curve with increasing distance (~0.1–1.6 m). The curve for northwest Germany (Vink et al., 2007) is based on selected data previously published by Behre (2003, 2007) and corrected for their indicative meaning by Vink et al. (2007), which led to a smoother curve than the original one. Taking a closer look at the discrepancies during the first phase, these data (top of basal peats and base of intercalated peat) are definitely influenced by compaction (Vink et al., 2007). Furthermore, the six data points originate from a very large section of

the German coast, reaching from Emden, close to the Dollart Bay, over Hooksiel and Wilhelmshaven (Jade Bay) to the 'Land Wursten' region (>10 km south of Cuxhaven) and none are from an area near Norderney, implying an inter-regional significance of the different RSL index points (Bungenstock and Weerts, 2010, 2012). Considering different local effects (compaction rates, mean tidal range, GIA), our curve is therefore associated with a higher significance, at least for the present study area. Looking at the database of Behre (2003) for the time of the second phase of the present curve, a similar pattern becomes apparent concerning the compaction-prone database (top and base of upper peats and intercalated peat). The dataset is not as widespread for this phase, possibly representing a significance for the area around the Jade Bay, but not for the tidal basin of Norderney. Therefore, also for the second phase, our curve is expected to be more reliable. However, the possible amount of compaction influencing the TF data can only be estimated from the compared trends described above and from peat-growth rates reconstructed for the basal peat of VVC17 (Bulian et al., 2019) compared to those estimated for central Europe (0.5–1.5 mm/a; Succow and Reimer, 1986) leading to a minimum of ~0.5 m, which would still provide an error band smaller than that of the curve for northwest Germany (Vink et al., 2007).

The present curve cannot be connected to the curve from the West Frisian islands for the last 2000 years (De Groot et al., 1996) due to the exclusion of the reworking-affected tidal-flat samples and the compaction uncertainties remaining for the third phase of the curve. In order to enable a connection between the two curves, a compaction of ~2 m and a trend similar to the second phase would be necessary, which cannot be verified by this research.

Comparing the TF-based RSL data to a new peat-based curve from the East Frisian island of Langeoog (~10 km east of Norderney, Fig. 6.9; Bungenstock et al., *in revision*) should enable more local conclusions on compaction and other potential driving factors. The present data plot generally below the Langeoog curve, but mostly with overlapping error bands. The trends are similar for the first two phases, whereas the present curve has a smaller error band. Since the Langeoog curve is depicted as an upper-limit line and a downward error band, the discrepancies are measured from the upper limit of the error band of the present curve. For the first phase, differences of ~1.7–1.4 m are documented and the deceleration of the RSL rise is reconstructed similarly. In the second phase the differences amount to ~1.7–1.9 m. The comparison for the third phase is again complicated by the assumed enhanced compaction effects of the present data resulting in discrepancies increasing over time (~1.9–2.8 m). The fact that the TF plots below the basal-peat curve (Bungenstock et al., *in revision*) around 4000–3000 cal BP is possibly the most important discrepancy between the two curves. The TF provides information about the sample elevation relative to the mean sea level at the time of deposition, whereas the mean sea level is

also influenced by the tidal range, i.e. the elevation of mean high water (MHW) and mean low water (MWL). If changes in tidal range happen equally for MHW and MLW, the mean sea level remains unchanged, but if one of the two changes stronger, mean sea level follows. Therefore, changes in palaeo-tidal range could have affected the RSL curve. Within the North Sea region, the tidal range amplified during the Holocene transgression until ~7000 BP, when the North Sea and Southern Bight (North Sea region between the Netherlands, Belgium and the UK) were finally connected, and did not change significantly since then (van der Molen and de Swart, 2001; Uehara et al., 2006; Haigh et al., 2019). However, the TF data plotting below the base of the basal peat could either be explained by a relatively lower MHW, which departed from MLW in time until today, or by a lower MWL, which approximated closer to MHW until today (Fig. 6.10). For different locations of the western North Sea, locally different tidal-range changes are recorded throughout the Holocene, all showing an increase in MHW, which results in predictions of RSL change below the observations (Shennan et al., 2000). Although the major changes are reported prior to ~6000 BP,

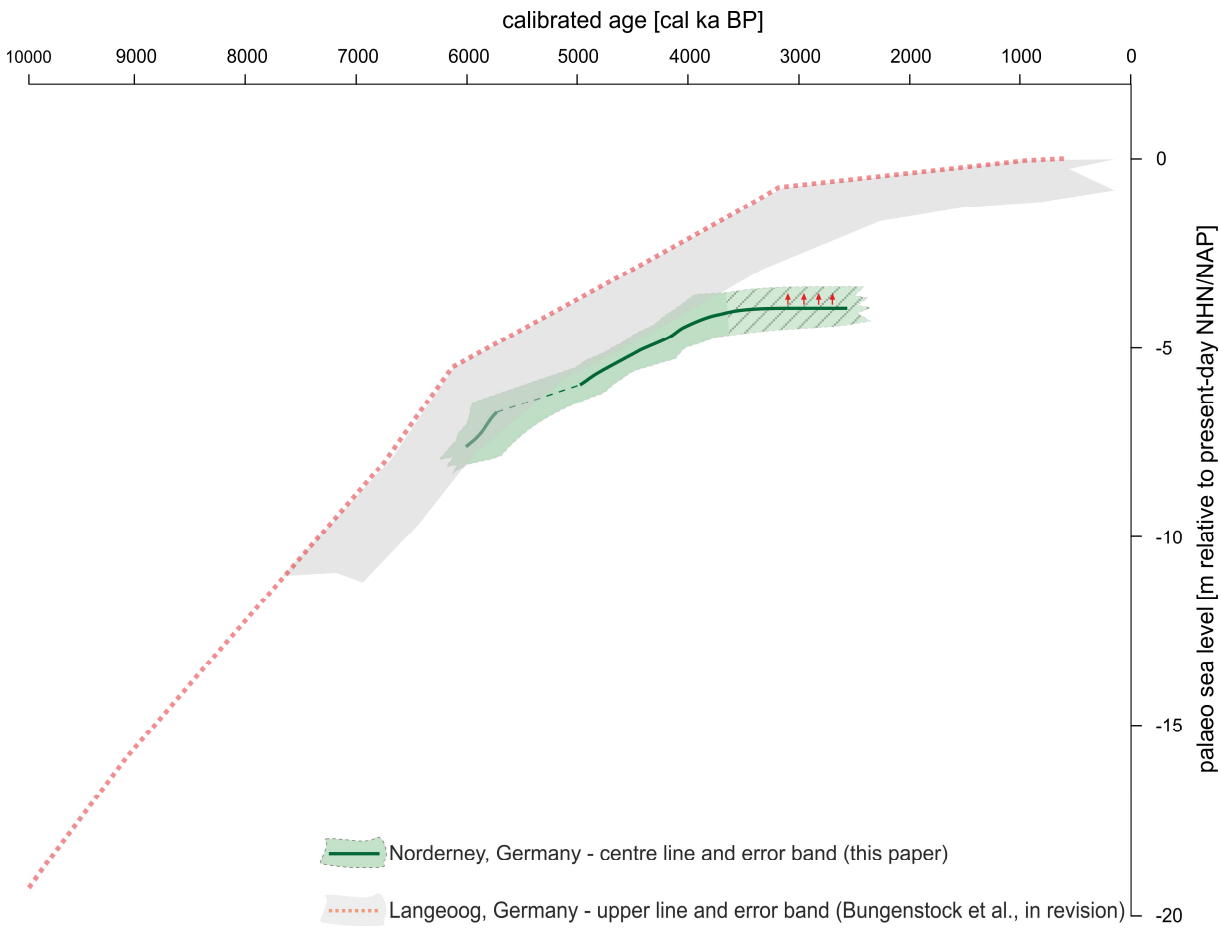

Fig. 6.9 Compilation of our RSL data and new data from the East Frisian island of Langeoog recently published by Bungenstock et al. (*in revision*).

the TF data suggest a continued increase in MHW, which would fit the documentation of Töppe (1994) about an increased rise in MHW compared to MLW within the last 150 years. A combined effect of changes in palaeo-tide and peat compaction is also conceivable. An

adjustment of the TF for different palaeo-tide models could therefore represent an aim for future studies.

From the comparison of the present RSL data with existing curves from the southern North Sea coast, the low reliability of the two lowest tidal-flat samples was confirmed, which is why they were discarded for the final RSL curve for Norderney. In general, the reworking that influences the reliability of the tidal-flat samples can only be circumvented by investigating sediment archives from inner-dyke locations providing younger salt-marsh deposits. Along a transect perpendicular to the coastline, these could also capture fossil tidal-flat deposits that have not been influenced by intense reworking. The potential compaction of peats within the Norderney tidal basin, possibly partially influencing sample depths and therefore RSL reconstruction, can only be estimated to be at least ~0.5 m. Nevertheless, the present TF-based curve provides a smaller error band than most of the consulted curves. Furthermore, it provides promising indications for palaeo-tide changes after 7000 BP, in contrast to existing reconstructions.

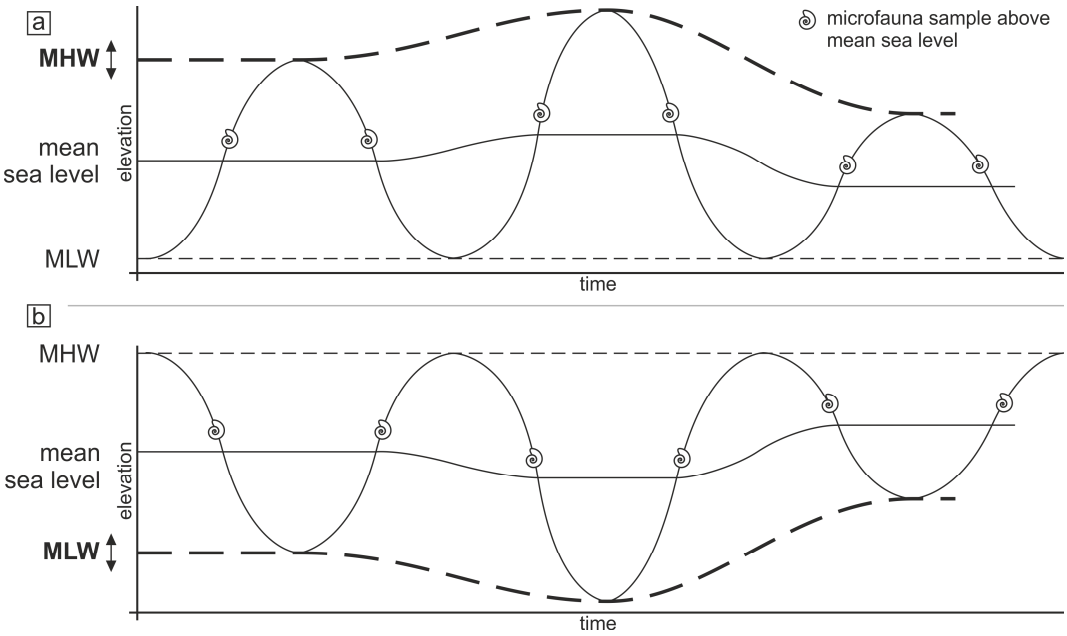

Fig. 6.10 Schematic depiction of different changes in the tidal range and the resulting absolute position of the TF sample from its reconstructed elevation relative to mean sea level. a: changing mean high water (MHW) – higher MHW: higher elevation of sample, lowered MHW: lower elevation of sample. b: changing mean low water (MLW) – lowered MLW: lower elevation of sample, higher MLW: higher elevation of sample.

6.7 Conclusion and outlook

The inclusion of additional samples from the vicinity of the surface transect (Scheder et al., 2019) helped to improve the performance of the preliminary transfer function (TF) for relative sea level (RSL). Once again, the vertical error of the common TF model, using only dead foraminifers, could be improved by ±8 cm by including dead ostracods. The final TF

provides an R^2_{boot} of 0.89 and a vertical error of 29.7 cm, accounting for ~11% of the tidal range of Spiekeroog (BSH, 2018).

The Holocene stratigraphic sequence of the back-barrier area of Norderney starts with Pleistocene deposits, which are overlain by the basal peat resulting from rising groundwater levels associated with the early to mid-Holocene trangression (Streif, 2004; Bungenstock and Schäfer, 2009). Peat growth started around 7500–8000 cal BP in the west and expanded further east. A salt-marsh layer on top of the basal peat indicates increasing marine influence, with a short-term stagnant phase in the west (intercalated peat in VVC17 connected to RSL). In general, peat and salt-marsh formation continue to the east with a delay, following the RSL rise in the back of the gradually forming barrier island. The tidal-flat record starts with a massive hiatus (~1000–3300 years), and ^{14}C ages suggest reworking throughout the complete layer, which is mainly connected to the change in hydrodynamics associated with dyke construction (Trusheim, 1929; Lüders, 1934; Reineck and Siefert, 1980; van der Spek, 1996). In general, the foraminifer and ostracod taxa documented in the modern tidal flat and salt marsh of Spiekeroog, also occur in the fossil record of the Norderney tidal basin.

The first Holocene RSL curve resulting from the application of a TF in the southern North Sea region shows a clear deceleration in sea-level rise between 6000 and 5000 cal BP. Due to the low reliability of the tidal-flat deposits, we were not able to reliably reconstruct RSL changes younger than ~2500 years, and uncertainties due to compaction effects after ~3500 cal BP remain. Nevertheless, the RSL curve provides smaller error bands than most of the peat-based curves (Denys and Baeteman, 1995; Vink et al., 2007; Meijles et al., 2018) and represents a more continuous record. A local comparison to a new peat-based curve for Langeoog implies potential changes in palaeo-tidal range for the time after ~6100 cal BP.

A correction for compaction, by determining the mean time of compaction (more ages from basal peat bases are necessary), and for tidal changes, by adjusting the TF, based on palaeo-tide models, remain goals for future studies.

6.8 Acknowledgements

The research reported here is part of the WASA project (*The Wadden Sea as an archive of landscape evolution, climate change and settlement history: exploration – analysis – predictive modelling*), funded by the 'Niedersächsisches Vorab' of the VolkswagenStiftung within the funding initiative 'Küsten und Meeresforschung in Niedersachsen' of the Ministry for Science and Culture of Lower Saxony, Germany (project VW ZN3197). Oxygen and TOC data were provided by Jennifer Schmitt (ICBM – Institute for Chemistry and Biology of

the Marine Environment) and Gesine Lange (University of Oldenburg) in the frame of the BEFmate project. Dirk Enters (Lower Saxony Institute for Historical Coastal Research), Alexander Bartholomä and Ruggero Capperucci (Senckenberg am Meer) are acknowledged for macroscopic core description, as well as Annastasia Elschner (University Bonn), Shirin Nurshan Rahman (Senckenberg am Meer) and Anika Symanczyk (University of Cologne) for laboratory assistance. Furthermore, we gratefully acknowledge Torsten Janßen (Senckenberg am Meer) for extensive organisational work concerning radiocarbon dating. The EasyCopy company is acknowledged for providing the core-drawing software (EasyCore).

Data Availability Statement:

The data that supports the findings of this study are available in the supplementary material of this article.

6.9 References

Athersuch, J., Horne, D.J., Whittaker, J.E., 1989. Marine and brackish water ostracods (superfamilies Cypridacea and Cytheracea): keys and notes for the identification of the species. Brill Archive, Leiden.

Baeteman, C., 1999. The Holocene depositional history of the IJzer palaeovalley (Western Belgian coastal plain) with reference to the factors controlling the formation of intercalated peat beds. Geologica Belgica 2, 39–72.

Baeteman, C., Waller, M., Kiden, P., 2011. Reconstructing middle to late Holocene sea-level change: A methodological review with particular reference to ‘A new Holocene sea-level curve for the southern North Sea’ presented by K.-E. Behre. Boreas 40, 557–572. https://doi.org/10.1111/j.1502-3885.2011.00207.x

Bakker, J.P., 2014. Ecology of Salt Marshes: 40 Years of Research in the Wadden Sea. Wadden Academy, Leeuwarden. https://doi.org/10.2307/2404318

Barlow, N.L.M., Shennan, I., Long, A.J., et al., 2013. Salt marshes as late Holocene tide gauges. Global and Planetary Change 106, 90–110. https://doi.org/10.1016/j.gloplacha.2013.03.003

Beck, H.E., Zimmermann, N.E., McVicar, T.R., et al., 2018. Present and future Köppen-Geiger climate classification maps at 1-km resolution. Scientific Data 5, 180214. https://doi.org/10.1038/sdata.2018.214

Behre, K.-E., 2003. Eine neue Meeresspiegelkurve für die südliche Nordsee. Probleme der Küstenforschung im südlichen Nordseegebiet 28, 9–63.

Behre, K.-E., 2007. A new Holocene sea-level curve for the southern North Sea. Boreas 36, 82–102. https://doi.org/10.1111/j.1502-3885.2007.tb01183.x

Behre, K.-E., Kučan, D., 1999. Neue Untersuchungen am Außendeichsmoor bei Sehestedt am Jadebusen. Probleme der Küstenforschung im südlichen Nordseegebiet 26, 35–64.

Birks, H.J.B., 1995. Quantitative palaeoenvironmental reconstructions, in: Maddy, D., Brew, J.S. (Eds.), Statistical Modelling of Quaternary Science Data. Quaternary Research Association, Cambridge, pp. 161–254.

Bittmann, F., 2019. Das Wattenmeer als Archiv zur Landschaftsentwicklung, Klimaänderung und Siedlungsgeschichte. Nachrichten des Marschenrats zur Förderung der Forschung im Küstengebiet der Nordsee 56, 25–27.

Blaauw, M., Christen, A., 2019. rbacon: Age-Depth Modelling using Bayesian Statistics. R package version 2.3.9.1. https://CRAN.R-project.org/package=rbacon.

BSH (Bundesamt für Seeschifffahrt und Hydrographie), 2018. Gezeitenkalender 2019: Hoch- und Niedrigwasserzeiten für die Deutsch Bucht und deren Flussgebiete. Bundesamt für Seeschifffahrt und Hydrographie, Hamburg.

Bulian, F., Enters, D., Schlütz, F., et al., 2019. Multi-proxy reconstruction of Holocene paleoenvironments from a sediment core retrieved from the Wadden Sea near Norderney, East Frisia, Germany. Estuarine, Coastal and Shelf Science 225, 106251. https://doi.org/10.1016/j.ecss.2019.106251

Bungenstock, F., Freund, H., Mauz, B., et al., 2021. Holocene relative sea level data for the Eastfrisian barrier coast (NW Germany). Netherlands Journal of Geosciences (in revision).

Bungenstock, F., Schäfer, A., 2009. The Holocene relative sea-level curve for the tidal basin of the barrier island Langeoog, German Bight, Southern North Sea. Global and Planetary Change 66, 34–51. https://doi.org/10.1016/j.gloplacha.2008.07.007

Bungenstock, F., Weerts, H.J.T., 2010. The high-resolution Holocene sea-level curve for Northwest Germany: global signals, local effects or data-artefacts? International Journal of Earth Sciences 99, 1687–1706. https://doi.org/10.1007/s00531-009-0493-6

Bungenstock, F., Weerts, H.J.T., 2012. Holocene relative sea-level curves for the German North sea coast. International Journal of Earth Sciences 101, 1083–1090. https://doi.org/10.1007/s00531-011-0698-3

Davis, J.C., 1986. Statistics and Data Analysis in Geology, 2nd ed. John Wiley & Sons, New York.

De Groot, T.A.M., Westerhoff, W.E., Bosch, J.H.A., 1996. Sea-level rise during the last 2000 years as recorded on the Frisian Islands (the Netherlands). Mededelingen Rijks Geologische Dienst 57, 69–78.

Denys, L., Baeteman, C., 1995. Holocene evolution of relative sea level and local mean high water spring tides in Belgium—a first assessment. Marine Geology 124, 1–19. https://doi.org/10.1016/0025-3227(95)00029-X

Edwards, R., Wright, A., 2015. Foraminifera, in: Shennan, I., Long, A.J., Horton, B.P. (Eds.), Handbook of Sea-Level Research. John Wiley & Sons, Chichester, pp. 191–217. https://doi.org/10.1002/9781118452547.ch13

Elschner, A., Scheder, J., Enters, D., et al., 2021. Microfauna- and sedimentology-based facies analysis for palaeo-landscape reconstruction in the back-barrier of Norderney (NW Germany). Netherlands Journal of Geosciences 100, e4.

Enters, D., Haynert, K., Wehrmann, A., Freund, H., Schlütz, F., 2021. A new ΔR value for the southern North Sea and its application in coastal research. Netherlands Journal of Geosciences 100, e1.

Flemming, B., Davis, Jr, R.A., 1994. Holocene evolution, morphodynamics and sedimentology of the Spiekeroog barrier island system (southern North Sea). Senckenbergiana maritima 24, 117–155.

Flemming, B.W., 2002. Effects of Climate and Human Interventions on the Evolution of the Wadden Sea Depositional System (Southern North Sea), in: Wefer, G., Berger, W.H., Behre, K.-E., et al. (Eds.), Climate Development and History of the North Atlantic Realm. Springer, Berlin, Heidelberg, pp. 399–413. https://doi.org/10.1007/978-3-662-04965-5_26

Flemming, B.W., Ziegler, K., 1995. High-resolution grain size distribution patterns and textural trends in the backbarrier environment of Spiekeroog Island (southern North Sea). Senckenbergiana maritima 26, 1–24.

Frenzel, P., Keyser, D., Viehberg, F.A., 2010. An illustrated key and (palaeo)ecological primer for Postglacial to Recent Ostracoda (Crustacea) of the Baltic Sea. Boreas 39, 567–575. https://doi.org/10.1111/j.1502-3885.2009.00135.x

Frenzel, P., Tech, T., Bartholdy, J., 2005. Checklist and annotated bibliography of Recent Foraminiferida from the German Baltic Sea coast. Studia Geologica Polonica 124, 67–86.

Freund, H., Streif, H., 2000. Natürliche Pegelmarken für Meeresspiegelschwankungen der letzten 2000 Jahre im Bereich der Insel Juist. Petermanns Geographische Mitteilungen

143, 34–45.

Gerdes, G., Petzelberger, B.E.M., Scholz-Böttcher, B.M., et al., 2003. The record of climatic change in the geological archives of shallow marine, coastal, and adjacent lowland areas of Northern Germany. Quaternary Science Reviews 22, 101–124. https://doi.org/10.1016/S0277-3791(02)00183-X

Haigh, I.D., Pickering, M.D., Green, J.A.M., et al., 2019. The Tides They Are A-Changin': A comprehensive review of past and future nonastronomical changes in tides, their driving mechanisms, and future implications. Reviews of Geophysics 58, e2018RG000636. https://doi.org/10.1029/2018RG000636

Hammer, Ø., Harper, D.A.T., Ryan, P.D., 2001. Past: Paleontological statistics software package for education and data analysis. Palaeontologia Electronica 4, article 4.

Harper, D.A.T. (Ed.), 1999. Numerical Palaeobiology. Computer-Based Modelling and Analysis of Fossils and their Distributions. John Wiley & Sons, Chichester.

Hatté, C., Jull, A.J.T., 2007. Plant Macrofossils, in: Scott, A.E. (Ed.), Encyclopedia of Quaternary Science. Elsevier, Oxford, pp. 2958–2965.

Hesemann, M., 2015. The foraminifera.eu database: concept and status. Palaeontologia Electronica 18.3.48A, 1–14.

Hijma, M.P., Cohen, K.M., 2010. Timing and magnitude of the sea-level jump preluding the 8200 yr event. Geology 38, 275–278. https://doi.org/10.1130/G30439.1

Hofker, J., 1977. The foraminifera of dutch tidal flats and salt marshes. Netherlands Journal of Sea Research 11, 223–296. https://doi.org/10.1016/0077-7579(77)90009-6

Juggins, S., 2007. C2 Version 1.5: software for ecological and palaeoecological data analysis and visualisation. University of Newcastle, Newcastle upon Tyne.

Kemp, A.C., Horton, B.P., Vann, D.R., et al., 2012. Quantitative vertical zonation of salt-marsh foraminifera for reconstructing former sea level; an example from New Jersey, USA. Quaternary Science Reviews 54, 26–39. https://doi.org/10.1016/j.quascirev.2011.09.014

Kemp, A.C., Telford, R.J., 2015. Transfer functions, in: Shennan, I., Long, A.J., Horton, B.P. (Eds.), Handbook of Sea-Level Research. John Wiley & Sons, Chichester, pp. 470–499. https://doi.org/10.1002/9781118452547.ch31

Kiden, P., Denys, L., Johnston, P., 2002. Late Quaternary sea-level change and isostatic and tectonic land movements along the Belgian–Dutch North Sea coast: geological data and model results. Journal of Quaternary Science 17, 535–546.

https://doi.org/10.1002/jqs.709

Kottek, M., Grieser, J., Beck, C., et al., 2006. World map of the Köppen-Geiger climate classification updated. Meteorologische Zeitschrift 15, 259–263. https://doi.org/10.1127/0941-2948/2006/0130

Lange, G., Haynert, K., Dinter, T., et al., 2018. Adaptation of benthic invertebrates to food sources along marine-terrestrial boundaries as indicated by carbon and nitrogen stable isotopes. Journal of Sea Research 131, 12–21. https://doi.org/10.1016/J.SEARES.2017.10.002

Last, W.M., Smol, J.P., 2001. Tracking Environmental Change Using Lake Sediments. Volume 2: Physical and Geochemical Methods. Kluwer Academic Publishers, Dordrecht. https://doi.org/10.1007/0-306-47669-X

Leorri, E., Gehrels, W.R., Horton, B.P., et al., 2010. Distribution of foraminifera in salt marshes along the Atlantic coast of SW Europe: Tools to reconstruct past sea-level variations. Quaternary International 221, 104–115. https://doi.org/10.1016/J.QUAINT.2009.10.033

Lepš, J., Šmilauer, P., 2003. Multivariate analysis of ecological data Using CANOCO. Cambridge University Press, New York. https://doi.org/10.1017/CBO9781139627061

Long, A.J., Waller, M.P., Stupples, P., 2006. Driving mechanisms of coastal change: Peat compaction and the destruction of late Holocene coastal wetlands. Marine Geology 225, 63–84. https://doi.org/10.1016/J.MARGEO.2005.09.004

Lüders, K., 1934. Über das Wandern der Priele. Abhandlungen des Naturwissenschaftlichen Vereins zu Bremen 29, 19–32.

Lutze, G.F., Altenbach, A. V, 1991. Technik und Signifikanz der Lebendfärbung benthischer Foraminiferen in Bengalrot. Geologisches Jahrbuch 128, 251–265.

Meijles, E.W., Kiden, P., Streurman, H.-J., et al., 2018. Holocene relative mean sea-level changes in the Wadden Sea area, northern Netherlands. Journal of Quaternary Science 33, 905–923. https://doi.org/10.1002/jqs.3068

Milker, Y., Weinkauf, M.F.G., Titschack, J., et al., 2017. Testing the applicability of a benthic foraminiferal-based transfer function for the reconstruction of paleowater depth changes in Rhodes (Greece) during the early Pleistocene. PLoS ONE 12, 0188447. https://doi.org/10.1371/journal.pone.0188447

Müller-Navarra, K., Milker, Y., Schmiedl, G., 2016. Natural and anthropogenic influence on the distribution of salt marsh foraminifera in the Bay of Tümlau, German North Sea. Journal of Foraminiferal Research 46, 61–74. https://doi.org/10.2113/gsjfr.46.1.61

Murray, J.W., 2000. The enigma of the continued use of total assemblages in ecological studies of benthic Foraminifera. Journal of Foraminiferal Research 30, 244–245. https://doi.org/10.2113/0300244

Murray, J.W., 2006. Ecology and Applications of Benthic Foraminifera. Cambridge University Press, Cambridge.

Preuß, H., Vinken, R., Vorr, H.-H., 1991. Symbolschlüssel Geologie, 3rd ed. Niedersächsisches Landesamt für Bodenforschung und Bundesanstalt für Geowissenschaften und Rohstoffe, Hannover.

Rahman, S.N., 2018. Distribution of salt marsh foraminifera. Universität Oldenburg.

Rahmstorf, S., 2017. Rising hazard of storm-surge flooding. Proceedings of the National Academy of Sciences of the United States of America 114, 11806–11808. https://doi.org/10.1073/pnas.1715895114

Reimer, P.J., Bard, E., Bayliss, A., et al., 2013. IntCal13 and Marine13 Radiocarbon Age Calibration Curves 0–50,000 Years cal BP. Radiocarbon 55, 1869–1887. https://doi.org/10.2458/azu_js_rc.55.16947

Reineck, H.-E., Siefert, W., 1980. Faktoren der Schlickbildung im Sahlenburger und Neuwerker Watt. Die Küste 35, 26–51.

Scheder, J., Frenzel, P., Bungenstock, F., et al., 2019. Vertical and lateral distribution of Foraminifera and Ostracoda in the East Frisian Wadden Sea – developing a transfer function for relative sea-level change. Geologica Belgica 22, 99–110. https://doi.org/10.20341/gb.2019.007

Shennan, I., Lambeck, K., Flather, R., et al., 2000. Modelling western North Sea palaeogeographies and tidal changes during the Holocene. Geological Society, London, Special Publications 166, 299–319. https://doi.org/10.1144/GSL.SP.2000.166.01.15

Steffen, H., Kaufmann, G., Wu, P., 2006. Three-dimensional finite-element modeling of the glacial isostatic adjustment in Fennoscandia. Earth and Planetary Science Letters 250, 358–375. https://doi.org/10.1016/J.EPSL.2006.08.003

Streif, H., 1990. Das ostfriesische Küstengebiet. Nordsee, Inseln, Watten und Marschen. Sammlung Geologischer Führer 57, 2nd ed. Gebrüder Bornträger, Berlin.

Streif, H., 2004. Sedimentary record of Pleistocene and Holocene marine inundations along the North Sea coast of Lower Saxony, Germany. Quaternary International 112, 3–28. https://doi.org/10.1016/S1040-6182(03)00062-4

Succow, M., Reimer, P.J., 1986. Moore in der Landschaft. Urania-Verlag, Leibzig, Jena, Berlin.

Tilch, E., 2003. Oszillation von Wattflächen und deren fossils Erhaltungspotential (Spiekerooger Rückseitenwatt, Südliche Nordsee). Berichte, Fachbereich Geowissenschaften, Universität Bremen 222.

Töppe, A., 1994. Beschleunigter Meeresspiegelanstieg. Hansa-Schiffahrt-Schiffbau-Hafen 131, 78–82.

Trusheim, F., 1929. Zur Bildungsgeschwindigkeit geschichteter Sedimente im Wattenmeer, besonders solcher mit schräger Parallelschichtung. Senckenbergiana 11, 47–56.

Uehara, K., Scourse, J.D., Horsburgh, K.J., et al., 2006. Tidal evolution of the northwest European shelf seas from the Last Glacial Maximum to the present. Journal of Geophysical Research: Oceans 111. https://doi.org/10.1029/2006JC003531

van de Plassche, O., 1982. Sea-level change and water-level movements in the Netherlands during the Holocene. Mededelingen Rijks Geologische Dienst 36, 1–93.

van de Plassche, O., Bohncke, S.J.P., Makaske, B., et al., 2005. Water-level changes in the Flevo area, central Netherlands (5300-1500 BC): implications for relative mean sea-level rise in the Western Netherlands. Quaternary International 133–134, 77–93. https://doi.org/10.1016/j.quaint.2004.10.009

van der Molen, J., de Swart, H.E., 2001. Holocene tidal conditions and tide-induced sand transport in the southern North Sea. Journal of Geophysical Research: Oceans 106, 9339–9362. https://doi.org/10.1029/2000JC000488

van der Spek, A., 1996. Holocene depositional sequences in the Dutch Wadden Sea south of the island of Ameland. Mededelingen Rijks Geologische Dienst 57, 41–68.

van Dijk, G., Fritz, C., Straathof, N., et al., 2019. Biogeochemical Characteristics of the Last Floating Coastal Bog Remnant in Europe, the Sehestedt Bog. Wetlands 39, 227–238. https://doi.org/10.1007/s13157-018-1089-3

van Wijnen, H.J., Bakker, J.P., 2001. Long-term surface elevation change in salt marshes: A prediction of marsh response to future sea-level rise. Estuarine, Coastal and Shelf Science 52, 381–390. https://doi.org/10.1006/ecss.2000.0744

Vink, A., Steffen, H., Reinhardt, L., et al., 2007. Holocene relative sea-level change, isostatic subsidence and the radial viscosity structure of the mantle of northwest Europe (Belgium, the Netherlands, Germany, southern North Sea). Quaternary Science Reviews 26, 3249–3275. https://doi.org/10.1016/j.quascirev.2007.07.014

Walton, W.R., 1952. Techniques for recognition of living Foraminifera. Contribution Cushman Foundation of Foraminiferal Research 3, 56–60.

Weerts, H.J.T., 2013. Holocene sea-level change, sedimentation, coastal change and palaeogeography in the southern North Sea lowlands. A 2012 geological literature overview, in: Thoen, E., Borger, G.J., de Kraker, A.M.J., et al. (Eds.), Landscapes or Seascapes? The History of the Coastal Environment in the North Sea Area Reconsidered. CORN Publication Series, 13. Brepols Publishers, Turnhout, pp. 145–173.

Weisse, R., von Storch, H., Niemeyer, H.D., et al., 2012. Changing North Sea storm surge climate: An increasing hazard? Ocean and Coastal Management 68, 58–68. https://doi.org/10.1016/j.ocecoaman.2011.09.005

Woodroffe, C.D., Murray-Wallace, C. V., 2012. Sea-level rise and coastal change: the past as a guide to the future. Quaternary Science Reviews 54, 4–11. https://doi.org/10.1016/j.quascirev.2012.05.009

Supplementary material – Scheder et al. submitted to Journal of Quaternary Science

6.S1. Applied Methods (outside main focus of the paper)

6.S1.1 Laboratory analyses – Core drillings

Samples for microfaunal analysis were carefully shaken overnight with water, adding a dispersant (sodium pyrophosphate; $Na_4P_2O_7$; 46 g/l) to avoid adhesion of clay, and washed through sieves (63 and 100 µm) in order to separate microfossils (>100 µm) from finer-grained material. Where possible, 100–200 individuals were counted dry (for ostracods, valves were counted). However, a minimum of 40 individuals was considered acceptable for samples with very low abundance (Scheder et al., 2019). The analysed and residual materials were weighed to allow for extrapolation and calculation of microfaunal concentration. Species identification of foraminifers follows illustrations and taxonomic descriptions in Gehrels and Newman (2004), Horton and Edwards (2006), Murray (2006) and ostracod species were identified based on descriptions in Athersuch et al. (1989) and Frenzel et al. (2010). Due to problematic discrimination of juvenile individuals of *Leptocythere*, species were grouped under *Leptocythere* spp. for counting.

Sample material for sedimentological and geochemical analyses was dried (drying cabinet, 40 °C) and carefully pestled by hand. Pre-treatment for grain-size analysis included the dissolution of carbonates with hydrochloric acid (HCl; 10%) and of organic matter with hydrogen peroxide (H_2O_2; 15%), as well as the treatment with sodium pyrophosphate ($Na_4P_2O_7$; 46 g/l) in order to prevent aggregation. Afterwards, the grain-size distribution was measured on the <2 mm fraction using a laser particle size analyser (Beckman Coulter LS 13320; laser beam 780 nm) applying the Fraunhofer optical mode (Eshel et al., 2004). The grain-size distribution is an important tool in the interpretation of hydro-energetic levels and sediment origin and can be related to microfaunal associations, since species often prefer specific substrates (Blott et al., 2004; Frenzel et al., 2010).

The concentration of total organic carbon (TOC, accounting for c. 50% of the organic matter) was measured after grinding the samples to determine the organic content using an elemental analyser (elementar, Vario EL Cube). This enabled the simultaneous measurement of nitrogen (N) and the determination of total inorganic carbon (TIC, accounting for c. 12% of the calcium carbonate [$CaCO_3$]). The finally derived C/N ratio provides information about the origin of organic matter (aquatic/terrestrial) (Last and Smol, 2001).

6.S1.2 Data processing – Core drillings

Univariate statistical grain-size measures after Folk and Ward (1957) were calculated using GRADISTAT software (Blott and Pye, 2001). Spearman's correlation coefficients were calculated between microfaunal data and environmental parameters (sand amount, mean grain size, TOC, TIC, N, C/N) to detect possible auto-correlations. Foraminifer and ostracod distributions and environmental parameters where subsequently analysed by means of multivariate statistics (PCA) in order to evaluate driving factors and support facies identification (for details, see Elschner et al., 2021). Following the latter, intertidal and supratidal facies were used for the application of the TF by means of the software C2 (Juggins, 2007).

6.S2. Results – modern samples and core drillings

6.S2.1 Microfauna – taxa and ecological information

Species list

Superdomain Biota

Kingdom Animalia
1 Phylum Arthropoda
1 Subphylum Crustacea
1 Superclass Oligostraca
1.1 Class **Ostracoda**
1.2 Subclass Podocopa
1.2.1 Order Podocopida
1.2.1.1 Suborder Cytherocopina
1.2.1.1.1 Superfamily Cytheroidea (Baird, 1850)
1.2.1.1.1.1 Family Cushmanideidae (Puri, 1974)
Cushmanidea elongata (Brady, 1868)
Ecology: shallow marine, lagoons and open sea; euryhaline (Frenzel et al., 2010); sublittoral, on sandy substrate; estuaries to open sea (Athersuch et al., 1989)
1.2.1.1.1.2 Family Cytherideidae (Sars, 1925)
Cyprideis torosa (Jones, 1850)
Ecology: common in brackish waters, but found in a wide range from almost freshwater to salinities up to 60 psu, inland ponds, lakes, marginal marine environments (e.g. lagoons, estuaries), prefers mud or sandy mud (Athersuch et al. 1989); very shallow to shallow waters, salt marshes (Frenzel et al., 2010).
1.2.1.1.1.3 Family Cytheruridae (Müller, 1894)
Semicytherura (Wagner, 1957)
Ecology: differing between species; mainly very shallow to shallow marine; open sea, phytal zone (Frenzel et al., 2010)
Semicytherura striata (Sars, 1866)
Ecology: shallow to deep, open sea, phytal, sand, pebbles and shelly, endobenthic, polyhaline to euhaline (Frenzel et al. 2010)
1.2.1.1.1.4 Family Krithidae (Mandelstam, 1958)
Krithe (Crosskey & Robertson, 1874)

Ecology: open sea, deep marine; polyhaline to euryhaline (Frenzel et al., 2010)

1.2.1.1.1.5 Family Leptocytheridae (Hanai, 1957)

Leptocythere (Sars, 1925)

Ecology: useful environmental indicator, some species exclusively marine (e.g. L. pellucida), others typical for inner estuarine and salt marsh environments (e.g. L. castanea, L. lacertosa), differentiation between species is difficult (Athersuch et al., 1989), therefore this study summarises occurring Leptocythere species with Leptocythere spp.

1.2.1.1.1.6 Family Neocytherideididae (Puri, 1957)

Sahnicythere retroflexa (Klie, 1936)

Ecology: fine-sandy substrate, littoral to sublittoral (Athersuch et al., 1989)

1.2.1.1.1.7 Family Paradoxostomatidae (Brady & Norman, 1889)

Cytherois fischeri (Sars, 1866)

Ecology: very shallow to shallow, lagoons and open sea, salt marsh, sediment and phytal, endobenthic, high oxygen (Frenzel et al. 2010)

Cytherois pusilla (Sars, 1928)

Ecology: very shallow to shallow, lagoons and open sea (Frenzel et al., 2010); shallow marine, living amongst littoral algae (Athersuch et al., 1989).

Kingdom Chromista

Subkingdom Harosa

Infrakingdom Rhizaria

2 Phylum **Foraminifera**

2.1 Class Globothalamea

2.2 Subclass Textulariia

2.2.1 Order Lituolida

2.2.1.1 Suborder Trochamminina

2.2.1.1.1 Superfamily Trochamminoidea (Schwager, 1877)

2.2.1.1.1.1 Family Trochamminidae (Schwager, 1877)

2.2.1.1.1.1.1 Subfamily Jadammininae (Saidova, 1981)

Entzia macrescens (Brady, 1870)

Ecology: Euryhaline species, land-bound parts of salt marshes, sand flats also, in 0.1 to 0.3 m water depth and 8.5 to 19 psu on mud to medium sand and within the phytal zone of the southern Baltic; extremely euryhaline (Lehmann 2000); controlled more by substrate than salinity (Murray 2006).

2.2.1.1.1.1.2 Subfamily Polystomammininae (Brönnimann & Beurlen, 1977)

Deuterammina balkwilli (Brönnimann & Whittaker, 1983)

Ecology: Epifaunal, attached mobile, sediment, normal marine, shelf (Murray 2006).

2.2.1.1.1.1.3 Subfamily Trochammininae (Schwager, 1877)

Trochammina inflata (Montagu, 1808)

Ecology: Euryhaline brackish water species, shallow water, typical for salt marshes (Lehmann, 2000); high and middle marsh environments (Horton and Edwards 2006).

2.2.2 Order Rotaliida

2.2.2.1.1 Superfamily Rotalioidea (Ehrenberg, 1839)

2.2.2.1.1.1 Family Ammoniidae (Saidova, 1981)

2.2.2.1.1.1.1 Subfamily Ammoniinae (Saidova, 1981)

Ammonia tepida (Cushman, 1926)

Ecology: sheltered, shallow marine, often slightly brackish, intertidal environments, may extend onto low and mid marshes (Murray 2006).

2.2.2.1.1.2 Family Elphidiidae (Galloway, 1933)

2.2.2.1.1.2.1 Subfamily Elphidiinae (Galloway, 1933)

Cribroelphidium williamsoni (Haynes, 1973)

Ecology: shallow parts of intertidal mud flats, estuaries, lagoons and sea-bound parts of salt marshes (Murray 2006); mainly less than 20 cm water depth, found in 0.1 to 0.5 m water depth and between 8 and 19 psu on mud to medium sand, also within the phytal zone, brackish water species, mainly temperate climate (Lehmann, 2000).

2.2.2.1.1.3 Family Haynesinidae (Mikhalevich, 2013)

Haynesina germanica (Ehrenberg, 1840)

Ecology: middle and low marshes, tidal flats (Horton and Edwards 2006); shallow marine, intertidal environments, may extend onto low and mid marshes (Murray 2006).

2.3 Class Tubothalamea

2.3.1 Order Miliolida

2.3.1.1 Suborder Miliolina

2.3.1.1.1 Superfamily Cornuspiroidea (Schultze, 1854)

2.3.1.1.1.1 Cornuspiridae (Schultze, 1854)

Cornuspira involvens (Reuss, 1850)

Ecology: epifaunal, widespread in marginal marine and shelf environments in low abundance (Murray, 2006)

2.3.1.1.2 Superfamily Miliolacea (Ehrenberg, 1839)

2.3.1.1.2.1 Family Miliamminidae (Saidova, 1981)

Miliammina fusca (Brady, 1870)

Ecology: salt marshes and lagoons, brackish (Murray, 2006)

2.3.1.1.3 Superfamily Milioloidea (Ehrenberg, 1839)

2.3.1.1.3.1 Family Hauerinidae (Schwager, 1876)

2.3.1.1.3.1.1 Subfamily Miliolinellinae (Vella, 1957)

Triloculina oblonga (Montagu, 1803)

Ecology: Salt marshes (Lehmann 2000).

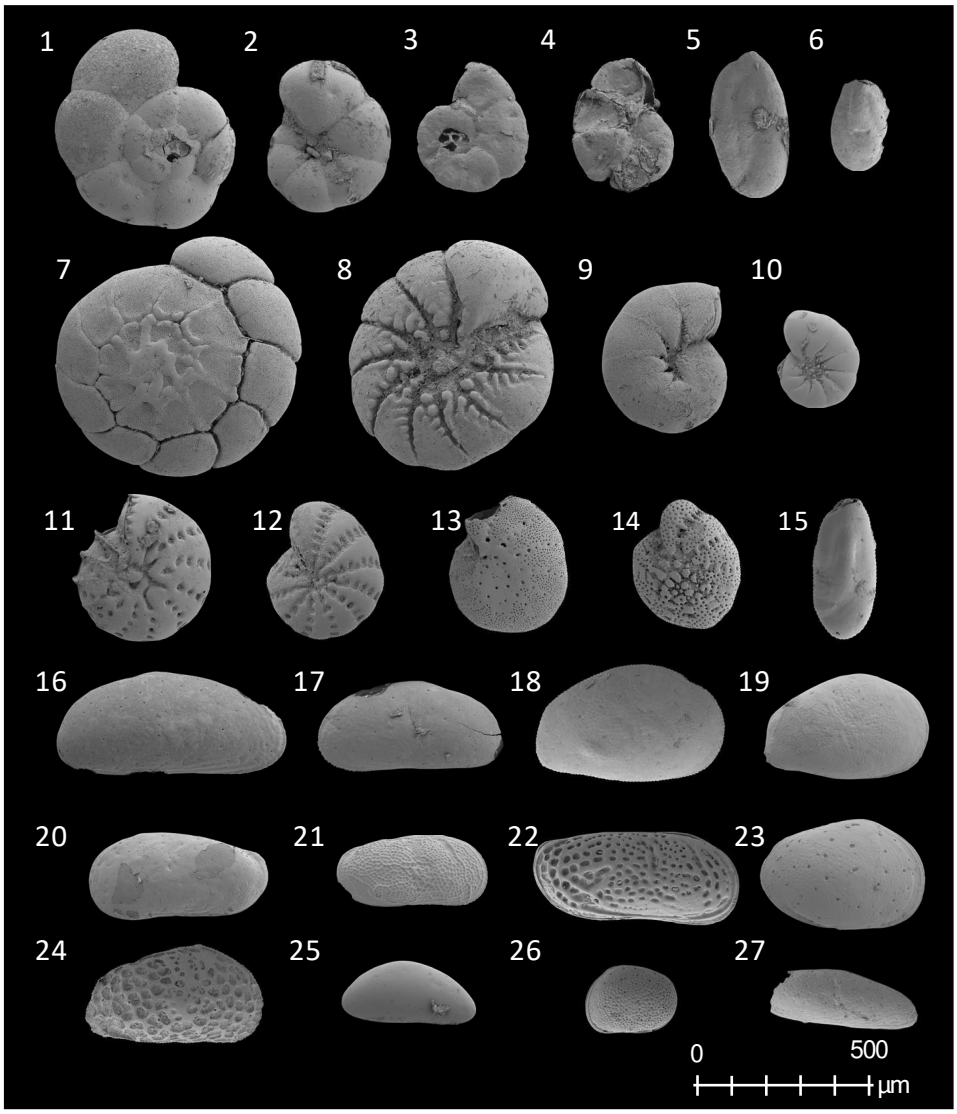

Fig. 6.S1.1 SEM images of frequently documented foraminifer (1–15) and ostracod (16–27) species. 1, 2: *Trochammina inflata* (Montagu, 1803); 3, 4: *Entzia macrescens* (Brady, 1870); 5, 6: *Miliammina fusca* (Brady, 1870); 7, 8: *Ammonia tepida* (Cushman, 1926); 9, 10: *Haynesina germanica* (Ehrenberg, 1840); 11, 12: *Cribroelphidium williamsoni* (Haynes, 1973); 13, 14: *Elphidium* spp. (Montfort, 1808): 13: *E. cuvillieri* (Levy, 1966), 14: *E. gunteri* (Cole, 1931); 15: *Triloculina oblonga* (Montagu, 1803); 16, 17: *Cushmanidea enlongata* (Brady, 1868), 17: juvenile; 18, 19: *Cyprideis torosa* (Jones, 1850), juvenile; 20-22: *Leptocythere* (Sars, 1925): 20: *L. lacertosa* (Hirschmann, 1912), juvenile, 21: *L. castanea* (Sars, 1866), juvenile, 22: *L. pellucida* (Baird, 1850); 23: *Loxoconcha elliptica* (Brady, 1868), juvenile; 24: *Urocythereis britannica* (Athersuch, 1977), juvenile; 25: *Cytherois* cf. *pusilla* (Sars, 1928), juvenile; 26: *Hirschmannia viridis* (Mueller, 1785) juvenile; 27: *Sahnicythere retroflexa* (Klie, 1936), juvenile. Not all species documented here are representated in the results of each core, since rare species were excluded for this paper. Depiction after Elschner et al. (2021).

6.S2.2 Results of modern samples

Additional surface transect

Tab. 6.S2.1 List of foraminifers, mean density (ind./m2) of A) living foraminifers and B) dead foraminifers and standard deviation (SD) of foraminiferal species of the 11 transect stations.

A) Density of living foraminifera (ind./ m^2)

Living species	Transect 1		Transect 2		Transect 3		Transect 4		Transect 5		Transect 6		Transect 7		Transect 8		Transect 9		Transect 10		Transect 11	
>63 µm	Mean	SD	Mean	SD	Mean	SD	Mean	SD	Mean	SD	Mean	SD	Mean	SD	Mean	SD	Mean	SD	Mean	SD	Mean	SD
Agglutinated species																						
Trochammina inflata	12902	8233.25	58400	20098.54	120195	12223.20	120195	42096.66	54325	37138.18	12223	7345.23	16298	8148.80	4074	0.00						
Jadammina macrescens	6791	8233.25	30558	17759.90	22409	16675.20	52967	12223.20	23088	15425.43	9167	4321.55	21730	2352.36								
Miliammina fusca			4074	0.00	2037	0.00	7470	7712.71	14260	0.00	6112	7057.07	4074	0.00								
Deuterammina balkwilli					4074	0.00			6112	0.00												
Miolid species																						
Cornuspira involvens			4074	0.00	2037	0.00	14260	13358.81	6112	5389.92	27502	21607.77	4074	0.00								
Triloculina oblonga	4074	2881.04	184706	35422.29	107293	32360.93	392501	199212.05	157543	71920.18	88279	24559.32	28521	7057.07								
Hyalin species																						
Ammonia tepida			17656	16592.03	175878	177614.56	617951	370352.28	526956	365933.14	324594	190130.18	12223	0.00	5433	2352.36	4074	0.00			4074	0.00
Elphidium excavatum	2037	0.00	24446	0.00	4074	0.00	6112	7057.07	5093	1440.52	5433	1176.18	74697	47223.22	14939	15425.43			25805	24895.00	130381	138349.73
Elphidium williamsoni																			40744	0.00		
Elphidium incertum																					48893	0.00
Elphidium albiumbilicatum	2037	0.00																	4074	0.00		
Haynesina germanica	2037	0.00	16298	0.00	4074	0.00	6791	2352.36	29879	11220.02	27842	8481.54	17656	8481.54	12223	4074.40	4074	0.00	14939	15425.43	36670	18671.25

B) Density of dead foraminifera (ind./ m^2)

Dead species	Transect 1		Transect 2		Transect 3		Transect 4		Transect 5		Transect 6		Transect 7		Transect 8		Transect 9		Transect 10		Transect 11	
>63 µm	Mean	SD	Mean	SD	Mean	SD	Mean	SD	Mean	SD	Mean	SD	Mean	SD	Mean	SD	Mean	SD	Mean	SD	Mean	SD
Agglutinated species																						
Trochammina inflata	17656	3111.87	74018	16466.49	122911	81343.57	74018	40811.85	25125	7712.71	17656	3111.87	12223	5762.07								
Jadammina macrescens	23767	26273.83	34632	14690.46	43460	45795.48	63832	19254.86	31916	21783.12	21051	9186.24	33953	4704.71								
Miliammina fusca			7470	4240.77	9507	3111.87	31916	23611.61	21730	14737.47	11544	7154.41										
Deuterammina balkwilli			4074	0.00	4074	0.00			2037	0.00												
Miolid species																						
Cornuspira involvens					8149	0.00	4753	3111.87	6112	5762.07	12223	0.00	5433	2352.36								
Triloculina oblonga	2037	0.00	47535	27128.69	110009	59184.08	198967	60100.28	137851	66211.61	66549	42942.58	29879	30580.63								
Hyalin species																						
Ammonia tepida			16298	20167.25	169088	124719.24	427812	154249.81	626779	450457.74	208473	204911.67	14939	9409.42	6112	2881.04	8149	5762.07			4074	0.00
Elphidium excavatum			7470	2352.36	6112	3528.53	16298	17759.90	47874	21607.77	21730	18485.09	154827	72428.12	10186	2881.04	19014	2352.36	36670	28520.80	70623	27733.87
Elphidium williamsoni													4074	0.00							57042	74906.93
Elphidium incertum																						
Elphidium albiumbilicatum							2037	0.00									4074	0.00				
Haynesina germanica			8828	11761.78	36670	20064.09	37349	19254.86	96427	65486.82	84883	88854.00	38028	16466.49	10186	8643.11	32595	14690.46	8149	0.00	5433	2352.36

Tab. 6.S2.2 Total organic carbon (TOC) values of the 11 transect stations

Transect	Zonation	TOC [%]
T1	upper salt marsh	6.90
T2		6.45
T3	lower salt marsh/ transition zone	5.08
T4		4.62
T5		4.61
T6		4.48
T7		1.80
T8		0.53
T9	tidal flat	0.39
T10		0.20
T11		0.22

Tab. 6.S2.3 Replicated oxygen values (n=3), mean oxygen ± standard deviation (SD) of the 11 transect stations.

Transect	Zonation	Replicate	O_2 [µmol/l]	O_2 mean [µmol/l]	O_2 SD [µmol/l]
T1	upper salt marsh	1	259.2	208.8	44.73
		2	193.4		
		3	173.8		
T2		1	280.4	171.8	94.14
		2	122.2		
		3	112.9		
T3	lower salt marsh/ transition zone	1	243.3	154.4	77.01
		2	111.7		
		3	108.2		
T4		1	266.3	273.2	6.13
		2	275.1		
		3	278.1		
T5		1	64.3	128.3	56.27
		2	169.9		
		3	150.8		
T6		1	279.8	259.9	35.77
		2	218.6		
		3	281.3		
T7		1	225.1	244.1	22.13
		2	238.8		
		3	268.4		
T8		no measurement			
T9	tidal flat	1	177.6	169.3	34.70
		2	199.1		
		3	131.2		
T10		1	304.1	270.5	30.36
		2	262.5		
		3	245.0		
T11		1	260.2	279.0	17.60
		2	295.1		
		3	281.6		

Combined dataset

Tab. 6.S2.4 Foraminifer- and ostracod counts of the combined dataset (Scheder et al. 2019 and additional transect).

sample no.	elevation [m NHN]	*T. inflata*	*T. oblonga*	*E. macrescens*	*M. fusca*	*C. involvens*	*A. tepida*	*C. williamsoni*	*H. germanica*	*C. torosa*	*Leptocythere* spp.	*C. pusilla*
2015/02	0.468	0	0	0	0	0	1	1	0	0	4	0
2015/03	0.629	0	0	0	0	0	0	0	0	0	2	0
2015/04	0.757	1	0	0	0	0	9	9	10	0	0	0
2015/05	0.903	108	69	28	0	0	9	6	23	0	7	2
2015/06	0.359	0	0	0	0	0	1	0	0	0	0	0
2015/07	0.209	0	0	0	0	0	3	0	11	0	0	0
2015/08	0.040	0	0	0	0	0	1	1	0	0	0	0
2015/09	-0.102	0	0	0	0	0	0	1	1	0	0	0
2015/10	-0.259	0	0	0	0	0	0	0	0	0	0	0
2015/11	-0.391	0	0	0	0	0	11	12	46	0	0	2
2015/12	-0.519	1	0	0	0	0	30	11	89	0	0	0
2017/12	-0.518	0	0	0	0	0	51	5	71	0	1	0
2015/13	-0.661	0	0	0	0	0	45	8	226	0	2	0
2015/14	-0.803	0	0	0	0	0	28	15	110	1	3	1
2015/15	-0.982	1	0	0	0	0	27	9	89	0	0	0
2015/16	-1.126	0	0	0	0	0	44	21	156	0	2	1
2015/17	-1.206	0	0	0	0	0	58	17	230	0	4	2
2015/18	0.430	0	0	0	0	0	6	8	4	0	0	0
2017/18	-1.340	0	0	0	0	0	73	4	36	0	0	0
2015/19	0.693	1	10	0	7	0	41	35	93	50	22	12
2015/20	1.027	38	78	96	21	8	26	1	17	0	0	0
2017/20	1.178	6	15	0	6	0	180	42	66	2	8	4
2017/22	1.329	12	44	1	5	0	74	4	10	0	2	0
2017/24	1.478	25	87	20	13	4	30	5	9	0	0	0
1A	1.934	10	0	26	0	0	0	0	0	0	0	0
1B	1.929	7	1	8	0	0	0	0	0	0	1	0
1C	1.925	9	0	1	0	0	0	0	0	0	0	0
2A	1.459	41	32	25	6	0	15	5	11	0	8	0
2B	1.482	43	30	15	2	0	0	3	1	0	5	0
2C	1.506	27	8	11	3	0	1	3	1	0	4	2
3A	1.398	32	56	2	5	0	147	5	29	0	5	0
3B	1.395	45	24	16	3	0	25	2	10	0	5	0
3C	1.392	106	82	46	6	4	77	2	15	0	9	0
4A	1.374	21	110	28	10	1	222	4	15	0	2	0
4B	1.322	59	119	42	30	4	279	18	29	0	5	0
4C	1.269	29	64	24	8	2	129	2	12	0	7	0

Continued on next page

sample no.	elevation [m NHN]	*T. inflata*	*T. oblonga*	*E. macrescens*	*M. fusca*	*C. involvens*	*A. tepida*	*C. williamsoni*	*H. germanica*	*C. torosa*	*Leptocythere* spp.	*C. pusilla*
5A	1.262	8	35	4	6	1	226	31	84	0	1	1
5B	1.253	14	68	18	19	0	139	5	24	0	12	0
5C	1.243	13	100	23	4	0	558	16	34	0	16	0
6A	1.264	10	27	10	6	0	61	12	18	0	12	0
6B	1.269	9	15	6	2	6	29	1	15	0	11	0
6C	1.274	7	56	15	9	0	217	19	92	0	6	0
7A	1.107	4	3	9	0	1	5	19	5	0	8	2
7B	1.141	2	16	7	0	1	5	45	12	0	17	0
7C	1.176	0	3	9	0	1	2	51	11	0	2	0
8A	0.794	0	0	0	0	0	1	2	1	0	27	4
8B	0.791	0	0	0	0	0	0	0	0	0	38	0
8C	0.788	0	0	0	0	0	2	3	4	0	34	2
9A	0.707	0	0	0	0	0	3	5	4	0	20	13
9B	0.666	0	0	0	0	0	0	6	9	0	13	7
9C	0.625	0	0	0	0	0	1	6	11	0	35	8
10A	0.813	0	0	0	0	0	0	16	0	0	12	0
10B	0.794	0	0	0	0	0	0	9	0	0	16	0
10C	0.774	0	0	0	0	0	0	2	2	0	23	0
11A	0.929	0	0	0	0	0	1	25	1	0	62	1
11B	0.909	0	0	0	0	0	1	16	2	0	41	2
11C	0.890	0	0	0	0	0	0	28	12	0	46	1

6.S2.3 Sedimentological, geochemical and microfaunal results of core drillings

Figures 6.S2.2–6.S2.8 show the detailed results of sedimentological, geochemical and microfaunal investigations. For detailed results of VVC17, please see Bulian et al. (2019). The location of cores is indicated in Fig. 1 of the main text.

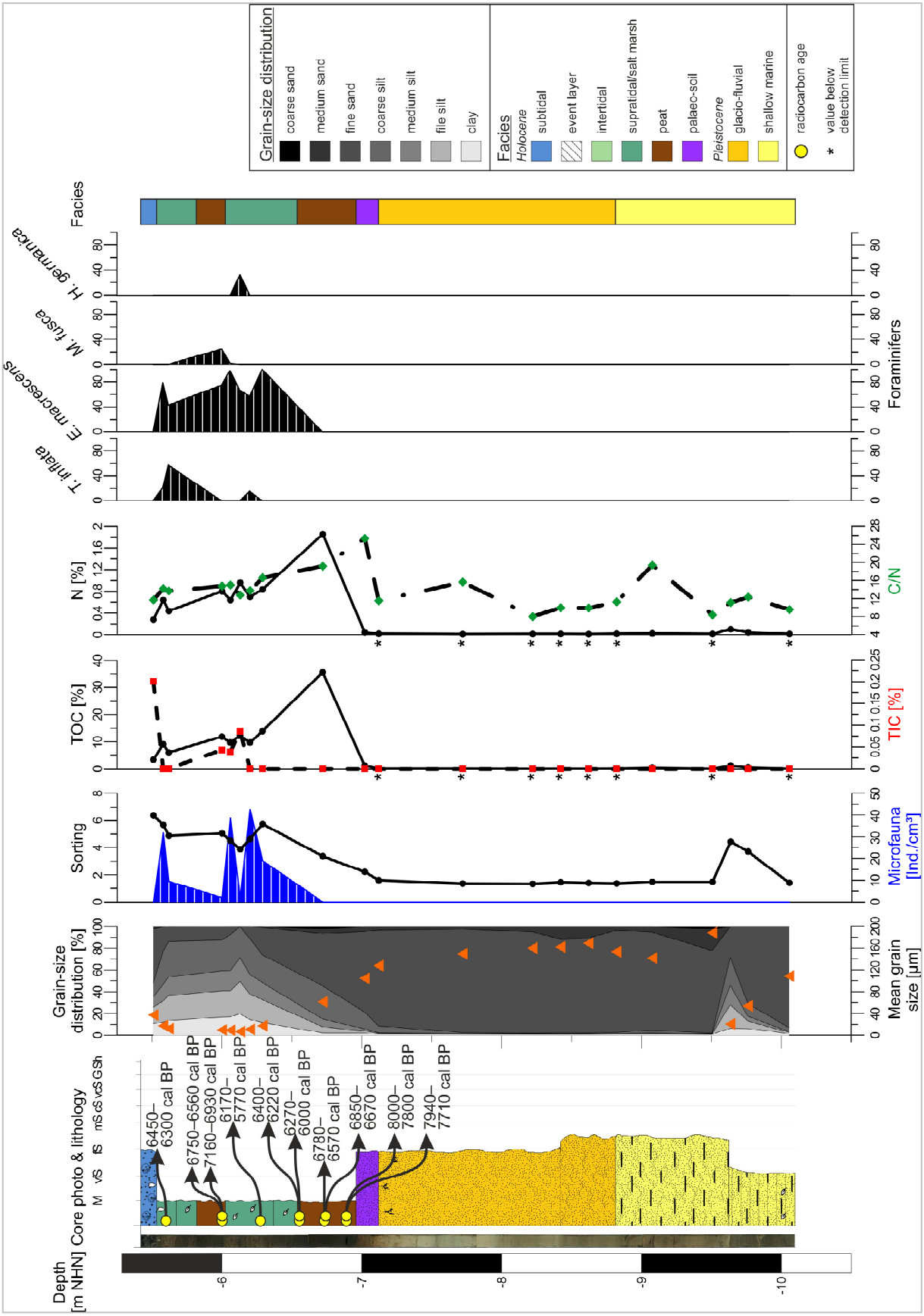

Fig. 6.S2.2 Sedimentological, geochemical and microfaunal results as well as facies interpretation of VVC16.

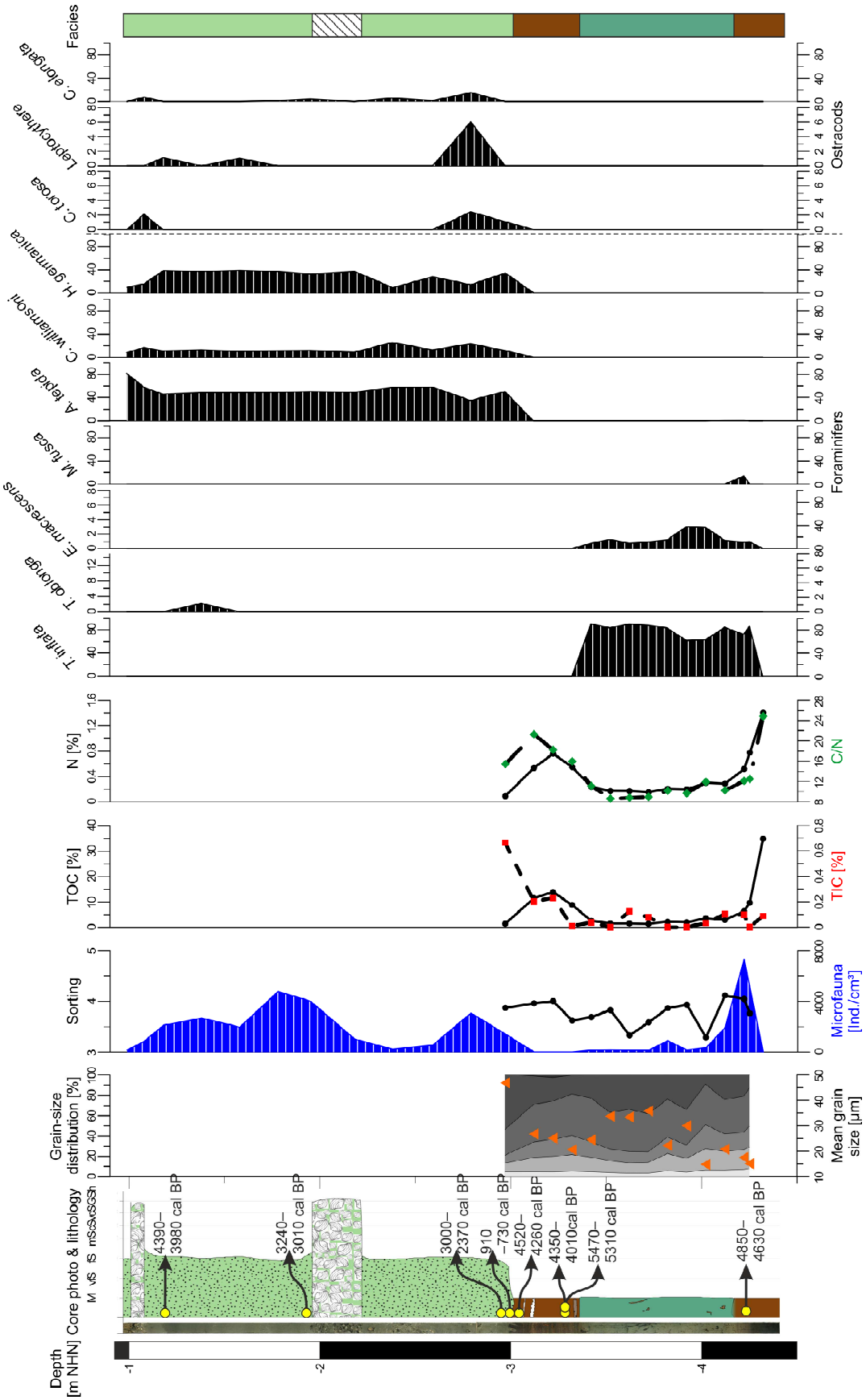

Fig. 6.S2.3 Sedimentological, geochemical and microfaunal results as well as facies interpretation of N49. Legend in Fig. 6.S2.2.

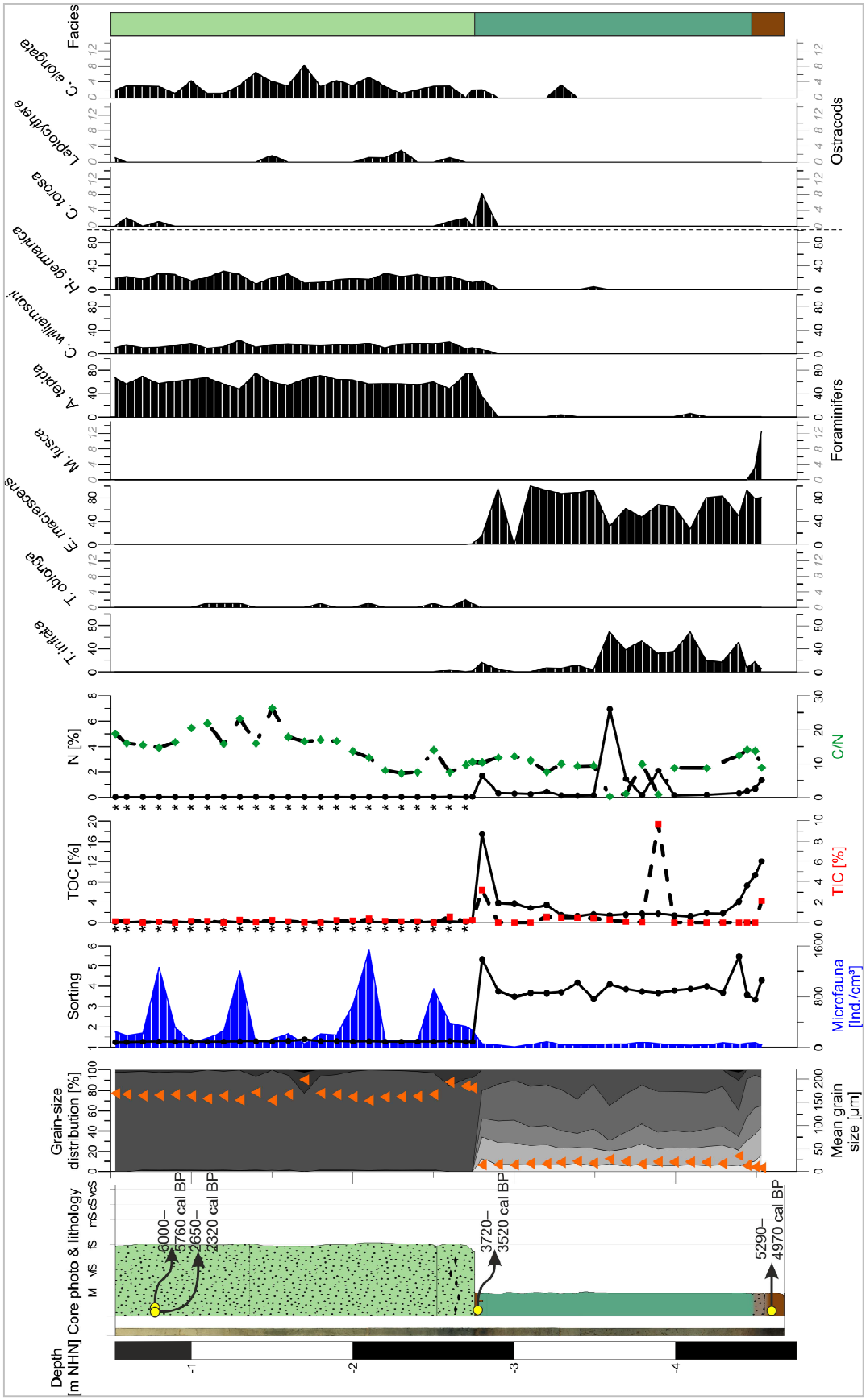

Fig. 6.S2.4 Sedimentological, geochemical and microfaunal results as well as facies interpretation of N43. Legend in Fig. 6.S2.2.

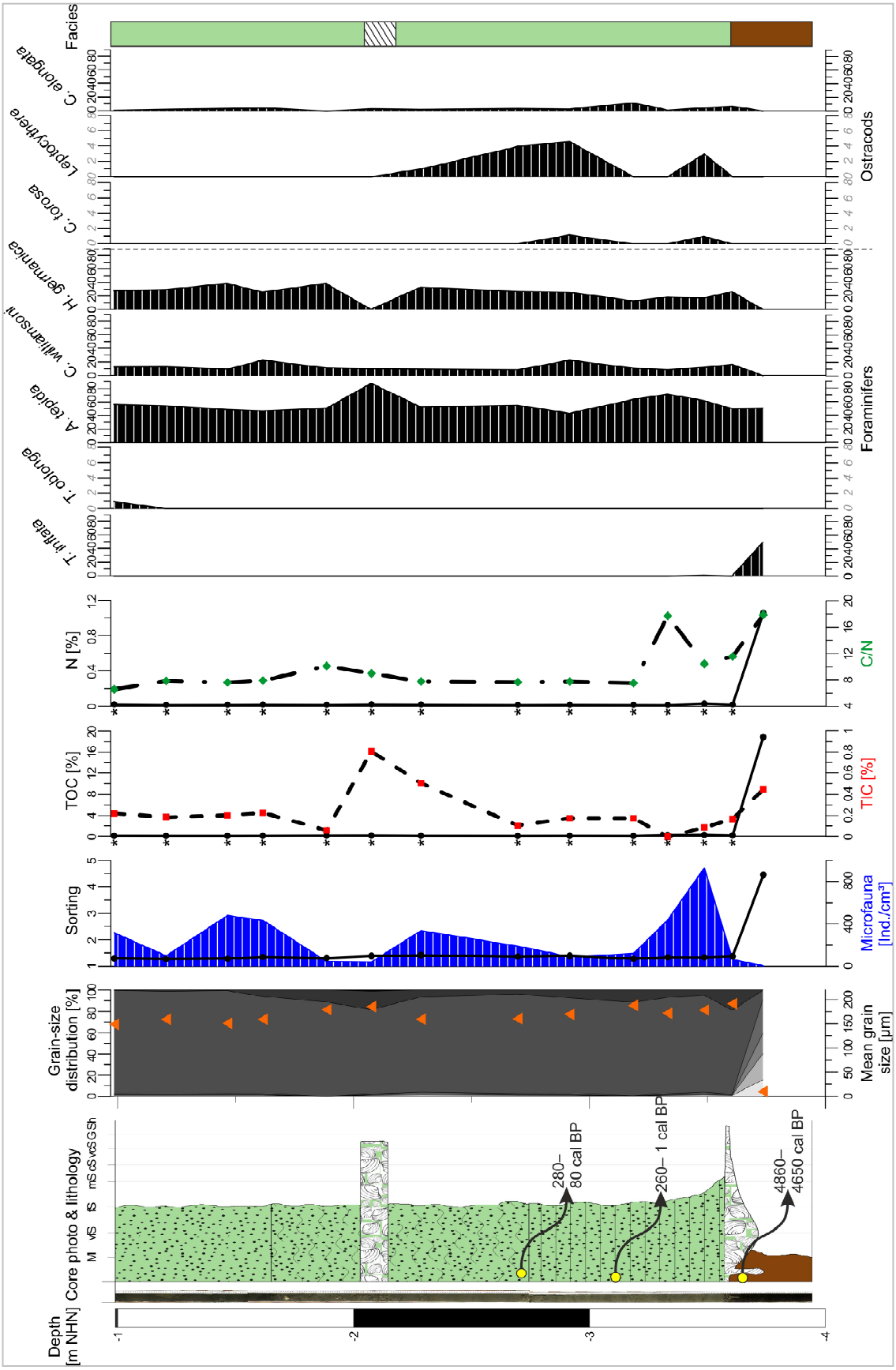

Fig. 6.S2.5 Sedimentological, geochemical and microfaunal results as well as facies interpretation of VC03. Legend in Fig. 6.S2.2.

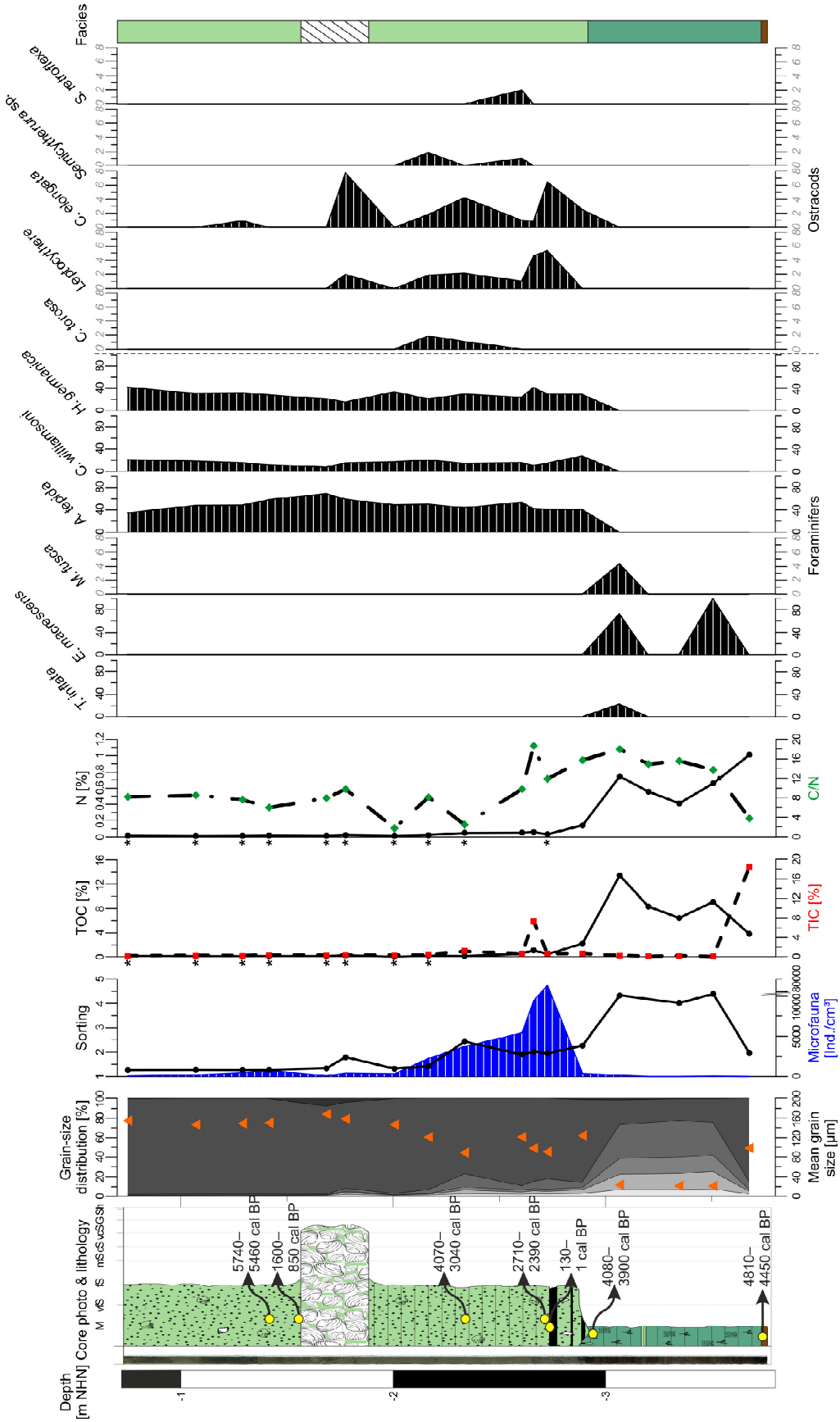

Fig. 6.S2.6 Sedimentological, geochemical and microfaunal results as well as facies interpretation of VC13. Legend in Fig. 6.S2.2.

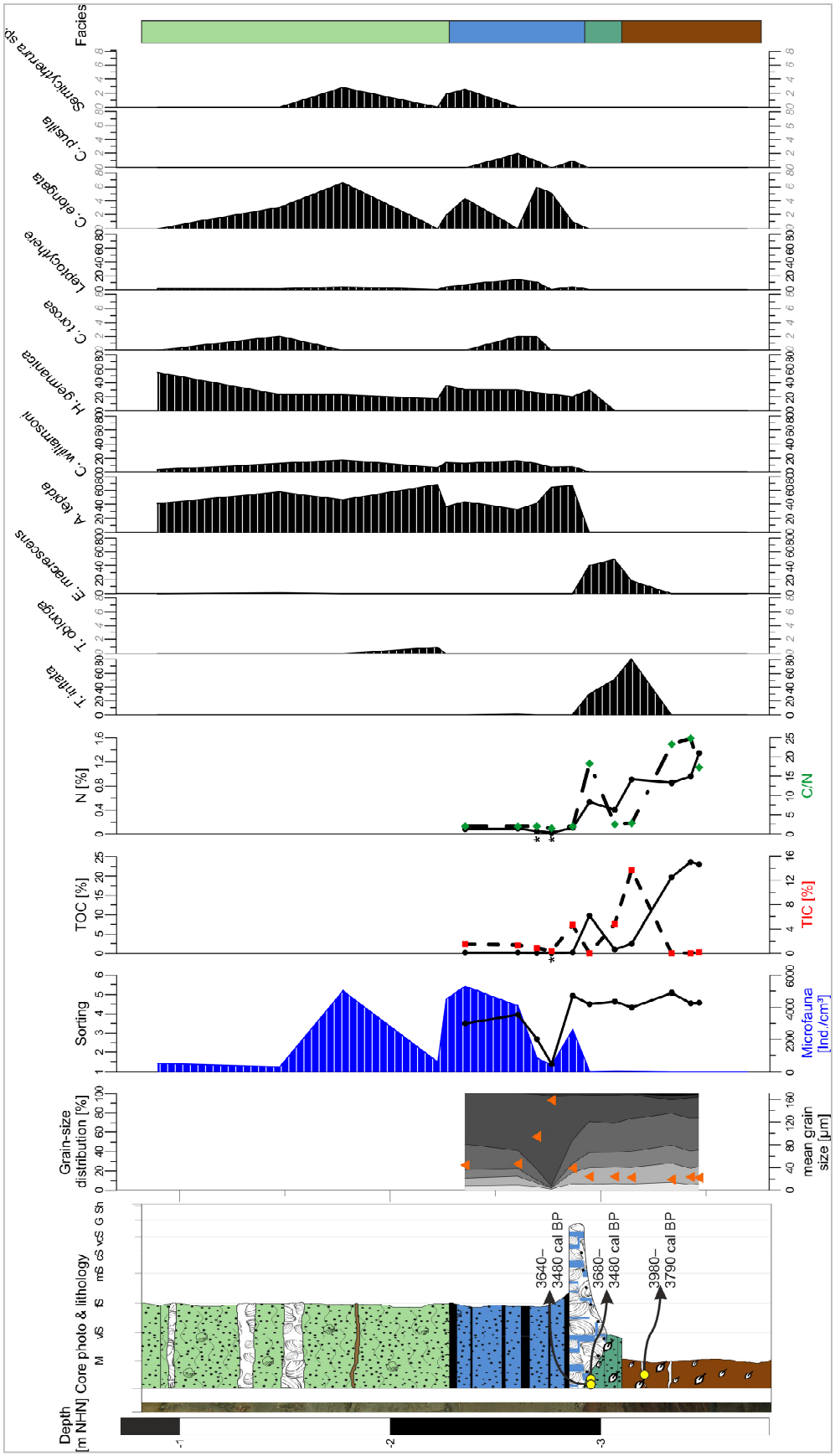

Fig. 6.S2.7 Sedimentological, geochemical and microfaunal results as well as facies interpretation of N44. Legend in Fig. 6.S2.2.

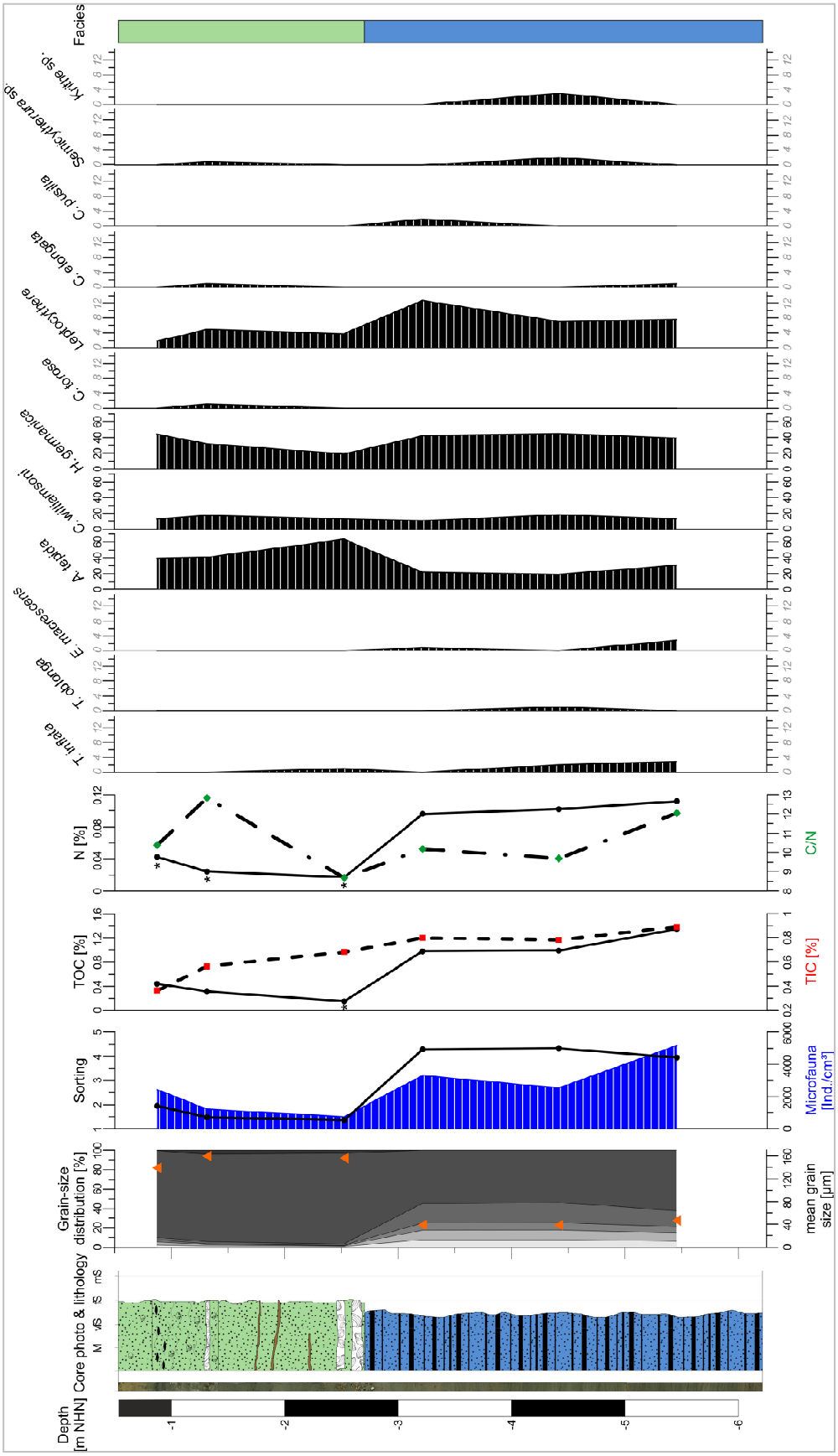

Fig. 6.S2.8 Sedimentological, geochemical and microfaunal results as well as facies interpretation of N45. Legend in Fig. 6.S2.2.

Athersuch, J., Horne, D.J., Whittaker, J.E., 1989. Marine and brackish water ostracods (superfamilies Cypridacea and Cytheracea): keys and notes for the identification of the species. Brill Archive.

Blott, S.J., Croft, D.J., Pye, K., et al., 2004. Particle size analysis by laser diffraction. Forensic Geoscience: Principles, Techniques and Applications. https://doi.org/10.1144/GSL.SP.2004.232.01.08

Blott, S.J., Pye, K., 2001. GRADISTAT: a grain size distribution and statistics package for the analysis of unconsolidated sediments. Earth Surface Processes and Landforms 26, 1237–1248. https://doi.org/10.1002/esp.261

Bulian, F., Enters, D., Schlütz, F., et al., 2019. Multi-proxy reconstruction of Holocene paleoenvironments from a sediment core retrieved from the Wadden Sea near Norderney, East Frisia, Germany. Estuarine, Coastal and Shelf Science 225, 106251. https://doi.org/10.1016/j.ecss.2019.106251

Elschner, A., Scheder, J., Enters, D., et al., 2021. Microfauna- and sedimentology-based facies analysis for palaeo-landscape reconstruction in the back-barrier of Norderney (NW Germany). Netherlands Journal of Geosciences 100, e4.

Eshel, G., Levy, G., Mingelgrin, U., et al., 2004. Critical Evaluation of the Use of Laser Diffraction for Particle-Size Distribution Analysis. Reproduced from Soil Science Society of America Journal. Published by Soil Science Society of America. All copyrights reserved 68, 736–743. https://doi.org/10.2136/sssaj2004.0736

Folk, R.L., Ward, W.C., 1957. Brazos River bar [Texas]; a study in the significance of grain size parameters. Journal of Sedimentary Research 27, 3–26. https://doi.org/10.1306/74D70646-2B21-11D7-8648000102C1865D

Frenzel, P., Keyser, D., Viehberg, F.A., 2010. An illustrated key and (palaeo)ecological primer for Postglacial to Recent Ostracoda (Crustacea) of the Baltic Sea. Boreas 39, 567–575. https://doi.org/10.1111/j.1502-3885.2009.00135.x

Gehrels, W.R., Newman, S.W.G., 2004. Salt-marsh foraminifera in Ho Bugt, western Denmark, and their use as sea-level indicators. Geografisk Tidsskrift-Danish Journal of Geography 104, 97–106. https://doi.org/10.1080/00167223.2004.10649507

Horton, B., Edwards, R., 2006. Quantifying Holocene Sea Level Change Using Intertidal Foraminifera: Lessons from the British Isles, Cushman Foundation for Foraminiferal Research, Special Publication No. 40.

Juggins, S., 2007. C2 Version 1.5: software for ecological and palaeoecological data analysis and visualisation. University of Newcastle, Newcastle upon Tyne.

Last, W.M., Smol, J.P., 2001. Tracking Environmental Change Using Lake Sediments. Volume 2: Physical and Geochemical Methods. Kluwer Academic Publishers, Dordrecht. https://doi.org/10.1007/0-306-47669-X

Murray, J.W., 2006. Ecology and Applications of Benthic Foraminifera. Cambridge University Press, Cambridge.

Scheder, J., Frenzel, P., Bungenstock, F., et al., 2019. Vertical and lateral distribution of Foraminifera and Ostracoda in the East Frisian Wadden Sea – developing a transfer function for relative sea-level change. Geologica Belgica 22, 99–110. https://doi.org/10.20341/gb.2019.007

Chapter 7

7 Discussion

This research deals with coastal environments in NW Germany that were exposed to coastal and RSL changes during the Holocene. Detailed investigations were carried out in order to reconstruct the Holocene landscape evolution and to draw conclusions on RSL changes. Furthermore, a novel approach for directly reconstructing RSL histories for the East Frisian island of Norderney led to a new RSL curve, which can now help to determine between the local and regional differences of the underlying processes.

7.1 Holocene coastal changes in NW Germany

Hypothesis 1 – The reconstruction of Holocene coastal changes in the southern North Sea region can be connected to the RSL evolution

Objective A: Reconstructing Holocene landscape changes in the 'Land Wursten' region

During the Holocene, the 'Land Wursten' region (Chapter 2) was subject to significant landscape changes. It is a representive marsh environment which formed during the Holocene transgression. The *dwog* horizons, fossil bog soils, which were buried during marine inundations, provide evidence for RSL changes and sometimes can be connected to coastal progradation, when laterally transitioning into intercalated peat layers (Bungenstock and Weerts, 2012). As soil formation requires stable landscape conditions over a certain time, *dwog* horizons are important for the reconstruction of Holocene coastal changes. In the wet depressions of the marshlands, they are dependent on a falling groundwater level, which in coastal areas is directly related to RSL. Therefore, aside from their importance for archaeological investigations due to their potential of carrying settlements (Streif, 1990), they also enable to draw conclusions on the local RSL development.

Analyses of archive core data from the 'Landesamt für Bergbau, Energie und Geologie' (LBEG, Hannover) for correlation proved to be challenging due to different and partially incomplete facies descriptions (as a result of different processors). However, based on three newly conducted drillings in the area, a calibration of the archive data was possible and the palaeo-landscape could be reconstructed over an area of ~4 km².

The investigated sedimentary record originates in the Holocene; this was determined as none of the drillings reached the Holocene base. Salt-marsh deposits were documented in

the west of the study area (LAN 3), mainly identified from their high mud content indicating an environment of mid-energetic levels. Lamination reflecting occasional inundations supports this interpretation (Bungenstock and Weerts, 2012), although the microfaunal associations do not contain the typical salt-marsh species but rather shallow-marine species tolerant of brackish waters and also occuring in salt marshes (Horton and Edwards, 2006; Murray, 2006). The position only ~1.5 m above the modelled Holocene base, suggests that this salt marsh might have developed from the local basal peat following the rising marine influence of the slowly ingressing sea. However, one of the archive cores (146) in the southeastern part of the study area documents a tidal-flat deposit below this salt-marsh layer. Although the possibility of an incorrect identification due to problematic descriptions in the archive material remains, sequences like this have been discussed earlier in terms of pro- and retrograding coastlines, which would be connected to the ratio of accommodation space and sediment supply (A/S ratio) (Bungenstock and Weerts, 2010, 2012). By assuming an increased sediment supply, the development of a salt marsh on top of this tidal-flat layer is reasonable. Several explanations are possible: repeated marine inundations depositing sediments in the higher, vegetated zones of the tidal flats could have initiated the vertical and lateral growth of the salt-marsh areas; or the deceleration of the RSL rise could have caused a smaller A/S ratio, resulting in coastline progradation (Bungenstock and Weerts, 2012). Due to the proximity of the river Weser, an increased fluvial sediment supply also has to be considered, possibly induced by enhanced soil erosion due to a combination of anthropogenic influences (intensified agricultural ativities) and more humid climate conditions (Holocene climatic optimum) (cf. Kalis et al., 2003).

A rise in groundwater levels in the northwest of the study area, most likely connected to the rising sea level (Bungenstock and Schäfer, 2009; Meijles et al., 2018), probably caused the development of a peat environment from the decaying salt-marsh vegetation. This peat is not documented in the archive core (146) in the southeast, which could be due to the fact that the peats in the study area do not show visual signs of decomposed plant material and are permeated with clastic material, hence, they might just not be described as such for the archive core data. Another possibility is the partial erosion of this peat during the subsequent high-energy marine inundation, which is indicated by the grain-size distribution, the presence of shallow marine foraminifers and the very low thickness of the overlying deposit. This interpretation as a high-energy event is supported by reworked peat intraclasts in this layer. Due to the lack of chronological data, the association with a specific event or phase of increased storm activity remains difficult, but due to its stratigraphic position, it could possibly correlate with an event marker documented for the time period around ~3600–2400 cal BC (Wartenberg et al., 2013). However, without numerical age data, this remains

an assumption. The overlying peat layer either indicates a re-establishment of the swamp conditions prior to the marine inundation or it could be still connected to the underlying high-energy event. In this case, the layer intercalated between the two peat layers would be referred to as '*Klappklei*' (Wildvang, 1938). This formation develops when a peat cliff is ripped open laterally during a storm surge, causing the upper part of the peat to float on top of the marine inundation. After the event, the peat layer settles down on top of the accumulated marine sediments leading to an age inversion in the sedimentary sequence (Wildvang, 1938; Streif, 1990; Behre and Kučan, 1999; van Dijk et al., 2019). This could only be verified by dating of the peat and the intercalated event layer. In general, the very low thickness of the interrupted peat layer could imply an influence of post-depositional or auto-compaction as well as erosion by the higher-energy event.

Subsequently, a tidal-flat environment developed, since peat growth could not keep up with the rising sea, maybe attributed to an increased rate of RSL rise (e.g. Bungenstock and Weerts, 2012). The tidal-flat deposits documented in the cores (Chapter 2) show higher energy levels than the first documented tidal-flat deposit, a high carbonate content, organic laminae (resulting from periodical inundations), and mollusc fragments. Shallow marine, intertidal foraminifer associations support this interpretation. The tidal flat was cut by several tidal channels and energy levels were decreasing from the west towards the *Geest* ridge of Pleistocene deposits in the east, which is in accordance with the shore-normal energy gradient (Nyandwi and Flemming, 1995). One of the tidal channels was running in the area east of the later settlement area ('Barward', Chapter 2). It cannot be determined how long this tidal flat prevailed, since no ^{14}C ages are available for this facies.

As tidal flats slowly grow vertically, this tidal flat aggraded above the mean high-tide level, initiating the formation of a second salt marsh in the transitional area between marine and terrestrial environments (Bungenstock and Weerts, 2012). The most likely reason for this development is an increased sediment supply originating from the sea, which could have been deposited via a phase of repeated flooding events, like during spring tides or storm surges. The accumulated sediments were trapped by vegetation probably leading to accelerated aggradation and possibly also coastline progradation. Salt-marsh deposits in some of the former tidal channels indicate a filling of these channels during this phase.

In the east, peat formation on top of the salt marsh indicates freshwater input, probably from dewatering of the *Geest* ridge (cf. Jelgersma, 1961, 1979; Wolters et al., 2010), whereas in the west and northwest, signs of initial transition to terrestrial conditions by continued vertical growth are indicated by upwardly decreasing hydraulic energy levels (i.e. finer-grained sediments).

The overlying unit was interpreted as a former marsh environment that grew above the supratidal area. The study area was subject to subaerial conditions, which led to processes of subsidence, desalination, oxidation and decalcification in the course of pedogenesis (Müller-Ahlten, 1994).

On top of this decalcified marsh deposit, the first soil could form representing the Late Bronze Age surface. This *dwog* horizon was dated to 1128–969 cal BC (Chapter 2), approximately matching a stagnation phase of the RSL reported by Bungenstock and Weerts (2010) and a potential marine inundation afterwards, (which would explain the burial of this *dwog*), reported by Wartenberg et al. (2013). Still, a possible incorporation of older ^{14}C from groundwater in the marsh has to be considered, leading to a slight age overestimation. Since this *dwog* is not present in the core located in the tidal channel (LAN 1) east of the 'Barward' area, it can be assumed that the channel was still active during this time. However, the area was not yet settled.

The Late Bronze Age surface was buried during a marine inundation, indicated by a high-energy layer on top of the *dwog*. This could have been a single, severe storm surge or a period of increased storm activity, possibly correlating with the event reported by Wartenberg et al. (2013) around 4000–1000 cal BC. During this inundation, the still active channel was probably infilled, since the second *dwog* could also be documented at this location.

This second *dwog* was dated to cal AD 1426–1467, which seems too young due to the fact that the area was protected by dykes since the first continuous dyke systems around AD 1300 (Bungenstock and Schäfer, 2009) complicating the explanation of the clastic layer above the *dwog*. Hence, either the dating results underlie methodological errors (contamination with younger ^{14}C through bioturbation, field sampling, fungal growth or pre-treatment in the laboratory) or the overlying deposit represents a high-energy event. As shown in Chapter 2, the time after this *dwog* horizon was characterised by several storm surges with possible dyke breaches (for a list of all important storm surges, see Streif, 1990), which would be a reasonable explanation for the overlying clastic deposit, provided a correct age of the *dwog*. The deposition of this layer could have happened during one or several of these storm surges at shorter intervals during the 16th century. Besides that, a possible reactivation of the 'Barward' drainage system in the course of the short-term Medieval re-occupation (Chapter 2) could also explain the clastic deposits. However, this would not explain the extent of the layer even in non-tidal-channel areas of the study area. Finally, the

presence of shallow marine foraminifers supports a marine influence of the layer. The weakening of the period of increased storm activity lead to the re-establishment of subaerial conditions and to the development of the present-day land surface.

The investigations presented in Chapter 2 were able to provide detailed reconstructions of Holocene landscape changes in the 'Land Wursten' region eludicating phases of coastal pro- and retrogradation combined with increased sediment supply. This information is supposed to support conclusions on the RSL development (see Objective C).

Objective B: Reconstructing Holocene landscape changes in the back-barrier of Norderney

The East Frisian island of Norderney belongs to the chain of barrier islands, which formed since the deceleration of the RSL rise (6–7 ka BP) (Freund and Streif, 2000; Flemming, 2002; Bungenstock and Schäfer, 2009). The study area in the back-barrier of the island was also subject to massive landscape changes since the LGM. Three studies have been carried out in order to reconstruct these landscape changes. The first one provides small-scale information based on detailed multi-proxy investigations of a single drilling core (Chapter 3), whereas the second gives information on a more extensive base due to the investigation of several cores, which were then combined with archive core data (LBEG) along a transect (~6 km in a WSW–ENE direction, Chapter 4). The third study complements these data by means of additional cores and dating results (Chapter 6, in particular section 6.5).

The results of the analyses reveal up to seven different facies units representing different depositional environments. Sedimentation history begins with shallow-marine deposits likely of Eemian age, which were documented in the western part of the study area (VVC16). The subsequent Pleistocene deposits were also exclusively documented in the west (VVC16, VVC17 and N77) and were identified based on the grain-size distribution and the lack of carbon (organic and inorganic) and microfauna. The latter indicates a non-aquatic habitat supporting their interpretation as terrestrial deposits of pre-Holocene, likely Weichselian times, when the area was subject to periglacial conditions and aeolian and glacio-fluvial accumulation (Streif, 1990, 2004). Deposits of older glaciations have not been found in the investigated areas. A degradation of the organic matter is also reported (VVC17, Chapter 3) indicating the formation of a palaeosol on top of the aeolian and glacio-fluvial sands. The top of this palaeosol represents the Holocene base, which was not reached in any of the other cores and was therefore modelled based on information from archive core data (LBEG, Chapters 4 and 6).

Subsequently, a basal peat (fen peat) developed marking the start of the Holocene sequence, identified based on high organic content. In the western part, the basal peat started

to form from ~7500 cal BP and lasted until ~6000 cal BP (VVC17, Chapter 3), while more to the east a delay in peat formation can be assumed due to ^{14}C dating of the upper part of the basal peat layer to ~4700 cal BP (N49). A reconstruction of the start of peat growth in the east is not possible due to the fact that none of the drillings reached the base of the peat (i.e. the Holocene base). Fen peat formation was probably bound by rising groundwater levels associated with the RSL rise (Bungenstock and Schäfer, 2009) and the channel situation in the west, and followed the slightly higher topography towards the east. Furthermore, the area became protected since ~6–7 ka BP by the developing barrier island, which maintained the sheltered conditions required for peat growth during a rising RSL (Freund and Streif, 2000; Flemming, 2002; Bungenstock and Schäfer, 2009). Based on ^{14}C ages of the peat (Chapter 3), the general growth rates of the peat documented in VVC17 (~0.4 mm/a) are lower than the rates estimated for central Europe (~1 mm/a, Bungenstock and Schäfer, 2009) implying high post-depositional or auto-compaction of the peat. Provided that the peat was subject to auto-compaction by decomposition or water loss, this would have resulted in a lowering of the peat surface leading to enhanced accommodation space (changed A/S ratio), possible marine inundation and increased compaction by water load (cf. Long et al., 2006). Towards the top of the peat, introduced foraminifers and marine diatoms support an increasing marine influence.

Due to this increasing marine influence from the west most likely accompanied by frequent flooding of the peat due to the ingressing sea along adjacent channels, a salt marsh formed ~6000 cal BP burying the basal peat. This interpretation is based on the microfaunal association, the grain-size distribution and C/N ratios (Horton and Edwards, 2006; Khan et al., 2015). The salt marsh prevailed until ~5900–5500 cal BP in the western part of the transect. Since the salt marsh further to the east started to develop much later (after ~4700 cal BP), it is possible that during this time the east was still under terrestrial conditions and peat had not even started to form.

However, an intercalated peat in the west that was documented only in one core (VVC17, Chapter 3) from ~5900–5300 cal BP indicates a decreased marine influence. Due to higher sediment supply peat growth was probably able to resume (Baeteman, 1999). This peat growth happened at the same time as the basal-peat growth in the eastern part of the transect, verifying the connection to the RSL of the basal peat in the east. The fact that this peat is documented in VVC17 but neither in VVC16 (Chapter 6; relocated peat) nor N77 (Chapter 4) could either result from the positions of these cores possibly being closer to a palaeochannel, leading to a continuation of flooding, or it could indicate that this peat was eroded

by subsequent processes associated with the overlying unit. Since both the peat and overlying salt-marsh deposit in VVC16 are relocated (Chapter 6, section 6.5), the latter seems more reasonable.

An additional intercalated peat developed ~4300 cal BP on top of the salt marsh, which is exclusively documented in one core (N49, Chapters 4 and 6). It could have formed locally due to locally sheltered conditions, which would explain the absence of this peat in the other cores further to the east. However, its top is characterised by an erosive contact leading to the assumption that it was partially eroded. In this case, erosion of the peat entirely in the adjacent cores is also conceivable. This is supported by erosional contacts documented in the cores further east (N43, VC03, VC13 after ~3900 cal BP and N44 after ~3600 cal BP) indicating a hiatus. Hence, it is possible that peat growth reached this area and was then subsequently eroded. Due to the documentation of further intercalated peats in this area (LBEG, Chapters 4 and 6), an extensive peat area is assumed for the time between at least ~4300 and 3600 cal BP.

During this time, the main channel had already shifted to the western part of the study area, probably following the southeastwards shifting barrier island (e.g. Flemming, 2002; Streif, 2004). It caused reworking and erosion, (indicated by salt-marsh foraminifers in the top layer of VVC17), which appears as tidal-flat facies and represents the core surface in the present-day channel (Chapters 3 and 6).

East of the main channel, a tidal-flat environment formed resulting from the rising RSL. In the east, this tidal flat was cut by another tidal channel, which was either infilled subsequently or shifted its location. Chronological data of foraminifer tests and molluscs (N43, N49, VC03, VC13) (Chapter 6, Tab. 6.1), document the hiatus at the base of the tidal-flat sediments as well as sediment reworking (age inversions) within the complete unit. The differences in the length of the hiatus possibly arise from the different topographical situations of the respective cores; the “channel” situation of N49 and VC03 (Fig. 6.5) led to more intense reworking and a longer hiatus (~3500 years), whereas the higher-situated erosive contact in N43 and VC13 seems to be connected to a shorter hiatus (~1500 years), likely associated with less intense initial reworking. Possible artefacts caused by effects associated to ^{14}C dating in general, which could have caused the age inversions, can mainly be excluded due to one specific dating result: an articulated bivalve (*Barnea candida*) was documented directly inside its borehole within the erosive peat-tidal-flat contact and provided an age of 905–733 cal BP in a depth of ~-3.0 m NHN. This bivalve in its living position is expected to provide the most reliable age within the complete transect (c.f. Hayward and Ryland, 1990), which is why all overlying and older ages suggest the influence of sediment

reworking. In general, two different reworking layers are expected, separated by the undisturbed storm deposit which was documented in at least three cores (N49, VC03 and VC13) and can only be associated to a time after ~2300 cal BP (youngest reliable ages from N49 and VC13). The sediment reworking is most likely to be connected to the beginning of dyke construction on the German North Sea coast, with first continuous dyke systems around AD 1300 (e.g. Gerdes et al., 2003). The resulting changes in tidal-flat hydro-dynamics may have led to the reworking of up to 50% of the complete tidal-flat deposits, which could enable disturbance down to >20 m depth (Trusheim, 1929; Lüders, 1934; Reineck and Siefert, 1980; van der Spek, 1996). Reworking in the younger part of the tidal-flat deposits (overlying the storm deposit), may relate not only to dyke construction but also to recent tidal dynamics and the present-day tidal channel between N43 and VC03. For the complete tidal-flat deposit, reworking is expected to ensure only proximal sediment transport, since the documented microfauna mainly does not show clear signs of relocation (Hofker, 1977). Investigations by Tilch (2003) from the tidal flat between Langeoog and Spiekeroog, showing vertical erosion and spatially shifted accumulation of approximately the same sediment amounts, also hint to only proximal transport.

Summarising, the multi-proxy investigations in the back-barrier of Norderney provide valuable information on palaeo-landscape changes connected to the Holocene transgression. However, the intense reworking reconstructed for the complete tidal flat permits a continuous chronological classification of the Holocene sedimentary sequence.

Objective C: Relating coastal changes to the local RSL history

Every reconstructed facies layer in the study areas has a specific relation to the sea level, lying either above, at or below the RSL (e.g. Streif, 2004). Thus, statements can be made from the reconstruction of the different depositional environments both in the ‘Land Wursten’ area and in the back-barrier of Norderney. Different approaches have been chosen to achieve conclusions on the RSL history.

For each reconstructed facies in the ‘Land Wursten’ study area (Chapter 2), the position below, at or above the sea level is approximately known based on literature and local modern analogues, which leads to the following development: no absolute elevation for the sea level at the time of the first tidal flat can be assumed. However, the fact that a salt marsh developed on top of this tidal-flat layer indicates a relative lowering of the sea level, which can be connected to a lateral shift of the coastline in combination with a stagnation or slow rise of the RSL (Bungenstock and Schäfer, 2009; Bungenstock and Weerts, 2012). The subsequently recorded peat indicates a decreased marine influence or an increased sediment supply preventing periodic flooding (Baeteman, 1999), which suggests further

lowering of the RSL, aggradation and/or coastal progradation. The tidal-flat deposits overlying the peat indicate a RSL rise, since they are situated in the intertidal zone approximately at the MSL, which was again followed by a salt marsh indicating a RSL lowering or stagnation. This could be connected to coastal progradation due to an increased sediment supply (as discussed above), which continued until peat formation resumed. The terrestrial conditions that started after the peat formation and prevailed until today indicate falling groundwater levels, which this close to the coast are directly related to the RSL (Meijles et al., 2018).

Hence, this information allows only crude estimates about RSL changes, which is why Chapter 2 also describes the approach to relate the reconstructed facies model to an existing RSL curve for the Jade Weser region (Bungenstock and Weerts, 2010), as well as to include the dated *dwog* horizons in the curve. The older salt marsh documented in LAN 3 was related to the slower RSL rise between ~5200 and 3200 cal BC. Since the salt marsh lies deeper than the reconstructions by Bungenstock and Weerts (2010), a compaction effect has to be expected here leading to increased uncertainties. The tidal-flat facies, connected to a transgressive phase, was associated to the increased RSL rise in the time from ~3200–2600 cal BC. The younger salt marsh was related to the decelerated RSL rise between ~2600 and ~1100 cal BC as well as the overlying decalcified marsh, which was situated higher above the RSL. After ~1100 cal BC the RSL rise decelerated again, which correlates with the older *dwog* (1128–969 cal BC) documented in the drillings. The increased RSL after the turn of eras until ~AD 300, possibly connected to a rise in storm-surge levels, could be the reason for the burial of the older *dwog*, whereas the subsequent stagnation phase (~AD 300–1644) could explain the formation of the second *dwog* (cal AD 1426–1467). The burial of this younger *dwog* cannot be related to any part of the RSL curve. As can be seen in Fig. 2.11 (Chapter 2), the vertical position of the older *dwog* is ~2 m above the RSL curve error band, whereas the younger *dwog* is situated directly on top of the error band. This exemplifies the difficulty of interpreting the indicative meaning of such stratigraphic layers that are known to develop above the MSL. Furthermore, different compaction rates, which cannot be estimated for the study area, could have influenced the elevation of the *dwogs* leading to falsified statements provided the vertical distance of their formation to the sea level would be known. Hence, reconstructions based on the available data bear uncertainties.

For the study area of Norderney (Chapters 3, 4 and 6), the same relative statements on the sea level can be made from the different identified Holocene facies (peat = above MSL, salt marsh = supratidal area, tidal-flat = at MSL, channel = at MSL), but the erosive contact with the overlying hiatus prevents a chronological classification of any RSL statement regarding

the time after the salt-marsh developed. In order to integrate a part of the data into existing RSL reconstructions, the dated peat layers, as well as the palaeosol documented in VVC17 (Chapter 3), were compared with previous RSL data for the southern North Sea (see Fig. 3.7). In general, the data show a relatively good accordance with local reconstructions from Langeoog (Bungenstock and Schäfer, 2009) as well as with reconstructions from the Dutch Wadden Sea (Meijles et al., 2018). However, with the exception of one data point, the Langeoog curve does not cover the same time span and a connection of both can only be assumed. The fit with the curve for the complete German Bight (Behre, 2007) has to be considered with caution, since the curve has been debated in terms of oscillations of underlying, locally varying effects (e.g. tidal range, compaction rates, GIA); the reliability of specific RSL index points and the missing correction for compaction and GIA (Vink et al., 2007; Bungenstock and Weerts, 2010, 2012; Baeteman et al., 2011). The integration of the palaeosol, once again, shows the uncertainty connected to the indicative meaning, since it represents a clear outlier in the compilation of RSL data in Chapter 3. Furthermore, a closer look at the comparison to the Dutch RSL curve (Meijles et al., 2018), shows one peat from VVC17 with a reconstructed RSL above the Netherlands curve whereas the others lie below it. The higher glacial isostatic subsidence in the northern part of the considered area (Meijles et al., 2018) could explain the lower course of VVC17. However, the higher position of the oldest peat sample, originating from the base of the basal peat, is not in accordance with this explanation, questioning the indicative meaning of this peat.

In general, the reconstructed coastal changes can be related to the RSL, thus, verifying **Hypothesis 1**, but uncertainties remain when integrating the data and comparing it to existing RSL curves from the southern North Sea coast. These uncertainties include under- and possibly also overestimation of the compaction of peats and fine-grained Holocene sediments, which cannot always be quantified accurately, coupled with the unclarified indicative meanings of peats and *dwog* horizons or other palaeosols (details in Chapters 1.2 and 5). Accordingly, the need for more precise RSL data has been expressed repeatedly (Vink et al., 2007; Bungenstock and Schäfer, 2009; Bungenstock and Weerts, 2010, 2012; Baeteman et al., 2011; Meijles et al., 2018).

In order to demonstrate a possibility for more precise RSL reconstructions from the ‘Land Wursten’ record, Fig. 7.1 shows a test application of a foraminifer-based TF which was established based on foraminifer data from the western coast of Schleswig-Holstein (Halebüll) (Lehmann, 2000). Since only the *dwog* horizons were dated for the three investigated cores, the reconstruction can only be depicted in relation to sample depth and is therefore not showing the RSL development in time. The model shows a vertical error of ±17 cm, which leads to very small sample-specific errors for the reconstructed curve.

Hence, it is already visible that this approach provides much more detailed information than the existing approach discussed in this section and also in Chapters 2, 3 and 4. Due to the lack of age data, the curve shows a continuous and relatively linear RSL rise, verifying the potential of this approach. The uppermost sample of LAN 2 is an outlier in this context, since it reconstructs a RSL drop (Fig. 7.1). This is the only sample with a high number of agglutinated salt-marsh species from the younger salt-marsh deposit, definitely indicating a salt-marsh environment. Since none of the other salt-marsh layers contained agglutinated foraminifers and they were mainly identified based on other criteria, this could lead to a misinterpretation of the palaeo-elevation provided by the TF. Another possible explanation would be an increased sediment supply from the hinterland, which led to an aggradation of the eastern study area resulting in a relatively lower sea level. Nonetheless, all remaining samples still eludicate the high potential of this approach, since they provide high-resolution data on the RSL.

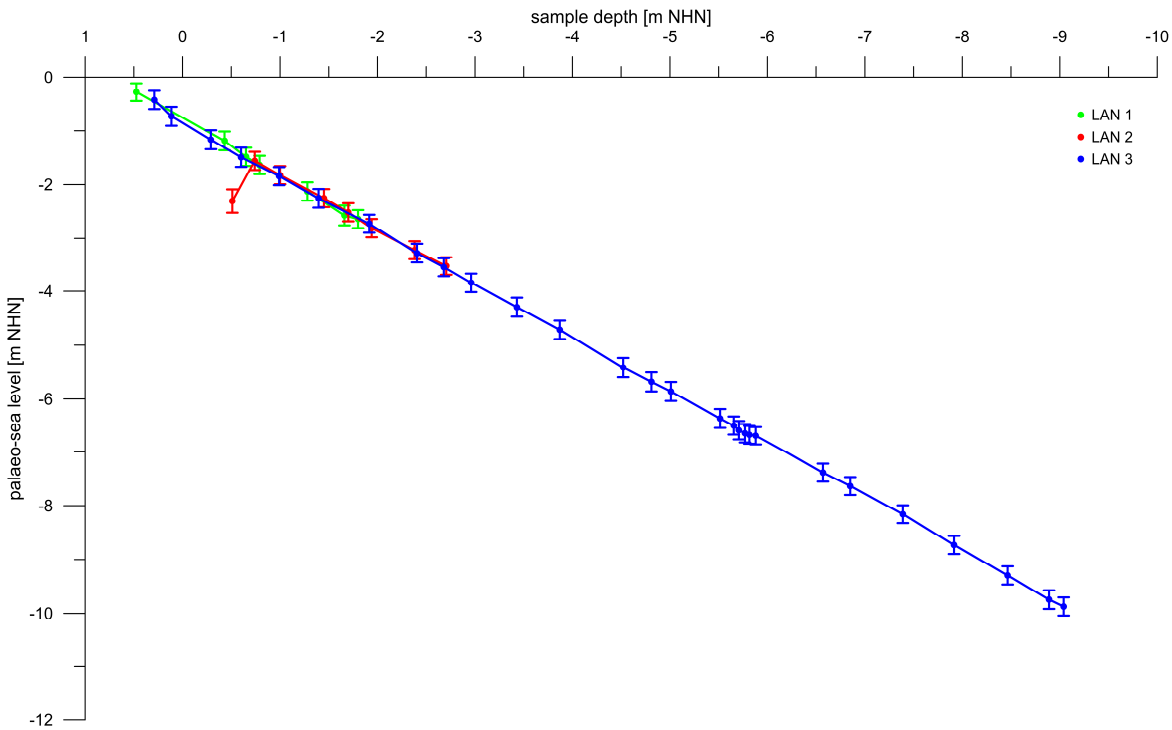

Fig. 7.1 Test application of a TF based on modern data of Lehmann (2000) to the cores of the 'Land Wursten' area. The palaeo-sea level is plotted against sample depth due to the lack of datings within the cores (own design).

7.2 A transfer function for relative sea-level change

Hypothesis 2 – Reconstructions of the Holocene RSL on the German North Sea coast can be improved by using a transfer function based on microfaunal data

Objective D: Investigating the vertical and lateral zonation of foraminifer and ostracod associations on the southern coast of Spiekeroog

Chapter 7.1 shows that inferences on RSL changes based on individual facies are possible, but also that uncertainties remain. The approach of applying a microfauna-based TF for RSL change to the Holocene samples seems promising, but poses inherent difficulties due to regional differences. Therefore, a local modern training set was developed on the southern coast of Spiekeroog, representative for the East Frisian islands (Chapter 5), in order to establish a TF that can be applied to the WASA cores.

Firstly, the vertical and lateral zonation of foraminifer and ostracod associations was investigated to identify the driving environmental parameters and to find out if the modern associations are suitable for the development of a TF for RSL change. The investigations described in Chapter 5 led to the identification of six zones reaching from the middle salt marsh (~1.51 m NHN) to the transition to the tidal channel (~-1.31 m NHN). The middle salt marsh (~1.51–1.13 m NHN) is characterised by low hydro-energetic levels and increasing marine influence towards the lower elevations. A high diversity in the microfaunal association and the high abundances verify suitable living conditions for a variety of species. Ostracods exhibit much lower abundances than foraminifers but the general microfaunal concentration increases towards the lower elevations. The well-preserved tests and the fact that the percentage of living individuals is much lower than that of dead individuals indicates good test preservation in this environment. Here, a part of the documented number of individuals could also have been introduced during spring tides or storms (De Rijk and Troelstra, 1999), which represent the only flooding of this part of the salt marsh (Streif, 1990; Bungenstock and Weerts, 2012).

The adjacent lower salt marsh (~1.06–0.86 m NHN) shows increasing energy levels towards the lower elevations and the proximity to the sea. Here, the microfauna is dominated by agglutinated salt-marsh foraminifers accompanied by calcareous shallow marine species. Ostracods again appear in low numbers compared to foraminifers. A salt-marsh pool with permanent water coverage shows higher marine influence, slightly enhanced numbers of living individuals, dominances of calcareous shallow marine species and high numbers of living ostracods. The ratio of living and dead individuals in this zone implies either poorer test preservation or better living conditions, which could mainly be explained by the higher

inundation frequency in this zone. Especially in the salt-marsh pool, probably oxygen-rich water inundates during high tide and rainfall, which together with root-bioturbation and diffusion provide the ideal living conditions for microorganisms (De Rijk and Troelstra, 1999; Berkeley et al., 2007). The permanent water coverage is enabled through the protection provided by the surrounding vegetation of the lower salt marsh, resulting in the high number of living individuals, especially ostracods, which are not removed by the current (e.g. Athersuch et al., 1989; Murray, 2006). However, a combination of better living conditions and poorer preservation is also conceivable.

The pioneer zone (~0.86–0.48 m NHN) exhibits increasing hydro-energetic levels, typical for the transition area between the salt marsh and the tidal flat (Nyandwi and Flemming, 1995), and much lower microfauna concentrations with a dominance of living *C. williamsoni*, a shallow marine foraminifer that prefers sandy substrates (Murray, 2006). Due to the higher energy levels, an introduction of dead individuals could be assumed.

The sand flat (~0.48–-0.30 m NHN) shows the highest energy levels correlated with the lowest microfauna concentrations. Towards the lower part of this zone, the dynamics seem to become too turbulent for the survival or settlement of microfauna or dead tests are removed frequently by the currents (Hofker, 1977). Furthermore, processes of early diagenesis (Berkeley et al., 2007) could influence test preservation and cause the dissolution of $CaCO_3$.

In the mixed flat (-0.30–-1.14 m NHN), foraminifers and ostracods reappear, connected to slightly increased mud contents. The microfaunal association is dominated by typical tidal-flat species (Chapter 5) and similar numbers of living and dead individuals indicate a good fossilisation potential (Smith, 1987), whereas ostracods in the lower part could have experienced *post mortem* transport towards the tidal channel (c.f. Edwards and Horton, 2000; Frenzel and Boomer, 2005).

The transition to the tidal flat (~-1.14–-1.31 m NHN) shows high but decreasing microfauna concentrations towards the lower elevations, which can probably be attributed to the proximity to the tidal channel. The low number of living individuals could again indicate very good preservation of empty tests, since dead shells are generally easier to redistribute by the current. Furthermore, the current of the channel could also complicate the settlement of living microfauna (Hofker, 1977; Murray, 2006).

The general zonation is clearly visible from the results presented in Chapter 5. In order to find out, which environmental factors influence the microfaunal associations, multivariate statistics were performed for all samples with statistically relevant proportions (>40 individuals, leading to the exclusion of almost all sand-flat samples). Principle component analysis

(PCA) revealed a 'tidal flat vs. salt marsh' factor for the most important component, which is interpreted to relate to the duration of water cover or the inundation frequency, i.e. the elevation. The second important factor seems to be the salinity, due to confrontation of species with different salinity preferences by the second component. In general, the salinity rises from the salt marsh towards the tidal channel and with increasing water depths (Kaiser and Niermeyer, 1999; Flöser et al., 2011) suggesting an additional importance of the elevation here. Hence, the PCA already indicates a high influence of the elevation on the microfaunal distribution. A canonical correspondence analysis (CCA) should verify this and shows that the elevation has high scores for both axes (see Fig. 5.6), which together explain ~93% of the variance in the dataset. Furthermore, the arrangement of foraminifer and ostracod species within the CCA plot suggest a main influence of the TOC content and the elevation on species distribution. Since the organic content is strongly related to the elevation (verified by the high Pearson correlation coefficient of ~0.75) and the elevation related to both important axes, a major influence of the elevation, related to the inundation frequency and water depth, is assumed, satisfying the main criterion of the TF for RSL change.

These correlations show that the modern training set from the southern coast of Spiekeroog is well suited for the development of a TF, which can be used for RSL reconstructions.

Objective E: Using a combination of foraminifers and ostracods for TF development

So far, studies focussing on TFs for RSL change use exclusively foraminifers, some of them also exclude calcareous species due to their potential dissolution within the fossil record (e.g. Edwards and Horton, 2000; Gehrels and Newman, 2004; Horton and Edwards, 2006; Barlow et al., 2013; Kemp et al., 2013; Milker et al., 2017; Müller-Navarra et al., 2017). In order to enable the application of the TF also to widespread tidal-flat sediments within the study area of the Norderney tidal basin (Chapters 3, 4 and 6), this study includes samples from the recent tidal flat (Chapter 5), as calcareous species are not dissolved in the study area. This also results in an enhancement of the investigated elevation gradient. The novel approach of including ostracods for TF development shall lead to more detailed habitat information due to their specific ecological preferences. Living associations of foraminifers and ostracods can very well be affected by seasonal differences (temperature, salinity, storm activity, etc.), which is why the samples, taken during different seasons in 2015 and 2017, may lead to diverging results. Therefore, only dead assemblages (Chapter 5) were used for the development of the TF. These should represent the result of habitat preferences and taphonomic changes over an average of several years (e.g. Murray, 2006).

Prior to TF development, the species-environment relationship had to be tested, which was performed by means of detrended correspondence analysis (DCA) including the microfaunal data and the strongest environmental factor (elevation). From the DCA plot (Fig. 5.7), the length of the environmental gradient was determined as 3.3 SD (standard deviation), indicating a rather unimodal species response (e.g. Birks, 1995; Lepš and Šmilauer, 2003). This knowledge is important in order to chose the correct method for TF development, in this case the weighted averaging-martial least squares (WA-PLS) method (for more methodological detail, see Chapter 5).

In order to point out potential differences between the common approach of using exclusively foraminifers and the new approach of a joint foraminifer-ostracod dataset, two models were developed for the TF (Fig. 5.8). Model I represents the common approach and Model II the new approach. The most appropriate component (component 2) of the modelling was chosen based on the highest correlation (R^2_{boot}) and the lowest vertical error (RMSEP). The investigated elevation gradient was reduced to a vertical distance of 2.69 m (+1.51 to -1.18 m NHN) due to the exclusion of outliers and samples with low abundance (<40 individuals; i.e. almost the complete sand-flat samples), which left a total of 16 samples.

Model I (exclusively foraminifers) exhibits an R^2_{boot} of 0.82 and an RMSEP of 54.2 cm, accounting for 20.2% of the elevation gradient and 20.1% of the mean tidal range. There is no trend in the TF over- or underestimating samples related to their observed elevation, nor are there structures of residuals.

Model II (foraminifers and ostracods) shows an R^2_{boot} of 0.84 and an RMSEP of 49.1 cm, which accounts for 18.3% of the elevation gradient and 18.2% of the mean tidal range. Again, no trends in over- or underestimation or structures of residuals are visible.

Comparing the two models, it becomes clear that the inclusion of the ostracod data indeed improves the TF performance, as for R^2_{boot} and RMSEP. Barlow et al. (2013) reporting a vertical error of typically 10–15% of the mean tidal range, thus, an error of 18.3% seems acceptable. However, a vertical error of ~49 cm, resulting in an error range of the indicative meaning of ~1 m, is still relatively large, especially when considering the low topography of the landscape of the German North Sea coast. Possible ways to improve the vertical error would be reducing the environmental gradient by focussing on the salt marsh (c.f. Edwards and Horton, 2000; Gehrels and Newman, 2004; Kemp et al., 2013; Müller-Navarra et al., 2017) or increasing the number of samples for TF development. Most studies (e.g. Kemp et al., 2012; Müller-Navarra et al., 2016, 2017; Milker et al., 2017) base their TF on modern datasets consisting of at least 40 samples, resulting in smaller errors. The present TF

(Chapter 5) was developed based on only 16 samples, wherefore an improvement in TF performance (R^2_{boot} and RMSEP) is expected from an increased total number of samples. This was accomplished in the next step of the study (Chapter 6 and section 7.3). Further differences between the present study and previous TF studies relate to sampling thickness, pre-treatment and dry-counting. In general, studies focussing on microfaunal surface distributions use the uppermost 1 cm, mostly based on the fact that foraminifers are epifaunal, i.e. on top of the substrate (Horton and Edwards, 2006). However, the conditions in the meso-tidal Wadden Sea are characterised by high dynamics, wherefore infaunal foraminifer taxa are expected to be living down to a depth of 5 cm (Hofker, 1977). After testing the vertical distribution of living individuals, the thickness for investigation was set to 3 cm, thus accounting their known habitat range. Furthermore, the TF provides a dm-scale accuracy, which is why an error imposed by the vertical integration of 3-cm samples should be negligible. As for pre-treatment of microfaunal samples, concerns might arise about the use of sodium pyrophosphate ($Na_4P_2O_7$) as dispersant to prevent adhesion of clay particles and possible destruction of agglutinated tests, which consist of foreign material (e.g. sediment grains or detritus) cemented by proteinaceous, carbonate or ferric oxide cements (Lowe and Walker, 1997). In order to test possible destruction of agglutinated tests during this procedure, representative individuals of agglutinated foraminifers (8x *Entzia macrescens* and 1x *Trochammina inflata*) from fossil samples were shaken with either pure $Na_4P_2O_7$ solution (46 g/l) or tap water with 1 ml of $Na_4P_2O_7$ solution for approximately five days. No differences in test appearance or identifiability were documented compared to appearance and identifiability prior to shaking. Many existing studies focussing on foraminifers for landscape or RSL reconstruction pick the individuals wet to prevent drying of organic residuum and damaging of agglutinated tests (e.g. de Rijk, 1995; Edwards and Wright, 2015; Milker et al., 2016; Müller-Navarra et al., 2016, 2017). Therefore, testing was performed by wet-picking and subsequent drying of agglutinated foraminifers (*E. macrescens*, *T. inflata* and *Miliammina fusca*) in micro cells. Furthermore, three salt-marsh samples were split, counting one replicate wet and one replicate dry. Again, no significant effects of drying could be documented, neither on test preservation nor on species associations. These findings corroborate previous investigations, e.g. by Schönfeld et al. (2013). Hence, the chosen methodological procedures are expected to provide results comparable to those of previous studies.

Objective F: Comparing the TF with presently used RSL index points

The most commonly used RSL index points for the southern North Sea area are basal and intercalated peats (e.g. Denys and Baeteman, 1995; Baeteman, 1999; Vink et al., 2007; Bungenstock and Schäfer, 2009; Hijma and Cohen, 2010; Meijles et al., 2018). In general, a vertical error range of ~1 m (Model I of the TF), (seeming relatively high when compared

to previous TF studies) is significantly smaller than error ranges of existing peat-based RSL reconstructions for the southern North Sea coast of up to 3–5 m (e.g. Long et al., 2006; Bungenstock and Schäfer, 2009; Bungenstock and Weerts, 2010, 2012; Baeteman et al., 2011). There are several arguments for the improved performance using the TF as opposed to the use of peats as RSL indicators.

One major problem when using peats, is post-depositional compaction influencing the depth of peat layers and thus resulting in high vertical uncertainties of peat-based RSL reconstructions. Post-depositional compaction by sediment load has a significant impact on intercalated peats as well as the upper part of basal peats and only the lowermost part of a basal peat can be expected compaction-free. For example,Horton and Shennan (2009) reported average compaction rates of 0.4±0.3 mm/a for peat beds buried in Holocene sedimentary sequences along the east coast of the United Kingdom. Since the TF can be applied to a range of intertidal and supratidal deposits, stratigraphic sequences comprising large amounts of compaction-prone peat can be avoided, still providing a more continuous record than the only occasionally occurring peat layers.

Another problem in the use of peats for RSL reconstruction is their indirect relation to the sea level. In terms of the indicative meaning of peat, still no universal definition exists (e.g. Baeteman, 1999; van de Plassche et al., 2005; Bungenstock and Schäfer, 2009; Wolters et al., 2010). A basal peat does not always have to be related to RSL, which was shown for example, for the early Holocene by Wolters et al. (2010). They reported a basal peat that started to form when RSL was ~17 m below the investigated location. In special topographic conditions, sea-level independent paludification and peat growth is described for example by Jelgersma (1961), Lange and Menke (1967) and Baeteman (1999). However, widespread intercalated peat beds are generally used for RSL reconstructions, but careful consideration of forming processes is crucial (Bungenstock and Schäfer, 2009; Bungenstock and Weerts, 2010). In contrast to this, the TF provides a direct relation to the sea level, since it relates recent associations to their elevation relative to MSL (Leorri et al., 2010; Kemp et al., 2012; Kemp and Telford, 2015), providing a well-constrained indicative meaning.

In addition, uncertainties can arise in the use of peats as RSL index points due to the occurrence of relocated peats. These are ripped off at peat cliffs in so called '*Dargen*' and can be transported over large distances (Streif, 1990; Behre and Kučan, 1999; van Dijk et al., 2019). This can result in age inversions within Holocene sedimentary records and result in invalid RSL reconstructions. An example for relocated peat and associated age inversions was documented in one of the WASA cores (VVC16) and is described in Chapter 6 and

section 7.1. By applying the TF to the microfaunal record, these uncertainties can also be avoided.

Finally, the TF has the potential to provide information on RSL also from the youngest part (last 2000 years) of the Holocene sequence, where peats are usually lacking, but microfauna are still well represented.

Hence, the TF provides a promising tool for RSL reconstructions with much higher resolution, smaller error ranges and less uncertainties than the classical peat-based reconstructions in the southern North Sea, thus, verifying **Hypothesis 2**. Nevertheless, the aforementioned vertical error of the present TF was expected to be improved by the measures discussed in the following section.

7.3 RSL reconstructions for Norderney using microfaunal data

Hypothesis 3 – The application of a microfauna-based TF leads to more precise RSL reconstructions for the East Frisian islands

Objective G: Improving the performance of the TF

Even though the established TF already outperforms the use of peats as RSL index points in terms of vertical error range, indicative meaning and continuity of data, an improvement of the TF performance is still preferable. Therefore, additional samples along a surface transect (Transect 2) adjacent to Transect 1 (Chapter 5 and section 0) were included into the TF development. This second transect was investigated and the data were liberally provided by Dr. Kristin Thomsen and Dr. Achim Wehrmann (Senckenberg am Meer) (Chapter 6). Transect 2 is located c. 180 m west of Transect 1 and reaches across a distance of c. 230 m in a general N-S direction. It covers the natural salt marsh and c. 100 m of the tidal flat of Spiekeroog (for detailed maps, see Fig. 6.1).

After transformation of elevations of both datasets to the most recent vertical datum (DHHN2016, '*Deutsches Haupthöhennetz*'), the same uni- and multivariate statistics as for Transect 1 were performed for the joint dataset (except for CCA, since TOC data were not available for all replicates). Pearson and Spearman's correlation coefficients show no autocorrelations between taxa, but the PCA reveals the elevation as the most relevant component (31.99% variance) and the oxygen availability as the second component (17.61% variance) and finally, the DCA indicates a unimodal species-environment relation (gradient length 3.86 SD). Therefore, the final TF could be modelled again using the WA-PLS method and the resulting TF was again tested by bootstrapping cross-validation. For comparability to the preliminary TF (Chapter 5), again two models were developed: Model I considers

exclusively foraminifers and Model II also includes the available ostracod data. The appropriate component was chosen as in Chapter 5 and section 0 (highest R^2_{boot} and lowest RMSEP) and once again, outliers were excluded from the dataset leading to a final set of 41 samples. The resulting elevation gradient exhibits a vertical distance of 2.71 m (+1.506 to -1.206 m NHN), which is again comparable to the mean tidal range of Spiekeroog (2.70 m; BSH, 2018).

Model I provides an R^2_{boot} of 0.81 and an RMSEP of 37.8 cm accounting for ~13.92% of the elevation gradient and 13.98% of the mean tidal range. This already represents an improvement of the vertical error of 16.4 cm compared to Model I of the preliminary TF (Chapter 5). As can be seen from Fig. 6.4, the TF underestimation of samples related to their observed elevation seems to be higher than the overestimation.

Model II shows a quite high R^2_{boot} of 0.89 and an RMSEP of only 29.7 cm, which accounts for 10.98% of the elevation gradient and 11.02% of the mean tidal range. This represents a more pronounced improvement of 19.4 cm compared to Model II of the preliminary TF (Chapter 5). As shown in Fig. 6.4, the underestimation was reduced compared to Model I, also demonstrating the improved precision of the TF.

Moreover, for the joint dataset of both transects, the inclusion of ostracods leads to a clear improvement of the vertical error by ~8 cm, leading to an improvement of the previous error range of ~16 cm. Furthermore, the preliminary TF (Chapter 5 and section 0) could be improved by >19 cm of vertical error by increasing the total number of samples, now providing an error of ~11% of the mean tidal range. This way, it could be verified that a TF for RSL change may well include recent tidal-flat areas and still provide an error that lies at the lower limit of the typical error of 10–15% of the mean tidal range (c.f. Barlow et al., 2013). The next step will be the application of the final TF to the Holocene sedimentary record.

Objective H: Reconstructing the RSL history of Norderney

According to the reconstructed landscape changes, facies units could be selected for the application of the TF. Non-marine samples from Pleistocene deposits as well as semi-terrestrial peat facies were excluded for the application. Furthermore, the previously indicated reworking within the tidal flat resulted in the exclusion of most tidal-flat samples, as their microfaunal assemblages might not reflect the true RSL during the time of deposition. The lowermost samples of the base of the tidal-flat sediments of N43 were included due to the expected lesser intensity of reworking (Chapter 6) and the lower part of the tidal-flat deposit of VVC17 was also included, as only very few (<7%) salt-marsh foraminifers were documented in these samples, and reworking is mainly expected to occur within the upper half of this unit.

The reworking effects identified within the tidal-flat facies led to the subsequent exclusion of 101 samples (including non-aquatic samples), a matter which needs to be considered and avoided during future studies. This could be accomplished by investigating cores from inner-dyke locations along a coastline-perpendicular transect, possibly targeting younger salt-marsh and tidal-flat deposits which have not yet been subject to intense reworking connected to the dyke construction.

After the exclusion of the samples mentioned above, the TF was applied to 38 remaining samples from seven sediment cores. As Model II provided the best vertical error and correlation (RMSEP and R^2_{boot}), only this model was used for the RSL reconstructions, including the joint data of foraminifers and ostracods (total=100%) of each core. Since the TF provides a palaeo-elevation of each sample relative to the palaeo-sea level, values had to be converted to an absolute elevation (m NHN) as described in Chapter 6 (section 6.6.1). The resulting RSL curve (Fig. 6.6) starts at ~6100 cal BP within the transition phase of the steeper RSL rise, moving to a decelerated rise with rates of ~0.5 m per century. This first phase of the curve lasts until ~5700 cal BP and is followed by a gap which matches approximately the time of basal-peat formations in the area of the East Frisian coast, coinciding with the deceleration of the RSL rise (Freund and Streif, 2000; Streif, 2004; Bungenstock and Schäfer, 2009).

The second phase (~5000–3700 cal BP) shows a clear deceleration of the RSL rise, which continues at a rate of ~0.16 m per century. As can be seen from Fig. 6.6, some outlier samples have been excluded from the error band of the curve. These data points represent samples situated directly on top of the erosive contact discussed above (Objective H), where hydro-dynamics might have been too turbulent for the initial phase, (i.e. after the hiatus but before the re-establishment of short-term calmer conditions). The outliers from VC03 and VC13 (light and dark red data points in Fig. 6.6) originate from within a mollusc borehole inside the peat (no articulated bivalve within), which indicates a possible overestimation of the ages of these samples by the age-depth models. Due to these collective reasons, the outlier samples were excluded from subsequent investigations.

The third phase of the curve (~3700–1700 cal BP) represents a stagnation phase. For the considered time, no peat formation is reported for the tidal basin of Norderney, but a regressive signal around this time was documented for the tidal basin of Langeoog (Bungenstock and Schäfer, 2009), wherefore a stagnation seems plausible. However, due to the hiatus at the base of the tidal-flat sediments and the subsequent reworking, uncertainties concerning the general reliability of this part of the curve remain. The first uncertainty arises from the estimated length of the hiatus in N43, resulting in an uncertain temporal position for the two

youngest samples of the curve. Furthermore, the estimated age of the samples would imply a RSL rise of nearly 4 m within the last 2 ka, which does not correspond to any existing RSL reconstruction for the southern North Sea coast (e.g. Denys and Baeteman, 1995; De Groot et al., 1996; Bungenstock and Schäfer, 2009; Meijles et al., 2018). The two samples from N43 were therefore also excluded from further investigations, resulting in a cut-off of the curve at ~2500 cal BP. The second uncertainty arises from the vertical position of the sample from on top of the intercalated peat in VVC17, possibly influenced by compaction of the underlying peat. Hence, this data point might underestimate the RSL at this time and the curve may plot higher. Due to the exclusion of most tidal-flat samples, RSL changes after ~1700 cal BP cannot be reconstructed.

Another noteworthy characteristic is a fairly small error band of the curve for the phase between ~5000 and ~4000 cal BP, despite several cores which have been plotted together in this phase. The data originate from salt-marsh layers, confirming their high potential for continuous, high-resolution and accurate RSL reconstructions.

In an attempt to close the gap (~5700–5000 cal BP) between the first and the second phase, peat data available from within the investigated cores were included into the RSL curve (Fig. 6.7). Only peat data with undisputable sea-level induced growth were used here, i.e. the base of the intercalated peat of VVC17, correlating with the basal peat further east (see section 7.1, Objective B), and the base of the intercalated peat of N49. For the basal peats of N43 and N49, only the uppermost ages are known, representing the transgressive contact. Comparing the peat data and the TF curve, the peats lie within the error band but show different positions relative to the reconstructed MSL line. On tidal coasts, the basal peat forms at, or slightly above the local MHW level and therefore, generally reflects MHW when used as RSL indicator. The effects lowering or amplifying MHW are locally different. The flood-basin effect causes a lowering of local MHW (compared to MHW of an open coast), due to dissipation of the tidal wave from tidal inlets into large intertidal storage basins (e.g. Vink et al., 2007; Weerts, 2013; Meijles et al., 2018). This could partially apply for the tidal basin of Norderney, at least after the formation of the barrier islands, representing the incomplete flood-basin effect with a slightly lowered MHW (Vink et al., 2007; Weerts, 2013). However, this would rather apply on the more eastern cores of the transect and not on the two tidal-inlet cores (VVC16 and VVC17). The estuary effect causes an amplification of MHW, comparable to the damming effect of the narrower part of the German Bight, due to confinement of the tidal wave in a narrow embayment or estuary (e.g. Vink et al., 2007; Weerts, 2013). This effect does not seem to apply on the tidal basin of Norderney. The river-gradient effect, referring to a gently dipping groundwater surface in rivers, also leads to an amplified MHW along the estuary (upstream), which does not apply to the study area.

Hence, depending on the local amplification/lowering of the tidal wave, the basal peat forms at a very local MHW level, which can vary between MSL and coastal MHW (MHW of an open coast at this location), or above (but never below) MSL. Therefore, the position of the two basal peat-top samples relative to the TF curve (below the MSL line in the second phase), indicates that they are under the influence of compaction that happened prior to the salt-marsh development, since they should plot above MSL. An effect of auto-compaction by decomposition of the peat, associated with a lowering of the surface, resulting in enlarged accommodation space and subsequent flooding, sedimentation and salt-marsh formation is conceivable (cf. Long et al., 2006). However, it cannot be verified that compaction was complete when the salt marsh further aggraded and hence, an additional amount of compaction should also be assumed for the salt-marsh layer, but not as large as for the basal peat. In order to plot above the MSL line and error band, the basal peat would have to be shifted upwards for at least ~0.7 m, suggesting a compaction of this layer by the same amout. The same should be valid for the intercalated peat bases, which plot at or above the MSL line, but should rather be situated above the error band, suggesting an overall compaction of at least ~0.9 m for VVC17 and ~0.3 m for N49. Whether this compaction happened by oxidation and decomposition (cf. Long et al., 2006; Weerts, 2013) or post-depositionally by sediment or water load cannot be clarified, since the overlying sediments are mainly not suitable for the TF application. However, the stagnation trend during the third phase of the curve (represented by one tidal-flat sample from VVC17) could suggest an additional influence of post-depositional compaction by sediment load.

In order to evaluate the reliability and trans-regional significance of the established RSL curve, it was compared to several existing curves from the southern North Sea region (Fig. 6.8). As it lies below most of the existing curves, this probably confirms regional differences are a factor. When comparing the TF curve to curves from Belgium (Denys and Baeteman, 1995) and Zeeland (Kiden, 1995), a similar trend (albeit a lower course) with differences decreasing with time are noticeable. The differences lie around ~3.5–4 m in the first phase (~6100–5700 cal BP), but they decrease to ~3.8–2.8 m in the second phase (~5000–3700 cal BP). During the third phase (~2500–1700 cal BP), discrepancies increase again to 2.8–3.2 m. The general lower course of the TF curve could be explained by higher glacial isostatic subsidence in East Frisia due to the position relative to the glacial forebulge (see Fig. 1.3). The tendency of the TF curve to the Belgium and Zeeland curves towards younger times could be related to slowly decreasing GIA in time (Kiden et al., 2002; Weerts, 2013; Meijles et al., 2018). However, the compaction influences discussed above must not be neglected, since they could also play a role in causing the apparent discrepancies. A com-

bined influence of the differences in GIA and local compaction effects could also seem reasonable. Due to this “doubled” compaction effect (basal peat and most likely intercalated peat) in the third phase, the TF curve needs to be interpreted with caution, as it might plot too low. A significant reworking influence is not expected for this part of the curve, since the representing sample (VVC17) only exhibits a very low percentage of salt-marsh foraminifers within the tidal-flat deposit (<3.5%). If a trend similar to the curve of Denys and Baeteman (1995) would be assumed, a compaction of ~0.5 m could be implied. However, since the curves should further approximate in time, due to decreasing subsidence rates over time (cf. Kiden et al., 2002; Vink et al., 2007), the minimum compaction value mentioned above (~0.9 m) seems more likely.

Smaller discrepancies can be documented with curves from the western (Hijma and Cohen, 2010) and central Netherlands (van de Plassche et al., 2005) and from the Dutch Wadden Sea (Meijles et al., 2018), which all plot higher than the TF curve. The differences lie at ~2.6–1.5 m for the first phase, ~2.8–1.7 m for the second phase and increase in the third phase (~1.7–2.9 m). The curve showing the most similar trend originates from the Flevo area, using samples from the lowermost part of the basal peat as RSL index points (van de Plassche et al., 2005). Hence, their curve is most likely not influenced by compaction effects. However, the Flevo area is situated in the basin of the Ijsselmeer and experiences the complete flood-basin effect (cf. Weerts, 2013), whereas the tidal basin of Norderney experiences an incomplete flood-basin effect, if at all. This suggests a more intense reduction of MHW in the Flevo area than in the tidal flat of Norderney, explaining the lower discrepancies between the two curves, when compared to the curve from the Dutch Wadden Sea (Meijles et al., 2018). The generally similar trend but lower course of the TF curve compared to the three mentioned curves could again be related to differences in GIA rates (Steffen et al., 2006; Meijles et al., 2018). However, the increasing differences within the third phase rather emphasise increased compaction effects on the TF curve.

With the exception of the third phase, (which still contains some uncertainties), the TF curve shows an overlap with the curve for northwest Germany. This curve is based on selected data published by Behre (2003), and corrected for their indicative meaning by Vink et al. (2007). The TF data plot above the northwest Germany curve in the first phase (~0.4–0.9 m) with distances increasing in time (but still within the error band), whereas in the second phase, the TF plots below the existing curve (~0.1–1.6 m) again departing from each other with overlapping error bands. The data used for the first phase by Vink et al. (2007) (top basal peats and base intercalated peat), are certainly affected by compaction and, moreover, originate from very distant locations along the German coast. Namely from the Dollart-Bay area, crossing Wilhelmshaven (Jade Bay) to the ‘Land Wursten’ region (with currently

no data points close to Norderney), implying an inter-regional significance of the RSL index points (Bungenstock and Weerts, 2010, 2012; Baeteman et al., 2011). Due to existing local differences in compaction rates, mean tidal range, MHW and GIA, the TF curve is associated with a higher significance for the tidal basin of Norderney. Also for the database of Vink et al. (2007) (top and base upper peats and intercalated peat) during the second phase of the TF curve, an effect of compaction must be considered for the northwest Germany curve. Furthermore, considering the data locations, this part of the curve seems to be more significant for the area around the Jade Bay, but not for the Norderney tidal basin, suggesting the TF data to be more reliable for the study area. Even when factoring in these estimated minimum compaction rates for the TF curve, the data would still provide an error band smaller than the curve for northwest Germany (Vink et al., 2007).

To account for compaction and other possible impact factors, the TF data were compared to a new peat-based RSL curve from Langeoog (~10 km east of Norderney) by Bungenstock et al. (*in revision*), Fig. 6.9 and Fig. 7.2. This enabled conclusions on a more local scale. The TF data generally plot below the Langeoog data with mostly overlapping error bands. The TF curve shows a similar trend and a narrower error band. The differences are measured from the upper limit of the TF error band to the upper limit of the Langeoog curve. For the first phase they lie at ~1.7–1.4 m, and the deceleration of the RSL rise is reconstructed very similarly. During the second phase, the differences are around ~1.7–1.9 m and for the third phase, comparison is again difficult due to the established uncertainties, wherefore the differences increase in time (~1.9–2.8 m). These differences could indicate that compaction rates are higher than estimated above. However, the fact that the TF data plot below data from the lowermost part of the basal peat (at least in the time around 4000–3000 cal BP), (black data points in Fig. 7.2), could also reveal another important influencing factor. Since the TF provides an elevation for each sample relative to MSL at the time of deposition, which is also influenced by the tidal range, i.e. the height of MHW and MLW (mean low water), unequal changes in tidal range can also affect the elevation reconstructed by the TF.

It is generally assumed that the tidal range within the North Sea region was amplified throughout the Holocene transgression until ~7000–6000 BP (when the North Sea and the Southern Bight connected), without significant changes since (van der Molen and de Swart, 2001; Uehara et al., 2006; Haigh et al., 2019). However, the TF data plotting below the lowermost part of the basal peat could indicate that either MHW or MLW changed more strongly than the other, in which case MSL would follow (Fig. 6.10). With these insights, the lower course of the TF curve could be explained either by an increased rise in MHW departing from MLW (since ~4000 cal BP), or by an increased rise of MLW approximating towards

MHW until today. Shennan et al. (2000) report locally different changes in tidal range throughout the Holocene related to an increasing MHW, for different locations of the western North Sea. Even though the major changes should have happened prior to ~6000 BP, the TF data suggest a continued increase in MHW, which is in accordance with investigations about a notable rise in MHW compared to MLW within the last 150 years (Töppe, 1994). Of course, a combined effect of palaeo-tidal changes and peat compaction is conceivable for the course of the TF curve, especially for the third phase where uncertainties persist. Adjusting the TF for different models of palaeo-tides could therefore represent a goal for future investigations.

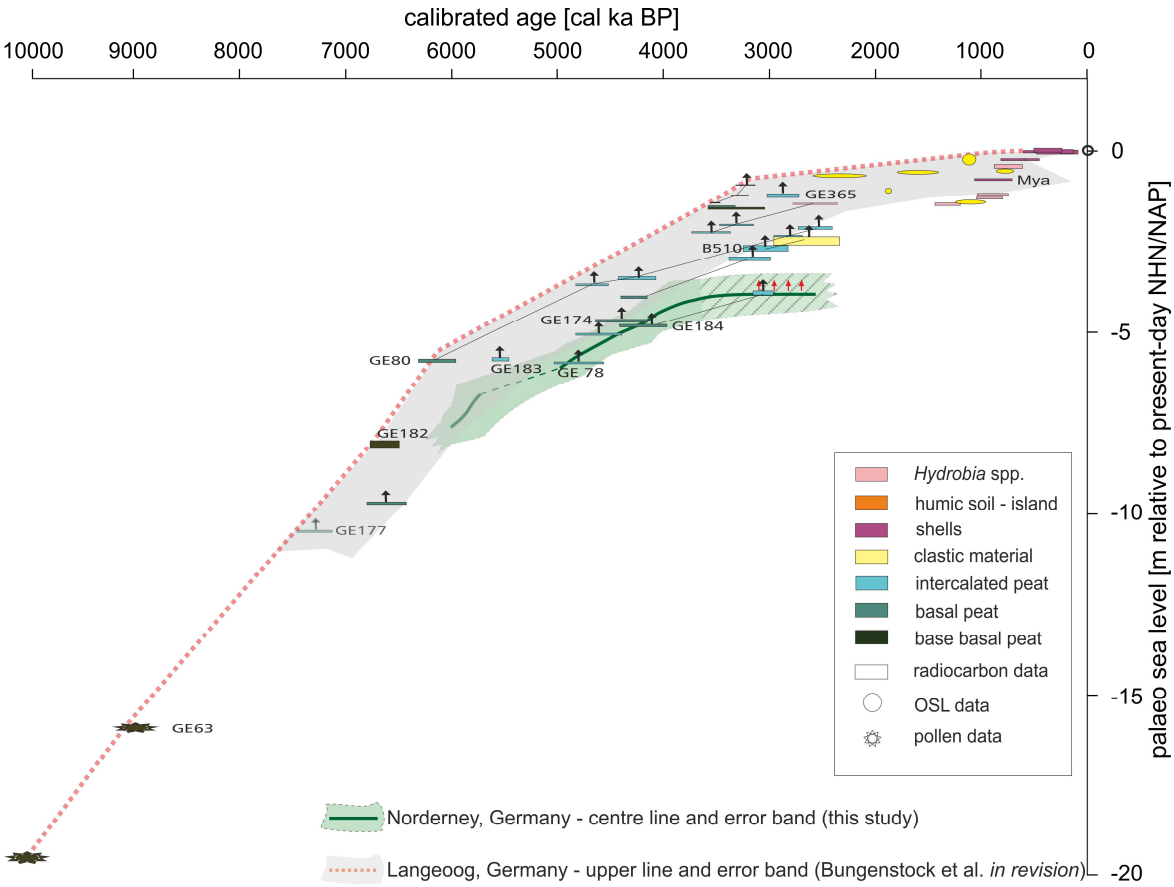

Fig. 7.2: Compilation of the TF data and new data from the East Frisian island of Langeoog by Bungenstock et al. (*in revision*) including all used RSL index points. The phase still affected by main uncertainties is cross-hatched. (own design 2020).

Summarising the evaluation of the RSL curve based on TF application, it can be documented that the low reliability of the lowest tidal-flat samples was verified leading to their exclusion from the final RSL curve for the tidal basin of Norderney. The overall high impact of sediment reworking in the tidal-flat deposits can be avoided by investigating archives from inner-dyke locations in future studies, which along a coastal-perpendicular transect, could also capture fossil tidal-flat layers that have not yet been influenced by additional reworking driven by dyke-construction. The potential effects of (auto- and post-depositional)

peat compaction, which partially influence the RSL reconstruction within the tidal basin of Norderney, can only be estimated to at least ~0.5–0.9 m. Moreover, the TF data provide promising indications on palaeo-tidal changes after 6000 BP, which is in contrast to reconstructions to date.

This research demonstrates that the application of the microfauna-based TF leads to RSL reconstructions with a much higher resolution and generally narrower error ranges than solely peat-based RSL reconstructions, for the Netherlands and the East Frisian island of Langeoog, thus, verifying **Hypothesis 3**. However, some uncertainties due to possible peat compaction, which cannot be reliably quantified with the currently available data remain.

Chapter 8

8 Conclusion and Outlook

The research presented in this thesis provides new insights into the Holocene landscape evolution on the German North Sea coast, by discussing possibilities and limitations to drawing conclusions on local RSL changes based on existing approaches, and offers a new approach in reconstructing Holocene RSL changes with a much higher precision.

The palaeo-landscape changes in the 'Land Wursten' region (Chapter 2) and in the tidal basin of Norderney (Chapters 3, 4 and 6) were reconstructed by identifying different depositional environments based on their microfaunal, sedimentological and geochemical characteristics. These landscape changes could be related to: (i) the Holocene transgression, leading to a generally increasing marine influence, (ii) coastal pro- and retrogradations, which led to alternations of supra-, intertidal and semi-terrestrial environments, (iii) (auto- and/or post-depositional) peat compaction leading to changes in A/S ratio and surface lowering, (iv) human intervention by dyke construction, leading to terrestrial conditions or intense sediment reworking in tidal-flat areas and (v) high-energy events which inundated the early swamp landscapes, tidal flats as well as the anthropogenic surfaces, resulting in the formation of *dwog* horizons. Moreover, the landscape changes enabled conclusions about the RSL evolution in the area: the supratidal, intertidal, semi-terrestrial and terrestrial alternations could be related to phases with different rates of RSL rise, and the *dwog* horizons were related to stagnation phases or phases of decelerated RSL rise after Bungenstock and Weerts (2010). However, uncertainties due to compaction and indicative meaning remain.

The intense reworking of the back-barrier tidal flat of Norderney still permits a continuous chronological classification and thus, conclusions on the RSL are further complicated for these deposits. Hence, the palaeo-landscape reconstructions have confirmed the necessity for more precise, quantitative RSL data. These could be provided in the form of modern foraminifer and ostracod associations, investigated in the tidal basin of Spiekeroog (Chapters 5 and 6). A modern training set, established from two surface transects (reaching from supratidal (salt marsh) to shallow subtidal (tidal channel) environments, crossing the intertidal tidal flat), could be related to an elevation-driven vertical and lateral zonation. Therefore, this thesis presented the first approach combining foraminifers and ostracods for a

RSL TF, which definitely led to an improved TF performance compared to the classic approach of using exclusively foraminifers. Since the combination of two transects provided an improved TF performance in terms of vertical error (29.7 cm) and correlation (0.89), it was confirmed that larger datasets (sample quantity of at least 40) are essential for the quality of a TF. The resulting vertical error range (~59 cm) outperforms the error ranges of existing peat-based RSL curves, which are associated with large uncertainties resulting from peat compaction and unclarified indicative meanings, frequently leading to error ranges of 3–5 m.

The first application of the final TF to Holocene samples from the southern North Sea coast led to the establishment of a new RSL curve for the tidal basin of Norderney (Chapter 6). This curve repeatedly confirmed the reworking effect on the tidal-flat deposits, indicating that tidal-flat cores are not suitable for RSL reconstructions for the younger part of the Holocene (after ~2.5 ka BP). Nonetheless, the TF application led to a RSL curve showing a clear deceleration of the RSL rise around 6–5 ka BP, in accordance with the known deceleration phase. Furthermore, the high suitability of fossil salt-marsh samples was confirmed by the small error band (~1 m) associated with the second phase of the RSL curve (~5–3.7 ka BP). This error band is smaller than that of most of the peat-based curves consulted for comparison. This comparison was able to confirm higher glacial isostatic subsidence rates on the East Frisian coast, compared to coastal sections further to the south (Belgium, central Netherlands). Comparing the TF-based RSL curve to available peat data from the same cores, revealed influences of peat compaction of at least ~0.7 m, which probably partially occurred due to oxidation and decomposition, creating accommodation space for the rapid accumulation of sediments and salt-marsh formation. Most likely, compaction continued due to sediment and water load, also influencing the intercalated peat which therefore might have been subject to double-compaction and thus, more intense subsidence. The compaction rates of the intercalated peat could also only be estimated to at least 0.3–0.9 m from their position relative to the TF-based RSL curve. Due to these compaction influences, the third phase of the presented RSL curve remains uncertain, and diverges from all existing RSL curves for the southern North Sea, wherefore in time decreasing GIA rates could not be confirmed. Potential palaeo-tidal changes for the time after ~6.1 ka BP were revealed from local comparison of the TF curve for Norderney and a new peat-based curve for Langeoog. This is in contrast to existing palaeo-tidal reconstructions, but still fits the investigations about a stronger rise in MHW compared to MLW during the last 150 years (Töppe, 1994). In case of a relatively lower MHW and stronger rise compared to MLW until today, the TF would underestimate the RSL in the past and explain the low course of the presented curve

In order to provide a TF-based RSL curve for the younger time period, prevention of collecting tidal-flat sediments affected by reworking would be necessary. This could be accomplished for example, by investigating sediment archives from inner-dyke locations instead of tidal-flat cores. If situated along a coastal-perpendicular transect, these should provide younger salt-marsh layers, (which have been shown to be best suited for TF application), as well as possible pre-dyke tidal-flat sediments, which have not yet been subject to intense reworking. However, a correction for compaction of peats by determination of the main time span of compaction remains necessary, in order to verify the reliability of overlying supra- and intertidal sediments. Furthermore, adjusting the TF, based on palaeo-tide models, would help to verify potential local changes in the palaeo-tidal range. Finally, the application of the new approach (TF utilising both foraminifers and ostracods) to other regions, such as the Dutch Wadden Sea, could provide valuable insights on locally different palaeo-tidal evolutions as well as local differences in peat compaction and GIA.

References

Ad-hoc-Arbeitsgruppe, B., 2005. Bodenkundliche Kartieranleitung, 5th ed. Bundesanstalt für Geowissenschaften und Rohstoffe, Hannover.

Asmus, W.D., 1949. Neuere Ausgrabungen in der Eisenzeitlichen Dorfsiedlung auf der Barward bei Dingen. Kr. Wesermünde. Hammaburg 2, 116–130.

Athersuch, J., Horne, D.J., Whittaker, J.E., 1989. Marine and brackish water ostracods (superfamilies Cypridacea and Cytheracea): keys and notes for the identification of the species. Brill Archive, Leiden.

Aufderhaar, I., Brandt, I., Schwank, S., Siegmüller, A., 2013. Aktuelle Untersuchungen im Umfeld der Wurt Fallward, Ldkr. Cuxhaven. Nachrichten des Marschenrates zur Förderung der Forschung im Küstengebiet der Nordsee 50, 41–44.

Baeteman, C., 1999. The Holocene depositional history of the IJzer palaeovalley (Western Belgian coastal plain) with reference to the factors controlling the formation of intercalated peat beds. Geologica Belgica 2, 39–72.

Baeteman, C., Waller, M., Kiden, P., 2011. Reconstructing middle to late Holocene sea-level change: A methodological review with particular reference to 'A new Holocene sea-level curve for the southern North Sea' presented by K.-E. Behre. Boreas 40, 557–572.

Barlow, N.L.M., Shennan, I., Long, A.J., Gehrels, W.R., Saher, M.H., Woodroffe, S.A., Hillier, C., 2013. Salt marshes as late Holocene tide gauges. Global and Planetary Change 106, 90–110.

Barsch, H., Billwitz, K., Bork, H. (Eds.), 2000. Arbeitsmethoden in Physiogeographie und Geoökologie. Justus Perthes Verlag Gotha GmbH, Gotha.

Beck, H.E., Zimmermann, N.E., McVicar, T.R., Vergopolan, N., Berg, A., Wood, E.F., 2018. Present and future Köppen-Geiger climate classification maps at 1-km resolution. Scientific Data 5, 180214.

Behre, K.-E., 2003. Eine neue Meeresspiegelkurve für die südliche Nordsee. Probleme der Küstenforschung im südlichen Nordseegebiet 28, 9–63.

Behre, K.-E., 2007. A new Holocene sea-level curve for the southern North Sea. Boreas 36, 82–102.

Behre, K.-E., Kučan, D., 1999. Neue Untersuchungen am Außendeichsmoor bei Sehestedt am Jadebusen. Probleme der Küstenforschung im südlichen Nordseegebiet 26, 35–64.

Berkeley, A., Perry, C.T., Smithers, S.G., Horton, B.P., Taylor, K.G., 2007. A review of the ecological and taphonomic controls on foraminiferal assemblage development in intertidal environments. Earth-Science Reviews 83, 205–230.

Bird, M.I., Fifield, L.K., Chua, S., Goh, B., 2004. Calculating Sediment Compaction for Radiocarbon Dating of Intertidal Sediments. Radiocarbon 46, 421–435.

Birks, H.J.B., 1995. Quantitative palaeoenvironmental reconstructions, in: Maddy, D., Brew, J.S. (Eds.), Statistical Modelling of Quaternary Science Data. Quaternary Research Association, Cambridge, pp. 161–254.

Bittmann, F., 2019. Das Wattenmeer als Archiv zur Landschaftsentwicklung, Klimaänderung und Siedlungsgeschichte. Nachrichten des Marschenrats zur Förderung der Forschung im Küstengebiet der Nordsee 56, 25–27.

Blaauw, M., Christen, A., 2019. rbacon: Age-Depth Modelling using Bayesian Statistics. R package version 2.3.9.1. https://CRAN.R-project.org/package=rbacon.

Blott, S.J., Croft, D.J., Pye, K., Saye, S.E., Wilson, H.E., 2004. Particle size analysis by laser diffraction. Forensic Geoscience: Principles, Techniques and Applications.

Blott, S.J., Pye, K., 2001. GRADISTAT: a grain size distribution and statistics package for the analysis of unconsolidated sediments. Earth Surface Processes and Landforms 26, 1237–1248.

Blume, H.P., Stahr, K., Leinweber, P., 2011. Bodenkundliches Praktikum. Eine Einführung in pedologische Arbeiten für Ökologen, Landund Forstwirte, Geo- und Umweltwissenschaftler. Spektrum, Heidelberg.

BSH (Bundesamt für Seeschifffahrt und Hydrographie), 2018. Gezeitenkalender 2019: Hoch- und Niedrigwasserzeiten für die Deutsch Bucht und deren Flussgebiete. Bundesamt für Seeschifffahrt und Hydrographie, Hamburg.

Bulian, F., Enters, D., Schlütz, F., Scheder, J., Blume, K., Zolitschka, B., Bittmann, F., 2019. Multi-proxy reconstruction of Holocene paleoenvironments from a sediment core retrieved from the Wadden Sea near Norderney, East Frisia, Germany. Estuarine, Coastal and Shelf Science 225, 106251.

Bungenstock, F., Freund, H., Mauz, B., Bartholomä, A., 2021. Holocene relative sea level data for the Eastfrisian barrier coast (NW Germany). Netherlands Journal of Geosciences (*in revision*).

Bungenstock, F., Schäfer, A., 2009. The Holocene relative sea-level curve for the tidal basin of the barrier island Langeoog, German Bight, Southern North Sea. Global and Planetary Change 66, 34–51.

Bungenstock, F., Weerts, H.J.T., 2010. The high-resolution Holocene sea-level curve for Northwest Germany: global signals, local effects or data-artefacts? International Journal of Earth Sciences 99, 1687–1706.

Bungenstock, F., Weerts, H.J.T., 2012. Holocene relative sea-level curves for the German North sea coast. International Journal of Earth Sciences 101, 1083–1090.

De Groot, T.A.M., Westerhoff, W.E., Bosch, J.H.A., 1996. Sea-level rise during the last 2000 years as recorded on the Frisian Islands (the Netherlands). Mededelingen Rijks Geologische Dienst 57, 69–78.

De Rijk, S., 1995. Salinity control on the distribution of salt marsh foraminifera (Great Marshes, Massachusetts). Journal of Foraminiferal Research 25, 156–166.

De Rijk, S., Troelstra, S., 1999. The application of a foraminiferal actuo-facies model to salt-marsh cores. Palaeogeography, Palaeoclimatology, Palaeoecology 149, 59–66.

Denys, L., Baeteman, C., 1995. Holocene evolution of relative sea level and local mean high water spring tides in Belgium—a first assessment. Marine Geology 124, 1–19.

Edwards, R.J., Horton, B.P., 2000. Reconstructing relative sea-level change using UK salt-marsh foraminifera. Marine Geology 169, 41–56.

Edwards, R.J., Wright, A., 2015. Foraminifera, in: Shennan, I., Long, A.J., Horton, B.P. (Eds.), Handbook of Sea-Level Research. John Wiley & Sons, Chichester, pp. 191–217.

Ehlers, J., Gibbard, P.L., 2004. Quaternary glaciations – Extent and chronology. Part I: Europe, Developments in Quaternary Science 2. Elsevier, Amsterdam.

Ehlers, Jürgen, Grube, A., Stephan, H.J., Wansa, S., 2011. Pleistocene glaciations of North Germany-New results, in: Ehlers, J, Gibbard, P.L., Hughes, P.D. (Eds.), Quaternary Glaciations - Extent and Chronology (Developments in Quaternary Science, Volume 15). Elsevier, Amsterdam, pp. 149–162.

Elschner, A., Scheder, J., Enters, D., Bartholomä, A., Becker, T., Capperucci, R., Wehrmann, A., Schlütz, F., Bungenstock, F., Hoffmann, G., 2021. Microfauna- and sedimentology-based facies analysis for palaeo-landscape reconstruction in the back-barrier of Norderney (NW Germany). Netherlands Journal of Geosciences 100, e4.

Engelhart, S.E., Horton, B.P., 2012. Holocene sea level database for the Atlantic coast of the United States. Quaternary Science Reviews 54, 12–25.

Enters, D., Haynert, K., Wehrmann, A., Freund, H., Schlütz, F., 2021. A new ΔR value for the southern North Sea and its application in coastal research. Netherlands Journal of Geosciences 100, e1.

Eshel, G., Levy, G., Mingelgrin, U., Singer, M., 2004. Critical Evaluation of the Use of Laser Diffraction for Particle-Size Distribution Analysis. Soil Science Society of America Journal 68, 736–743.

Filipescu, S., Kaminski, M., 2011. Re-discovering Entzia, an agglutinated foraminifer from the Transylvanian salt marshes. Proceedings of the Eighth International Workshop on Agglutinated Foraminifera. Grzybowski Foundation Special Publication 16, 29–35.

Flemming, B.W., 2002. Effects of Climate and Human Interventions on the Evolution of the Wadden Sea Depositional System (Southern North Sea), in: Wefer, G., Berger, W.H., Behre, K.-E., Jansen, E. (Eds.), Climate Development and History of the North Atlantic Realm. Springer, Berlin, Heidelberg, pp. 399–413.

Flöser, G., Burchard, H., Riethmüller, R., 2011. Observational evidence for estuarine circulation in the German Wadden Sea. Continental Shelf Research 31, 1633–1639.

Folk, R.L., Ward, W.C., 1957. Brazos River bar [Texas]; a study in the significance of grain size parameters. Journal of Sedimentary Research 27, 3–26.

Frenzel, P., Boomer, I., 2005. The use of ostracods from marginal marine, brackish waters as bioindicators of modern and Quaternary environmental change. Palaeogeography, Palaeoclimatology, Palaeoecology 225, 68–92.

Frenzel, P., Keyser, D., Viehberg, F.A., 2010. An illustrated key and (palaeo)ecological primer for Postglacial to Recent Ostracoda (Crustacea) of the Baltic Sea. Boreas 39, 567–575.

Freund, H., Streif, H., 2000. Natürliche Pegelmarken für Meeresspiegelschwankungen der letzten 2000 Jahre im Bereich der Insel Juist. Petermanns Geographische Mitteilungen 143, 34–45.

Gehrels, W.R., Belknap, D.F., Black, S., Newnham, R.M., 2002. Rapid sea-level rise in the Gulf of Maine, USA, since AD 1800. The Holocene 12, 383–389.

Gehrels, W.R., Newman, S.W.G., 2004. Salt-marsh foraminifera in Ho Bugt, western Denmark, and their use as sea-level indicators. Geografisk Tidsskrift-Danish Journal of Geography 104, 97–106.

Gerdes, G., Petzelberger, B.E.M., Scholz-Böttcher, B.M., Streif, H., 2003. The record of climatic change in the geological archives of shallow marine, coastal, and adjacent lowland areas of Northern Germany. Quaternary Science Reviews 22, 101–124.

Gerlach, A., 1999. Pflanzengesellschaften auf Spülsäumen, in: Umweltatlas Wattenmeer. Band 2, Wattenmeer Zwischen Elb- Und Emsmündung. Ulmer, Stuttgart, pp. 58–59.

Haigh, I.D., Pickering, M.D., Green, J.A.M., Arbic, B.K., Arns, A., Dangendorf, S., Hill, D.F., Horsburgh, K., Howard, T., Idier, D., Jay, D.A., Jänicke, L., Lee, S.B., Müller, M., Schindelegger, M., Talke, S.A., Wilmes, S.-B., Woodworth, P.L., 2019. The Tides They Are A-Changin': A comprehensive review of past and future nonastronomical changes in tides, their driving mechanisms, and future implications. Reviews of Geophysics 58, e2018RG000636.

Hajdas, I., 2008. Radiocarbon dating and its applications in Quaternary studies. E&G Quaternary Science Journal 57, 2–24.

Hammer, Ø., Harper, D.A.T., Ryan, P.D., 2001. Past: Paleontological statistics software package for education and data analysis. Palaeontologia Electronica 4, article 4.

Hayward, P.J., Ryland, J.S., 1990. The Marine Fauna of the British Isles and North-West Europe. Volume 2. Molluscs to Chordates, The Marine Fauna of the British Isles and North-West Europe. Volume 2. Molluscs to Chordates. Oxford University Press, Oxford.

Hijma, M.P., Cohen, K.M., 2010. Timing and magnitude of the sea-level jump preluding the 8200 yr event. Geology 38, 275–278.

Hofker, J., 1977. The foraminifera of dutch tidal flats and salt marshes. Netherlands Journal of Sea Research 11, 223–296.

Horton, B.P., Edwards, R., 2006. Quantifying Holocene Sea Level Change Using Intertidal Foraminifera: Lessons from the British Isles, Cushman Foundation for Foraminiferal Research, Special Publication No. 40. Lawrence.

Horton, B.P., Shennan, I., 2009. Compaction of Holocene strata and the implications for relative sealevel change on the east coast of England. Geology 37, 1083–1086.

Jelgersma, S., 1961. Holocene sea level changes in the Netherlands. Mededelingen van de Geologische Stichting C, 1–100.

Jelgersma, S., 1979. Sea-level changes in the North Sea Basin, in: Ole, E., Schüttenhelm, R.T.E., Wiggers, A.J. (Eds.), The Quaternary History of the North Sea. Uppsala University, Uppsala, pp. 233–248.

Jöns, H., 2015. SINCOS, SPLASHCOS und SUBLAND – Geschichte, Gegenwart und Perspektiven von „Submerged Prehistoric Research“ als europäische Forschungsdisziplin. Siedlungs- und Küstenforschung im südlichen Nordseegebiet 38, 13–27.

Juggins, S., 2007. C2 Version 1.5: software for ecological and palaeoecological data analysis and visualisation. University of Newcastle, Newcastle upon Tyne.

Kaiser, R., Niermeyer, H.D., 1999. Wasser-Beschaffenheit, in: Henke, R.M., Andrae, C. (Eds.), Umweltatlas Wattenmeer. Band 2, Wattenmeer Zwischen Elb- Und Emsmündung. Ulmer, Stuttgart, pp. 32–33.

Kalis, A.J., Merkt, J., Wunderlich, J., 2003. Environmental changes during the Holocene climatic optimum in central Europe - human impact and natural causes. Quaternary Science Reviews 22, 33–79.

Karle, M., Frechen, M., Wehrmann, A., 2017. Holocene coastal lowland evolution: reconstruction of land-sea transitions in response to sea-level changes (Jade Bay, southern North Sea, Germany). Zeitschrift der Deutschen Gesellschaft für Geowissenschaften 168, 21–38.

Kemp, A.C., Horton, B.P., Vann, D.R., Engelhart, S.E., Grand Pre, C.A., Vane, C.H., Nikitina, D., Anisfeld, S.C., 2012. Quantitative vertical zonation of salt-marsh foraminifera for reconstructing former sea level; an example from New Jersey, USA. Quaternary Science Reviews 54, 26–39.

Kemp, A.C., Telford, R.J., 2015. Transfer functions, in: Shennan, I., Long, A.J., Horton, B.P. (Eds.), Handbook of Sea-Level Research. John Wiley & Sons, Chichester, pp. 470–499.

Kemp, A.C., Telford, R.J., Horton, B.P., Anisfeld, S.C., Sommerfield, C.K., 2013. Reconstructing Holocene sea level using salt-marsh foraminifera and transfer functions: lessons from New Jersey, USA. Journal of Quaternary Science 28, 617–629.

Khan, N.S., Vane, C.H., Horton, B.P., 2015. Stable carbon isotope and C/N geochemistry of coastal wetland sediments as a sea-level indicator, in: Shennan, I., Long, A.J., Horton, B.P. (Eds.), Handbook of Sea-Level Research. John Wiley & Sons, Chichester, pp. 295–311.

Kiden, P., 1995. Holocene relative sea-level change and crustal movement in the southwestern Netherlands. Marine Geology 124, 21–41.

Kiden, P., Denys, L., Johnston, P., 2002. Late Quaternary sea-level change and isostatic and tectonic land movements along the Belgian–Dutch North Sea coast: geological data and model results. Journal of Quaternary Science 17, 535–546.

Kottek, M., Grieser, J., Beck, C., Rudolf, B., Rubel, F., 2006. World map of the Köppen-Geiger climate classification updated. Meteorologische Zeitschrift 15, 259–263.

Lambeck, K., Rouby, H., Purcell, A., Sun, Y., Sambridge, M., 2014. Sea level and global ice volumes from the Last Glacial Maximum to the Holocene. Proceedings of the National Academy of Sciences 111, 15296–15303.

Lange, W., Menke, B., 1967. Beiträge zur frühpostglazialen erd- und vegetationsgeschichtlichen Entwicklung im Eidergebiet, insbesondere zur Flußgeschichte und zur Genese des sogenannten Basistorfes. Meyniana 17, 29–44.

Last, W.M., Smol, J.P., 2001. Tracking Environmental Change Using Lake Sediments. Volume 2: Physical and Geochemical Methods. Kluwer Academic Publishers, Dordrecht.

Lehmann, G., 2000. Vorkommen, Populationsentwicklung, Ursache fleckenhafter Besiedlung und Fortpflanzungsbiologie von Foraminiferen in Salzwiesen und Flachwasser der Nord- und Ostseeküste Schleswig - Holsteins. PhD Thesis (unpublished). Christian-Albrechts-Universität zu Kiel.

Leorri, E., Gehrels, W.R., Horton, B.P., Fatela, F., Cearreta, A., 2010. Distribution of foraminifera in salt marshes along the Atlantic coast of SW Europe: Tools to reconstruct past sea-level variations. Quaternary International 221, 104–115.

Lepš, J., Šmilauer, P., 2003. Multivariate analysis of ecological data Using CANOCO. Cambridge University Press, New York.

Long, A.J., Waller, M.P., Stupples, P., 2006. Driving mechanisms of coastal change: Peat compaction and the destruction of late Holocene coastal wetlands. Marine Geology 225, 63–84.

Lowe, J.J., Walker, M.J.C., 1997. Reconstructing Quaternary Environments, 2nd ed. Longman, London.

Lüders, K., 1934. Über das Wandern der Priele. Abhandlungen des Naturwissenschaftlichen Vereins zu Bremen 29, 19–32.

Mehra, O.P., Jackson, M.L., 1958. Iron oxide removal from soils and clays by a dithionite-citrate system buffered with sodium bicarbonate. Clay Clay Miner 7, 317–327.

Meijles, E.W., Kiden, P., Streurman, H.-J., van der Plicht, J., Vos, P.C., Gehrels, W.R., Kopp, R.E., 2018. Holocene relative mean sea-level changes in the Wadden Sea area, northern Netherlands. Journal of Quaternary Science 33, 905–923.

Milker, Y., Horton, B.P., Nelson, A.R., Engelhart, S.E., Witter, R.C., 2015. Variability of intertidal foraminiferal assemblages in a salt marsh, Oregon, USA. Marine Micropaleontology 118, 1–16.

Milker, Y., Nelson, A.R., Horton, B.P., Engelhart, S.E., Bradley, L.A., Witter, R.C., 2016. Differences in coastal subsidence in southern Oregon (USA) during at least six prehistoric megathrust earthquakes. Quaternary Science Reviews 142, 143–163.

Milker, Y., Weinkauf, M.F.G., Titschack, J., Freiwald, A., Krüger, S., Jorissen, F.J., Schmiedl, G., 2017. Testing the applicability of a benthic foraminiferal-based transfer function for the reconstruction of paleowater depth changes in Rhodes (Greece) during the early Pleistocene. PLoS ONE 12, 0188447.

Müller-Ahlten, W., 1994. Zur Genese der Marschböden. II. Kalksedimentation, Entkalkung. Zeitschrift für Pflanzenernährung und Bodenkunde 157, 333–343.

Müller-Navarra, K., Milker, Y., Schmiedl, G., 2016. Natural and anthropogenic influence on the distribution of salt marsh foraminifera in the Bay of Tümlau, German North Sea. Journal of Foraminiferal Research 46, 61–74.

Müller-Navarra, K., Milker, Y., Schmiedl, G., 2017. Applicability of transfer functions for relative sea-level reconstructions in the southern North Sea coastal region based on salt-marsh foraminifera. Marine Micropaleontology 135, 15–31.

Murray, J.W., 2006. Ecology and Applications of Benthic Foraminifera. Cambridge University Press, Cambridge.

Nyandwi, N., Flemming, B., 1995. A hydraulic model for the shore-normal energy gradient in the East Frisian Wadden Sea (southern North Sea). Senckenbergiana maritima 25, 163–171.

Paul, M.A., Barras, B.F., 1998. A geotechnical correction for post-depositional sediment compression: examples from the Forth valley, Scotland. Journal of Quaternary Science 13, 171–176.

Pedersen, J.B.T., Svinth, S., Bartholdy, J., 2009. Holocene evolution of a drowned melt-water valley

in the Danish Wadden Sea. Quaternary Research 72, 68–79.

Preuß, H., Vinken, R., Vorr, H.-H., 1991. Symbolschlüssel Geologie, 3rd ed. Niedersächsisches Landesamt für Bodenforschung und Bundesanstalt für Geowissenschaften und Rohstoffe, Hannover.

Reimer, P.J., Bard, E., Bayliss, A., Beck, J.W., Blackwell, P.G., Ramsey, C.B., Buck, C.E., Cheng, H., Edwards, R.L., Friedrich, M., Grootes, P.M., Guilderson, T.P., Haflidason, H., Hajdas, I., Hatté, C., Heaton, T.J., Hoffmann, D.L., Hogg, A.G., Hughen, K.A., Kaiser, K.F., Kromer, B., Manning, S.W., Niu, M., Reimer, R.W., Richards, D.A., Scott, E.M., Southon, J.R., Staff, R.A., Turney, C.S.M., van der Plicht, J., 2013. IntCal13 and Marine13 Radiocarbon Age Calibration Curves 0–50,000 Years cal BP. Radiocarbon 55, 1869–1887.

Reineck, H.-E., Siefert, W., 1980. Faktoren der Schlickbildung im Sahlenburger und Neuwerker Watt. Die Küste 35, 26–51.

Reise, K., 2015. Kurswechsel Küste. Was tun, wenn die Nordsee steigt? Wachholtz Murmann Publishers, Hamburg.

Scheder, J., Engel, M., Bungenstock, F., Pint, A., Siegmüller, A., Schwank, S., Brückner, H., 2018. Fossil bog soils (‘dwog horizons’) and their relation to Holocene coastal changes in the Jade Weser region, southern North Sea, Germany. Journal of Coastal Conservation 22, 51–69.

Scheder, J., Frenzel, P., Bungenstock, F., Engel, M., Brückner, H., Pint, A., 2019. Vertical and lateral distribution of Foraminifera and Ostracoda in the East Frisian Wadden Sea – developing a transfer function for relative sea-level change. Geologica Belgica 22, 99–110.

Schönfeld, J., Golikova, E., Korsun, S., Spezzaferri, S., 2013. The Helgoland Experiment – assessing the influence of methodologies on Recent benthic foraminiferal assemblage composition. Journal of Micropalaeontology 32, 161–182.

Schoute, J.F.T., Griede, J.W., Roeleveld, W., Mook, W.G., 1981. Radiocarbon dating of vegetation horizons, illustrated by an example from the Holocene coastal plain in the northern Netherlands. Geologie en Mijnbouw 60, 453–459.

Schwertmann, U., 1964. Differenzierung der Eisenoxide des Bodens durch Extraktion mit Ammoniumoxalat-Lösung. Zeitschrift für Pflanzenernährung, Düngung, Bodenkunde 105, 194–202.

Scott, D.B., Medioli, F.S., Schafer, C.T., 2001. Monitoring in Coastal Environments Using Foraminifera and Thecamoebian Indicators, Monitoring in Coastal Environments Using Foraminifera and Thecamoebian Indicators. Cambridge University Press, Cambridge.

Shennan, I., Lambeck, K., Flather, R., Horton, B., McArthur, J., Innes, J., Lloyd, J., Rutherford, M., Wingfield, R., 2000. Modelling western North Sea palaeogeographies and tidal changes during the Holocene. Geological Society, London, Special Publications 166, 299–319.

Siegmüller, A., 2017. Die römisch-kaiserzeitlichen Wurten Barward und Fallward im Land Wursten (Ldkr. Cuxhaven). Aktuelle Auswertungen und struktureller Vergleich mit der Feddersen Wierde, in: Eriksen, B. V, Abegg-Wigg, A., Bleibe, R., Ickerodt, U. (Eds.), Interaktion Ohne Grenzen. Beispiele Archäologischer Forschungen Am Beginn Des 21. Jahrhunderts 1. Festschrift Für C. von Carnap-Bornheim Zum 60. Schleswig, pp. 169–179.

Smith, R.K., 1987. Fossilization potential in modern shallow-water benthic foraminiferal assemblages. Journal of Foraminiferal Research 17, 117–122.

Steffen, H., Kaufmann, G., Wu, P., 2006. Three-dimensional finite-element modeling of the glacial isostatic adjustment in Fennoscandia. Earth and Planetary Science Letters 250, 358–375.

Streif, H., 1990. Das ostfriesische Küstengebiet. Nordsee, Inseln, Watten und Marschen. Sammlung Geologischer Führer 57, 2nd ed. Gebrüder Bornträger, Berlin.

Streif, H., 2004. Sedimentary record of Pleistocene and Holocene marine inundations along the North Sea coast of Lower Saxony, Germany. Quaternary International 112, 3–28.

Strempel, R., 2016. Wadden Sea, in: German Commission for UNESCO, Perspectives of Transboundary Cooperation in World Heritage Sharing Experiences in and around Germany (Conference Report).

Tamm, O., 1932. Über die Oxalat-Methode in der chemischen Bodenanalyse. Meddelanden från Statens skogsförsöksanstalt 27, 1–20.

Tilch, E., 2003. Oszillation von Wattflächen und deren fossiles Erhaltungspotential (Spiekerooger Rückseitenwatt, Südliche Nordsee). Berichte, Fachbereich Geowissenschaften, Universität Bremen 222, Bremen.

Töppe, A., 1994. Beschleunigter Meeresspiegelanstieg. Hansa-Schiffahrt-Schiffbau-Hafen 131, 78–82.

Trusheim, F., 1929. Zur Bildungsgeschwindigkeit geschichteter Sedimente im Wattenmeer, besonders solcher mit schräger Parallelschichtung. Senckenbergiana 11, 47–56.

Uehara, K., Scourse, J.D., Horsburgh, K.J., Lambeck, K., Purcell, A.P., 2006. Tidal evolution of the northwest European shelf seas from the Last Glacial Maximum to the present. Journal of Geophysical Research 111, C09025.

van de Plassche, O., Bohncke, S.J.P., Makaske, B., van der Plicht, J., 2005. Water-level changes in the Flevo area, central Netherlands (5300–1500 BC): implications for relative mean sea-level rise in the Western Netherlands. Quaternary International 133–134, 77–93.

van der Molen, J., de Swart, H.E., 2001. Holocene tidal conditions and tide-induced sand transport in the southern North Sea. Journal of Geophysical Research: Oceans 106, 9339–9362.

van der Spek, A., 1996. Holocene depositional sequences in the Dutch Wadden Sea south of the

island of Ameland. Mededelingen Rijks Geologische Dienst 57, 41–68.

van Dijk, G., Fritz, C., Straathof, N., van de Riet, B., Hogeweg, N., Harpenslager, S.F., Roelofs, J.G.M., Behre, K.-E., Lamers, L.P.M., 2019. Biogeochemical Characteristics of the Last Floating Coastal Bog Remnant in Europe, the Sehestedt Bog. Wetlands 39, 227–238.

Vink, A., Steffen, H., Reinhardt, L., Kaufmann, G., 2007. Holocene relative sea-level change, isostatic subsidence and the radial viscosity structure of the mantle of northwest Europe (Belgium, the Netherlands, Germany, southern North Sea). Quaternary Science Reviews 26, 3249–3275.

Walton, W.R., 1952. Techniques for recognition of living Foraminifera. Contribution Cushman Foundation of Foraminiferal Research 3, 56–60.

Wartenberg, W., Vött, A., Freund, H., Hadler, H., Frechen, M., Willershäuser, T., Schnaidt, S., Fischer, P., Obrocki, L., 2013. Evidence of isochronic transgressive surfaces within the Jade Bay tidal flat area, southern German North Sea coast – Holocene event horizons of regional interest. Zeitschrift für Geomorphologie, Supplementary Issues 57, 229–256.

Weerts, H.J.T., 2013. Holocene sea-level change, sedimentation, coastal change and palaeogeography in the southern North Sea lowlands. A 2012 geological literature overview, in: Thoen, E., Borger, G.J., de Kraker, A.M.J., Soens, T., Tys, D., Vervaet, L., Weerts, H.J.T. (Eds.), Landscapes or Seascapes? The History of the Coastal Environment in the North Sea Area Reconsidered. CORN Publication Series, 13. Brepols Publishers, Turnhout, pp. 145–173.

Wildvang, D., 1938. Die Geologie Ostfrieslands. Abhandlungen der Preußischen Geologischen Landesanstalt N. F. 181, Berlin.

Wolters, S., Zeiler, M., Bungenstock, F., 2010. Early Holocene environmental history of sunken landscapes: pollen, plant macrofossil and geochemical analyses from the Borkum Riffgrund, southern North Sea. International Journal of Earth Sciences 99, 1707–1719.

Paper contribution

1. **Scheder, J.**, Engel, M., Bungenstock, F., Pint, A., Siegmüller, A., Schwank, S., Brückner, H., 2018. Fossil bog soils ('dwog horizons') and their relation to Holocene coastal changes in the Jade Weser region, southern North Sea, Germany. Journal of Coastal Conservation 22 (1), 51-69. doi: 10.1007/s11852-017-0502-z.

   Geländearbeit: 100 %
   Erhebung der Daten im Labor: 100 %
   Auswertung und Interpretation: 70 %
   Verfassen der Publikation: 80 %

2. Bulian, F., Enters, D., Schlütz, F., **Scheder, J.**, Blume, K., Zolitschka, B., Bittmann, F., 2019. Multi-proxy reconstruction of Holocene paleoenvironments from a sediment core retrieved from the Wadden Sea near Norderney, East Frisia, Germany. Estuarine, Coastal and Shelf Science 225. doi: 10.1016/j.ecss.2019.106251.

   Geländearbeit: 50 %
   Erhebung der Daten im Labor: 20 %
   Auswertung und Interpretation: 20 %
   Verfassen der Publikation: 20 %

3. Elschner, A., **Scheder, J.**, Bungenstock, F., Schlütz, F., Hoffmann, G., Bittmann, F. Microfauna- and sedimentology-based facies analysis for palaeo-landscape reconstruction in the back-barrier area of Norderney (NW Germany). Netherlands Journal of Geosciences 100, e4. doi: 10.1017/njg.2020.16.

   Geländearbeit: 50 %
   Erhebung der Daten im Labor: 75 %
   Auswertung und Interpretation: 70 %
   Verfassen der Publikation: 20 %

4. **Scheder, J.**, Frenzel, P., Bungenstock, F., Engel, M., Brückner, H., Pint, A., 2019. Vertical and lateral distribution of Foraminifera and Ostracoda in the East Frisian Wadden Sea – developing a transfer function for relative sea-level change. Geologica Belgica 22 (3-4), 99-110. doi: 10.20341/gb.2019.007.

   Geländearbeit: 80 %
   Erhebung der Daten im Labor: 100 %
   Auswertung und Interpretation: 75 %
   Verfassen der Publikation: 80 %

5. **Scheder, J.**, Bungenstock, F., Engel, M., Pint, A., Frenzel, P., Schlütz, F., Elschner, A., Brückner, H. Unravelling relative sea-level change in the southern North Sea using an improved micro-fauna-based transfer function. (*submitted to Journal of Quaternary Science, Manuscript number: JQS-20-0040*).

   Geländearbeit: 50 %
   Erhebung der Daten im Labor: 80 %
   Auswertung und Interpretation: 70 %
   Verfassen der Publikation: 80 %

Erklärung

"Hiermit versichere ich an Eides statt, dass ich die vorliegende Dissertation selbstständig und ohne die Benutzung anderer als der angegebenen Hilfsmittel und Literatur angefertigt habe. Alle Stellen, die wörtlich oder sinngemäß aus veröffentlichten und nicht veröffentlichten Werken dem Wortlaut oder dem Sinn nach entnommen wurden, sind als solche kenntlich gemacht. Ich versichere an Eides statt, dass diese Dissertation noch keiner anderen Fakultät oder Universität zur Prüfung vorgelegen hat; dass sie - abgesehen von unten angegebenen Teilpublikationen und eingebundenen Artikeln und Manuskripten - noch nicht veröffentlicht worden ist sowie, dass ich eine Veröffentlichung der Dissertation vor Abschluss der Promotion nicht ohne Genehmigung des Promotionsausschusses vornehmen werde. Die Bestimmungen dieser Ordnung sind mir bekannt. Darüber hinaus erkläre ich hiermit, dass ich die Ordnung zur Sicherung guter wissenschaftlicher Praxis und zum Umgang mit wissenschaftlichem Fehlverhalten der Universität zu Köln gelesen und sie bei der Durchführung der Dissertation zugrundeliegenden Arbeiten und der schriftlich verfassten Dissertation beachtet habe und verpflichte mich hiermit, die dort genannten Vorgaben bei allen wissenschaftlichen Tätigkeiten zu beachten und umzusetzen. Ich versichere, dass die eingereichte elektronische Fassung der eingereichten Druckfassung vollständig entspricht."

Nachfolgend genannte Publikationen und Manuskripte zur Veröffentlichung liegen vor:

1. **Scheder, J.**, Engel, M., Bungenstock, F., Pint, A., Siegmüller, A., Schwank, S., Brückner, H., 2018. Fossil bog soils ('dwog horizons') and their relation to Holocene coastal changes in the Jade Weser region, southern North Sea, Germany. Journal of Coastal Conservation 22 (1), 51-69. doi: 10.1007/s11852-017-0502-z.
2. Bulian, F., Enters, D., Schlütz, F., **Scheder, J.**, Blume, K., Zolitschka, B., Bittmann, F., 2019. Multi-proxy reconstruction of Holocene paleoenvironments from a sediment core retrieved from the Wadden Sea near Norderney, East Frisia, Germany. Estuarine, Coastal and Shelf Science 225. doi: 10.1016/j.ecss.2019.106251.
3. Elschner, A., **Scheder, J.**, Bungenstock, F., Schlütz, F., Hoffmann, G., Bittmann, F. Microfauna- and sedimentology-based facies analysis for palaeo-landscape reconstruction in the back-barrier area of Norderney (NW Germany). Netherlands Journal of Geosciences 100, e4. doi: 10.1017/njg.2020.16.

4. **Scheder, J.**, Frenzel, P., Bungenstock, F., Engel, M., Brückner, H., Pint, A., 2019. Vertical and lateral distribution of Foraminifera and Ostracoda in the East Frisian Wadden Sea – developing a transfer function for relative sea-level change. Geologica Belgica 22 (3-4), 99-110. doi: 10.20341/gb.2019.007
5. **Scheder, J.**, Bungenstock, F., Engel, M., Pint, A., Frenzel, P., Schlütz, F., Elschner, A., Brückner, H. Unravelling relative sea-level change in the southern North Sea using an improved microfauna-based transfer function. (*submitted to Journal of Quaternary Science, Manuscript number: JQS-20-0040*).

Köln, den 11.04.2021

(Juliane Scheder)

Curriculum Vitae

Juliane Michaela Scheder
[redacted]
Germany

Primary email: schederj@uni-koeln.de
Secondary email: scheder@nihk.de
Phone: [redacted]

Date & place of birth:	02/05/1987, Bad Homburg
Nationality:	German

Education

01/2016–06/2020	**Doctoral studies in Physical Geography**, Lower Saxony Institute for Historical Coastal Research, Wilhelmshaven, and Institute of Geography, University of Cologne Project: *The Wadden Sea as an archive of landscape evolution, climate change and settlement history: Exploration – analysis – predictive modelling* (acronym: WASA)
10/2011–12/2013	**Master of Science (M.Sc.) Physical Geography**, University of Cologne Master thesis: *"Fossil bog soils (dwog horizons) and their relation to Holocene coastal changes in the Jade Weser region" (grade: 1.0; best mark possible)*
10/2007–09/2011	**Bachelor of Science (B.Sc.) Geography**, University of Cologne Bachelor thesis: *"Mikrofaunistische Untersuchungen im Mündungsbereich der Quebrada Pachingo, Bahia Tongoy (Zentralchile) – spätholozäne Umweltveränderungen und ihre möglichen Ursachen" (grade: 2.0)*
10/2006–09/2007	**Bachelor of Science (B.Sc.) Geophysics and Meteorology**, University of Cologne

Awards

10/2019	**GSGS Stipend Grant** (GSGS-2019X-15) of the Graduate School of Geosciences, University of Cologne
06/2016	**Dr. Prill Award for excellent MSc thesis** ("Dr. Prill-Preis") of the Cologne Society of Geography ("Gesellschaft für Erdkunde zu Köln e.V.")
01/2016–09/2016	**Start-up Honours Grant** of the Graduate School of Geosciences (GSGS), University of Cologne
04/2014	**3rd place poster award** at the 32nd annual conference of the German Working Group of "Geography of Seas and Coasts", 3–6 April 2014, Wilhelmshaven

Work experience

Since 05/2020	**Research assistant** (Prof. Dr. H. Brückner, University of Cologne) Activities: *Preparations for research proposal*
Summer terms 2017 & 2018	**Lectureship**, University of Cologne Field and laboratory course 'Gelände- und Laborpraktikum zur Landschaftsgeschichte der Nordseeküste' (together with Dr. M. Engel, Dr. S. Opitz)

10/2016–09/2019	**Research associate** (Dr. F. Bittmann, Lower Saxony Institute for Historical Research, Wilhelmshaven) Activities: *Microfaunal analysis of modern sediment samples and core drillings, development of a sea-level transfer function, statistical and sedimentological data analysis, field work (core drillings in tidal flats and onshore, surface sampling)*
01/2016–09/2016	**Research assistant** covered by a Start-up Honours Grant of the GSGS at the University of Cologne (Dr. K. Boessenkool) Activities: *preparatory work for the doctoral project*
10/2015–12/2015	**Research assistant** (Prof. Dr. H. Brückner, University of Cologne) Activities: *microfaunal, statistical and sedimentological analysis, field work (drillings, surface sampling)*
06/2011–09/2015	**Student assistant** (Prof. Dr. H. Brückner, University of Cologne) Activities: *microfaunal, statistical and sedimentological analysis, field work (drillings, surface sampling)*
Since 10/2011	**Freelancer** (EMF-Institut Dr. Nießen, Siebengebirgsallee 60, 50939 Cologne – Germany) Activities: *digital mapping and analysing of electromagnetic radiation of mobile communications and other sources of electric, magnetic and electromagnetic radiation*

Practical experience

05/2018	**Field work (Neuharlingersiel, German North Sea coast)** with the field course 'Gelände- und Laborpraktikum zur Landschaftsgeschichte der Nordseeküste' (Pint, Scheder, Seeliger)
06/2017	**Field work (Hilgenriedersiel, German North Sea coast)** with the field course 'Gelände- und Laborpraktikum zur Landschaftsgeschichte der Nordseeküste' (Engel, Opitz, Scheder)
05/2017	**Field work (Wadden Sea – German North Sea coast)** in the course of the WASA project
11/2013	**Self-guided field work (Langen, German North Sea coast)** for the MSc thesis
09/2011	**Internship** at EMF-Institut Dr. Nießen, Siebengebirgsallee 60, 50939 Köln
03/2011	**Internship** at Land Surveying and Registry Office (Amt 62), Willy-Brandt-Platz 1, 50126 Bergheim

Training

04/2018–07/2018	**English course 'for Scientists'** at 'Linguarama Spracheninstitut GmbH' 13 April–6 July 2018
02/2017	**European School on Ostracoda** organised by the Society of Friends of IRGO (International Research Group on Ostracoda) e.V. 13–17 February 2017, Jena.

Extra-curricular activites

02/2019–05/2019	**Member of the organisation committee** of the 37th annual conference of the 'Arbeitskreis Geographie der Meere und Küsten', 09–10 May, Cologne
08/2017–01/2018	**Member of the organisation committee** of the 5th Research Conference of the GSGS, 19 January 2018, Cologne
02/2013–04/2013	**Organising assistant** of the 31st annual conference of the German Working Group of "Geography of Seas and Coasts", 18–21 April 2013, Cologne

09/2012	**Organising assistant** of the 14th International German Ostracodologists' Meeting (IGOM). 11–14 October 2012, Cologne
07/2012–08/2012	**Organising assistant** of the 32nd International Geographical Congress (IGC) 2012, 26–30 August 2012, Cologne

International peer-reviewed publications

2021

Elschner, A., **Scheder, J.**, Bungenstock, F., Schlütz, F., Hoffmann, G., Bittmann, F. Micro-fauna- and sedimentology-based facies analysis for palaeo-landscape reconstruction in the back-barrier area of Norderney (NW Germany). Netherlands Journal of Geosciences 100, e4. doi: 10.1017/njg.2020.16.

2020

Scheder, J., Bungenstock, F., Haynert, K., Pint, A., Schlütz, F., Frenzel, P., Wehrmann, A., Brückner, H., Engel, M., 2020. Unravelling Holocene relative sea-level change in the southern North Sea using an improved microfauna-based transfer function. Journal of Quarternary Science (submitted, manuscript number: *JQS-20-0040*).

2019

Scheder, J., Frenzel, P., Bungenstock, F., Engel, M., Brückner, H., Pint, A., 2019. Vertical and lateral distribution of Foraminifera and Ostracoda in the East Frisian Wadden Sea – developing a transfer function for relative sea-level change. Geologica Belgica 22 (3-4), 99-110. doi: 10.20341/gb.2019.007

Bulian, F., Enters, D., Schlütz, F., **Scheder, J.**, Blume, K., Zolitschka, B., Bittmann, F., 2019. Multi-proxy reconstruction of Holocene paleoenvironments from a sediment core retrieved from the Wadden Sea near Norderney, East Frisia, Germany. Estuarine, Coastal and Shelf Science 225. doi: 10.1016/j.ecss.2019.106251

2018

Scheder, J., Engel, M., Bungenstock, F., Pint, A., Siegmüller, A., Schwank, S., Brückner, H., 2018. Fossil bog soils ('*dwog* horizons') and their relation to Holocene coastal changes in the Jade Weser region, southern North Sea, Germany. Journal of Coastal Conservation 22 (1), 51–69. doi: 10.1007/s11852-017-0502-z

Other publications

2019

Scheder, J., Pint, A., Engel, M., Bungenstock, F., Frenzel, P., Brückner, H., 2019. Foraminiferen und Ostrakoden im Ostfriesischen Wattenmeer – Ein Beitrag zur Meeresspiegelrekonstruktion. Nachrichten des Marschenrates 56, 39–44.

Conference contributions

2019

1st International Conference 'Drowned paleo-landscapes. Current Archaeological and Natural Scientific research in the Wadden Sea and the North Sea basin' 2019, 19–20 September, Delmenhorst (talk). **Scheder, J.**, Engel, M., Pint, A., Bungenstock, F., Frenzel, P., Schlütz, F., Brückner, H. Foraminifers and ostracods as a tool for unravelling relative sea-level change in the East Frisian Wadden Sea.

20th Congress of the 'International Union for Quaternary Research' (INQUA) 2019, 25–31 July, Dublin (talk). **Scheder, J.**, Pint., A., Frenzel, P., Bungenstock, F., Engel, M., Schlütz, F., Brückner, H. Distribution of foraminifers and ostracods in the East Frisian Wadden Sea – A transfer function for relative sea-level change.

37th annual conference of the 'Arbeitskreis Geographie der Meere und Küsten' 2019, 09–10 May, Cologne (talk). **Scheder, J.,** Pint, A., Frenzel, P., Bungenstock, F., Engel, M., Schlütz, F., Brückner, H. Distribution of foraminifers and ostracods in the East Frisian Wadden Sea – A transfer function for relative sea-level change.

6th Research Conference of the Graduate School of Geosciences, 18 January 2019, Cologne (talk). **Scheder, J.,** Pint, A., Frenzel, P., Bungenstock, F., Engel, M., Schlütz, F., Brückner, H. Vertical and lateral zonation of Foraminifera and Ostracoda in the German Wadden Sea – Establishment and first application of a transfer function for Holocene relative sea-level changes.

2018
3rd annual meeting of the 'IGCP Project 639 – Sea Level Change from Minutes to Millennia' 2018, 16–23 September, 'Crossing southern Italy: a travelling meeting from Taranto to Siracusa' (talk). **Scheder, J.,** Bungenstock, F., Engel, M., Pint, A., Frenzel, P., Schlütz, F., Brückner, H. Vertical and lateral zonation of Foraminifera and Ostracoda in the German Wadden Sea – Establishment and first application of a tranfer function for Holocene relative sea-level changes.

36th annual conference of the 'Arbeitskreis Geographie der Meere und Küsten' 2018, 18–21 April, Braunschweig (poster). Scheder, J., Bungenstock, F., Engel, M., Pint, A., Frenzel, Brengelmann, T., P., Brückner, H. Vertical and lateral zonation of Foraminifera and Ostracoda in the German Wadden Sea – Establishing a transfer function for Holocene relative sea-level changes.

5th Research Conference of the Graduate School of Geosciences, 19 January 2018, Cologne (poster). **Scheder, J.,** Bungenstock, F., Engel, M., Pint, A., Frenzel, P., Brückner, H. Holocene relative sea-level reconstructions at the German North Sea coast using microfaunal and sedimentological data. (*updated version*)

2017
35th annual conference of the German Working Group of “Geography of Seas and Coasts”, 19–22 April 2017, Kiel (poster). **Scheder, J.,** Bungenstock, F., Engel, M., Pint, A., Frenzel, P., Brückner, H. Holocene relative sea-level reconstructions at the German North Sea coast using microfaunal and sedimentological data.

2016
Annual conference of the German Working Group of “Geomorphology”, 5–8 October 2016, Jena (poster). **Scheder, J.**, Bungenstock, F., Engel, M., Pint, A., Frenzel, P., Freund, H., Siegmüller, A., Schwank, S. & Brückner, H. Microfaunal and sedimentological data as proxies for Holocene sea-level and coastal changes at the German North Sea coast.

34th annual conference of the German Working Group of “Geography of Seas and Coasts”, 20–23 April 2016, Rostock-Warnemünde (oral presentation). **Scheder, J.**, Bungenstock, F., Engel, M., Pint, A., Frenzel, P., Freund, H., Siegmüller, A., Schwank, S. & Brückner, H. Microfaunal and sedimentological data as proxies for Holocene sea-level and coastal changes at the German North Sea coast.

2015
33rd annual conference of the German Working Group of “Geography of Seas and Coasts”, 6–9 May 2015, Hamburg (poster). **Scheder, J.**, Pint, A., Bungenstock, F., Engel, M., Siegmüller, A., Schwank, S., Brückner, H. Microfaunal investigations in the Weser marshland – Holocene coastal changes at the German North Sea coast.

2014
32nd annual conference of the German Working Group of “Geography of Seas and Coasts”, 3–6 April 2014, Wilhelmshaven (poster). **Scheder, J.**, Bungenstock, F., Siegmüller, A., Schwank, S., Brückner, H. Fossil bog soils (dwog horizons) as a key to reconstruct Holocene palaeotopography and coastal evolution.

2013
31st annual conference of the German Working Group of “Geography of Seas and Coasts”, 18–21 April 2013, Cologne (oral presentation). Pint, A., **Scheder, J.**, May, S.M., Kelletat, D., Brückner, H. Paläoumweltrekonstruktion mit Hilfe der Mikrofauna (Foraminiferen, Ostrakoden) – Methodischer Ansatz, Potential und ein Anwendungsbeispiel aus Zentralchile.

2012
14th International German Ostracodologists’ Meeting (IGOM), 11–14 October 2012, Cologne (poster). **Scheder, J.**, May, S.M., Pint, A., Kelletat, D., Rixhon, G., Brückner, H. Microfaunal investigation of the Quebrada Pachingo coastal swamp (Bahía Tongoy, northern central Chile) – Late Holocene environmental changes and their potential causes.

32nd International Geographical Congress (IGC) Cologne, 26–30 August 2012, Cologne (poster). **Scheder, J.**, May, S.M., Pint, A., Kelletat, D., Rixhon, G., Brückner, H. Microfaunal investigation of the Quebrada Pachingo coastal swamp (Bahía Tongoy, northern central Chile) – Late Holocene environmental changes and their potential causes.

Further qualifications and memberships

Language competence	English (C1.2), French & Spanish (basic knowledge)
IT experience	MS Office, image processing, ArcGIS, NIRView, PAST, Grapher
Memberships	German Working Group of “Geography of Seas and Coasts” Gesellschaft für Erdkunde zu Köln e.V.

Cologne, 26 June 2020